Optical characterisation of long wavelength self-assembled Quantum Dot lasers

Thomas James Badcock

Thesis submitted for PhD

Department of Physics and Astronomy

University of Sheffield

March 2008

In memory of my grandparents…

Chapter 1

Introduction

1.1 Low dimensional semiconductors

According to Heisenberg's uncertainty principle, the confinement of carrier motion along a given direction increases the kinetic energy of the particle in that direction by an amount that is inversely proportional to the length scale of the confinement. If this energy is comparable to the carrier thermal energy (= $\frac{1}{2}k_BT$ per degree of freedom), then the effects of this 'quantum confinement' are able to be observed. Due to the typical values of electron effective mass and working temperatures, quantum confinement effects are only observed when the carriers are restricted to regions of a few nanometers at most. Semiconductor heterostructures that contain a few nanometers of a narrow bandgap (E_g) semiconductor placed within wider E_g semiconductor provide an ideal means of investigating such effects. The thin films of material required for these studies may now be realised with an extremely high level of precision due to the advent of epitaxial growth techniques such as Molecular Beam Epitaxy (MBE) and Metal Organic Vapour Phase Epitaxy (MOVPE).

In a complementary way, the reduction of the periodicity of the crystal lattice to only a few repeats in the direction of the confinement results in a strong modification to the electronic density of states (DOS). The DOS may be modified further by restricting the carrier motion in additional (perpendicular) directions. Systems with confinement in one, two and three directions are referred to as quantum wells, wires and dots respectively. The evolution of the DOS with increasing 'dimensionality' of the confinement is shown schematically in Fig 1.1.

As the dimensionality of the structure reduces, the DOS continuum in the bulk (3D) material breaks down in to sub-'bands', for quantum well (QW) and quantum wire structures. Since the onset of the first sub-band in a QW occurs at a higher energy than the bulk E_g, injected carriers are not wasted filling up lower energy states in order to reach the required DOS for lasing to occur. Therefore the

threshold gain in QW devices is able to be obtained at a lower carrier injection level than in bulk, resulting in reduced threshold current densities[1].

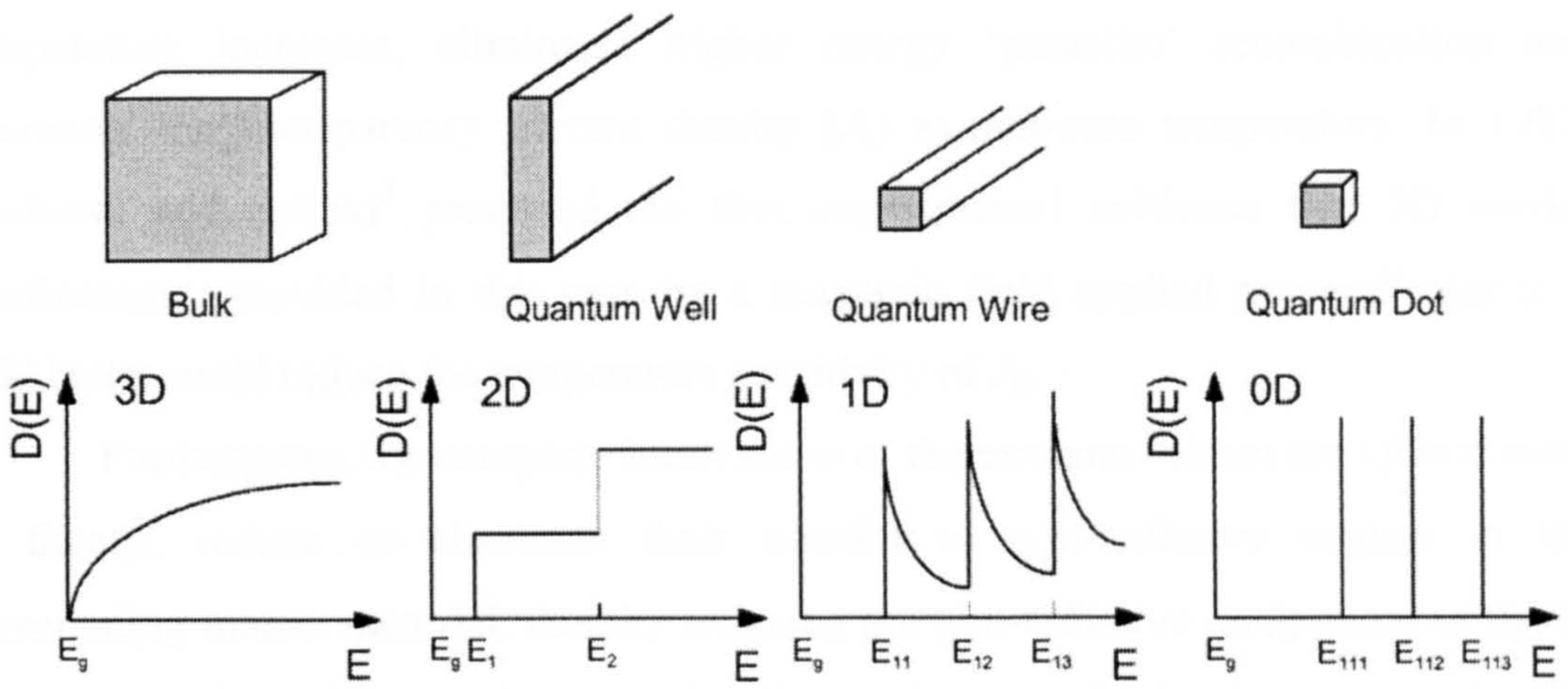

Fig. 1.1 Evolution in the density of electronic states (DOS) as the dimensionality of the confinement (system) is increased (reduced). In 2D and 1D systems, the DOS breaks down into sub-bands, with edges denoted by E_1, E_{11} etc. Free carrier motion is still possible in in the unconfined directions. In a quantum dot, discrete electronic states are formed (E_{111} etc.) with no free carrier motion.

In addition, as the dimensionality is decreased the relative DOS at higher energies decreases with respect to that at the sub-band edge. Hence the number of available states into which carriers can be thermally excited decreases and this should result in a greater thermal stability for laser devices[1]. Furthermore, the enhancement of the DOS at the band edge in structures of reduced dimensionality is predicted to provide an increase in the available differential gain[2]. Since the modulation bandwidth of a device is proportional to the differential gain, devices containing low dimensional active regions are therefore very attractive candidates for optical communication applications operating at high modulation speeds.

The ultimate case of quantum confinement corresponds to the formation of a Quantum Dot (QD). Here the carrier motion is confined in all three dimensions such that the sub-band structure of QWs and quantum wires is lost and an atomic-like series of discrete states is produced. As long ago as 1976, before their physical realisation, it was predicted that if an ensemble of identical QDs could be incorporated into the active region of a laser diode, the temperature dependence of the threshold current density (J_{th}) would be eliminated[3]. This insight relies on the QD

states being well described by a delta function-like DOS, with separations that significantly exceed the thermal energy (k_BT). In principle, an infinitely narrow DOS results in all of the injected carriers recombining with an identical transition energy. The absence of a sub-band continuum, into which carriers may be excited as the temperature increases, eliminates higher energy 'parasitic' recombination and decreases the transparency current density (J_0) at non-zero temperature. In 1982, Arakawa and Sakaki[4] produced the first experimental evidence that 3D carrier confinement, provided in this case by a magnetic field applied perpendicular to a QW laser, could reduce the temperature sensitivity of J_{th}.

Furthermore, the complete localisation of the excitons within the QDs should, in theory, reduce or eliminate their transfer to non-radiative centres in the surrounding matrix material, thereby reducing the non-radiative component of J_{th}. In samples that have been subjected to irradiation damage, the luminescence of a QD laser structure has been found to be up to 1000 times more intense than that of a comparable QW device[5]. Indeed, both proton-irradiated[6] and annealed[7] QD structures have demonstrated improved luminescence efficiency with respect to as-grown structures, perhaps as a result of defect passivation within the GaAs matrix[8].

However, a potential disadvantage of the highly localised nature of the states in QDs was predicted in 1991: "the phonon bottleneck". Due to the fully quantized carrier confinement in a QD, there is no wavevector (k) dispersion in any direction. In higher dimensionality systems, carrier relaxation to the bottom of the respective band can proceed via the emission of a series of single LO phonons, which occurs very efficiently on a time scale of ~100 fs per phonon, followed by slower but still efficient LA phonon scattering. These processes are able to conserve both energy and momentum. The lack of continuum states within QDs inhibits such a process, it being very unlikely that the spacing between the discrete levels exactly matches the LO phonon energy. Therefore it was predicted that the carriers would remain trapped for several nanoseconds in the higher energy states and this mechanism was cited as an intrinsic reason for poor optical efficiency in original studies of QDs[9]. In addition, a slow carrier relaxation would limit the maximum modulation speed of a QD based laser. In early time resolved studies of QDs a long carrier relaxation time (τ_{rel}) was reported for higher energy states, reaching 1 ns for the transition between the two lowest lying states[10]. A τ_{rel} of over 7 ns was reported more recently,

attributed to a weaker exciton-LO phonon coupling in truncated pyramidal QDs[11]. In general however, literature reports suggest that τ_{rel} may be typically only a few ps in most QD systems[12, 13] and therefore that efficient phonon and/or carrier-carrier scattering processes are active, even at low temperature.

1.2 Stranski-Krastanow nucleation of InAs/GaAs QDs

A number of techniques have been developed to fabricate semiconductor QDs. Of these the self-assembly technique, based on the Stranski-Krastanow process, is the most successful for producing QDs suitable for electro-optical applications. This technique will now be described.

The self-assembly technique starts with the deposition of a relatively highly strained 2D layer on an underlying substrate. The elastic energy stored in this pseudomorphically strained film can be reduced via the formation of either misfit dislocations or the spontaneous 3D islanding of the deposited material. In the case of the latter, because the islands are initially unsurrounded by material, the lattice constant is able to relax parallel to the surface, reverting back to its unstrained value as the height of the dot increases. However there is an increase in surface energy and hence a transition from 2D layer to 3D islanding growth will occur when the decrease in elastic energy outweighs the increase in surface energy. For a system in which this occurs the transition between coherently strained 2D growth and the onset of 3D island growth is reached after a 'critical thickness' (θ_c) of epitaxial material has been deposited. This critical thickness is a function of the lattice mismatch (Δa_0) between the epitaxial material and the substrate and must occur before the critical thickness for the formation of mis-fit dislocations occurs. For the most commonly studied system consisting of InAs grown on GaAs, Δa_0 = 7%, and the resultant islands have dimensions of a few to 10s nm, sufficient for strong quantisation effects to be observed. The transition from a purely 2D to 3D growth during the deposition of a strained epitaxial layer is referred to as the Stranski – Krastanow (S-K) growth mode.

For InAs/GaAs QDs, S-K growth occurs after as little as 1.7 ML of InAs has been deposited[14]. Photoluminescence excitation spectroscopy studies have verified both the thickness[15] and the composition[16] of the thin InAs Wetting Layer (WL) on which the QDs are formed. The amount of required material (θ_c) increases with

decreasing Indium (In) fraction, reaching ~ 4 ML for $In_{0.5}Ga_{0.5}As$/GaAs QDs[17]. The lowest In composition that can support islanding of the $In_xGa_{1-x}As$ layer appears to be ~25%.

In later work, it was shown that the extent of the In segregation is a key determinant of θ_c for the S-K transition[18]. By monitoring the QD size as a function of growth temperature (T_G) using an in situ Scanning Tunnelling Microscopy (STM) technique, pure S-K growth has been shown to occur only when $T_G < 420$ °C. For $T_G > 420$ °C, the total QD volume is greater than the amount of additional InAs material deposited, implying that significant mass transport to the QDs occurs from the WL and GaAs substrate[19]. In addition, studies have shown that following overgrowth of the QDs with a matrix material, material can be lost from the QDs and/or alloying can occur. Hence the growth of 'real' self-assembled QDs can be much more complicated than that implied by the basic S-K mechanism.

Since the islanding of InAs in a GaAs matrix was first demonstrated in 1985[18], QD formation via the self-assembly technique has been demonstrated for many pairs of binary and ternary III-V compounds, e.g. InGaAs/GaAs[21], InGaAs/AlGaAs[22], InP/InGaP[23]. However, of these, the In(Ga)As/GaAs material system has remained the most extensively studied.

All of the samples studied in this thesis have been grown by MBE. In MBE, the constituent elements of the nanostructure are evaporated from their solid sources in the form of a "molecular beam", the material is subsequently deposited atomic layer by atomic layer on a heated crystalline substrate (e.g. GaAs). The thickness of the resulting epitaxial layers may be controlled with monolayer (ML) precision due to the low growth rates (a few Å/sec or less) and sub-second opening and closing of mechanical shutters placed in front of the cells that contain the elemental sources. This inherent controllability makes the MBE technique ideally suited for the growth of QDs. In addition, the growth can be monitored in-situ by techniques such as reflection high energy electron diffraction (RHEED) which provides real time monitoring of the growth surface.

1.3 Electronic structure of self-assembled InAs/GaAs QDs

A calculation of the electronic structure of self-assembled QDs is very difficult given their complicated shape and strain profile. In addition, the composition of the QDs may not be accurately known and is also likely to be non-uniform. However a number of general statements can be made. For example the number of confined electronic states increases with QD size and their separation decreases. In addition the degeneracy of the levels will generally increase with increasing quantum number(s) and hence energy. For a QD with cylindrical symmetry about the growth axis the lowest energy state (the ground state GS) is 1*s* which is able to contain a maximum of two electrons. The next state is 1p which is four fold degenerate. However departure from cylindrical symmetry may split the 1p state into two separate levels. Most self-assembled quantum dots have a height that is significantly smaller than the in-plane dimensions. Hence it is mainly the former which controls the quantisation energy of the lowest state but the latter which controls the separation between the confined states. However, the exact dependence of the quantised energy levels on the QD dimensions is a sensitive function of the confining potential, as determined by the QD shape[24, 25], strain[26] and piezoelectric field[27]. Full calculations of the electronic states of a QD require atomistic models run on a super computer[28], however reasonable approximations can be applied to use simpler models. For example, it is believed that large disk-like QDs provide a harmonic oscillator potential that results in uniformly spaced energy levels ($E = h\nu[n+½]$) and wavefunctions that can be represented by simple equations[29].

The InAs QDs studied in this thesis, have a GS to first excited state (ES1) separation of ~45 meV for electrons and ~12 meV for the holes[30]. The much larger effective mass of the holes in InAs (and all III-V semiconductors) always results in a smaller energy level separation for the holes than for electrons. Since the occupation of excited states is disadvantageous for QD laser operation (see next section) it is desirable to maximise this separation as much as possible in order to reduce the thermal excitation of carriers out of the GS, which is generally the lasing state. As discussed above it is believed that the GS – ES1 separation is predominantly determined by the lateral confinement provided by the QD[31]. Therefore, GS – ES1 may be increased by either decreasing the lateral extent of the QD or by confining it

in higher band gap material. In practice, it is difficult to tailor both inter and intra-band state separation energies simultaneously, due to the nature of the self-assembled QD growth process. However, InAs QDs with GS – ES1 separations (in this case the sum of both the electron and hole contributions) in excess of 100 meV have been achieved either when capped with GaAs[32] or InAlAs[33]. The beneficial effect of the increased sub-state separations on the lasing performance is reflected in the weaker temperature sensitivity of J_{th} around RT.

1.4 Limiting factors in QD laser performance

Initial calculations of the expected performance of QD lasers assumed idealized dots containing only one electron and one hole level and that all QDs in the laser were identical[4]. Real QDs contain multiple states, there are states external to the QDs, there may be defect related and Auger non-radiative recombination and the dots within an ensemble exhibit a significant distribution in size, shape and composition. Hence an important question is how far from the ideal behaviour a QD laser will deviate.

Although a gain medium containing QDs has the potential to offer simultaneously high differential gain and low transparency current density (J_0), a combination which can provide the lowest J_{th} at any cavity length, the full extent of this advantage can never be realised in practice. The material gain (g_{mat}) obtainable from the ground state (GS) transition of a single QD is inversely proportional to the homogeneous broadening of the transition. However the gain produced by a single QD is very small and hence in order to produce a total g_{mat} able to overcome the losses of a typical laser cavity a high density array of QDs must be produced. The 'self-assembly' technique, which was discussed in section 1.2, is able to produce a high density ensemble of QDs, with densities as high as ~10^{11} cm^{-2} possible, but suffers from the fact that there are intrinsic fluctuations in the QD size, shape and composition, which results in an inhomogeneous broadening of the optical transitions (typically of order 20~30meV). This inhomogeneous broadening "smears" out the DOS intrinsic to a single QD and is the dominant contribution to the emission linewidth, even in highly uniform ensembles of QDs[34]. In such an inhomogeneously broadened system, the peak DOS and therefore the lasing energy, corresponds to the

most probable size of QD in the array. For a QD ensemble of fixed in-plane QD density, any inhomogeneous broadening leads to a reduction in the peak DOS, resulting in lower saturated and differential gain. Although careful optimization of the growth conditions may reduce the degree of inhomogeneous broadening it appears difficult to reduce it below ~15meV[35].

The existence and population of excited QD states is also detrimental to device performance. Any population of excited states reflects wasted carriers which results directly in an increased threshold current density. In addition, since the saturated and differential gain is proportional to the degeneracy of the state involved in the lasing, any thermal occupation of these states may result in a switch from GS to ES1 or even the second excited state (ES2) lasing with increasing injection current or temperature. The population of excited states has also been correlated with an increase in the non-radiative current density, due to the greater number of non-radiative channels being accessible via these states[36].

Another factor that affects the performance of a QD laser is that, particularly at low temperatures, there may not be a thermal distribution of carriers within the QD ensemble. For example, the transition from a non-thermal to a thermal distribution is believed to cause the widely reported decrease of J_{th} with increasing temperature between 6 and 200 K, observed in nearly all QD lasers[37, 38]. An example of this behaviour is shown in Fig. 1.2, which shows the temperature dependence of J_{th} between 77 and 300 K for a QD laser structure with a large inhomogeneous broadening (Vn 57 – see chapter 3, section 3.4.2.2). At low temperatures electrons and holes recombine within the QD into which they are initially captured and hence the whole ensemble contributes to the emission; carriers in different QDs are effectively isolated from each other. As the temperature is raised the thermally induced transfer of carriers from QDs with shallower confinement to more deeply confining QDs is able to narrow the gain spectrum and consequently reduce J_{th}.

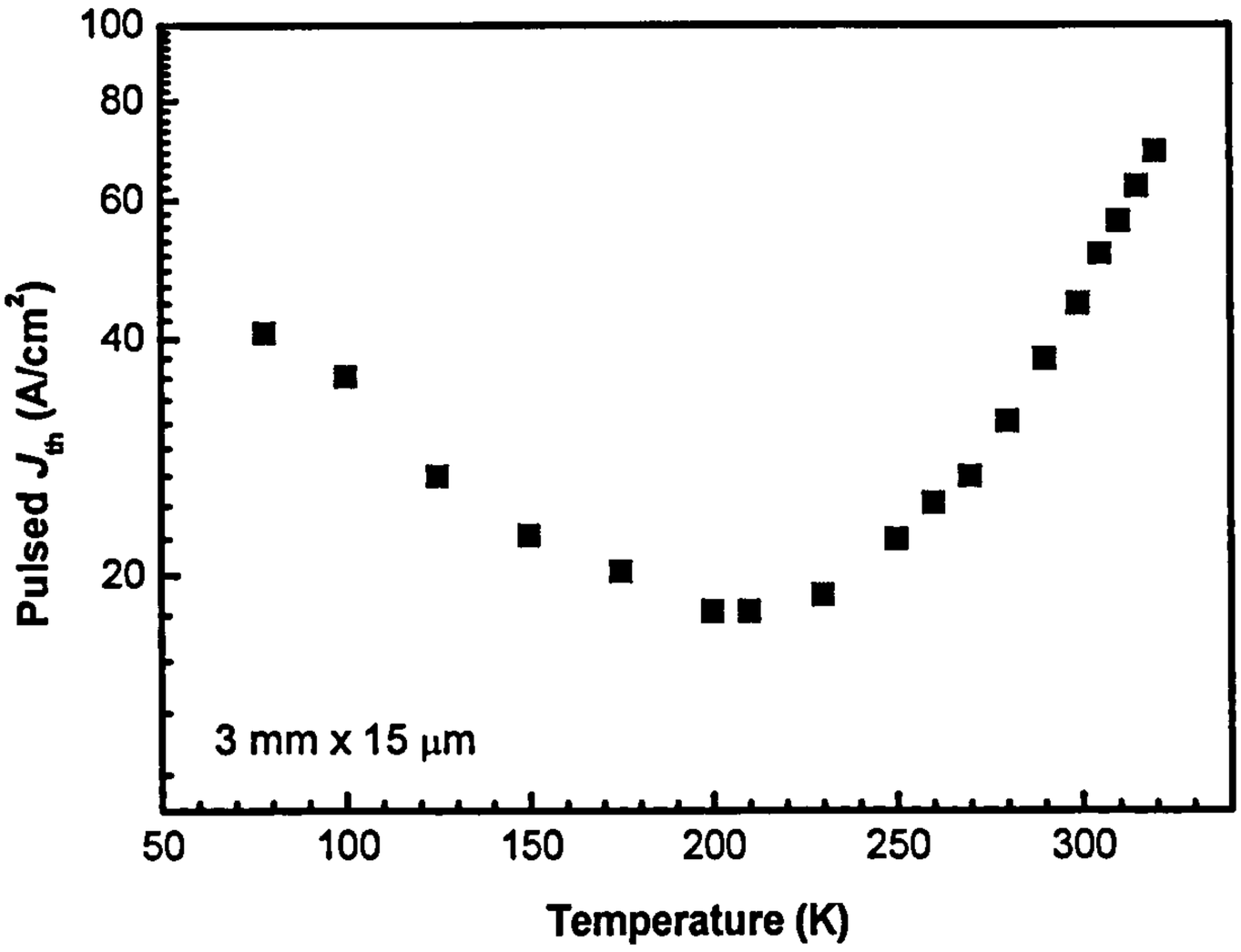

Fig. 1.2 J_{th} as a function of temperature under pulsed injection for a 3 mm cavity length of Vn 57 (see text). The J_{th} reduces with increasing temperature up to ~220 K. For higher temperatures, J_{th} increases monotonically.

The spectral form of the lasing emission is also determined by the carrier distribution within the inhomogeneously broadened QD states, ie. the temperature. At low temperatures, when carrier transfer between QDs is effectively suppressed, the lasing emission consists of a broad, multimode lasing spectrum[39]. On increasing the injection further above J_{th} additional lasing modes appear[40]. This behaviour results because there is no global clamping of the carrier density and QDs that initially are not lasing at threshold are able to continue to increase their carrier density until they reach lasing. At higher temperatures this process is suppressed once a thermal distribution within the ensemble is achieved.

Above 200 K, J_{th} is typically observed to increase slowly with temperature until an 'onset' temperature is reached, between 250 and 300 K, above which J_{th} increases relatively rapidly. In general, the temperature at which this onset occurs decreases with increasing threshold gain (increasing cavity loss)[41]. It has therefore been suggested that the degradation of J_{th} at high temperature originates mostly from the thermal population of the excited states, since the Fermi level increases with increasing threshold gain.

The threshold gain (g_{th}) of a semiconductor laser is given by

$$g_{th} = \frac{1}{\Gamma}\left[\alpha_i + \frac{1}{L}\ln\left(\frac{1}{R}\right)\right]$$

where Γ is the optical confinement factor, which represents the fractional overlap between the optical mode and the gain material; α_i is the internal loss of the structure due to photon scattering within the cavity and any absorption that does not return electrons and holes to the lasing transition; L is the cavity length and R is the reflectivity of the facets. In spite of the higher material gain potentially achievable in QD lasers, in general they have a much lower modal gain ($g_{mod} = \Gamma g_{mat}$) than QW lasers. This is due to the finite density of a QD array with only a low areal occupancy, typically ~5%, compared to the 'full' areal coverage provided by a QW. The modal gain may be increased by either adding more QD layers to the active region or increasing the in-plane QD density although there are limits to the increase achievable by both methods.

1.5 Motivation for the development of long wavelength GaAs-based lasers

An all optical method for data transmission offers several advantages over the high frequency co-axial cables conventionally used for these purposes. Because light has a much higher frequency than signals transmitted via co-axial cables, considerably higher modulation rates are possible. In addition signals transmitted as a series of light pulses are less sensitive to interference than are electrical signals. The attenuation spectrum of silica based optical fibres is determined by the absorption and scattering of the confined laser light within the material. Fig. 1.3 shows the attenuation curve for a typical silica fibre. A suitably matched telecoms laser should be designed to emit in one of the transparency windows centred at 1.3 or 1.55 μm. From Fig. 1.3 it can be seen that the minimum attenuation occurs at 1550 nm, which is the wavelength of choice for emitters used in long haul telecommunication applications. At 1310 nm, the attenuation is slightly stronger, but at this wavelength the dispersion for the propagating light pulses is a minimum, making it an ideal choice for high bit-rate data transmission over distances < 10 km.

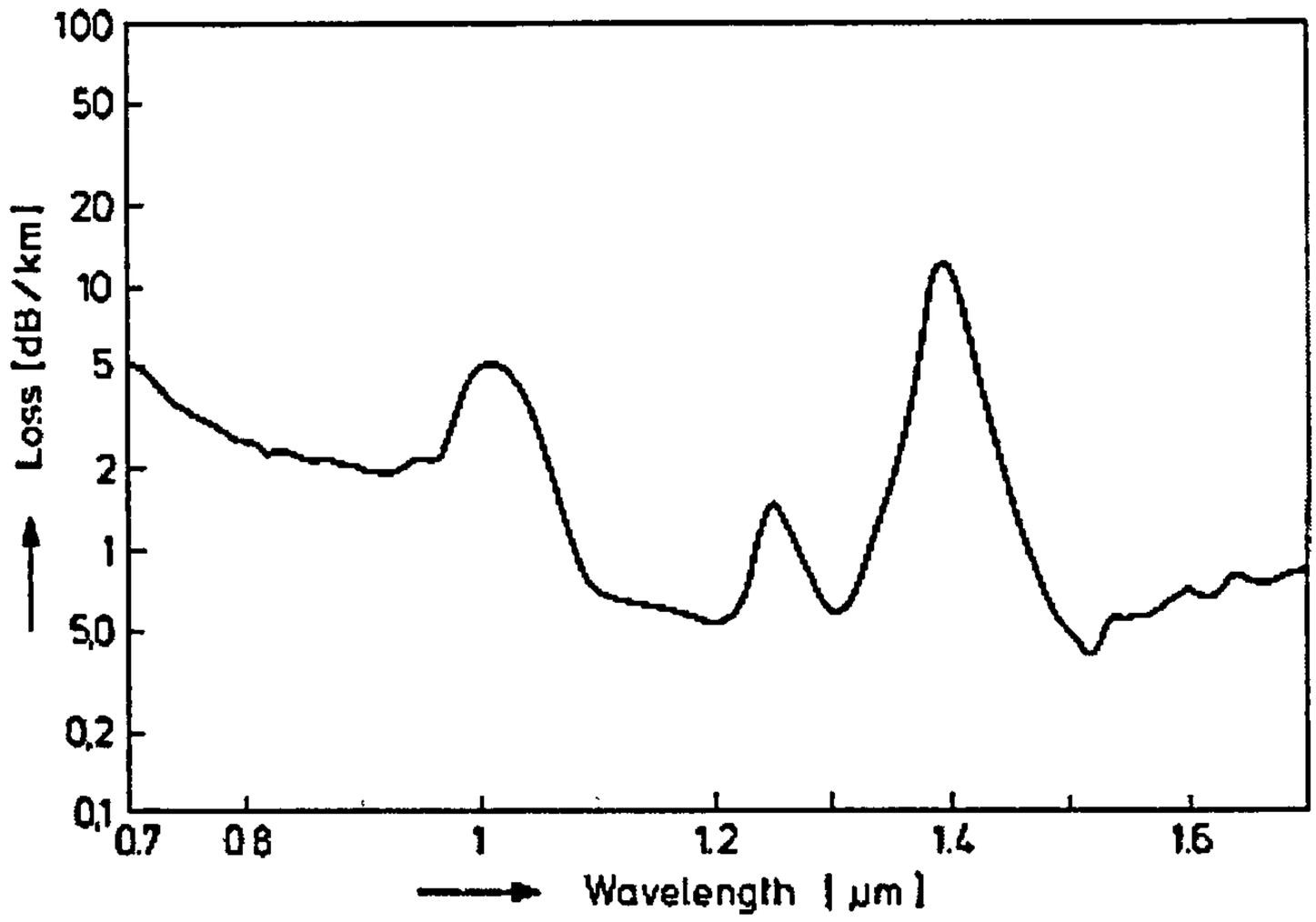

Fig. 1.3 Attenuation spectrum of a silica fibre as used in optical networks. Laser devices are targeted to operate in the transparency windows, centred at 1.3 or 1.55 µm.

Historically, InGaAsP QWs grown on InP substrates were used to achieve 1.3 µm emission[42]. However, these structures suffer from a low refractive index contrast ($\Delta n_i \sim 0.3$), poor thermal conductivity and small band offsets, all factors that serve to degrade the high temperature performance of fabricated devices[43]. In contrast, the wide bandgap AlGaAs cladding layers grown on GaAs substrates are able to combine good electrical and optical confinement in a material system which is closely lattice matched over a wide composition range. These benefits, coupled with inexpensive large area GaAs substrates, have allowed GaAs/AlGaAs hetero-structures to become the industry standard for 850 nm emitters.

In order for GaAs-based systems to reach 1.3 µm, various approaches are being actively pursued. Active regions comprising pseudomorphically strained InGaAs QWs are able to emit up to ~1.2 µm before the build up of strain results in the onset of misfit dislocation formation. GaAsSb QW devices have demonstrated 1.3 µm lasing at RT[44] with, however, poor temperature stability of J_{th} at RT[45]. Incorporating a very small amount (<1%) of nitrogen into either GaAs or (In)GaAs QWs, results in a large reduction of the bandgap, such that emission up to and beyond 1.3 µm may be achieved. However, reproducible growth of these structures is hampered by the poor miscibility of In and N, resulting in compositional inhomogeneities within the QW that lead to large fluctuations of the emission

wavelength. Nonetheless, these so-called 'dilute nitride' materials have the potential to reach 1.55 μm[46].

1.6 Long wavelength (>1.3 μm) InAs Quantum Dots

In comparison to all of the possibilities described above, the most promising means of obtaining optically efficient 1.3 μm emission at RT is by using self-assembled QDs. Using 'standard' growth conditions for the S-K formation of InAs QDs on GaAs, the room temperature (RT) emission wavelength may be extended out to ~1.24 μm for an InAs coverage of 4 monolayers (MLs)[47]. This limitation has driven crystal growers to pursue innovative growth methods in order to tailor the QD's size, strain and confinement environment to further redshift the emission.

The first report of RT 1.3 μm emission from an ensemble of In(Ga)As QDs was achieved using atomic layer epitaxy (ALE), a technique in which the In and Ga are deposited alternately under As_2 flux[48]. This method has been successfully employed in both MBE and MOCVD and results in large (10 nm high x 30 nm wide) lens shaped QDs. The first 1.3 μm QD laser to demonstrate GS lasing at RT, with a J_{th} of 405 A/cm^2, was grown using this technique[49]. However, ALE grown QDs are typically characterised by a low surface density (~10^{10} cm^{-2}) resulting from the large ad-atom migration distance[50]. Since the QD density is a critical determinant of the optical gain available in a laser structure, longer cavity lengths or high reflectivity mirror coatings are typically required for ALE-grown devices to operate at temperatures at and above RT.

An alternative method of increasing the PL peak wavelength and improving the homogeneity of the QD ensemble is to reduce the growth rate. Initial work demonstrated that when grown at relatively low temperatures (T_G ~ 490 °C) the composition of the QDs changes with growth rate, with lower growth rate (~0.0065 ML/s) QDs having higher In contents and hence longer emission wavelengths[51]. Furthermore, the slower surface diffusion allows the attainment of an equilibrium island shape prior to the capping with GaAs. Therefore the majority of the QDs are un-dislocated, when as much as 5 ML of InAs has been deposited[52]. However, as in ALE, the strain-driven surface kinetics of the In ad-atoms, resulting from the low growth rate, produces a low QD density (~10^{10} cm^{-2}).

A third alternative for obtaining 1.3 μm emitting QDs was realised by several research groups almost simultaneously. It was found that by 'capping' the QDs with a thin (few nm) layer of $In_xGa_{1-x}As$ before further overgrowth with GaAs, the emission wavelength of the QD could be extended towards 1.3 μm. In early studies of QD structures capped with a constant thickness of $In_xGa_{1-x}As$, it was found that the PL peak wavelength increased with increasing x, reaching 1.3 μm at x=0.4[53]. A reduction in the QD strain[54], QD size/height[55] enlargement, and increased In incorporation into the QDs[56] have all been suggested as mechanisms that may be responsible for this redshift of the emission. It is unlikely that the lower bandgap of the barrier material (InGaAs) has a dominant role in lowering the confinement energy of the QD GS as PL redshifts have also been reported for InAlAs capped QDs[57, 58]. This assertion is also supported by the PL excitation studies presented in chapter 3, section 3.2.

When the QDs are both grown on and overgrown with InGaAs the term dot-in-a-well (DWELL) is often used to describe the structure. In 1999, a QD laser demonstrated a lower J_{th} than that of a QW laser for the first time. The structure used consisted of a single layer DWELL with a 7.8 mm as-cleaved cavity that lased from the GS with a J_{th} of 26 A/cm^2 at 1.26 μm[59]. The DWELL design is now an established technique for obtaining high performance 1.3 μm emitting devices and is the structure used for the majority of laser devices studied in this thesis.

1.7 Overview of experimental thesis chapters

1.7.1 Chapter 3: 1.3 μm emitting InAs quantum-dot-in-a-well laser structures containing high growth temperature GaAs spacer layers

In this chapter the effect of the In composition (x) in the $In_xGa_{1-x}As$ DWELL on the QD emission properties is studied using photoluminescence (PL) and PL excitation (PLE) spectroscopy. An x value of 0.15 is found to be optimum for optically efficient RT 1.3 μm emission. Building on this result, multilayered $In_{0.15}Ga_{0.85}As$ DWELL laser structures were fabricated and investigated. The lasing performance of initially grown structures, containing GaAs spacer layers (SL) grown

at low temperature (510°C), is found to be very poor. Structural studies reveal that dislocated QD growth, originating in the second QD layer, is induced by an incomplete planarisation of the GaAs SL, a result of insufficient Ga ad-atom mobility at the growth temperature used.

However, by increasing the SL growth temperature to 585 °C after the initial 15 nm of GaAs growth, high quality multi-layer growth was achieved with dislocation densities estimated to be reduced by over a factor of 1000. SLs grown using this two-temperature technique are referred to as High Growth Temperature Spacer Layers (HGTSLs). The resultant improvement in material quality enabled a 5-layer structure to exhibit GS lasing from a 1.5 mm cavity and a 5 mm cavity device to operate from the ground state at 85 °C. A 3-layer device, containing 70 nm HGTSLs and high reflectivity coated facets, demonstrated one of the lowest ever reported J_{th} (19 A/cm^2) at room temperature. Despite the excellent material quality of the structures, the form of the low injection EL indicates the presence of a bimodal QD size distribution. Temperature dependent studies of the EL and J_{th} demonstrate the influence of carrier redistribution within the QD ensemble in determining the performance of the laser devices.

1.7.2 Chapter 4: Multilayer DWELL QD laser structures incorporating modified GaAs High Growth Temperature Spacer Layers (HGTSLs) and modified InGaAs capping layers

Due to the success of the HGTSL technique in improving the performance of multilayer DWELL laser structures, a new set of structures was grown that included 7 and 10-layer devices. The design of the active region was otherwise identical to that of the initial series, but the GaAs/AlGaAs waveguide thickness was reduced in an attempt to increase the optical confinement factor. However, decreasing the waveguide thickness is found to have little impact on device performance. None of the structures in this series demonstrated an improved performance with respect to the best structure of the previous series (Vn 61, 5-QD layers). The lowest cw J_{th} and maximum GS operating temperature were obtained from the 7-layer structure (70 A/cm^2 and 90 °C, respectively). Photocurrent spectroscopy indicates that each structure possesses a similar absorption strength *per QD layer* and therefore that a

reasonable level of repeatability had been achieved when multiple layers of QDs are grown up to a total of 10 layers. In addition EL measurements suggest that the optical efficiency per QD layer is maintained in structures with a high number of layers indicating that there is no increase in defect density as the layer number increases.

Having confirmed that the repeated stacking of the QD planes offers a limited improvement in performance, the HGTSL technique was re-optimised: the GaAs SL thickness was reduced to 35 nm and the growth temperature of the final 20 nm was increased to 620 °C. A 5-layer structure with a 1 mm cavity was able to operate cw from the GS at temperatures up to 60 °C. The mechanism for the improved performance was thought to be the same as that found in the initial development of the HGTSL step, ie. a smoothing of the QD nucleation surface. For this reduced SL thickness the initial HGTSL technique results in poor device performance.

A structure with an InGaAs capping layer having a graded In composition was studied. This design was intended to provide a smaller lattice mismatch between the QDs and capping matrix and hence reduce the QD strain. The EL is seen to be strongly bimodal, suggesting that the growth kinetics during capping had been altered. In spite of this, an unusually temperature stable lasing wavelength is achieved, attributed to the flat gain profile resulting from the broad QD size distribution.

The final part of this chapter focuses on the effect of post-growth annealing on the optical properties of DWELL laser structures. On the basis of these studies, the bimodal emission characteristic of all the laser structures studied in this thesis is attributed to the effect of *in-situ* annealing which occurs during the growth of the thick AlGaAs top cladding layer.

1.7.3 Chapter 5: Optical properties of *p*-type modulation doped Quantum Dot laser structures

Previous chapters have demonstrated that whilst the HGTSL technique can result in laser devices exhibiting very low threshold current densities at room temperature their temperature stability remains poor and at best only comparable to quantum well lasers. In an attempt to achieve better temperature stability p-type modulation doping, as initially studied by the Deppe group[60], was applied to the

lasers. Using this approach a 5-layer QD laser doped with 15 acceptors per QD exhibited a negative characteristic temperature between -50 and 45°C and a threshold current density below 50A/cm^2 at RT. The reason for this improved performance appears to be related to a delayed thermal redistribution of electrons within the QD ensemble due to an increased confinement potential provided by the extrinsic holes in the QDs. The contribution from a photon coupling model is also considered. A range of optical techniques applied to both undoped and doped QDs indicates a number of significant differences, including relative populations of the different QD states and the expected state blocking of absorption in the doped structures.

Time resolved PL studies of the low temperature carrier decay time as a function of p-type doping level reveals a lifetime that decreases with increasing doping. In addition, the PL efficiency decreases with increasing doping. This behaviour is attributed to a non-radiative Auger process which is enhanced by the extrinsic holes. However the dependency on hole density is weaker than in higher dimensionality systems, a result of the discrete QD energy states and strong transition selection rules.

1.7.4 Chapter 6: InAs QD structures with a thin antimony containing capping layer

In this chapter, the effects of a $GaAs_{1-x}Sb_x$ ($0.14<x<0.26$) capping matrix on the optical properties of InAs QDs are investigated. Initial attempts to form long wavelength (>1.3 μm) emitting InAs(Sb) QDs were not successful. The low temperature emission is blueshifted and becomes weaker with respect to a conventional InGaAs DWELL structure, which is attributed to the surfactant property of Sb. However, when the QDs are capped with a layer of $GaAs_{0.86}Sb_{0.14}$, 1.3 μm emission at RT is obtained with a narrow (20 meV) linewidth. For higher Sb contents ($x>0.14$), the emission redshifts strongly with increasing Sb composition and exhibits a pronounced blueshift with increasing laser excitation. This demonstrates the onset of a type-II transition occurring between electrons confined in the QDs and holes in the surrounding $GaAs_{1-x}Sb_x$ layer.

From a consideration of both the spatial modulation in the strain state of the $GaAs_{1-x}Sb_x$ capping layer and the spectral form of the blueshift, it is postulated that the hole wavefunction is located in a region of the $GaAs_{1-x}Sb_x$ layer directly above

the QD. PLE studies highlight differences in the carrier relaxation mechanisms and oscillator strengths between the type-I and type-II systems. The marked reduction in the oscillator strength of the type-II transition was confirmed by a long (~70 ns) radiative lifetime of the GS exciton in a structure with a $GaAs_{0.78}Sb_{0.22}$ capping layer, measured using time resolved PL. Despite the type-II nature of the transition for samples with x>0.14, magneto-PL studies revealed that the spatial extent of the GS exciton is not significantly extended compared with a type-I system.

The lasing performance of a structure with $GaAs_{0.86}Sb_{0.14}$ capped QDs was found to be equivalent to that of a device with an $In_{0.15}Ga_{0.85}As$ SRL. Type-II structures with $0.22 < x < 0.26$, engineered to emit at ~1.55 μm, failed to lase at RT, but exhibited novel emission and absorption properties. It remains unclear if this lack of lasing is a result of a low oscillator strength (intrinsic) or defects associated with the high Sb content (extrinsic).

References

1. Agrawal, G. P. *Semiconductor lasers : past, present, and future* Woodbury, N.Y. : American Institute of Physics, 1995.

2. Asada, M.; Miyamoto, Y.; Suematsu, Y. IEEE J. Quantum Electron. **22,** (9) 1915 (1986)

3. R. Dingle and C. H. Henry "Quantum Effects in Heterostructure Lasers" US Patent 3982207 (1976)

4. Y. Arakawa and H. Sakaki, Appl. Phys. Lett. **40,** 939 (1982)

5. P. G. Piva, R. D. Goldberg, I. V. Mitchell, D. Labrie, R. Leon, S. Charbonneau, Z. R. Wasilewski, and S. Fafard, Appl. Phys. Lett. **77,** 624 (2000)

6. R. Leon, G. M. Swift, B. Magness, W. A. Taylor, Y. S. Tang and K. L. Wang, Appl. Phys. Lett. **76,** 2074 (2000)

7. R. L. Sellin, Ch. Ribbat, M. Grundmann, N. N. Ledentsov, and D. Bimberg, Appl. Phys. Lett. **78,** 1207 (2001)

8. E. C. Le Ru, P. D. Siverns, and R. Murray, Appl. Phys. Lett. **77,** 2446 (2000)

9. H. Benisty, C. M. Sotomayor-Torrès, and C. Weisbuch, Phys. Rev. B **44,** 10945 (1991)

10. Kohki Mukai, Nobuyuki Ohtsuka, Hajime Shoji, and Mitsuru Sugawara, Phys. Rev. B **54,** R5243 (1996)

11. R. Heitz, H. Born, F. Guffarth, O. Stier, A. Schliwa, A. Hoffmann, and D. Bimberg, Phys. Rev. B **64,** 241305 (2001)

12. D Morris, N Perret, S Fafard, Appl. Phys. Lett. **75,** 3593 (1999)

13. P. Miska, J. Even, O. Dehaese, and X. Mariem, Appl. Phys. Lett. 92, 191103 (2008)

14. D. Leonard, K. Pond, and P. M. Petroff, Phys. Rev. B **50**, 11687 (1994)

15. A. S. Bhatti, M. Grassi Alessi, M. Capizzi, P. Frigeri, and S. Franchi, Phys. Rev. B **60**, 2592 (1999)

16. M. Hugues, M. Teisseire, J.-M. Chauveau, B. Vinter, B. Damilano, J.-Y. Duboz, and J. Massies, Phys. Rev. B **76**, 075335 (2007)

17. Egorov A Yu, Zhukov A E, Kop'ev P S, Ledentsov N N, Maximov M V and Ustinov V M, Semiconductors **28**, 809 (1994)

18. A.G. Cullis, D.J. Norris, T. Walther, M.A. Migliorato, and M. Hopkinson, Phys. Rev. B **66**, 081305 (2002)

19. P. B. Joyce, T. J. Krzyzewski, G. R. Bell, B. A. Joyce, and T. S. Jones, Phys. Rev. B **58**, R15981 (1998)

20. L. Goldstein, F. Glas, J. Y. Marzin, M. N. Charasse, and G. Le Roux, Appl. Phys. Lett. **47**, 1099 (1985)

21. D. Leonard, M. Krishnamurthy, C. M. Reaves, S. P. Denbaars, and P. M. Petroff, Appl. Phys. Lett. **63**, 3203 (1993)

22. A. E. Zhukov, A. Yu. Egorov, A. R. Kovsh, V. M. Ustinov, N. N. Ledentsov, M. V. Maksimov, A. F. Tsatsul'nikov, S. V. Zaitsev, N. Yu. Gordeev, P. S. Kop'ev, Zh. I. Alferov and D. Bimberg, Semiconductors **31**, 411 (1997)

23. N. Carlsson, W. Seifert, A. Petersson, P. Castrillo, M. E. Pistol, and L. Samuelson, Appl. Phys. Lett. **65**, 3093 (1994)

24. C. Y. Ngo, S. F. Yoon, W. J. Fan and S. J. Chua, Phys. Rev. B **74**, 245331 (2006)

25. Jeongnim Kim, Lin-Wang Wang and Alex Zunger, Phys. Rev. B **57**, R9408 (1998)

26. M. A. Migliorato, A. G. Cullis, M. Fearn, and J. H. Jefferson, Phys. Rev. B **65**, 115316 (2002)

27. Asryan, L.V., Grundmann, M., Ledentsov, N.N., Stier, O., Suris, R.A., Bimberg, D., IEEE J. Quantum Electron. **37**, (3) 418 (2001)

28. Lin-Wang Wang, Jeongnim Kim and Alex Zunger, Phys. Rev. B **59**, 5678 (1999)

29. G. Park, O. B. Shchekin, D. L. Huffaker, and D. G. Deppe, Appl. Phys. Lett. **73**, 3351 (1998)

30. I. R. Sellers, D. J. Mowbray, T. J. Badcock, J.-P. R. Wells, P. J. Phillips, D. A. Carder, H. Y. Liu, K. M. Groom, and M. Hopkinson, Appl. Phys. Lett. **88**, 081108 (2006)

31. P W Fry PhD Thesis.

32. Oleg B. Shchekin, Gyoungwon Park, Diana L. Huffaker, and Dennis G. Deppe, Appl. Phys. Lett. **77**, 466 (2000)

33. Z. Y. Zhang, B. Xu, P. Jin, X. Q. Meng, Ch. M. Li, X. L. Ye, and Z. G. Wang, J. Appl. Phys. **92**, 511 (2002)

34. A. Tackeuchi, R. Ohtsubo, K. Yamaguchi, M. Murayama, T. Kitamura, T. Kuroda, and T. Takagahara, Appl. Phys. Lett. **84**, 3576 (2004)

35. Zetian Mi and Pallab Bhattacharya, J. Appl. Phys. **98**, 023510 (2005)

36. Deppe, D.G., Huffaker, D.L., Zou, Z., Park, G., Shchekin, O.B., IEEE J. Quantum Electron. **35**, (8) 1238 (1999)

37. Nikolai N. Ledentsov, Dieter Bimberg, Victor M. Ustinov, Zhores I. Alferov and James A. Lott, Jpn. J. Appl. Phys. **39**, 3907 (2000)

38. I. Alghoraibi, T. Rohel, R. Piron, N. Bertru, C. Paranthoen, G. Elias, A. Nakkar, H. Folliot, A. Le Corre, and S. Loualiche, Appl. Phys. Lett. **91**, 261105 (2007)

39. H. Jiang and J. Singh, J. Appl. Phys. **85**, 7438 (1999)

40. L. Harris, D. J. Mowbray, M. S. Skolnick, M. Hopkinson, and G. Hill, Appl. Phys. Lett. **73**, 969 (1998)

41. A. E. Zhukov, A. R. Kovsh, N. A. Maleev, S. S. Mikhrin, V. M. Ustinov, A. F. Tsatsul'nikov, M. V. Maximov, B. V. Volovik, D. A. Bedarev, Yu. M. Shernyakov, P. S. Kop'ev, Zh. I. Alferov, N. N. Ledentsov and D. Bimberg, Appl. Phys. Lett. **75**, 1926 (1999)

42. K. Nakahara, K. Uomi, T. Haga, T. Taniwatari, and A. Oishi, IEEE Photon. Tech. Lett. **8**, (10) 1297 (1996)

43. Akira Sugimura, Appl. Phys. Lett. **42**, 17 (1983)

44. M. Yamada, T. Anan, K. Toukutome, A. Kamei, K. Nishi, and S. Sugou, IEEE Photon. Tech. Lett. **12**, (7) 774 (2000)

45. K. Hild, S. J. Sweeney, S. Wright, D. A. Lock, S. R. Jin, I. P. Marko, S. R. Johnson, S. A. Chaparro, S.-Q. Yu, and Y.-H. Zhang Appl. Phys. Lett. **89**, 173509 (2006)

46. H. Y. Liu, M. Hopkinson, P. Navaretti, M. Gutierrez, J. S. Ng, and J. P. R. David, Appl. Phys. Lett. **83**, 4951 (2003)

47. Egorov A Yu, Zhukov A E, Kop'ev P S, Ledentsov N N, Maximov M V and Ustinov V M, Semiconductors **28** 809 (1994)

48. Kohki Mukai, Nobuyuki Ohtsuka, Mitsuru Sugawara and Susumu Yamazaki, Jpn. J. Appl. Phys. **33**, (12A) L1710 (1994)

49. D. L. Huffaker, G. Park, Z. Zou, O. B. Shchekin, and D. G. Deppe, Appl. Phys. Lett. **73**, 2564 (1998)

50. D. L. Huffaker and D. G. Deppe, Appl. Phys. Lett. **73**, 520 (1998)

51. P. B. Joyce, T. J. Krzyzewski, G. R. Bell, T. S. Jones, S. Malik, D. Childs, and R. Murray, Phys. Rev. B **62**, 10891 (2000)

52. P. B. Joyce, T. J. Krzyzewski, G. R. Bell, T. S. Jones, E. C. Le Ru, and R. Murray Phys. Rev. B **64**, 235317 (2001)

53. V. M. Ustinov, N. A. Maleev, A. E. Zhukov, A. R. Kovsh, A. Yu. Egorov, A. V. Lunev, B. V. Volovik, I. L. Krestnikov, Yu. G. Musikhin, N. A. Bert, P. S. Kop'ev, Zh. I. Alferov, N. N. Ledentsov and D. Bimberg, Appl. Phys. Lett. **74**, 2815 (1999)

54. N.-T. Yeh, T.-E. Nee, J.-I. Chyi, T. M. Hsu and C. C. Huang, Appl. Phys. Lett. **76**, 1567 (2000)

55. Y. Q. Wei, S. M. Wang, F. Ferdos, J. Vukusic, A. Larsson, Q. X. Zhao, M. Sadeghi, Appl. Phys. Lett. **81**, 1621 (2002)

56. M. Arzberger, U. Käsberger, G. Böhm, and G. Abstreiter, Appl. Phys. Lett. **75**, 3968 (1999)

57. Kenichi Nishi, Hideaki Saito, Shigeo and Sugou, Jeong-Sik Lee, Appl. Phys. Lett. **74**, 1111 (1999)

58. B. V. Volovik, A. F. Tsatsul'nikov, D. A. Bedarev, A. Yu. Egorov, A. E. Zhukov, A. R. Kovsh, N. N. Ledentsov, M. V. Maksimov, N. A. Maleev, Yu. G. Musikhin, A. A. Suvorova, V. M. Ustinov, P. S. Kop'ev, Zh. I. Alferov, and D. Bimberg, Semiconductors 33, 901 (1999).

59. Lester, L.F.; Stintz, A.; Li, H.; Newell, T.C.; Pease, E.A.; Fuchs, B.A.; Malloy, K.J. Lester, IEEE Photon. Tech. Lett. **11**, (9) 931 (1999)

60. O. B. Shchekin and D. G. Deppe, Appl. Phys. Lett. **80**, 2758 (2002)

Chapter 2

Sample preparation and experimental methods

In this chapter the techniques used to fabricate the devices following wafer growth and the experimental techniques used to probe their various properties are briefly described.

2.1 Device fabrication

In this section, brief descriptions of the fabrication steps will be given that are required to produce electrically contacted devices from the MBE grown wafers containing doped AlGaAs cladding layers. Both mesa light emitting diode (LED) structures and ridge waveguide lasers were typically produced from such wafers using well established techniques such as optical lithography, wet chemical etching and metallisation.

2.1.1 Mesa diode processing

Cylindrical mesa LED structures were processed for use in spontaneous emission studies and photocurrent measurements. Prior to the initial photolithography step, the wafers are cleaved to ~1x1 cm^2 pieces and thoroughly cleaned using hot n-butyl acetate, acetone and isopropyl alcohol. The mask set used for the optical lithography contained apertures that produce either circular or square mesa devices, with diameters/side lengths of either 200 or 400 μm. Initially the metallisation of the n-type back contact was performed by evaporating ~200 nm InGe-Au onto the n^+ GaAs substrate. This was then alloyed for one minute at ~420 °C to ensure good ohmic contact with the substrate.

To allow optical access perpendicular to the growth plane, the top contact was applied to only a 5-10 μm wide circumference region around the edge of the device. This shape was defined by the first mask used in the photolithography. Following the evaporation of the back contact, the sample was re-cleaned and attached to a thin glass plate using hot wax, with the p-type surface facing upwards. The sample was then transferred to a room lit purely with yellow filtered light, where

the sample was baked on a hot-plate and spun with a ~1 μm covering of photoresist. The yellow light allowed the processing to be viewed but did not affect the photoresist which is only sensitive to UV light. The photoresist was baked again to evaporate solvent. The sample was then aligned to the mask defining the top contact and exposed to UV light for ~6 seconds, immersed in a developing solution for 1 minute and then rinsed immediately in de-ionised water and blow-dried before inspection under a microscope. Under these exposure and developing conditions, the features defined by the mask were found to be suitably sharp. If not however, acetone was used to remove the photoresist and the patterning process repeated.

The top p-type contact was then deposited on the patterned sample surface. As before, this was achieved by metallisation, in this case ~400 nm of Au-Zn-Au. The areas of photoresist covered with metal were then 'lifted off' by immersion in acetone prior to cleaning and alloying for 1 minute at 360 °C. Having deposited both *n*- and *p*-type contacts, the sample was re-patterned with the second mask that defined the circular or square mesa shape. This process requires that the new mask be aligned precisely with the existing contacts via the overlapping of 5 μm size alignment features present in both masks.

Following the exposure and development of the photoresist, the patterned sample was chemically etched using a mixture of Hydrobromic acid, Acetic acid and Potassium Dichromate solution in the ratio 1:1:1. This wet etch erodes only areas not covered with the photoresist ie. the regions of the sample in between the mesas. The etch is isotropic and the etch rate is ~4 μm/min. Typically, samples were etched to a depth of ~4 μm from the surface such that the active region is etched through and the etch terminates in the n^+ doped substrate. The profile of the etch and exact depth could be determined using a Talystep system. The photoresist covering the mesas was then finally removed and the sample re-cleaned.

The sample was next cleaved into pieces ~0.5 cm^2 using a diamond scriber in order for the individual pieces to be mounted using Au-epoxy on to a TO5 header package. The mesa contacts were then ultrasonically bonded to the pins of the TO5, using gold wire.

2.1.2 Laser processing

In many respects the processing of laser devices follows that of mesas, but is slightly more complicated. The same combination of metallisation materials was used to form the *n*- and *p*-type contacts and the exposure and developing conditions were identical to those employed in mesa fabrication. The top contacts form the 'ridge' of the laser and have widths ranging from 5 to 20 μm. Dry reactive ion etching was used to controllably etch material outside the area of the ridge. The initial structures studied were deep etched through the active region to a depth of ~3.2 μm. However, the good optical confinement provided by the *index guided* optical mode in such deep etched structures may be offset by the effect of increased non-radiative recombination at the sidewall surfaces as a result of the etching. It was thought that this may limit the device performance and the etching depth was consequently reduced to ~1.8 μm i.e. terminating before reaching the active region. A comparison of the results for deep and shallow etched devices is given in chapter 3, section 3.4.2.5.

One significant difference in the procedure for processing mesa and laser devices is the need for the deposition of a dielectric layer, in this case SiN_2, to electrically isolate the individual ridges. This also allows for enlarged Ti-Au bond pads to be used for contacting the ridges to the pins of the TO5.

In the next step the substrate was thinned to ~150 μm using a mechanical polishing unit in combination with Al_2O_3/H_2O paste that grinds the material away. Following a thorough clean, the back contact was formed by evaporation and alloying. The pieces of fully processed wafer were now ready to be cleaved into sections containing 5 or 6 devices and then cut into the desired cavity lengths with a diamond scribe, typically 0.5 – 5 mm. The laser 'chips' were then mounted and bonded on to the TO5 headers as described above.

2.2 Overview of the experimental setups

Figs. 2.1, 2.3, 2.5 and 2.7 outline the experimental setups used for photoluminescence (PL), electroluminescence (EL), photocurrent (PC) spectroscopy and photoluminescence excitation (PLE) measurements respectively. These techniques will be described individually in the following subsections, but before this is done some collective features of the instrumentation will be outlined.

In order to maximise the coupling efficiency, and hence throughput, of the light between each component in the setup (i.e. the lamp, the large and small monochromators and the cryostat) the focal length (f) of each lens was chosen according to the f- number of the relevant instrument. In practice this required lenses L_1, F_2 and C_1 to have $f \sim 5$ cm. Lenses L_2, M_1 and C_2 were chosen such that $15 < f < 30$ cm. All lenses had diameters of ~5 cm.

The long (0.75 m) single grating Czerny – Turner monochromator, labelled 'spex' in the figures, contained either a 1200 lines/mm grating (G), blazed at 1 μm or a 600 lines/mm grating, blazed at 1.3 μm depending on measurement and sample being studied. The 1200 lines/mm grating provides an instrumental resolution of 10 Å/mm which is doubled in the case of the 600 lines/mm grating. The 1.3 μm blazed grating was used in the work performed on the longer-wavelength Antimonide QD structures discussed in chapter 6. Permanently installed in the smaller equivalent of 'spex', labelled 'minimate' in the figures, was a 1 μm blaze grating with 600 lines/mm, providing a resolution of 40 Å/mm.

The 150 W lamp, used in the PLE and PC measurements, was mounted horizontally such that the longest dimension of the Tungsten filament was oriented parallel to the monochromator slits, thereby reducing the effect of vignetting (entendue).

A liquid nitrogen (LN_2) bath cryostat provided temperature control in the range 77 to 300 K, with a continuous flow He cryostat used for measurements at lower temperatures. Samples of epitaxial wafer were stuck to Cu sample sticks using vacuum grease.

In order to work at temperatures above RT, the devices were mounted on a copper stage containing a resistor. By passing a current through the resistor and using the resultant Joule heating to warm the copper block, stable temperatures of up to ~150 °C could be obtained within 5 mins of being set (assuming the use of suitable

feedback PID settings). This piece of instrumentation was designed by Dr A. Ramsey (Department of Physics and Astronomy, University of Sheffield) and was used for EL and LI measurements between RT and 140 °C.

2.2.1 Photoluminescence

PL spectroscopy is a well established technique used for the optical characterisation of semiconductor materials. In the case of bulk semiconductors, an excitation source, typically a laser or lamp generates electron-hole pairs at energies in excess of the bandgap (E_g) of the material being studied. The intra-band carrier relaxation processes, involving LO/LA phonon emission and carrier-carrier scattering occur on a timescale orders of magnitude shorter than the radiative recombination time. Therefore the carriers are able to relax to the bottom of their respective bands before recombining and emitting photons with energies close to E_g. This basic description of the PL mechanism is the same for all the InAs/GaAs QD structures studied in this thesis. The carriers are photo-generated in the GaAs matrix, using a variety of laser wavelengths (HeNe, Nd:YAG and Ar^+). They are then captured into the QD states on a sub-ns timescale and relax to the lowest lying (ground state) level before recombining. The choice of laser depends on the aim of the particular measurement. Temperature dependent PL measurements were typically carried out using a ~1 mW HeNe laser that resulted in occupation levels << 1 exciton/QD, effectively ruling out QD excited state emission from the spectra. Under these low excitation levels and at low temperature (~77K), when the states in the QD ensemble are electronically isolated, the spectral width of the emission provides information relating to the structural homogeneity of the QD ensemble. Excited state emission is a consequence of the limited degeneracy of the QD ground state and is observed when higher injection levels are used. Fig. 2.2 shows spectra acquired at 4K from an InAs DWELL structure under excitation from an Ar^+ laser operating at 514 nm, where neutral density filters have been used to attenuate the incident laser beam. Emission from the QD excited states at ~1125 and 1050 nm is clearly visible as the incident power is increased.

Fig. 2.1 shows a schematic diagram of the experimental setup typically used for temperature dependent PL using a 1 mW HeNe laser. The laser light from the

HeNe passes through a plasma line filter before being reflected and focussed to a spot of diameter <0.25 mm^2 on the sample surface. In order to minimise this spot size and reduce the amount of reflected laser light coupled into the spex, the normal to the sample surface was inclined at ~5° relative to the direction of the incident laser beam. PL was collected and collimated by C_1, then focussed into the spex by C_2 after being transmitted through a second long pass filter, placed before the slits.

Once dispersed by the spex, the PL is detected by a LN_2 cooled Ge photodiode and the signal voltage is recorded by a Keithley digital multimeter (DMM). A Labview program provided fully integrated control of the spex and DMM.

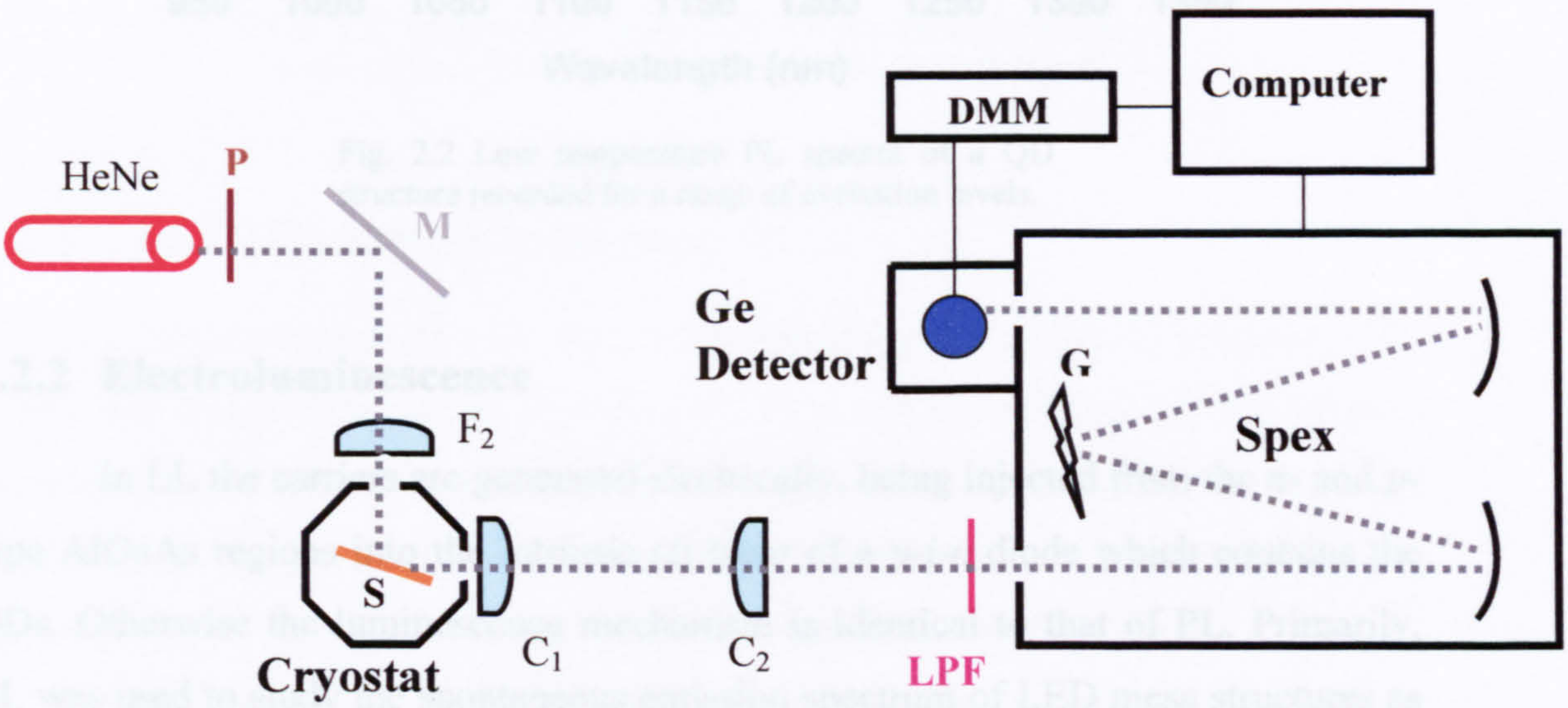

Fig. 2.1 Experimental setup used for photoluminescence measurements. The grey dotted line depicts the optical path.

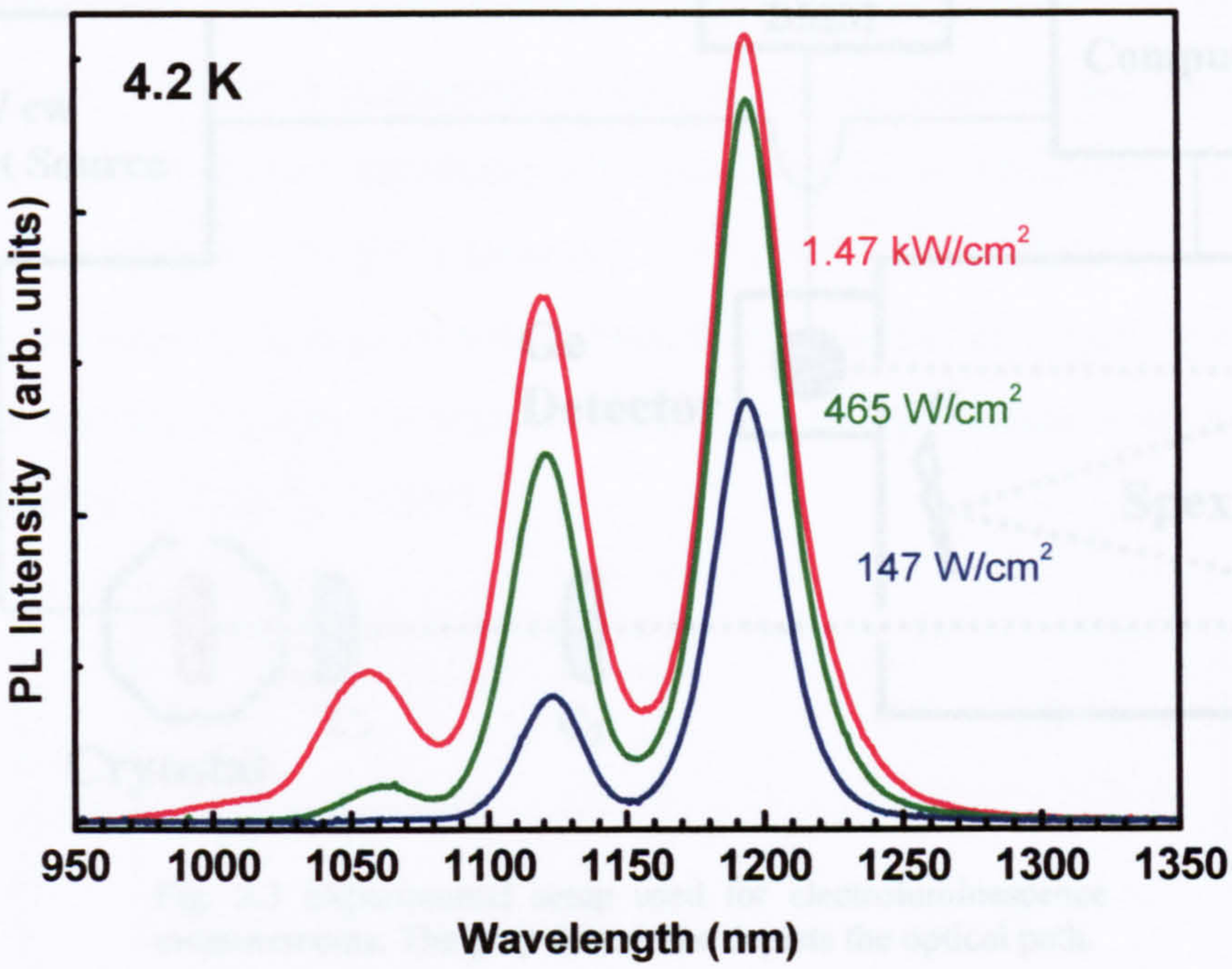

Fig. 2.2 Low temperature PL spectra of a QD structure recorded for a range of excitation levels.

2.2.2 Electroluminescence

In EL the carriers are generated electrically, being injected from the *n*- and *p*-type AlGaAs regions into the intrinsic (*i*) layer of a *p*-*i*-*n* diode which contains the QDs. Otherwise the luminescence mechanism is identical to that of PL. Primarily, EL was used to study the spontaneous emission spectrum of LED mesa structures as a function of either pulsed or cw injection current and/or temperature. The sample to be examined is mounted on a TO5 header package, which is electrically connected to a cw or pulsed current source via coaxial cables. Since the injection is supplied to a device of known area, EL measurements are preferential to PL when it is desirable to have a more exact knowledge of the QD state occupancy. Pulses 5 μs wide, driven at a duty cycle of 1% were used as standard for all measurements using pulsed injection. The pulsed and cw current sources, having maximum current outputs of 1 A and 200 mA respectively, were controlled remotely via Labview programs. Fig. 2.3 shows the experimental setup used for the EL measurements.

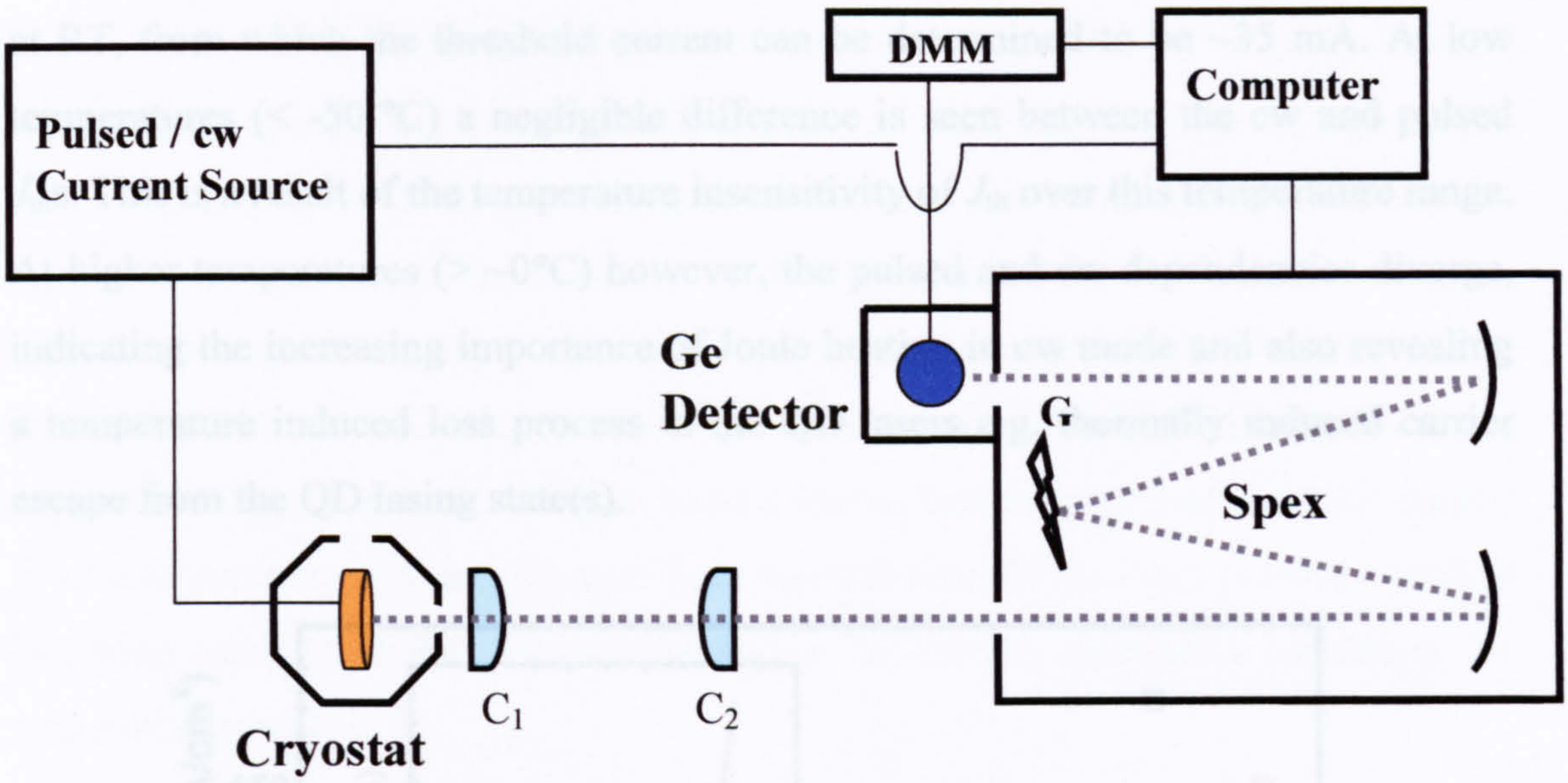

Fig. 2.3 Experimental setup used for electroluminescence measurements. The grey dotted line depicts the optical path.

2.2.3 Light – Current (LI) Measurements

LI measurements give the current dependence of the spectrally integrated EL. In practice this involves either replacing the spex and Ge detector with an InGaAs photodiode or setting the spex grating to 'zero' order and using the Ge detector. Typically, the former method was used for the characterisation of laser devices and the latter was employed in the study of spontaneous emission from mesas.

LI characterisation of laser structures yields important information, such as the threshold current density (J_{th}) required for lasing and the external differential efficiency of the cavity. The processed laser chips were aligned with a cleaved edge facing the InGaAs detector, which was connected to the Keithley DMM. Temperature dependent LIs were conducted in pulsed mode and the temperature variation of J_{th} was used to determine the characteristic temperature (T_0). Since T_0 is dependent on the temperature range over which it is measured, this range is given alongside all of the values listed in this thesis. cw mode operation produces significant Joule heating in the active region of the device. This results in a higher lattice temperature than that indicated by the temperature controller of the cryostat. Fig. 2.4 shows the results of a temperature dependent LI characterisation. The main part of the figure shows the temperature dependence of the threshold current density (J_{th}) under pulsed and cw current injection. The inset shows a cw LI curve, obtained

at RT, from which the threshold current can be determined to be ~35 mA. At low temperatures (< -50 °C) a negligible difference is seen between the cw and pulsed J_{th}s. This is a result of the temperature insensitivity of J_{th} over this temperature range. At higher temperatures (> ~0°C) however, the pulsed and cw dependencies diverge, indicating the increasing importance of Joule heating in cw mode and also revealing a temperature induced loss process in the QD lasers e.g. thermally induced carrier escape from the QD lasing state(s).

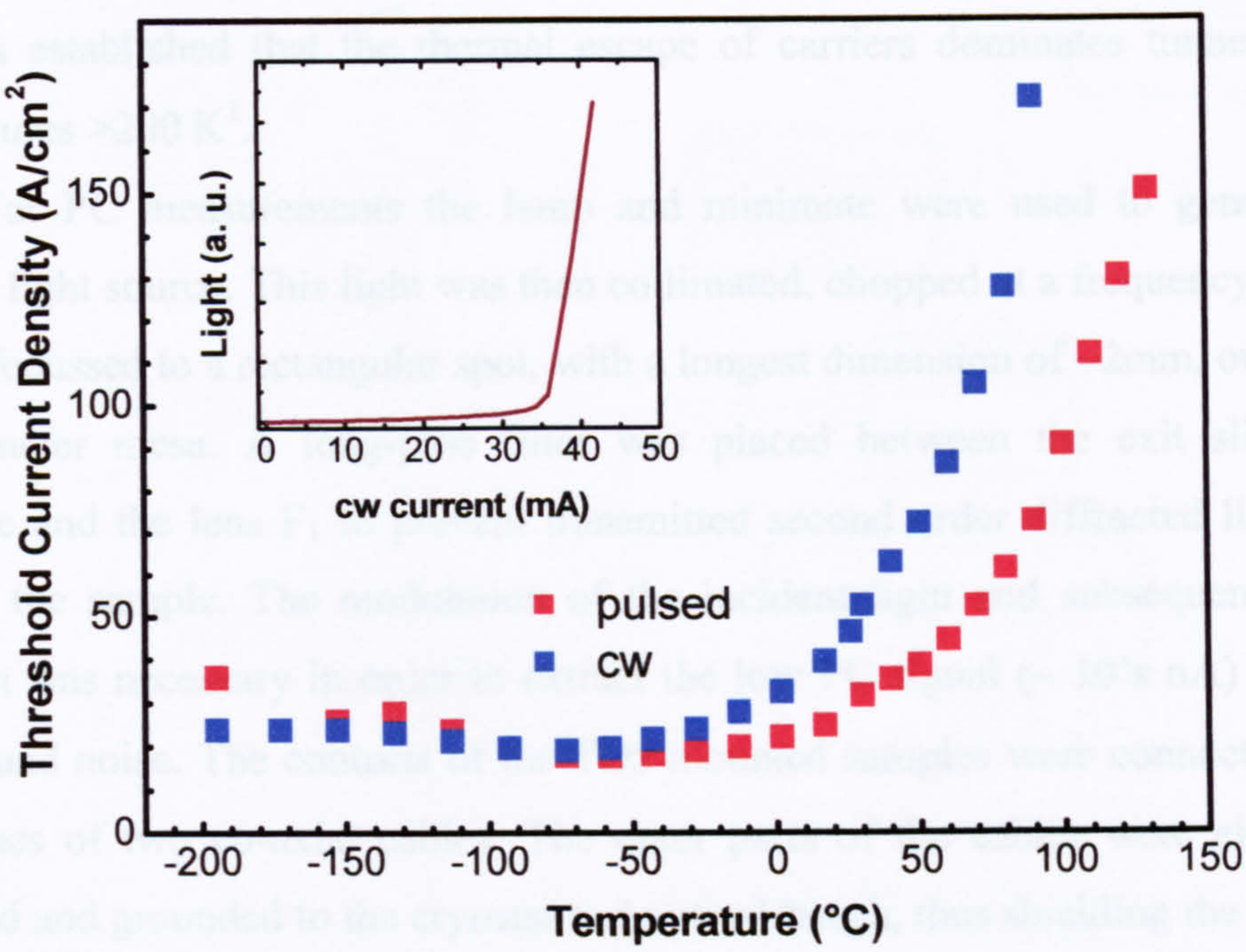

Fig. 2.4 Main part: plot of the temperature dependence of J_{th} between -200 and 150°C for a QD laser structure in pulsed and cw mode. Inset shows an L-I taken with cw current.

2.2.4 Normal incidence photocurrent spectroscopy

A photocurrent measurement is, in some respects, the inverse of EL. Incident light is absorbed in the *i* region of the structure, creating an electron-hole pair which may then escape to the *p* and *n* type contacts respectively. The magnitude of the photocurrent (PC) at a particular photon energy $h\nu$ is determined by a number of factors, including the applied electric field (E) across the *i* region, which controls carrier escape by tunneling, the lattice temperature, which controls carrier escape by thermal excitation, the joint density of states of the transition at the corresponding energy, which controls the absorption strength, and the radiative recombination time

(τ_{rad}) which provides a competing process to carrier escape. PC will only be detected if the carrier escape rate > carrier recombination rate ($=\tau_{rad}^{-1}$). At low temperatures and under zero bias (E=0), the measured PC is very low when the carrier pairs are created in the QD states. This results from their low tunnelling and thermal activation rates in this regime. By applying reverse biases of up to a few 100 kV/cm, the carrier tunnelling time may be reduced below the recombination rate and an increase in the measured PC is observed. At higher temperatures, thermally activated carrier escape is able to compete with any electric field induced tunnelling. From previous work it has been established that the thermal escape of carriers dominates tunnelling for temperatures >200 K[1].

For PC measurements the lamp and minimate were used to generate the tuneable light source. This light was then collimated, chopped at a frequency of ~160 Hz and focussed to a rectangular spot, with a longest dimension of ~2mm, onto a 400 μm diameter mesa. A long-pass filter was placed between the exit slit of the minimate and the lens F_1 to prevent transmitted second order diffracted light from exciting the sample. The modulation of the incident light and subsequent lock-in detection was necessary in order to extract the low PC signal (~ 10's nA) from the background noise. The contacts of the TO5 mounted samples were connected to the inner lines of two co-axial cables. The outer parts of the cables were electrically contacted and grounded to the cryostat and optical bench, thus shielding the small PC signal from external electromagnetic interference. A circuit box was designed to allow an external voltage source to be connected in parallel with the sample. A schematic diagram of the PC experimental setup is shown in Fig. 2.5.

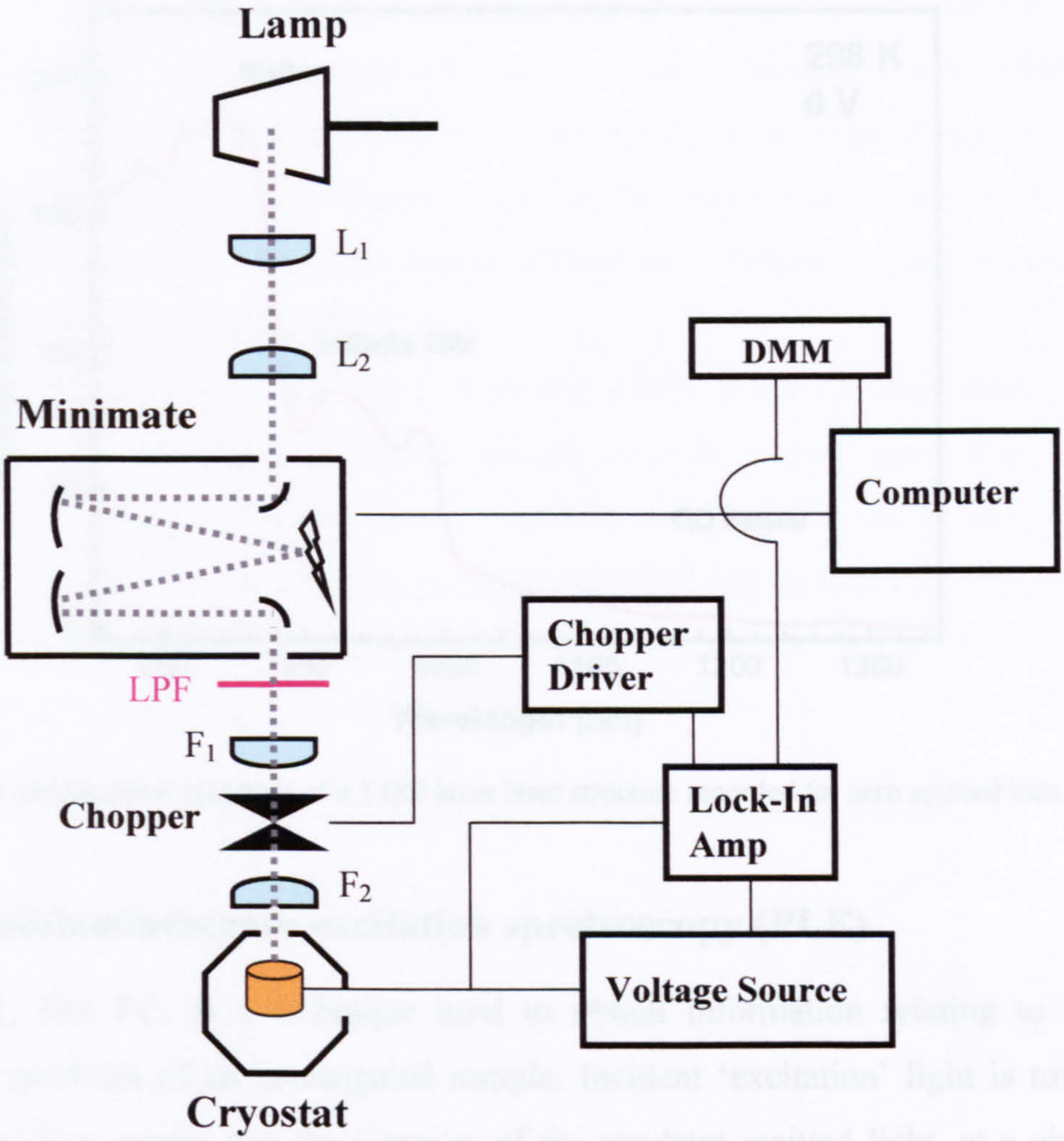

Fig. 2.5 Experimental setup used for photocurrent measurements. The grey dotted line depicts the optical path.

Fig. 2.6 depicts an example of a typical PC spectrum, recorded at RT and under zero applied bias, from a 5 layer DWELL structure. Strong absorption is seen for the bulk GaAs spacer layers (< 860 nm) and also for the QW surrounding the QDs (900-1000 nm). Absorption in to the QD states is much weaker, due to their low (~10 %) fractional occupancy of the sample area. However it is possible to make out three confined state transitions between 1100 and 1300 nm.

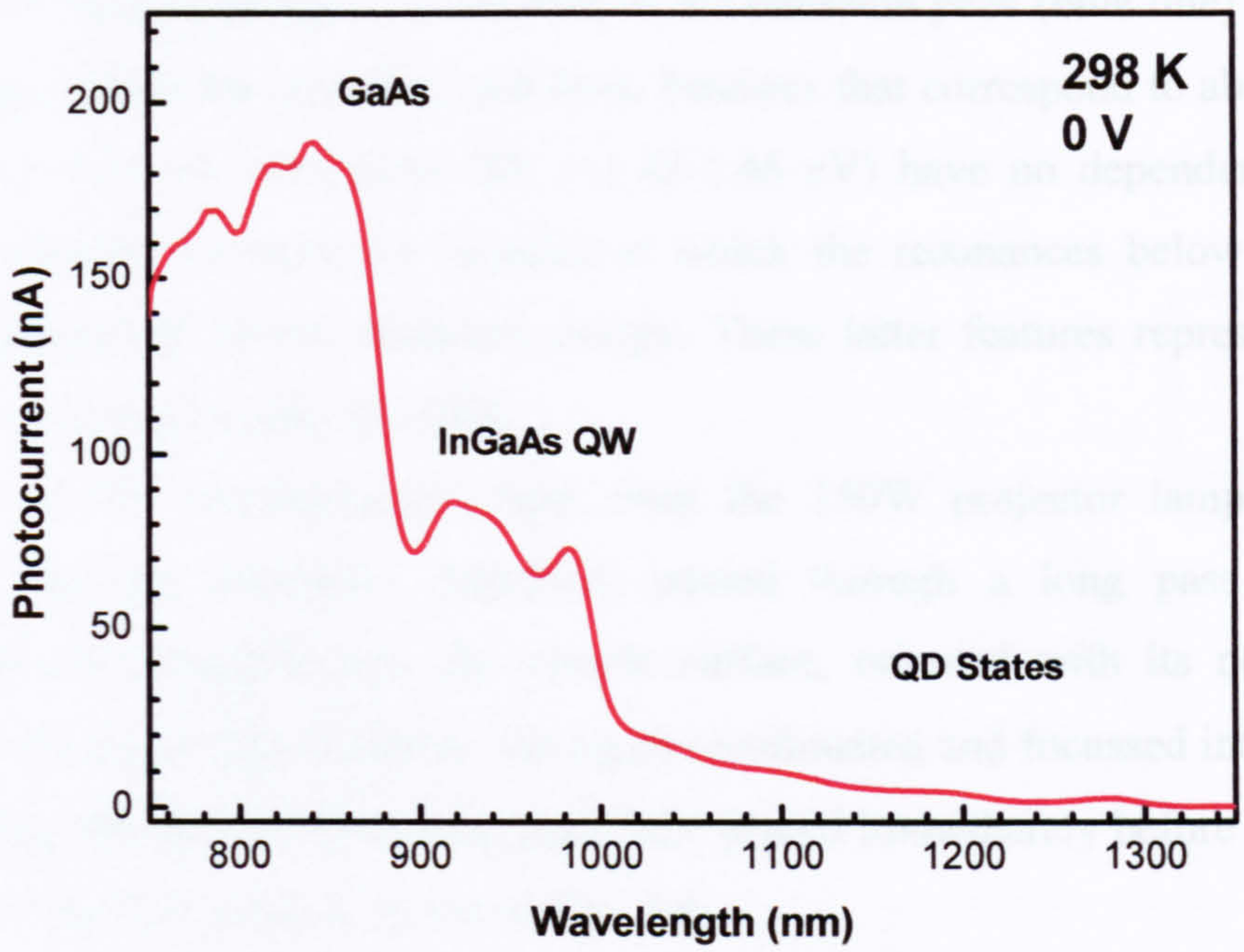

Fig. 2.6 RT photocurrent spectrum of a 5 QD layer laser structure recorded for zero applied bias.

2.2.5 Photoluminescence excitation spectroscopy (PLE)

PLE, like PC, is a technique used to obtain information relating to the absorption spectrum of an investigated sample. Incident 'excitation' light is tuned from high to low energy and the intensity of the resultant emitted light, at a given fixed energy, is monitored as a function of the excitation energy. Thus, the physical processes that determine the form of a PLE spectrum are not the same as those involved in PC. For the absorption of an incident photon to be 'recorded' in the detected signal, the photo-generated carriers must be able to relax to the energy level of the states being monitored (usually the GS in QD ensembles). Therefore the carrier relaxation mechanisms are embedded in the spectral form of the PLE. In bulk and quantum well systems this relaxation mechanism does not greatly distort the spectra. However in QDs, which because of their discrete electronic states and the resultant importance of effects related to the phonon bottleneck, carrier relaxation can dominate PLE spectra, with features observed at integer multiples of the LO phonon energy[2]. Unlike true absorption features, such features are not independent of the detection energy and can be attributed to relaxation processes specific to the subset of QDs probed in the measurement i.e. a narrow distribution of QDs having equivalent GS energies. This effect is clearly illustrated by noting the differences in

the two PLE spectra of Fig. 2.7, recorded at the emission peak (blue line) and on the high energy side of the emission (red line). Features that correspond to absorption in the GaAs (~1.51 eV) and InAs WL (~1.42-1.46 eV) have no dependence on the detection energy, whereas the energies at which the resonances below ~1.36 eV occur is dependent on the detection energy. These latter features represent carrier relaxation processes within the QDs.

As in PC measurements, light from the 150W projector lamp bulb was focussed into the minimate, dispersed, passed through a long pass filter, re-collimated and focussed onto the sample surface, oriented with its normal at a shallow (~5°) angle. The emission was again recollimated and focussed into the spex, after passing through a second long pass filter placed immediately before the slits. A diagram of the PLE setup is shown in Fig. 2.8.

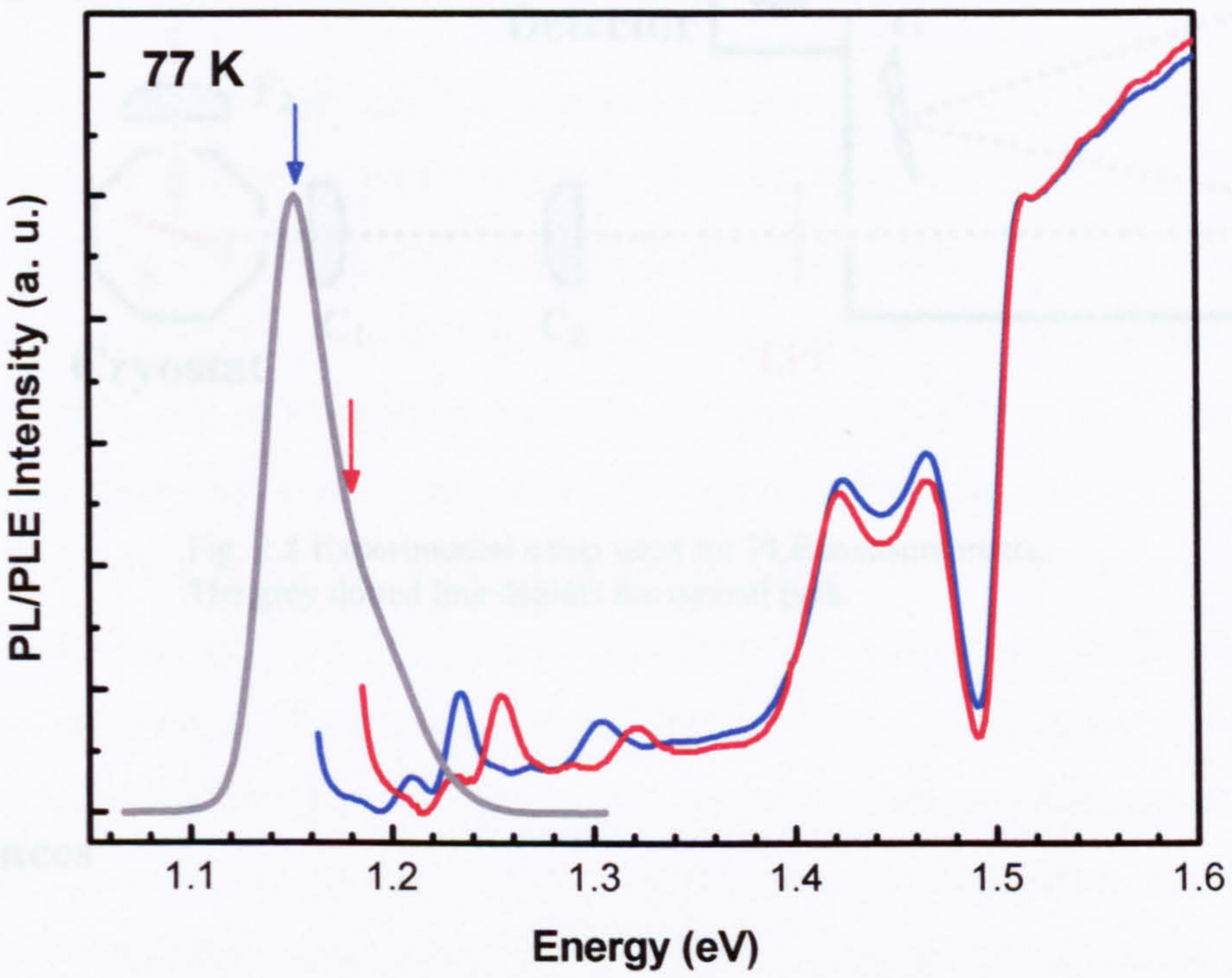

Fig. 2.7 PL (grey line) and PLE spectra (red and blue lines) recorded at 77K. The arrows indicate the detection energy of the corresponding PLE spectrum.

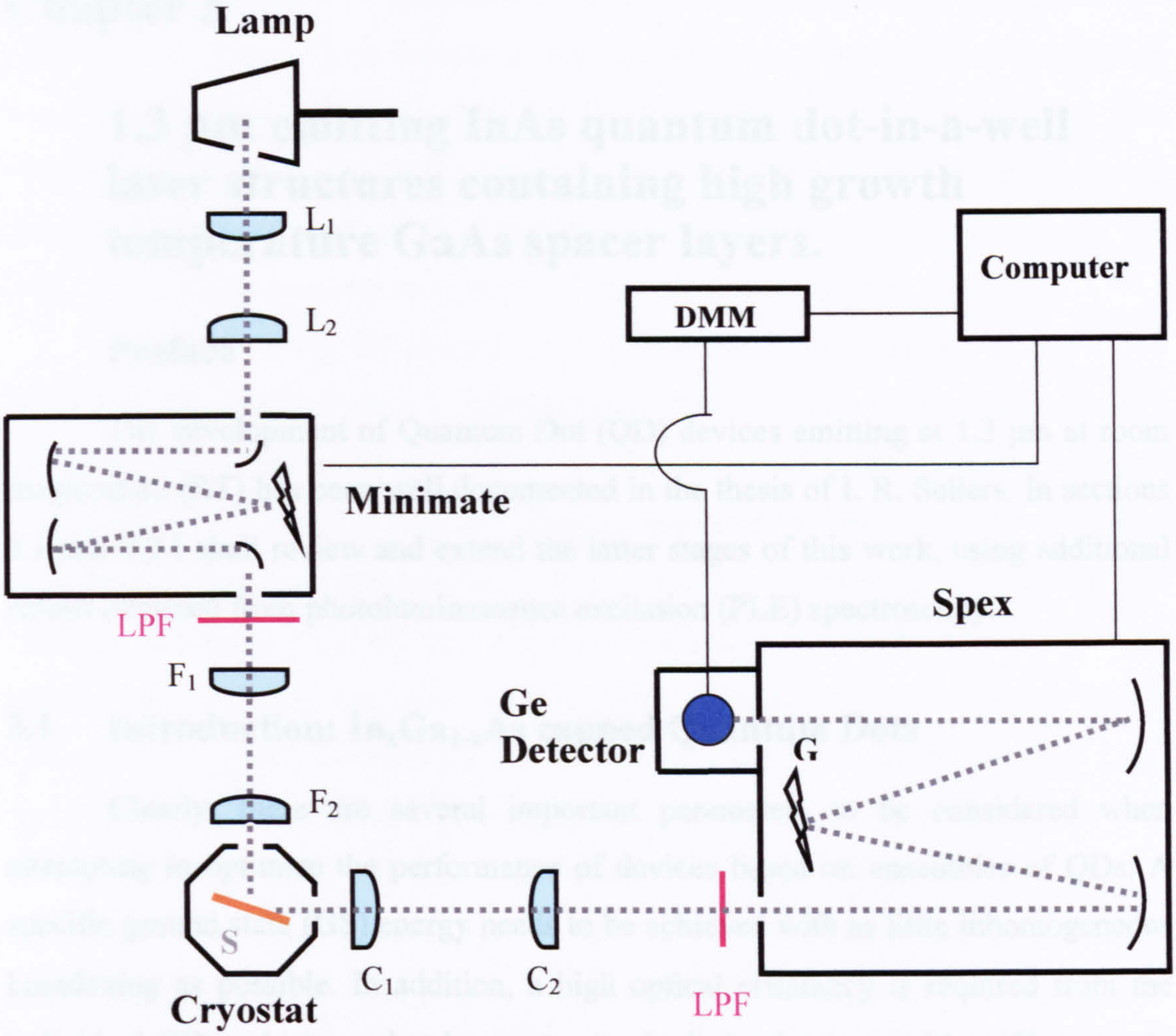

Fig. 2.8 Experimental setup used for PLE measurements.
The grey dotted line depicts the optical path.

References

1. P. W. Fry, I. E. Itskevich, S. R. Parnell, J. J. Finley, L. R. Wilson, K. L. Schumacher, D. J. Mowbray, M. S. Skolnick, M. Al-Khafaji, A. G. Cullis, M. Hopkinson, J. C. Clark, and G. Hill, Phys. Rev. B **62**, 16784 (2000)

2. M. J. Steer, D. J. Mowbray, W. R. Tribe, M. S. Skolnick, M. D. Sturge, M. Hopkinson, A. G. Cullis, C. R. Whitehouse and R. Murray, Phys. Rev. B **54**, 17738 (1996)

Chapter 3

1.3 μm emitting InAs quantum dot-in-a-well laser structures containing high growth temperature GaAs spacer layers.

Preface

The development of Quantum Dot (QD) devices emitting at 1.3 μm at room temperature (RT) has been well documented in the thesis of I. R. Sellers. In sections 3.1 and 3.2 I shall review and extend the latter stages of this work, using additional results obtained from photoluminescence excitation (PLE) spectroscopy.

3.1 Introduction: $In_xGa_{1-x}As$ capped Quantum Dots

Clearly, there are several important parameters to be considered when attempting to optimise the performance of devices based on ensembles of QDs. A specific ground state (GS) energy needs to be achieved with as little inhomogeneous broadening as possible. In addition, a high optical efficiency is required from the individual QDs, which need to be grown at a high density to provide sufficient gain for incorporation into a laser structure. The simultaneous achievement of each of these requirements in a single structure provides a considerable challenge.

Ensembles of InAs QDs grown within a GaAs matrix typically have peak emission wavelengths of ~1 μm at RT and are therefore unsuitable for incorporation into laser structures designed to emit at the longer telecoms wavelengths of 1.3 and 1.55 μm. A reduction in QD height, indium out-diffusion from the QDs and increased hydrostatic strain in the QDs are all proven consequences of their capping with GaAs. Each of these effects acts to reduce the GS emission wavelength in comparison to that of free-standing 'uncapped' InAs QDs, which may reach ~1.6 μm at RT[1]. However, the disadvantageous consequences associated with GaAs capping may be significantly reduced by growing a thin InGaAs layer immediately above the QDs before depositing the GaAs. The overgrowth of InAs QD ensembles with thin $In_xGa_{1-x}As$ capping layers has provided a viable route towards the achievement of optically efficient QD structures emitting at ≥1.3 μm. There are a number of possible

mechanisms that may be responsible for the extended QD emission wavelength when using this technique. These include: i) a strain driven decomposition of the capping layer that results in enlarged In(Ga)As QDs of possibly increased In content[2]; ii) a reduction in the hydrostatic strain within the QDs due to the smaller lattice mismatch between the QD and capping layer[3] and iii) a lower confinement potential for the QD states. The relative importance of these effects will be discussed in section 3.2.

In an early study, RT emission at 1.35 μm with a linewidth of ~ 21 meV was realised using this technique[4]. Subsequently, more extensive investigations have shown that the emission wavelength of such structures can be extended from 1.1 μm when capped with GaAs, to 1.35 μm when covered with $In_xGa_{1-x}As$ layers containing 30% In[5, 6]. These developments for QD test structures were soon incorporated into real laser structures. In 1999, for the first time, a long-wavelength (>1 μm) QD laser device was reported, operating with a lower threshold current density than a Quantum Well (QW) laser device at RT[7]. The structure in question contained a QD layer grown in the middle of a 10 nm $In_{0.15}Ga_{0.85}As$ QW, hence coining the term Dot-in-a-Well (DWELL) for this type of structure.

All of the samples studied in this thesis are based on structures that comprise active regions of InAs QDs grown within a thin (few nm) wide $In_xGa_{1-x}As$ QW. Initial growth studies, intended to optimise the In fraction, 'x', in the QW surrounding the QDs focussed on achieving optically efficient samples, comprising a uniform, high density array of QDs, emitting at a peak wavelength of 1.3 μm at RT and suitable for later incorporation into QD laser structures. These structures consisted of a single layer of QDs and lacked the waveguide structure of a laser device. Although these requirements are essential for producing high quality lasers, their realisation does not necessarily *guarantee* good laser performance. As shall be discussed in section 4.4 of chapter 4 the extra requirements of a laser structure involves the growth of multiple layers and the depositing of AlGaAs at a temperature ~100 °C higher than that used to grow the QDs, which appears to alter the size and shape distribution of the QDs and may also reduce their density.

3.2 Optimisation of the indium composition in the InGaAs DWELL

As has been outlined in the previous section, QDs grown within an $In_xGa_{1-x}As$ QW show superior emission characteristics to those grown directly on GaAs. To investigate the feasible parameter space for the growth of such DWELL structures, a series of five single layer test structures were grown, each differing only in the amount of Indium in the surrounding QW. All other aspects of the growth were kept constant. The structure of the samples was as follows: the QDs were formed by depositing 2.9 MLs of InAs at a rate of 0.09 ML/s on a 2 nm layer of $In_xGa_{1-x}As$. This thin layer of $In_xGa_{1-x}As$, on which the QDs nucleate, is referred to as the Strained Buffer Layer (SBL)[8]. The QDs were then capped by a 6 nm $In_xGa_{1-x}As$ QW referred to as a Strain Reducing Layer (SRL)[6] containing the same material composition as the SBL. Indium compositions (x) of 0, 0.06, 0.12, 0.15 and 0.2 were chosen. This 'full – DWELL' structure was grown at 510 °C. Finally, a 50 nm GaAs capping layer was grown above the DWELL.

The optical and structural properties of the samples were then studied via Photoluminescence (PL)/PLE spectroscopy and Atomic Force Microscopy (AFM). The latter technique required a separate series of structures to be grown, in which the growth is terminated following the deposition of a single layer of QDs. These QDs are grown on a 2 nm $In_xGa_{1-x}As$ SBL, as is used for the 'full' structures, and the purpose of these measurements is to ascertain the effect of the In composition in the SBL on the density of the QDs. On inspection of the PL/PLE spectra (Fig. 3.2), two systematic changes are seen in the QD emission characteristics as the Indium composition increases: the PL peak wavelength increases and the linewidth of the emission narrows. A further trend of increasing QD density with SBL Indium content is revealed in the AFM images. These properties are summarised in Table 3.1.

From these studies, an increase in QD density from 1.3×10^{10} cm^{-2} for x=0 to 3.6×10^{10} cm^{-2} for x=0.2 is found[9]. These values are consistent with previous findings that report increased densities for QDs grown on either thicker $In_xGa_{1-x}As$ SBLs, or SBLs with higher a In composition[10].

Indium %	RT PL Peak (μm)	QD Density (cm^{-2})	FWHM (meV)
0	1.17	1.3×10^{10}	33
6	1.2	2.5×10^{10}	30
12	1.25	3.1×10^{10}	29
15	1.32	3.5×10^{10}	28
20	1.35	3.5×10^{10}	26

Table 3.1. Variation of RT optical and structural parameters of $In_xGa_{1-x}As$ DWELL structures.

One possible explanation for the increase in QD density with greater Indium composition in the SBL may be related to changes in the equilibrium condition of the growth surface when growing the QDs on a SBL. Due to an increase in the amount of strained material at the growth front during the growth of the QDs on SBLs with higher In fractions, In and Ga atoms may be released from the surface of the SBL, ie. desorped, as 'x' increases. This material is then able to be incorporated into pre-existing QD islands or float on the surface, available for further QD nucleation.

Alternatively, differences in the strain fields below the QDs may be the cause of the variation in density. QDs are known to interact via their lateral strain fields during growth[11]. This repulsive interaction is proportional to the square of the lattice mismatch (Δa_0). Therefore, it is not unreasonable to assume that this interaction sets some limit to the maximum density that can be attained. It follows that as Δa_0 is less between $In_xGa_{1-x}As$ and InAs than it is between GaAs and InAs, a higher density is to be expected when the QDs are formed on $In_xGa_{1-x}As$ (as confirmed by the AFM results). The reason why the increase in QD density from x=0.15 and x=0.2 is so small as to be negligible is not completely clear. It may be that the dislocations that form at higher indium concentrations act as a sink for additional Indium atoms[12]. Evidence for dislocation formation when $x \geq 0.15$ is consistent with the behaviour of the integrated PL intensities of the structures: as x increases from 0 to 0.15 the integrated PL intensity increases by ~30%, but for x=0.2 the intensity is quenched by over an order of magnitude. Such a rapid decrease indicates that some critical limit for the allowed volume of strained material has been exceeded, and any further deposition results in strain relaxation and an increase in the concentration of non–radiative recombination centres.

Fig. 3.2 shows PL and PLE spectra, detected at the PL peak, for each sample (x=0, 0.06, 0.15 and 0.2) at a temperature of 6K. The respective PLE spectra have been normalised to the intensity at the GaAs bandgap, and the PL spectra have been normalised to a constant value.

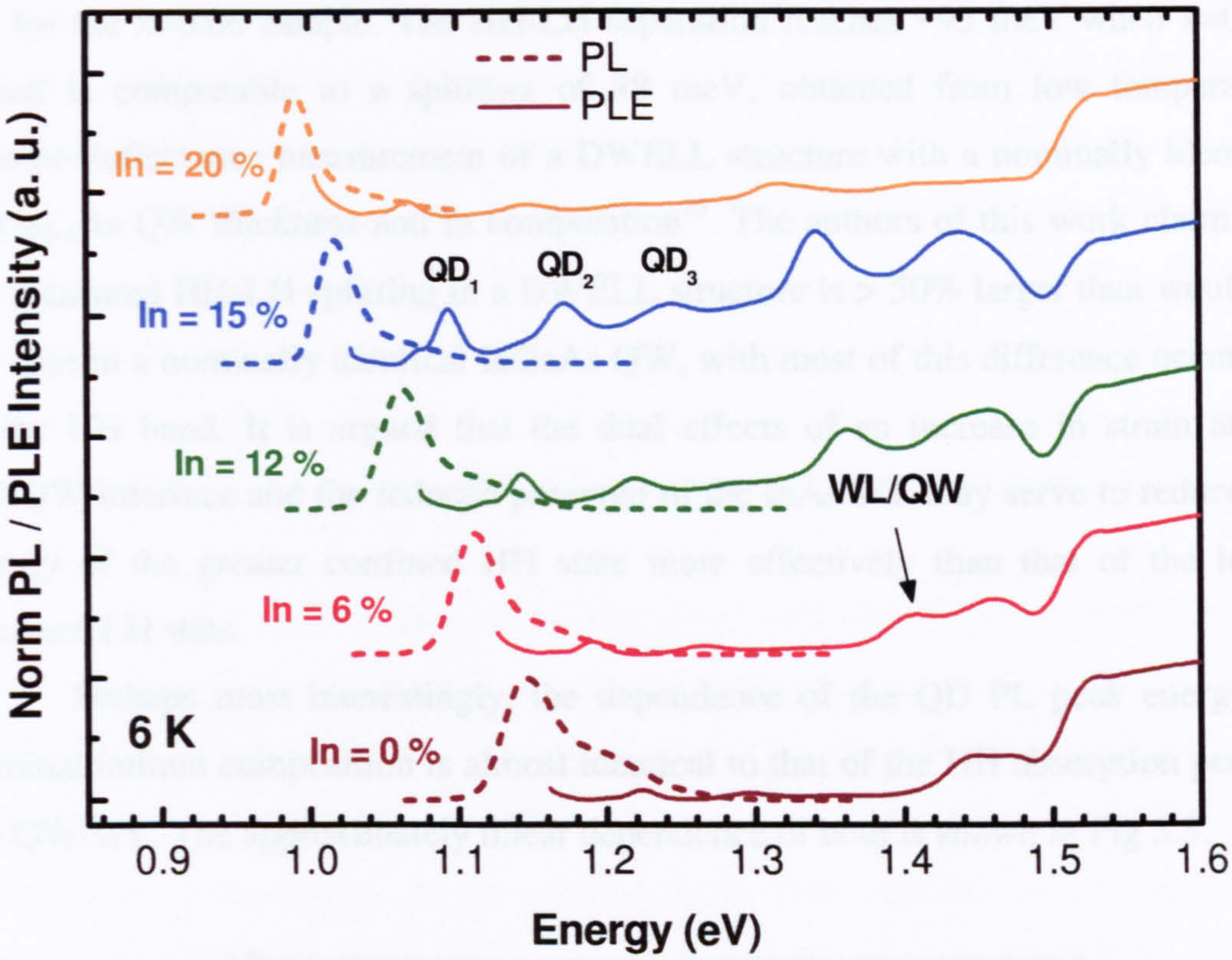

Fig. 3.2 Normalised 6 K PL (dotted line) and PLE (solid line) spectra of the $In_xGa_{1-x}As$ DWELL structures. PL was excited using semi-monochromatic light at 770 nm.

The spectra reveal some interesting changes in the electronic structure of the DWELL as the In composition is varied. In the sample where the QDs are formed on, and capped with GaAs, a double peaked feature, centred at ~1.46 eV, is observed. Its position is found to be independent of the detection energy (E_{det}) and it can therefore be attributed to interband absorption in the In(Ga)As wetting layer (WL). The separation between the two peaks (~35 meV) represents the energetic splitting of the light hole (LH) and heavy hole (HH) states in the WL. Similar HH-LH separations have been reported in PLE studies of other long wavelength InAs/GaAs QDs formed on GaAs[13, 14].

For the samples in which the QDs are embedded in an $In_xGa_{1-x}As$ QW, the shape of the PLE changes somewhat. Two absorption features are still seen, and

these redshift and separate with increasing In%. Their exact nature is uncertain, but they are tentatively attributed to absorption from the HH/LH states into the first confined electron state of the QW/WL composite. In a strained $In_xGa_{1-x}As$ QW the HH state occurs at a lower energy than the LH state due to the combined effects of strain and quantum confinement. The transition from the HH state is marked on Fig 3.2 for the x=0.06 sample. The HH-LH separation reaches ~95 meV when x=0.15, which is comparable to a splitting of 88 meV, obtained from low temperature Electro-Reflectance measurement of a DWELL structure with a nominally identical $In_xGa_{1-x}As$ QW thickness and In composition[15]. The authors of this work claim that the measured HH-LH splitting in a DWELL structure is > 50% larger than would be the case in a nominally identical InGaAs QW, with most of this difference occurring in the HH band. It is argued that the dual effects of an increase in strain at the QD/QW interface and the reduced potential of the InAs WL may serve to reduce the energy of the greater confined HH state more effectively than that of the lesser confined LH state.

Perhaps most interestingly, the dependence of the QD PL peak energy on nominal indium composition is almost identical to that of the HH absorption peak in the QW/WL. The approximately linear dependence of both is shown in Fig 3.3.

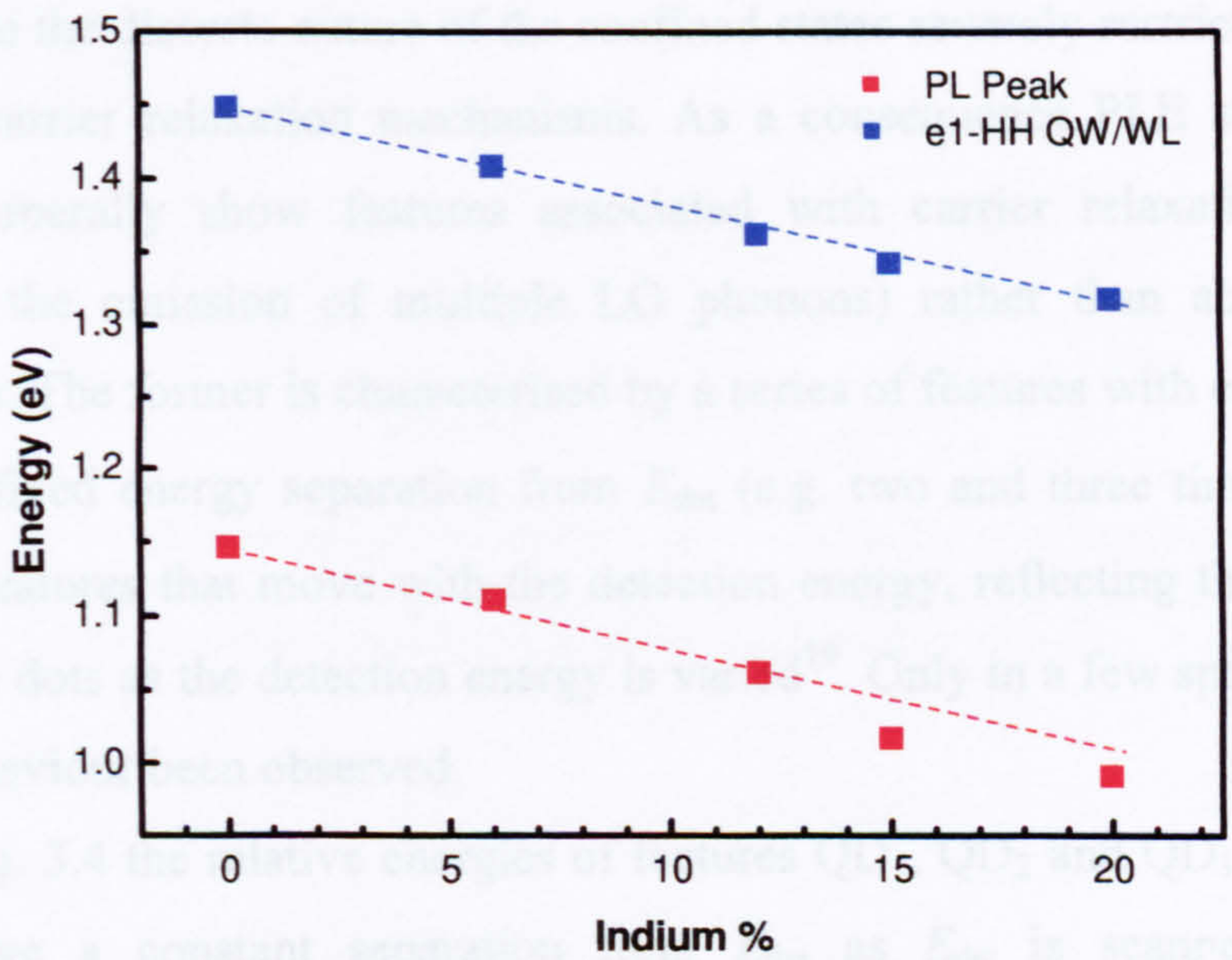

Fig. 3.3 PL peak energy and the lowest energy transition in the DWELL (e1 – HH) as a function of indium composition. The trends are approximately linear and have very similar dependencies.

This is an important result, as it implies that the confinement potential of the QD ground states with respect to the lowest energy InGaAs QW states is *virtually independent* of indium composition (over the composition range investigated). As a decrease in the depth of a potential well will not cause an equivalent decrease in the energy of a confined state (unless the states are very close to the top of the potential well), this result indicates that changes in the confinement potential are unlikely to be fully responsible for the redshift of the QD emission. Hence, the reduction of the QD GS energy with increasing In composition in the DWELL appears to have contributions from the effects of stimulated decomposition of the SRL and/or reduced hydrostatic strain in the QD. Complementary results from theory, PLE and TEM indicate that the reduction in QD strain dominates the GS redshift for an In composition < 0.15, whilst an enlargement of the QD height, due to In decomposition of the InGaAs DWELL, is the dominant mechanism for higher In contents[16].

Unlike the spectral form of the PLE in the bulk and WL regions, the features QD_1, QD_2 and QD_3 that appear in a ~270 meV energy window above the GS of the QDs do not represent the true absorption profile of the QD states. PLE will only resemble the real absorption profile when the carrier relaxation probabilities are independent of the energy of the exciting light. This condition is not met in QD systems, since the discrete nature of the confined states severely restricts the number of possible carrier relaxation mechanisms. As a consequence PLE studies of QD ensembles generally show features associated with carrier relaxation processes (particularly the emission of multiple LO phonons) rather than absorption into excited states. The former is characterised by a series of features with energies which remain at a fixed energy separation from E_{det} (e.g. two and three times $\hbar\omega_{LO}$[17, 18]) rather than features that move with the detection energy, reflecting the selection of different size dots as the detection energy is varied[19]. Only in a few special cases has the latter behaviour been observed.

In Fig. 3.4 the relative energies of features QD_1, QD_2 and QD_3 in the x=0.15 structure have a constant separation from E_{det} as E_{det} is scanned across the inhomogeneously broadened PL peak. Therefore, from previous work they appear to be due to discrete carrier relaxation channels within those QDs probed by the measurement. Similar features are seen in the spectra of the x=0, 0.06, 0.12 and 0.2

samples, but for clarity they have not been highlighted. From Fig. 3.4 it is seen that QD_1, QD_2 and QD_3 are positioned at energies 80, 155 and 225 meV respectively above the GS. Surprisingly these values are not particularly close to integer multiples of either the GaAs (36 meV) or InAs (~30 meV) LO phonon energies, hence their precise origin remains unclear.

The increase in the relative intensity of the QD_1, QD_2 and QD_3 features as x increases from 0 to 0.15, accompanies a similar increase of the WL/QW feature. This is likely to be related to an improvement in material quality, reducing the amount of non-radiative recombination and is consistent with the increase in PL efficiency over this range of 'x'. Additionally, there may be some increase in the exciton-phonon coupling strength due to the increased indium content or increased symmetry of the QDs[20].

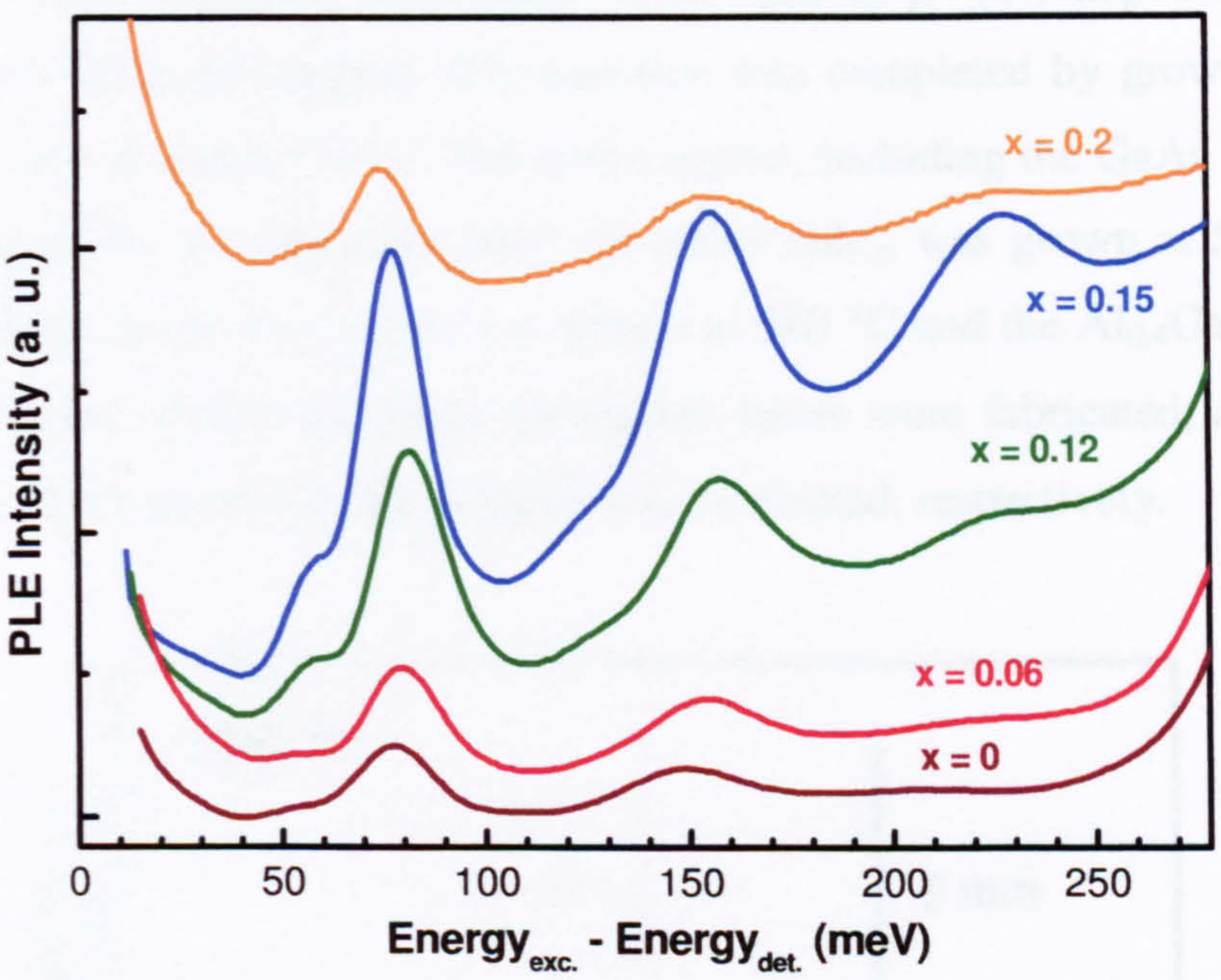

Fig. 3.4 PLE spectra of the DWELL structures plotted as a function of excess excitation energy ($E_{exc.} - E_{det.}$). The energies of the resonances are approximately independent of In fraction with respect to E_{det}.

3.3 Initial 1.3 μm DWELL laser structures

3.3.1 Lasing characteristics of 3 and 5-QD layer structures.

Combining the results of both optical (PL and PLE) and structural (AFM characterisation, it is clear that of the 5 structures tested, the QDs in the sample wit x=0.15 have the most desirable qualities required for the gain media in semiconductor laser designed for 1.3 μm emission; that is a strong PL intensit narrow FWHM, high density and a suitable GS transition energy (see Table 3.1).

As a result, two multilayer DWELL structures were then grown in a ne MBE reactor: Vn 17 consists of 3 DWELLs, separated by 50 nm spacer layers (SI of GaAs; Vn 20 has 5 DWELL layers, again with 50 nm GaAs spacer layers. Th active regions were embedded in the centre of a 150 nm $Al_{0.4}Ga_{0.6}As$/GaA waveguide, which was then surrounded by 1.5 μm of p^+ (n^+) doped $Al_{0.4}Ga_{0.6}A$ above (below) the active region. The structure was completed by growing 300 n GaAs as a *p*-doped contact layer. The active region, including the GaAs SLs and th initial 15 nm of the waveguiding layer (on either side), was grown at 510 °C. Th remaining GaAs in the waveguide was grown at 580 °C and the $Al_{0.4}Ga_{0.6}As$ at 62 °C. Circular mesa diodes and ridge waveguide lasers were fabricated, allowing th spontaneous emission and lasing properties to be studied, respectively.

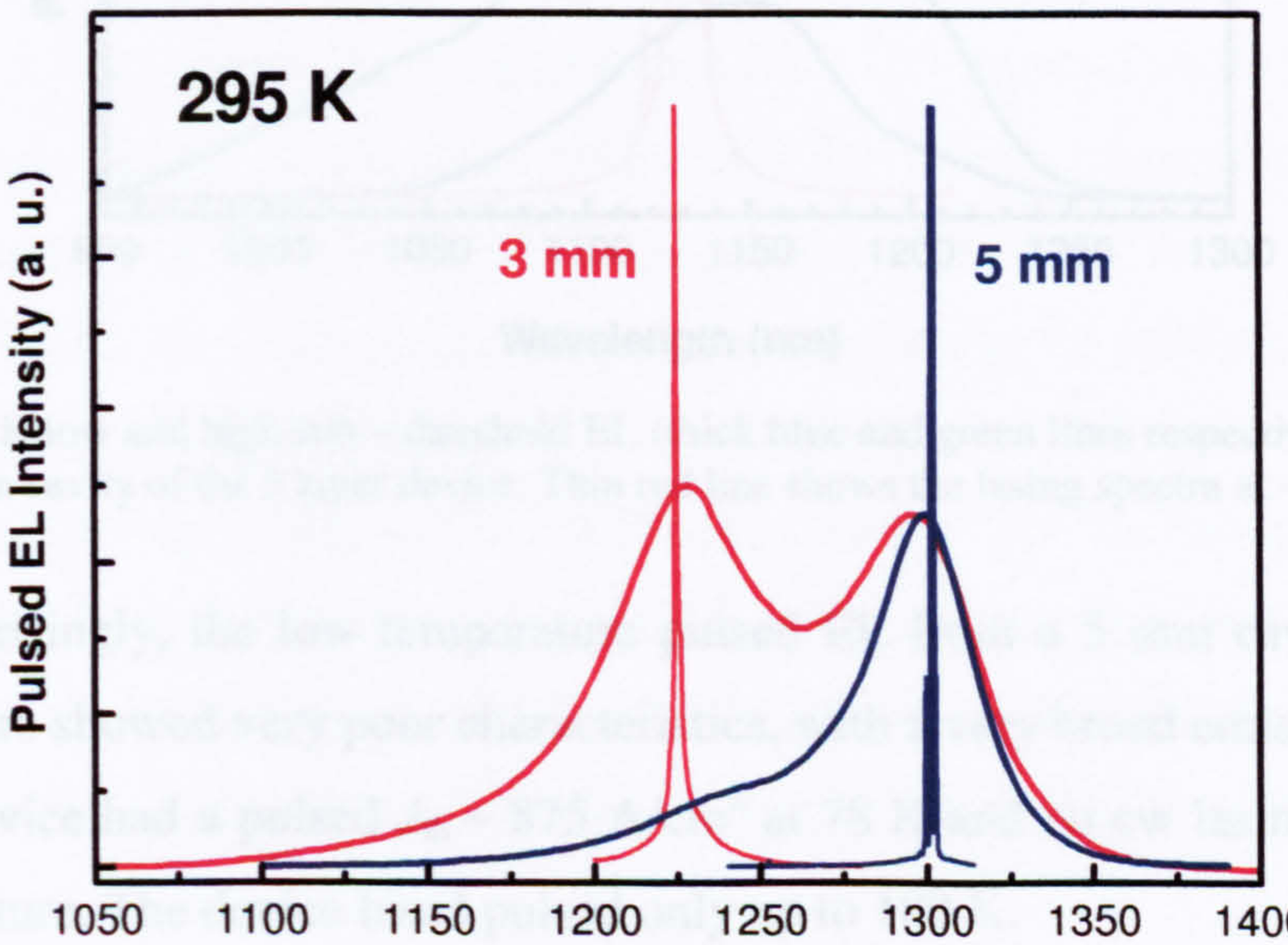

Fig. 3.5. Pulsed RT EL of the structure containing 3 QD layers (Vn 17). Sub – threshold EL from 3 mm and 5 mm cavities are shown using thick red and navy lines respectively. The thin lines are lasing spectra recorded at ~ 1.1 x J_{th}.

The RT, pulsed electroluminescence (EL), taken below and above threshold from laser devices fabricated from the 3-layer structure is shown in Fig. 3.5. Lasing occurs at 1.3 μm from a 5 mm cavity, with a pulsed threshold current density (J_{th}) of 135 A/cm^2, whereas in a 3 mm cavity, lasing is only possible from the first excited state, due to the insufficient GS gain. Continuous wave (cw) lasing was possible up to only 275 K in the 5 mm device. The strong temperature sensitivity of J_{th}, exhibited for all cavity lengths of this structure, is a direct result of a low modal gain. Multi-QD layer structures have been shown to increase the modal gain by 2 – 3 cm^{-1} per QD layer[21], thereby reducing the sensitivity of the GS to gain saturation and enabling shorter cavity length devices to operate with reduced J_{th}s[22]. It was with this consideration in mind, that an identically designed structure with 5 layers of QDs was grown.

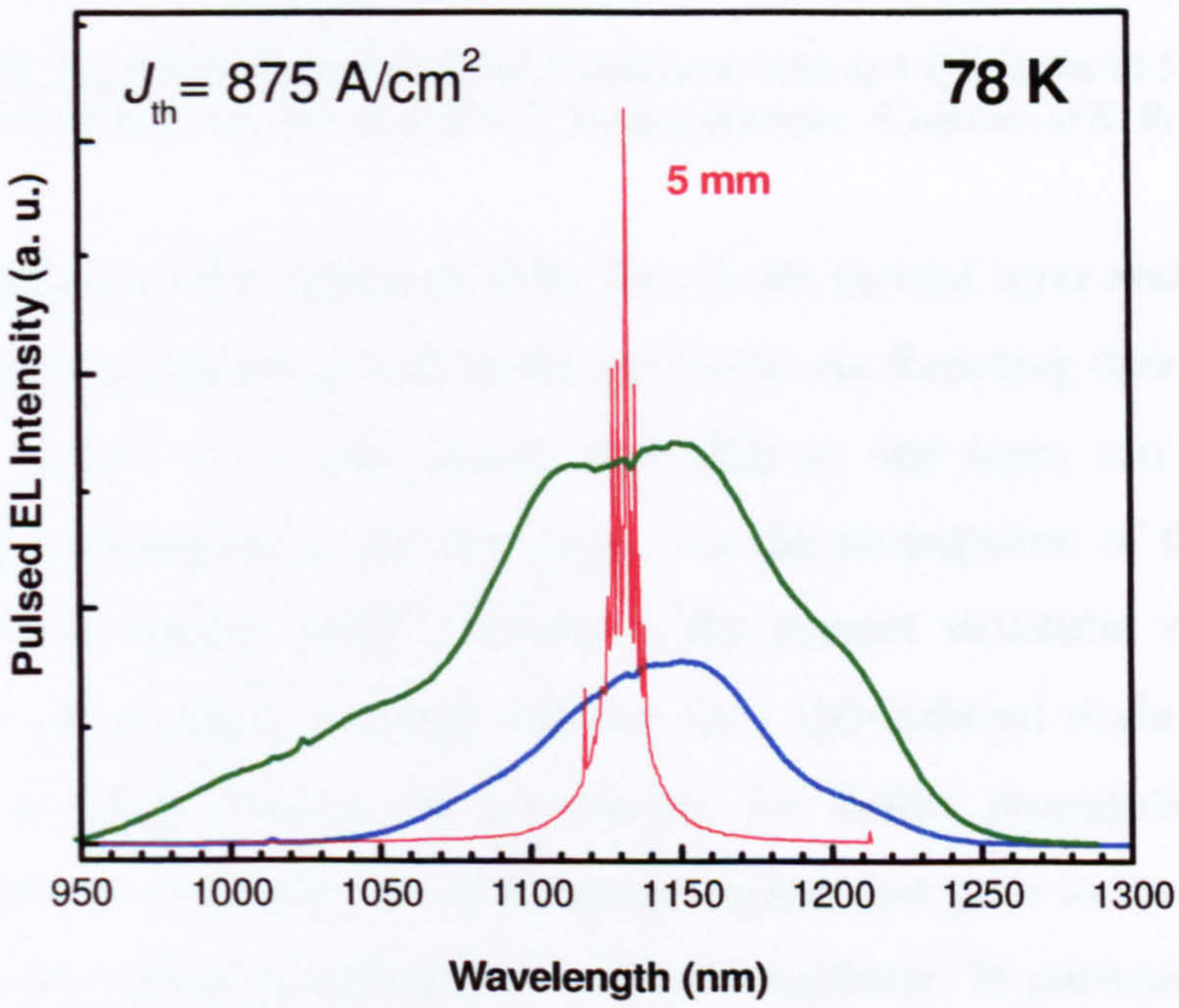

Fig. 3.6. 78 K low and high sub – threshold EL (thick blue and green lines respectively) taken from a 5 mm cavity of the 5 layer device. Thin red line shows the lasing spectra at ~ 1.1 x J_{th}.

Surprisingly, the low temperature pulsed EL from a 5 mm cavity of the 5-layer structure showed very poor characteristics, with a very broad emission (see Fig. 3.6). The device had a pulsed J_{th} ~ 875 A/cm^2 at 78 K and no cw lasing occurred at any temperature. The device lased pulsed only up to 180 K.

3.3.2 Structural investigation of the initial laser structures

The broad spontaneous emission and high J_{th} of the 5-layer device suggests that defective QD formation had occurred during the growth of the active region. Large dislocated QDs, present in the second and higher QD planes, are revealed in Transmission Electron Microscope (TEM) images of both the 3 and 5-layer devices as shown in Figs 3.7 a) and b).

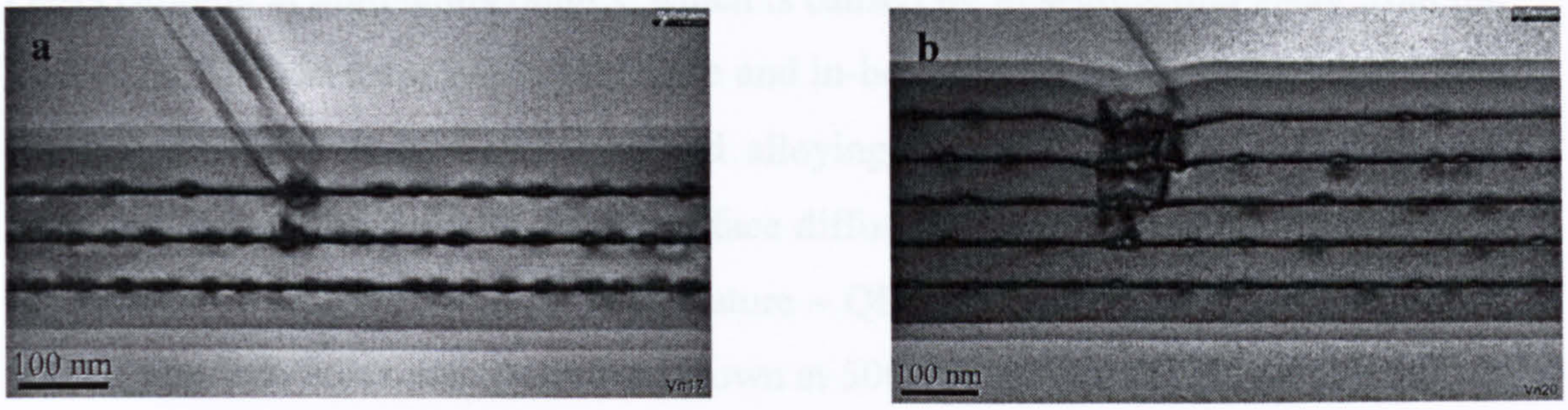

Fig. 3.7 Dark Field TEM images of DWELL structures with a) 3 QD layers b) 5 QD layers. The 50 nm GaAs SLs were grown at 515 °C in each structure. *(Courtesy of R. Beanland)*

The defective QDs appear to form first in the second layer and then are able to induce further incoherent growth in the next layer via threading dislocations in the GaAs spacer layer[23]. It is well known that QDs in one layer can influence the subsequent QD nucleation in the next layer, via the propagation of the strain field through the GaAs spacer layer[24]. However, the present structures contain spacer layers that are 50 nm thick – enough distance for a QD-induced strain field to decay to a negligible level. Hence, the mechanism for defect propagation cannot be attributed purely to strain effects. AFM images, taken just prior to the growth of the second QD layer, show a considerable *surface roughness*. In particular they reveal anisotropic undulations, consisting of 'mounds and pits' ~ 4 ML in amplitude and extending laterally up to 120 nm[25]. The density of these 'pits', where the QDs in the next layer are thought to nucleate, is similar to that of the QDs in the underlying layer. This indicates that the influence of the underlying QDs' on the next layer of growth is still being felt, although this is an indirect effect via the modulation of the growth of the GaAs spacer layer.

Recently, almost identical features to the ones observed in the present samples have been identified in the AFM and TEM images of similar multilayer

DWELL structures with GaAs SLs grown at a low temperature (500 °C)[26]. The presence of large coalesced QDs was found to induce 'pinhole-like' depressions in the GaAs grown above these QDs. The dimensions and densities of these depressions are comparable to those of the 'pits' observed in the present structures.

The strain-relief driven morphological changes that occur in InAs QDs during their overgrowth with GaAs have received considerable attention in the literature. Commonly observed is the 'levelling' of QDs during the initial stages (few ML) of GaAs capping at high temperatures, which is caused by In segregating away from the tops of the QDs to areas around the base and in-between the QDs (in the WL)[27]. The associated reduction in QD height and alloying of the WL have been attributed purely to thermodynamically driven surface diffusion processes that are independent of the overgrowth rate[28] but not temperature – QDs covered with GaAs deposited at 300 °C are 50% taller than those overgrown at 500 °C. In fact, the partial dissolution of the QDs into the surrounding InGaAs WL has been determined to occur on a timescale of < 20 s when GaAs is deposited at ~ 500 °C [29]. However, the planarisation rate of the *surface* above fully-overgrown QDs is sensitive to the deposition rate[28]. Slower rates produce increased surface diffusion lengths, with the result that the surface smoothing is enhanced. The influence of the strain effects that govern the stoichiometric balance of the evolving QD/matrix system can be minimised, to some extent, by capping with an InGaAs alloy.

3.3.3 Modification of the GaAs spacer layer growth conditions

Scanning Tunnelling Microscopy investigations of large, overgrown QDs, undertaken at Imperial College, London reveal that the growth front can remain non-planar even after 40 nm of GaAs deposition[30]. The cause of this surface roughness was attributed to the low growth temperature used during the deposition of the GaAs (510 °C), which is determined by the need to avoid intermixing of the QDs, since the additional of Ga will result in a blue shift of the emission. Gallium ad-atoms are relatively immobile at this temperature and their small migration distance is insufficient to fully re-planarise the growth front, even after the strain field has decayed to zero, hence a residual surface roughness remains. In an attempt to alleviate this problem, an annealing technique developed at the same institution was

employed during the GaAs growth. Using this method, multilayer structures with 40 nm spacer layers exhibited repeatable, coherent QD growth[31].

In light of this relatively straightforward solution, a similar technique was developed in Sheffield and employed for the next series of multilayer DWELL structures. The DWELL regions of the previous 3 and 5-layer structures were now re-grown as before, but with an important modification to the GaAs SL growth conditions. During the first 15 nm of GaAs SL deposition, the GaAs growth temperature was held at 510 °C, with the intention of preserving the QD composition. However, for the final 35 nm portion of the spacer layer, the GaAs was grown at 580 °C, allowing a buffer layer with a smooth surface morphology to be produced, exhibiting no 'memory' of the underlying QD growth. This technique for spacer layer growth is referred to as a High Growth Temperature Spacer Layer (HGTSL). A TEM image of a 5-layer HGTSL laser structure, shown in Fig. 3.8, reveals that the temperature increase during the spacer layer growth has resulted in a structure with far fewer dislocations than the non – HGTSL counterpart. ($<10^6$ and 10^9 cm^{-2} respectively)[23]. By using the HGTSL approach it is possible to achieve uncorrelated, coherent and repeatable QD growth in each of the 5 QD layers.

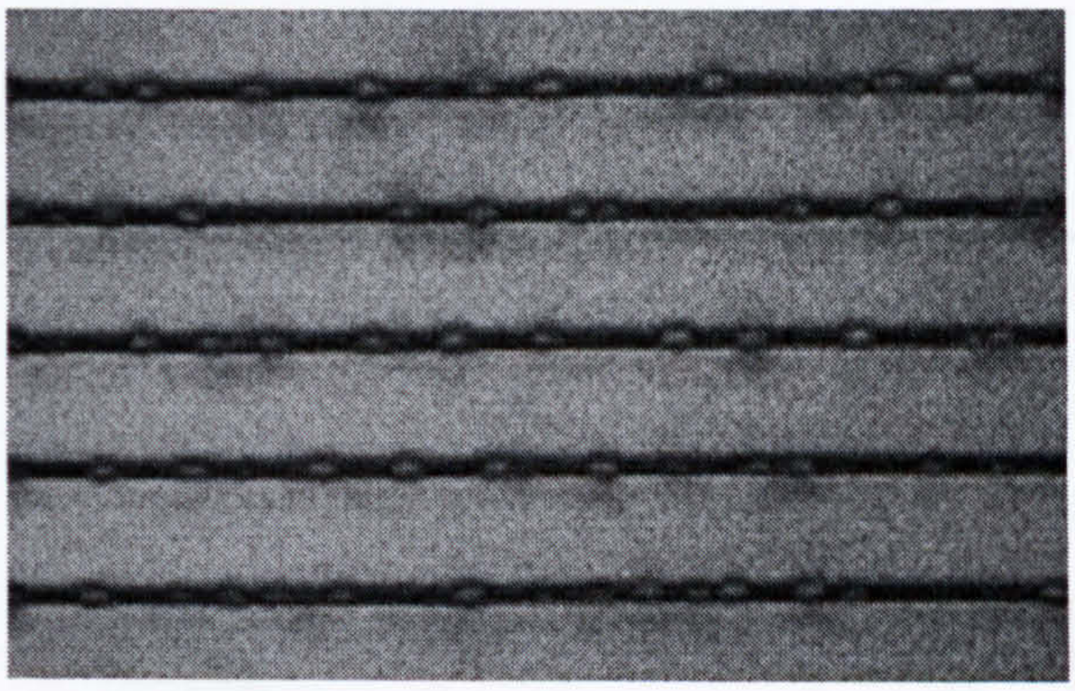

Fig. 3.8 Dark Field TEM image of a re-grown 5-layer DWELL structure with HGTSLs. *(Courtesy of R. Beanland)*

These improvements in the structural properties translate into greatly improved optical and electrical properties as will be described below. Before these are presented, it should be mentioned that an alternative, but not equivalent, method has been developed for eliminating defective QDs. This involves a two-stage heat treatment process. First, a thin layer of GaAs is deposited over the InAs QDs at a

temperature ~ 600 °C. InAs from any large incoherent QDs is evaporated during this overgrowth. The resulting voids are then filled with AlAs and subjected to heat treatment at 650 – 700 °C, effectively removing any buried defects[32]. In comparison, the HGTSL method, as well as being simpler, is a *preventative* approach to defect density reduction in QD structures.

3.4 DWELL QD laser structures incorporating HGTSLs

3.4.1 Optical and electrical properties of HGTSL devices

The improvement in the structural quality of the HGTSL samples is reflected in their superior optical efficiency. Comparative differences in the RT integrated EL intensities and the injection current dependence of the EL, are indicative of a large concentration of non-radiative centres being present in structures grown without HGTSLs. For example at RT, at an injection level of 0.8 A/cm^2, there is an order of magnitude reduction in the integrated EL intensity of a non-HGTSL device when compared to a HGTSL structure. This difference is reduced to a factor of two when the injection is raised to 40 A/cm^2. This variation in the comparative integrated EL with current is consistent with a non-radiative process being saturated as the injection level is increased.

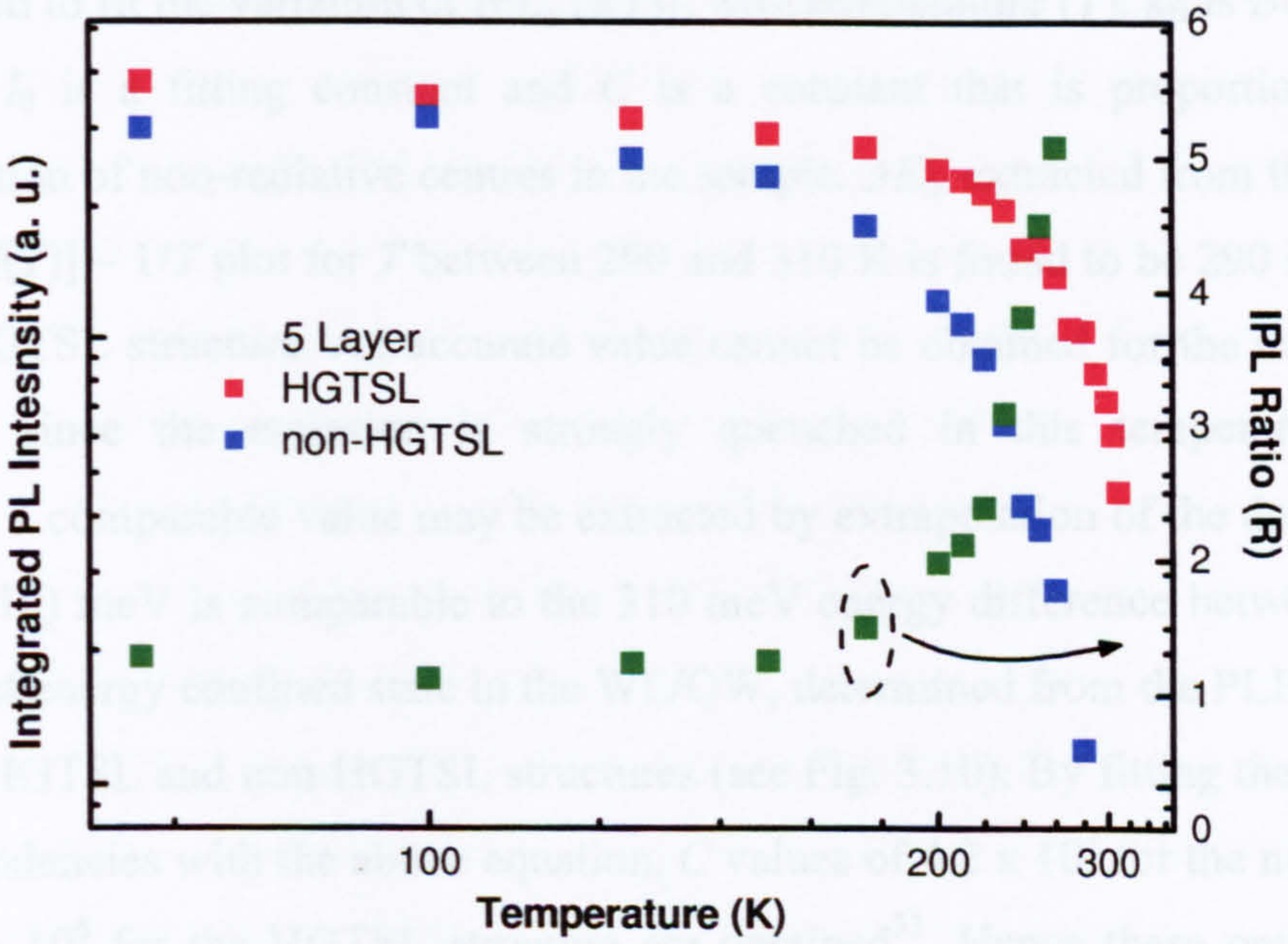

Fig. 3.9 Integrated PL Intensity plotted as a function of temperature for 5-layer test structures containing HGTSLs (red dots) and without HGTSLs (blue dots). The ratio of their integrated intensities is superposed (olive dots).

As expected, the presence of defects in non-HGTSL samples results in inferior temperature stability of the PL/EL intensity. Fig. 3.9 shows the temperature variation of the integrated PL intensity (IPL) for 5-layer test structures grown with and without HGTSLs. Also shown is the IPL ratio HGTSL: non-HGTSL (R). The PL was excited using a low power HeNe laser emission, resulting in a dot carrier occupancy << 1. Below 220 K, the PL intensity of both the HGTSL and non-HGTSL samples is fairly insensitive to temperature. In this temperature range the relative strengths of the emission are comparable, with the PL of the HGTSL structure less than a factor of 2 greater than that of the non-HGTSL structure ($R < 2$). However, as the temperature is raised above 220 K, the IPL ratio (R) increases rapidly, reflecting the faster quenching of the PL of the non-HGTSL structure.

The relative concentration of non-radiative centres in the two samples can be estimated using the data plotted in Fig. 3.9. In general, the high temperature PL efficiency [$I(T)$] is a function of the defect density in the sample and the energy required to thermally excite carriers from the emitting states to the defect states, referred to as the activation energy (ΔE_a).

An Arrhenius-type dependence of the form

$$I(T) = \frac{I_0}{1 + Ce^{-\Delta E_a / k_B T}}$$

can be used to fit the variation of IPL, [$I(T)$], with temperature (T). k_B is Boltzmann's constant, I_0 is a fitting constant and C is a constant that is proportional to the concentration of non-radiative centres in the sample. ΔE_a, extracted from the gradient of the $\ln[I(T)] - 1/T$ plot for T between 290 and 310 K is found to be 290 (±10) meV for the HGTSL structure. An accurate value cannot be obtained for the non-HGTSL structure, since the emission is strongly quenched in this temperature range. However, a comparable value may be extracted by extrapolation of the data. A value of 290 (±10) meV is comparable to the 310 meV energy difference between the GS and lowest energy confined state in the WL/QW, determined from the PLE spectra of both the HGTSL and non-HGTSL structures (see Fig. 3.10). By fitting the respective IPL dependencies with the above equation, C values of 4.2×10^7 for the non-HGTSL and 3.8×10^6 for the HGTSL structure are obtained[33]. Hence these optical results suggest that the defect density appears to be reduced by at least an order of

magnitude in the HGTSL structure. This reduction is however much less than the at least factor of 10^3 reduction suggested by the structural studies discussed above.

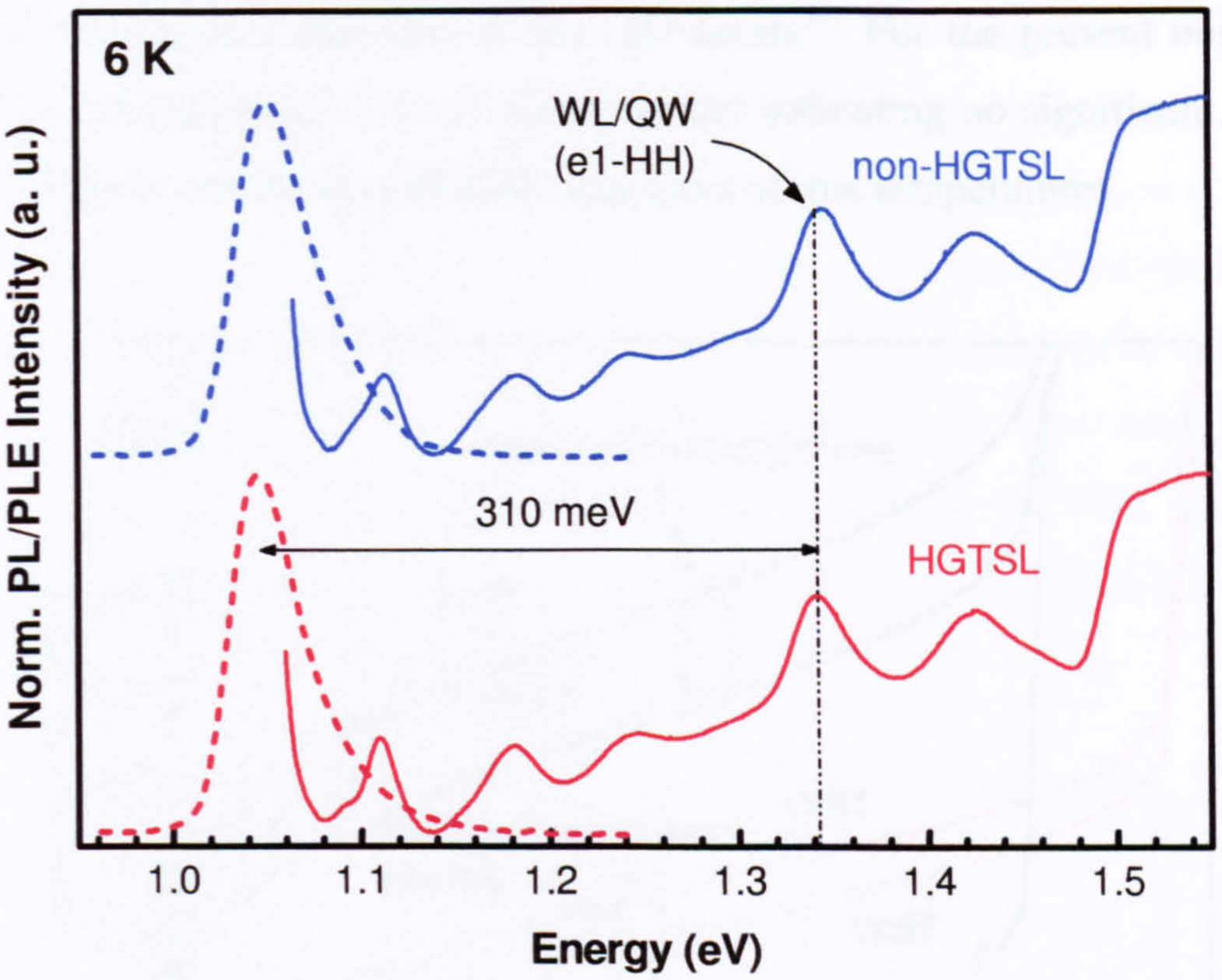

Fig. 3.10 6 K normalised PL (dotted lines) and PLE (solid lines) of the HGTSL structure (red lines) and non-HGTSL structure (blue line)

However, it is interesting to note that the spectral forms of the PLE for the HGTSL and non-HGTSL sample are essentially identical. This suggests that, at low temperatures where non-radiative recombination is suppressed, the carrier capture efficiency and relaxation into the QDs is unaffected by the HGTSL process. This may be understood if it is assumed that the proportion of 'high quality' GaAs involved in the transfer of carriers to the QDs is approximately the same for each sample (under these low temperature, low excitation conditions). An argument based on the decrease in the amount of high quality GaAs was used to explain the 'washing out' of the GaAs free exciton in multiple layer QD structures with 5 layers and thin (10-15 nm), low temperature (360 °C) grown GaAs spacer layers[34]. In contrast to this observation, there is no evidence from the comparison of the non-HGTSL and HGTSL samples for degraded GaAs close to the QDs in the former structures, at least at low temperatures. However the presence of non-radiative centres which become active at high temperatures cannot be discounted. Another relevant feature of the PLE comparison between single and multiple layers was a reduction for the latter

in the PLE intensity ratio for excitation above the GaAs band gap to excitation directly into the WL/QDs. Again this was accounted for by an assumed deterioration in the spacer layer material quality in the 5-layer structure, a result of the low growth temperature and small separation of the QD layers[34]. For the present non-HGTSL and HGTSL structures this ratio is equal, further indicating no significant reduction in the GaAs quality in the non-HGTSL structures at low temperatures.

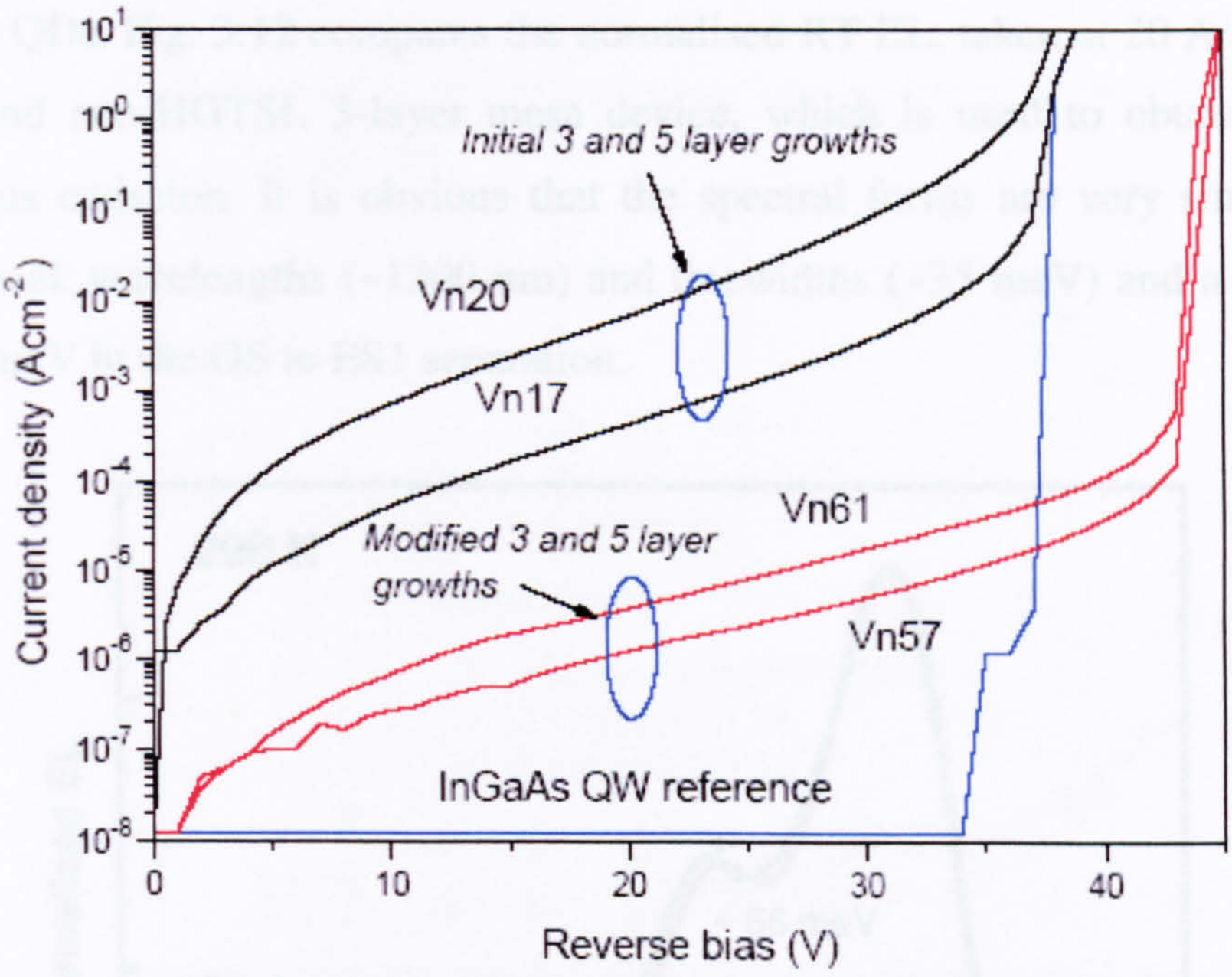

Fig. 3.11 Room temperature I-V characteristics of multilayer non-HGTSL and HGTSL mesa devices. The non-HGTSL and HGTSL structures are represented by black and red lines respectively. Vn 17 and Vn 57 are 3-layer structures and Vn 20 and Vn 61 are 5-layer structures. For comparison, the I-V of an InGaAs QW of nominally the same thickness (8 nm) and composition (15 % In) as the QW used in the DWELL structures is shown by the blue line. *(Measurements performed by M. Guittiarez)*

Further evidence for a higher defect concentration in non-HGTSL samples is obtained by comparing the reverse bias current-voltage characteristics for the two sets of devices, as shown in Fig. 3.11. Over a voltage range from -10 to -35 V the leakage current in the HGTSL devices (red lines) is between two and three orders of magnitude lower, than that of the non-HGTSL devices (black lines).

However it is interesting to note that the leakage current of the HGTSL devices is still greater than that of a reference InGaAs QW laser device. This difference, which is at least 1~2 orders of magnitude, with the characteristics of the QW laser being set by the noise floor of the system, suggests that a low density of

defects remains in the HGTSL structures[35]. These may remain undetected at densities ~10^3 cm^{-1} due to the limited area sampled by cross – sectional TEM. The leakage current increases with layer number, consistent with structural studies which show a higher density of defects in the 5-layer non-HGTSL samples than in the corresponding 3-layer samples.

Although the HGTSL process effectively reduces the proportion of defective QDs in the ensemble, it has little effect on the optical properties of the remaining (coherent) QDs. Fig. 3.12 compares the normalised RT EL, taken at 20 A/cm^2, of an HGTSL and non-HGTSL 3-layer mesa device, which is used to obtain the pure spontaneous emission. It is obvious that the spectral forms are very similar, with identical peak wavelengths (~1300 nm) and linewidths (~35 meV) and a difference of only 2 meV in the GS to ES1 separation.

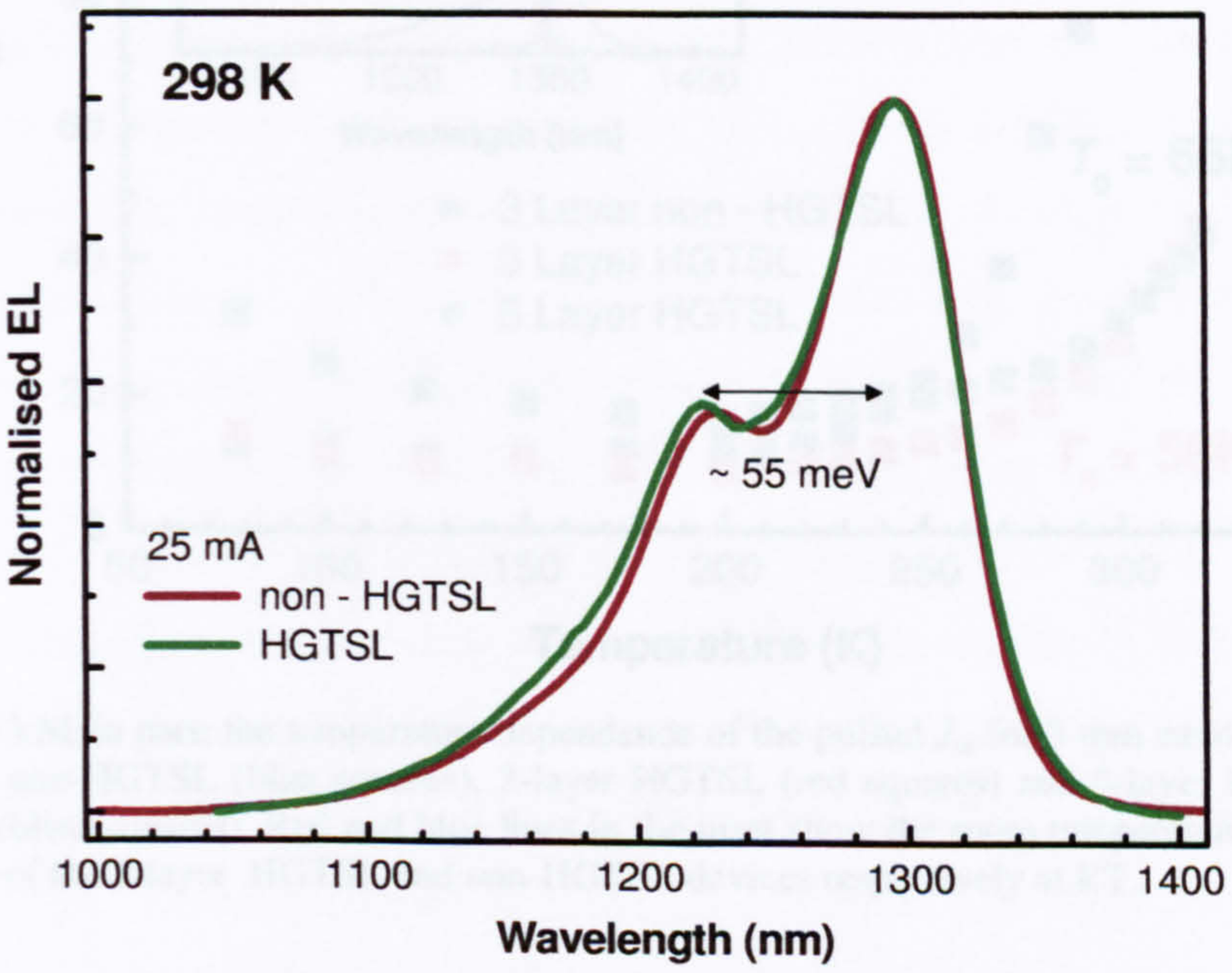

Fig. 3.12 Normalised RT EL spectra from non-HGTSL (maroon line) and HGTSL (olive line) 400 μm diameter mesa devices under 20 A/cm^2 injection.

3.4.2 Re-grown multilayer HGTSL DWELL lasers

3.4.2.1 Overview of laser characterisation results

The temperature dependence of J_{th} for a 5mm cavity of an HGTSL 3-layer structure is shown in Fig. 3.13 (red dots – Vn 58), along with the non-HGTSL device grown previously (blue dots – Vn 17). It is seen that, for T > 200 K, the temperature sensitivity of J_{th} is significantly improved by the incorporation of the HGTSLs.

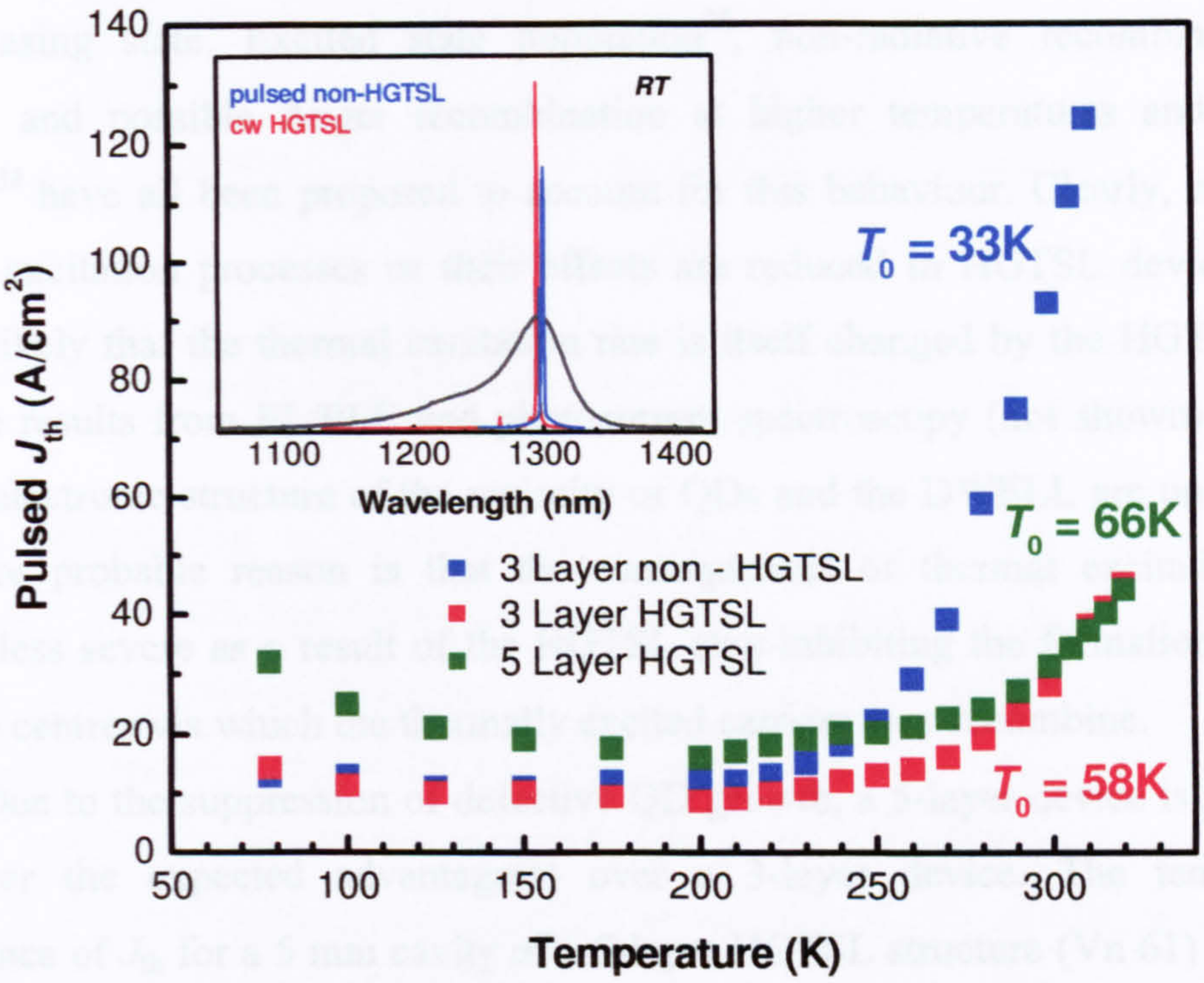

Fig. 3.13 Main part: the temperature dependence of the pulsed J_{th} for 3 mm cavities of a 3-layer non-HGTSL (blue squares), 3-layer HGTSL (red squares) and 5-layer HGTSL device (olive squares). Red and blue lines in the inset show the room temperature lasing spectra of the 3-layer HGTSL and non-HGTSL devices respectively at RT.

The 'Characteristic Temperature' (T_0) is a phenomenological parameter describing the temperature dependence of J_{th} in a semiconductor laser. It is defined by:

$$J_{th} = J_{th,0}\, e^{T/T_0}$$

where $J_{th,\,0}$ is a constant, T is the temperature and T_0 is the characteristic temperature. Clearly for J_{th} to be independent of T, T_0 must have a value of infinity – as predicted for ideal QD lasers. When J_{th} is not independent of T, as is always the case practically, the determined value of T_0 is generally dependent on the

temperature range over which the fit to the above equation is performed. For example, in all of the following results for HGTSL devices, a negative T_0 is found for temperatures between 78 and 200 K. At high temperatures the T_0 of the 3-layer HGTSL structure (Vn 58) is almost twice that of the 3-layer non-HGTSL structure (Vn 17) over the range $250 < T < 320$ K, with the RT J_{th} being reduced by more than a factor of four (decreasing from 130 to 31 A/cm^2) when the HGTSL step is included in the structure. The relatively rapid increase in J_{th} observed above ~250 K is seen in nearly all QD lasers and has been attributed to the thermal excitation of carriers out of the lasing state. Excited state population[36], non-radiative recombination at defects[37] and possible Auger recombination at higher temperatures and current densities[38] have all been proposed to account for this behaviour. Clearly, either the intrinsic excitation processes or their effects are reduced in HGTSL devices. It is most unlikely that the thermal excitation rate is itself changed by the HGTSL step, since the results from EL/PLE and photocurrent spectroscopy (not shown) indicate that the electronic structure of the majority of QDs and the DWELL are unchanged. The more probable reason is that the consequences of thermal excitation have become less severe as a result of the HGTSL step inhibiting the formation of non-radiative centres via which the thermally excited carriers may recombine.

Due to the suppression of defective QD growth, a 5-layer device is now able to deliver the expected advantage(s) over a 3-layer device. The temperature dependence of J_{th} for a 5 mm cavity of a 5-layer HGTSL structure (Vn 61) is shown in Fig. 3.13 (olive symbols). For temperatures below RT, J_{th} is larger than that for the HGTSL 3-layer structure, reflecting the increased transparency current density of the 5-layer structure. However above RT, the J_{th} - temperature sensitivity is slightly reduced in the 5-layer device, as reflected by the increase in T_0 from 58 to 66K, possibly due to the higher material (and therefore modal) gain of the 5-layer device.

Associated with the reduced temperature sensitivity of J_{th} in the HGTSL structures there should be an improvement in the performance of shorter cavity devices. For example, a 2 mm cavity of a 3-layer HGTSL structure (Vn 58) lases cw from the GS for temperatures up to 250 K, whereas the 5-layer counterpart (Vn 61) is able to operate up to 320 K with a cavity of 1.5 mm, exhibiting a cw $J_{th} = 108$ A/cm^2 at 320K (see Fig. 3.14).

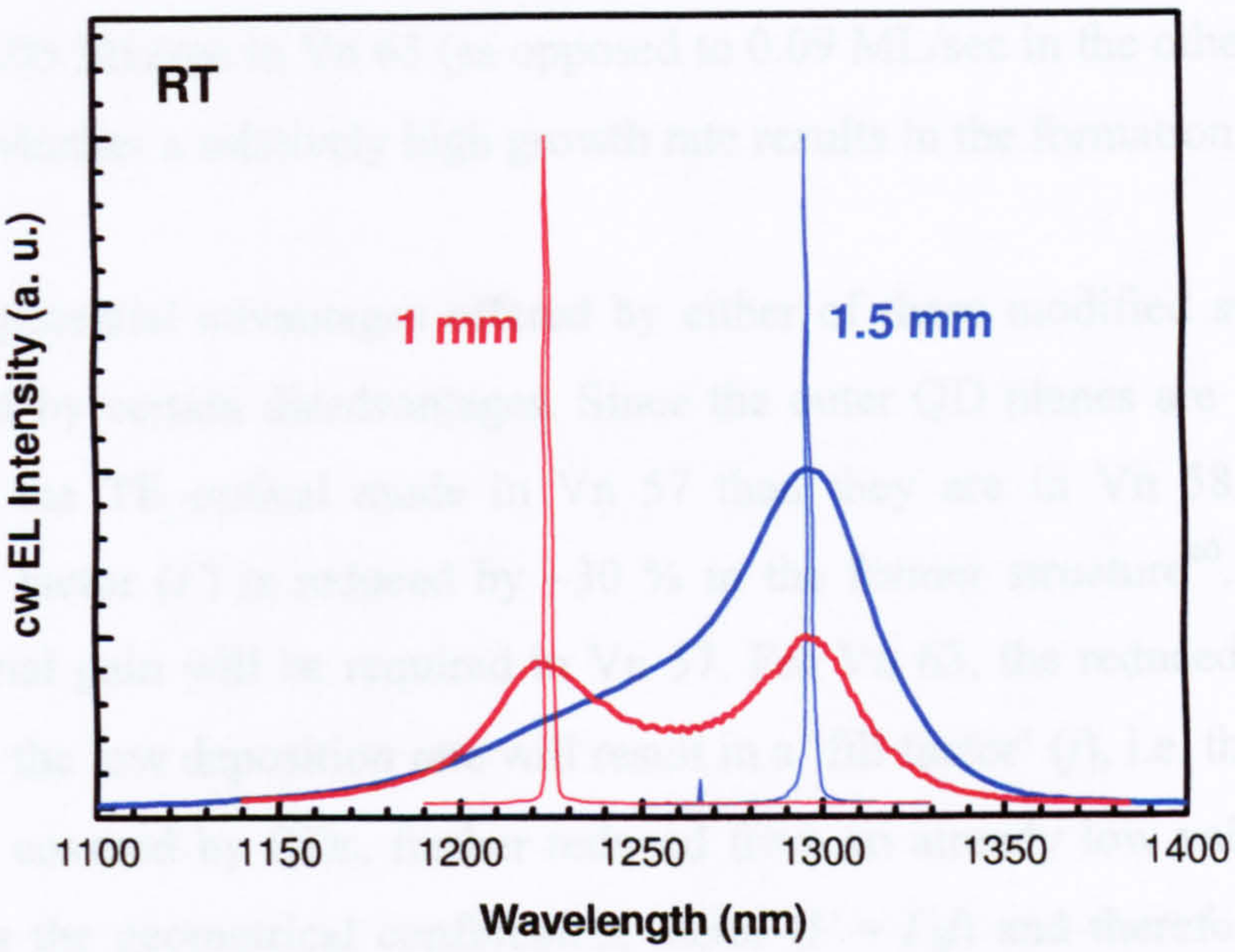

Fig. 3.14 Sub threshold EL (thick lines) and lasing spectra (thin lines) taken from a 1 mm cavity (red lines) and 1.5 mm cavity (blue lines) of a 5-layer HGTSL device (Vn 61).

A difference in the internal optical mode loss (α_i) in 5 layer structures with and without HGTSLs has been confirmed directly. This may be expected, since defective QDs can act as scattering centres, reducing the coherence of the optical mode. Measurements performed at Cardiff University derive the passive loss from an undriven section of a segmented-contact device. These reveal that α_i is reduced from 15 cm^{-1} to 3.5 cm^{-1} with the introduction of the HGTSLs[39]. Furthermore, these measurements allow the cavity length at which the lasing transition switches from the GS to the first excited state (ES1) to be calculated. In the 5-layer HGTSL device at 300K, the maximum GS net modal gain ($G-\alpha_i$) is ~8 cm^{-1}, corresponding to the highest sustainable mirror loss before the lasing transition switches to ES1. A cleaved cavity of 1.5 mm has this mirror loss, corresponding to the length where the switch is seen in the present devices (see Fig. 3.14).

Also grown as part of the HGTSL set of samples were two devices that had some modification to the basic structure. Vn 57 is another 3-layer structure, like Vn 58 except that the spacer layer thickness had been increased to 70 nm, and therefore 55 nm rather than 35 nm of GaAs was grown at 580 °C in the HGTSL step. This increased thickness will reduce any existing interactions between the QD planes, which may help to improve coherent QD growth and the resulting device performance. Vn 63 is a 5-layer structure, identical in design to Vn 61 but with QDs

formed at a lower deposition rate, and therefore a lower density. The QDs were grown at ~ 0.05 ML/sec in Vn 63 (as opposed to 0.09 ML/sec in the other structures) to ascertain whether a relatively high growth rate results in the formation of defective QDs.

Any potential advantages offered by either of these modified structures are compromised by certain disadvantages. Since the outer QD planes are further from the peak of the TE optical mode in Vn 57 than they are in Vn 58, the optical confinement factor (Γ) is reduced by ~30 % in the former structure[40]. Therefore a higher material gain will be required in Vn 57. For Vn 63, the reduced QD density produced by the low deposition rate will result in a 'fill factor' (f), i.e. the percentage of the plane covered by QDs, further reduced from an already low value of ~10%. This reduces the geometrical confinement factor ($\Gamma = \Gamma_z f$) and therefore the modal gain. Again, a higher material gain is required in Vn 63.

Fig. 3.15 shows the temperature dependence of the pulsed J_{th} for a 3 mm cavity of each of the four new HGTSL samples. Each structure displays a region of negative T_0 between 78 and 200 K – the logarithmic scale used to plot J_{th} emphasises this behaviour. Such behaviour is not uncommon in QD lasers and has been attributed to changes in either the carrier distribution within the ensemble[41]or the energetic coupling of the QD states mediated by their homogeneous broadening[42]. Measurements of the spontaneous emission performed on mesas fabricated from these samples provide evidence supporting the carrier redistribution model. These results will be presented in section 3.5.

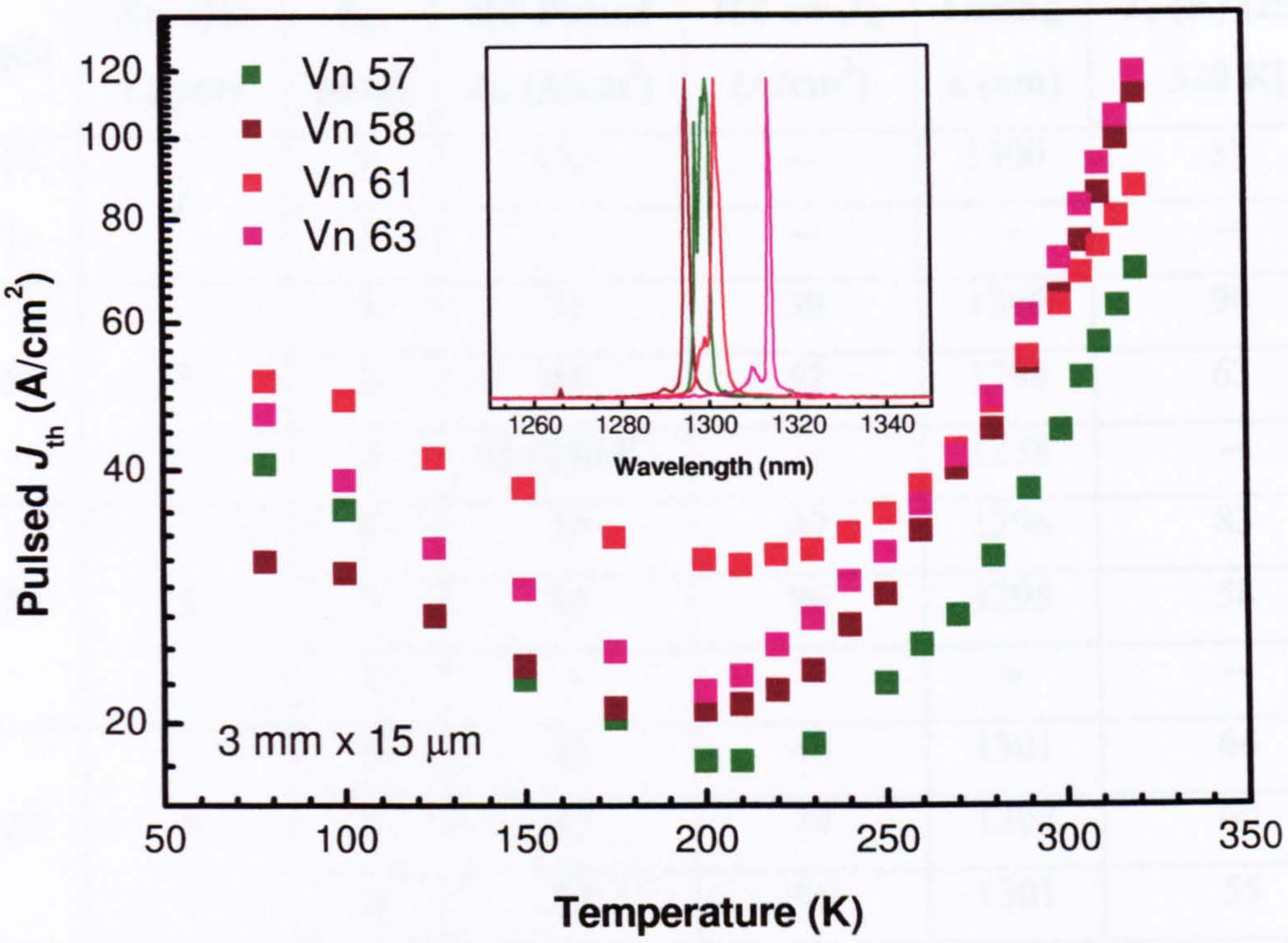

Fig. 3.15. The temperature dependence of the pulsed J_{th} for 3 mm cavity length, multilayer HGTSL structures.

Ultra low pulsed and cw J_{th}s are recorded at 299 K (RT) for all devices, with Vn 57 having the lowest pulsed J_{th} (44 A/cm^2). The cw J_{th}s and T_0s are listed for 5, 3 and 2 mm cavity lengths of each structure in Table 3.16. Shown in the inset of Fig 3.15 are lasing spectra taken at 1.1 x J_{th} at 299K from the 3 mm cavities. The emission occurs at 1298, 1295 and 1302 nm for Vn 57, Vn 58 and Vn 61 respectively. For Vn 63, the lasing is at the slightly longer wavelength of 1315 nm, this is most likely the result of the larger Indium rich QDs in this sample, a result of the reduced growth rate[43]. The spectral properties of this sample will be discussed further in section 3.5 of this chapter. In the sub-sections that follow, the laser characteristics of each sample will discussed in greater detail.

Sample	No. QD Layers	L_C (mm)	RT Pulsed J_{th} (A/cm^2)	RT cw J_{th} (A/cm^2)	Lasing λ (nm)	T_0 (K) [250-320 K]
Vn 17 (B)	3	5	135	--	1300	33
		3	--	--	--	--
Vn 57	3	5	31	30	1306	90
		3	44	52	1298	63
		2	92 (290 K)	--	1238	--
Vn 58	3	5	39	47	1296	83
		3	64	86	1295	58
		2	--	--	--	--
Vn 61	5	5	31	46	1301	66
		3	63	74	1303	60
		2	82	96	1301	55
Vn 63	5	5	52	61	1316	55
		3	71	93	1315	47
		2	162	232	1313	37

Fig. 3.16 Laser characteristics for 5, 3 and 2 mm cavity length devices fabricated from the multilayer HGTSL structures.

3.4.2.2 3-Layer HGTSL structure (70 nm spacer layers): Vn 57

Despite the very low pulsed and cw J_{th}s for the longer cavities, and hence excellent material quality, the temperature sensitivity of J_{th} is strongly dependent on the cavity length. The reduction of T_0 with decreasing cavity length is caused by the population of QD excited states[36]. In order to reach the increased gain required for shorter devices, higher injection current densities are required. As the injection quasi-Fermi level is raised towards the excited states of the QDs, a combination of non-complete GS population inversion and the greater degeneracy of the excited state produce a GS gain that saturates below the threshold value, resulting in the possible switching of the lasing state to the ES1 transition. This is seen in the 2 mm cavity for temperatures above 290 K. The lasing spectra for this sample (and others in this series) show a number of features that are unique to QD lasers.

Fig. 3.17 shows spectra from a 2 mm cavity of Vn 57 at 290 K, recorded at different current densities. Just above threshold (1.05 x J_{th}), lasing occurs at a wavelength (λ_s) 20 meV shorter than the peak of the spontaneous emission. However, spontaneous emission is still seen from the peak of the GS (λ_1) and from the emerging first excited state (λ_2). Clearly the carrier density has not clamped at this injection level, and on increasing the current further (to 1.2 x J_{th}), the lasing switches to pure first excited state lasing, with no emission observed at either λ_s or λ_1. The energy separation between λ_1 and λ_2 is ~ 45 meV.

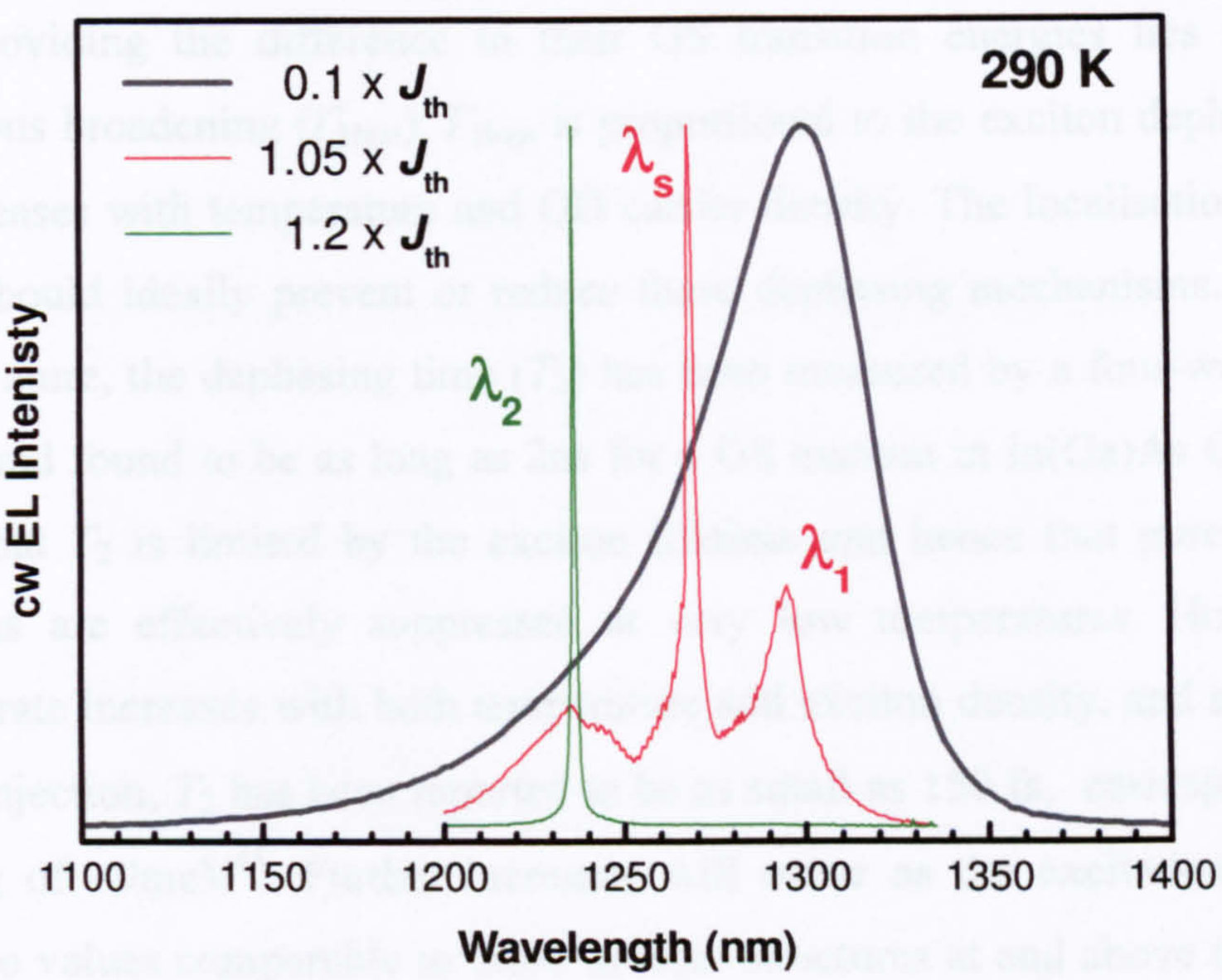

Fig. 3.17 Normalised RT lasing spectra (red and olive lines) and spontaneous emission from a 2mm cavity of Vn 57.

The origin of the intermediate-state lasing at λ_s is not totally clear. It will be shown in section 3.5 that the spontaneous emission properties of all of the samples in this series are characteristic of a bimodal QD size distribution. Therefore, it is possible that this inhomogeneity has an effect on the lasing properties. One possible explanation is that the GS gain of a sub-set of smaller, higher energy QDs, centred at λ_s, is able to exceed that of the main group of longer wavelength QDs at λ_1. As has just been mentioned, lasing from shorter cavities requires higher injection levels due to the larger mirror losses. Such injection raises the quasi-Fermi level higher into the conduction 'band' of the ensemble and may enable a significant proportion of smaller QDs to achieve population inversion and therefore contribute gain at a higher

energy. With an increase in injection current, the effect of gain saturation serves to reduce the differential gain at λ_l and so the emission at λ_s becomes dominant (see 1.05 x J_{th}). The energy difference between the peak emissions of these two sub-sets of QDs (λ_s-λ_l) is ~ 20 meV. Although the energetic separation of the GS spontaneous emissions of the two subsets of QDs is around twice this value (see section 3.5), their respective gain maxima will each be affected by a homogeneous broadening of ~ 5-10 meV, which may be effective in reducing the *effective* energy separation of the two sub-sets.

Individual, spatially isolated QDs of different GS energies may be able to interact, providing the difference in their GS transition energies lies within the homogeneous broadening (Γ_{Hom}). Γ_{Hom} is proportional to the exciton dephasing rate, which increases with temperature and QD carrier density. The localisation provided by a QD should ideally prevent or reduce these dephasing mechanisms. Indeed, at low temperature, the dephasing time (T_2) has been measured by a four-wave mixing technique and found to be as long as 2ns for a GS exciton in In(Ga)As QDs[44]. This indicates that T_2 is limited by the exciton lifetime and hence that pure dephasing mechanisms are effectively suppressed at very low temperatures. However, the dephasing rate increases with both temperature and exciton density, and at RT under electrical injection, T_2 has been reported to be as small as 150 fs, corresponding to a broadening of ~9meV[45]. Further increases will occur as the excitation density is increased to values comparable to those in laser structures at and above threshold. It is this effect that is believed to lead to the commonly observed single mode lasing observed at RT[46] . The separation of lasing modes in the multimode spectra of QD devices has been shown to correlate with the calculated homogeneous broadening at a given temperature, for example lasing peaks separated by 16-19 meV have been observed at room temperature[47]. This value corresponds closely with λ_s-λ_l in Fig. 3.17 and so an interaction mediated by homogeneous broadening seems reasonable in order to explain this intermediate-state lasing.

This interpretation is also consistent with the 8 meV blueshift in the room temperature lasing wavelength as the cavity length decreases from 5 to 3 mm (shown in Fig. 3.18). By increasing the threshold gain and corresponding injection level, a greater proportion of smaller, higher energy QDs are inverted, producing an overall blueshift in the gain peak. If the gain profile is relatively flat, as has been suggested

in QD lasers[48], then the lasing energy will depend sensitively on the homogeneous broadening.

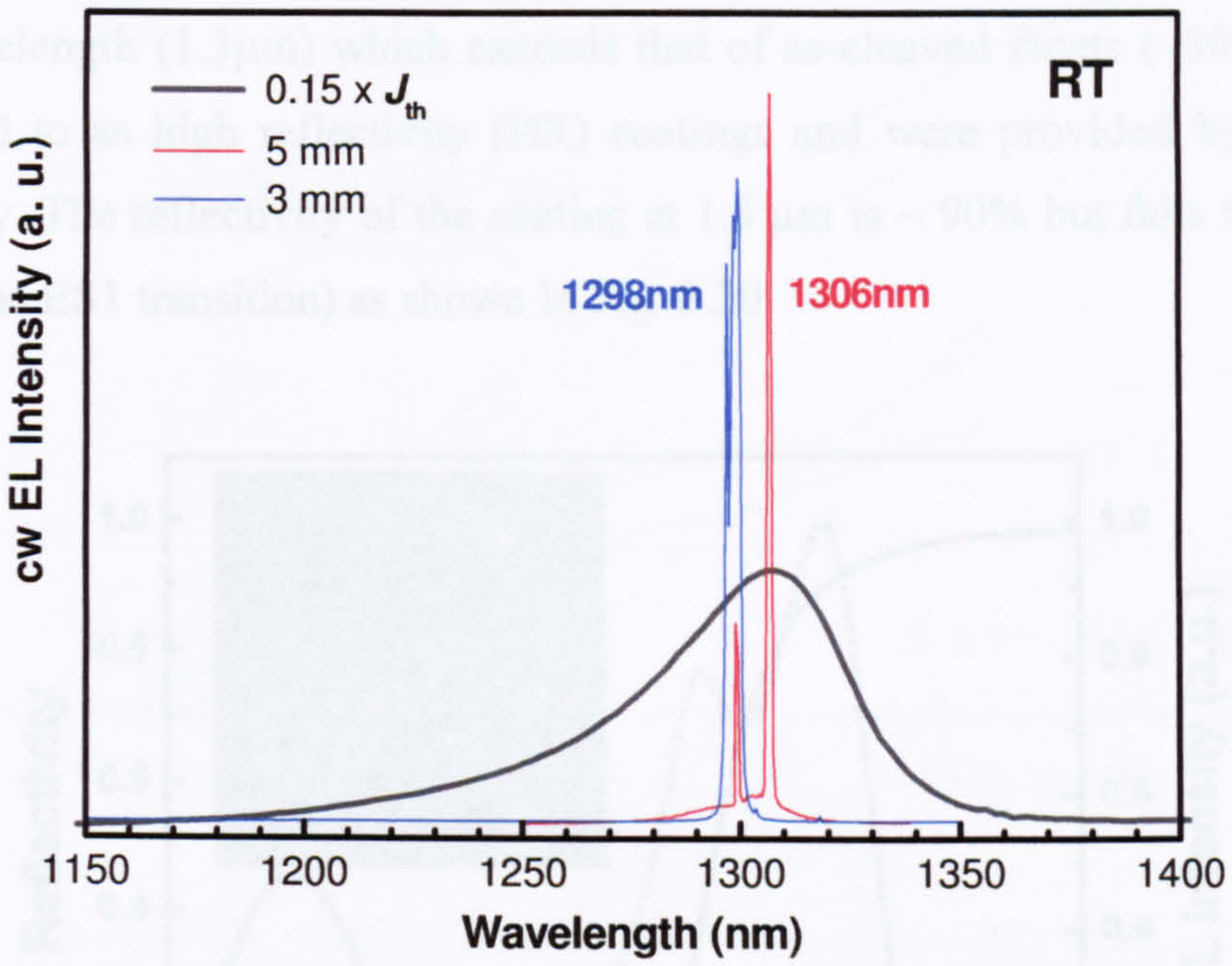

Fig. 3.18 RT spontaneous emission (black line) and cw lasing spectra of a 3 (blue line) and 5 (red line) mm cavity of Vn 57.

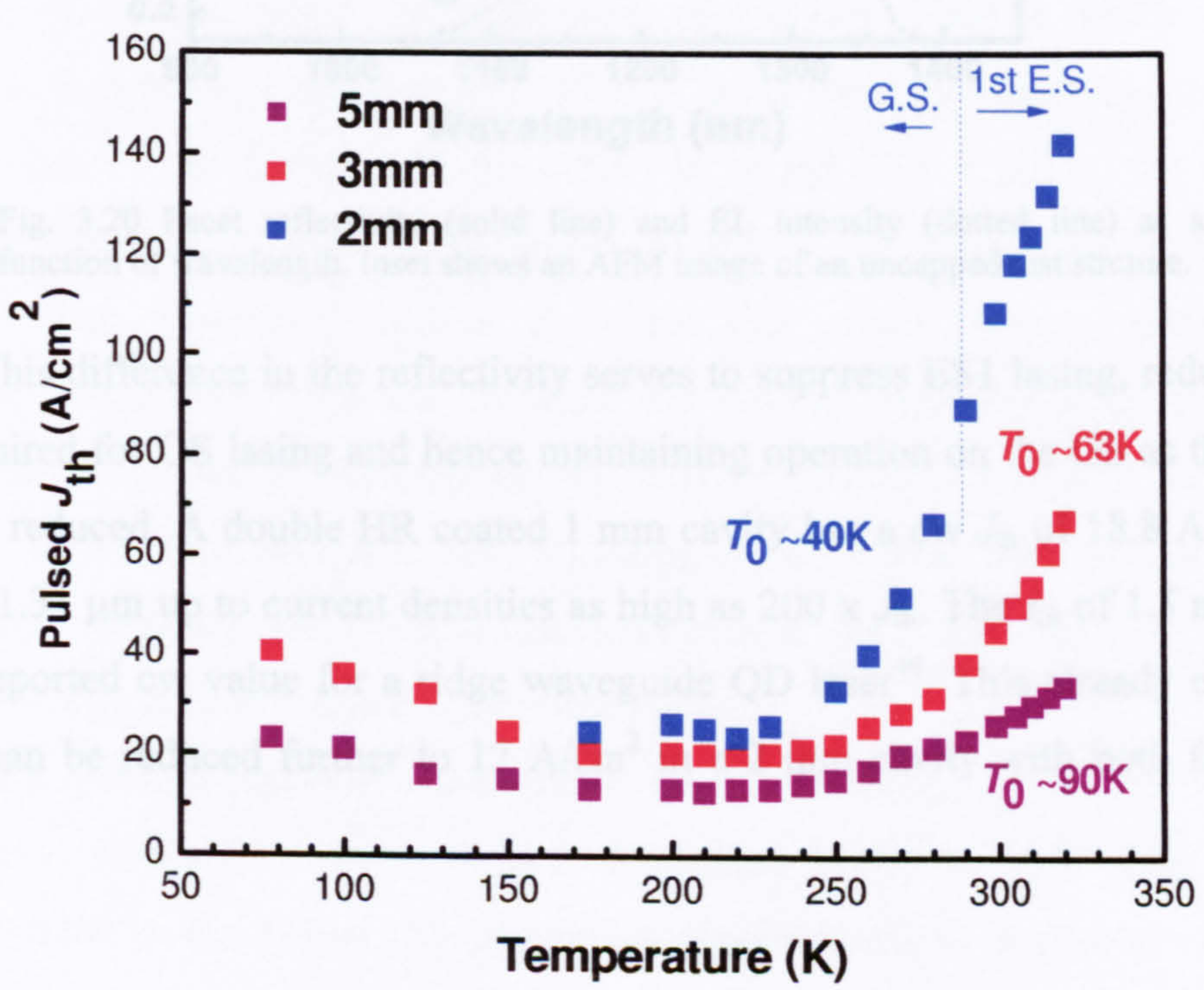

Fig. 3.19. The temperature dependence of the pulsed J_{th}s for 5, 3 and 2 mm cavity length devices of Vn 57.

Devices with cavity lengths shorter than 2mm demonstrated GS lasing at room temperature provided one or both facets were multilayer coated with Si-SiO_2, producing wavelength selective reflectivity with a peak reflectivity at the intended lasing wavelength (1.3μm) which exceeds that of as-cleaved facets (~30%) . These are referred to as high reflectivity (HR) coatings and were provided by Bookham Technology. The reflectivity of the coating at 1.3 μm is ~ 90% but falls to ~ 40% at 1.22 μm (the ES1 transition) as shown in Fig. 3.20

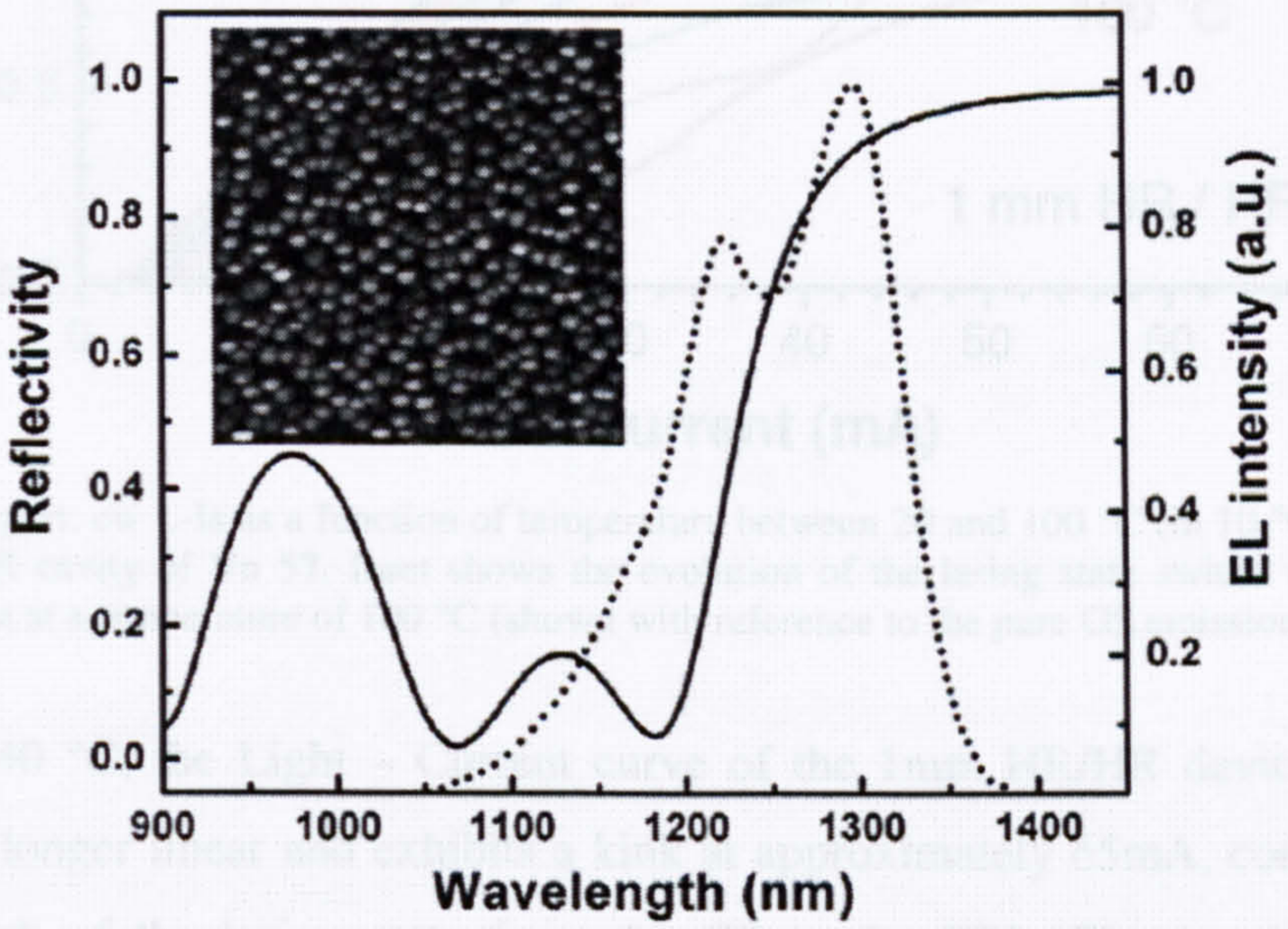

Fig. 3.20 Facet reflectivity (solid line) and EL intensity (dotted line) as a function of wavelength. Inset shows an AFM image of an uncapped test strcture.

This difference in the reflectivity serves to suppress ES1 lasing, reducing the gain required for GS lasing and hence maintaining operation on the GS as the cavity length is reduced. A double HR coated 1 mm cavity has a cw J_{th} of 18.8 A/cm^2 and emits at 1.31 μm up to current densities as high as 200 x J_{th}. The I_{th} of 1.5 mA is the lowest reported cw value for a ridge waveguide QD laser[49]. This already extremely low J_{th} can be reduced further to 17 A/cm^2 in a 2 mm cavity with both facets HR coated.

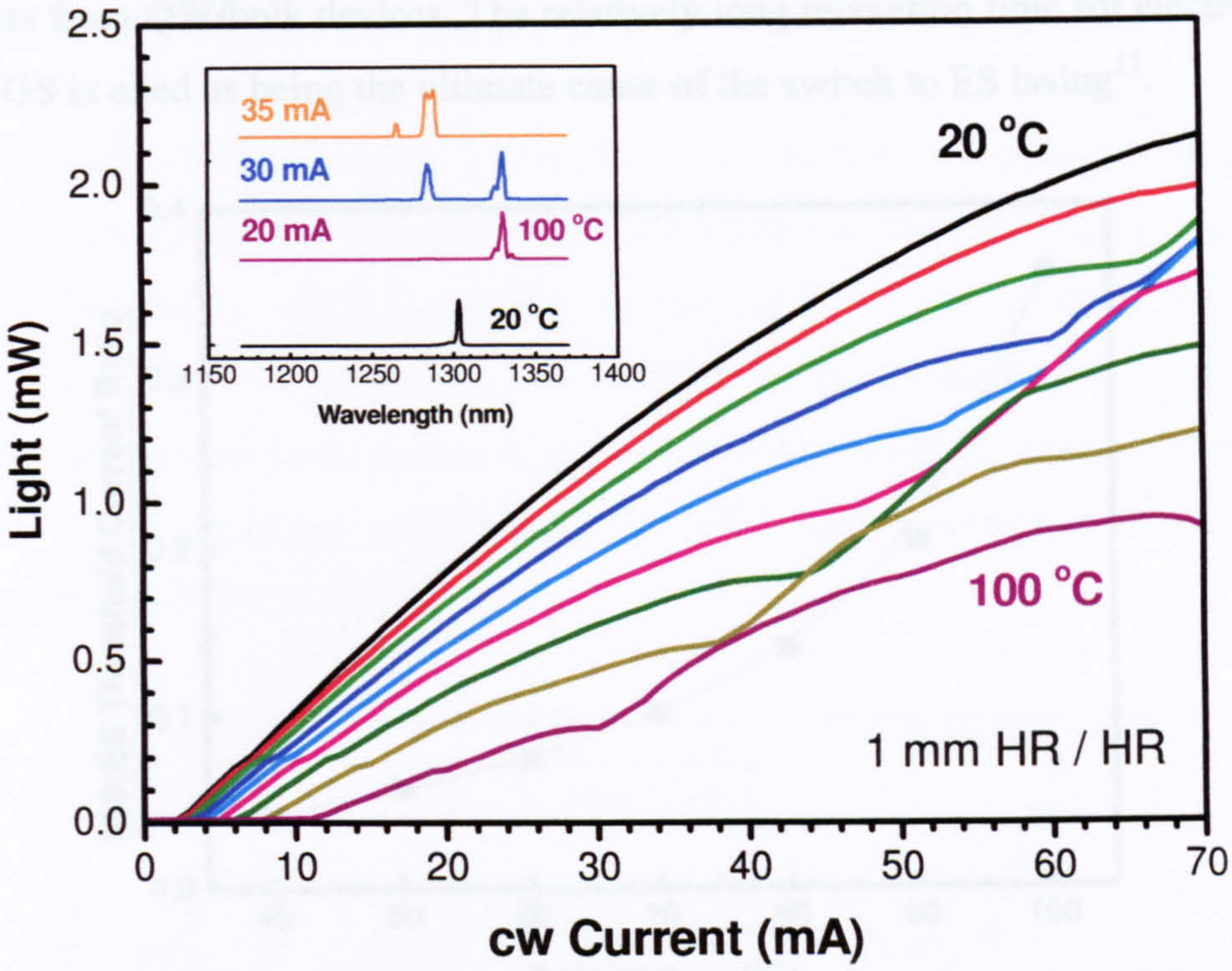

Fig. 3.21 Main part: cw L-Is as a function of temperature between 20 and 100 °C (in 10 °C intervals) for a 1 mm HR/HR cavity of Vn 57. Inset shows the evolution of the lasing state switch with increasing injection current at a temperature of 100 °C (shown with reference to the pure GS emission at 20 °C).

By 40 °C, the Light – Current curve of the 1mm HR/HR device (see Fig. 3.21) is no longer linear and exhibits a kink at approximately 65mA, corresponding to the switch of the lasing state from the GS to the ES1. Clearly, the effect of increasing temperature reduces the ability of the carrier density to clamp above threshold. The 'threshold' current at which this switch occurs reduces with increasing temperature. Spectra showing the current dependence of the lasing wavelength are shown in the inset of Fig. 3.21 for a temperature of 100 °C. At a particular current (e.g. 30 mA at 100 °C) lasing emission from both the GS and ES1 occurs simultaneously. The GS:ES1 threshold current ratio, obtained from Fig. 3.21, is plotted in Fig. 3.22 as a function of temperature.

In a previous report of simultaneous dual-state lasing, the GS:ES1 threshold current ratio was seen to increase with decreasing cavity length[50]. This effect is directly related to the higher GS population above threshold in shorter cavities, a result of the higher threshold gain. The increase in GS occupation causes a corresponding increase in the rate at which the ES1 population builds up with injected carrier density. Such behaviour is a clear manifestation of the state-blocking effects that increase the effective capture/relaxation times into the GS, distinguishing

QD lasers from QW/bulk devices. The relatively long relaxation time for electrons to the QD GS is cited as being the ultimate cause of the switch to ES lasing[51].

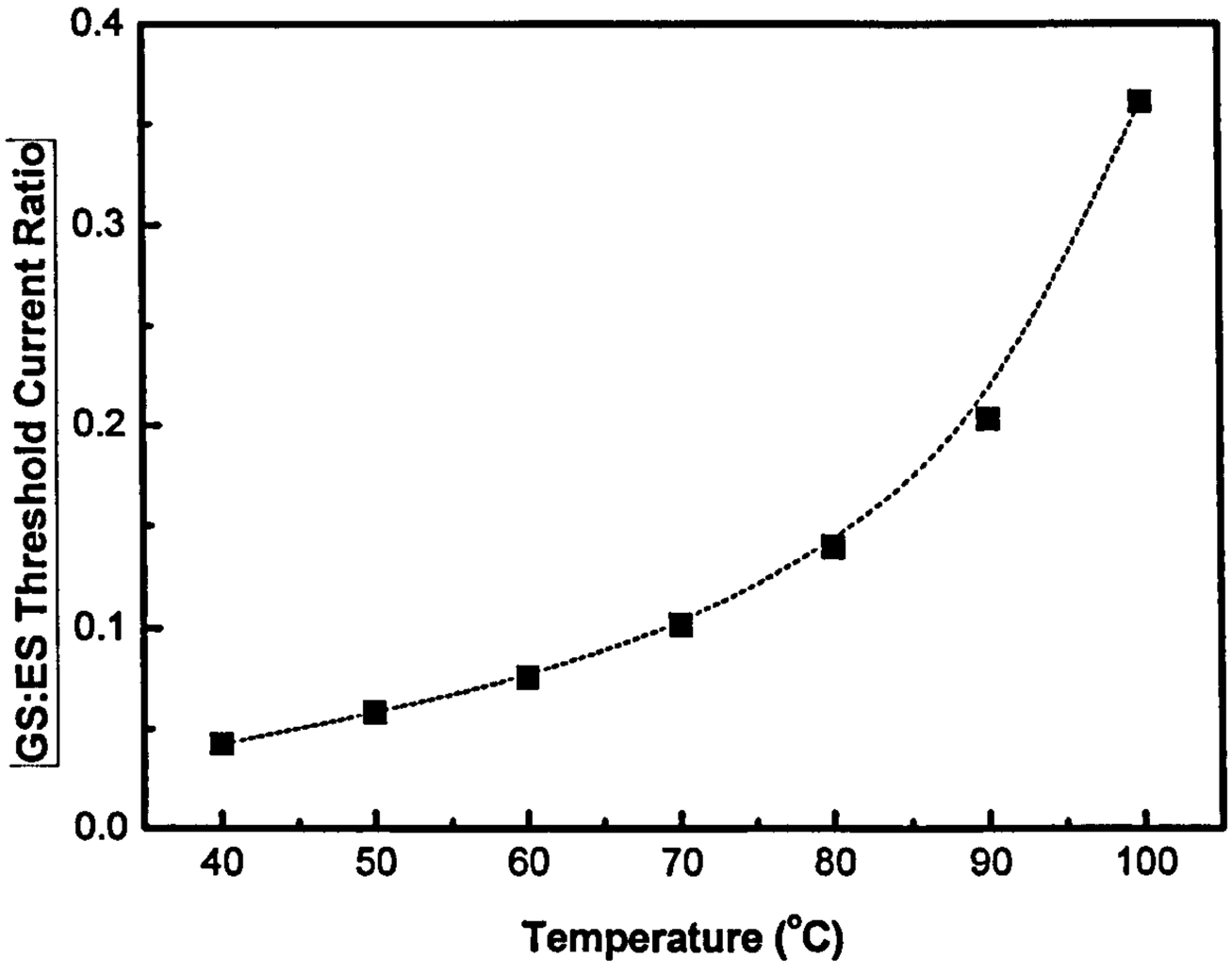

Fig. 3.22 GS:ES1 threshold current ratio between 40 and 100 °C for a 1 mm HR/HR cavity of Vn 57.

On inspection of Fig. 3.22, an increase in temperature has a similar effect to decreasing cavity length on the GS:ES1 threshold current ratio, but the underlying cause is somewhat different; as the temperature is increased, the quasi-Fermi level is raised further into the ES1 band of the QD ensemble due to the increased thermal energy of the carriers. In terms of the carrier dynamics within the QD, the increased thermal emission of carriers from the GS to the ES at higher temperatures represents an increase in their effective relaxation time to the GS.

This interpretation of the results shown in Figs. 3.21 and 3.22 is supported by the findings of a rate equation model which predicts a more effective clamping of the GS carrier population above threshold when both a larger GS Γ_{Hom} and faster carrier capture/escape times are assumed[51]. Respectively, the two effects serve to increase the interaction between energetically distinct QDs and the carrier equilibration rate within the ensemble.

3.4.2.3 3-Layer HGTSL structure (50 nm spacer layers): Vn 58

The other 3-layer sample, Vn 58, shows a temperature dependence of J_{th} that is similar to its counterpart for comparable cavity lengths. The absolute J_{th}s are lower in Vn 57, but the T_0 values are slightly higher, by 5 and 7 K in the 3 and 5 mm devices respectively. Unfortunately, this similarity in the temperature dependence of J_{th} extends to the poor performance of short (< 2 mm) as-cleaved devices. In a 2 mm cavity of Vn 58, the lasing switches from the GS to the ES between 250 and 260 K (see inset of Fig. 3.23).

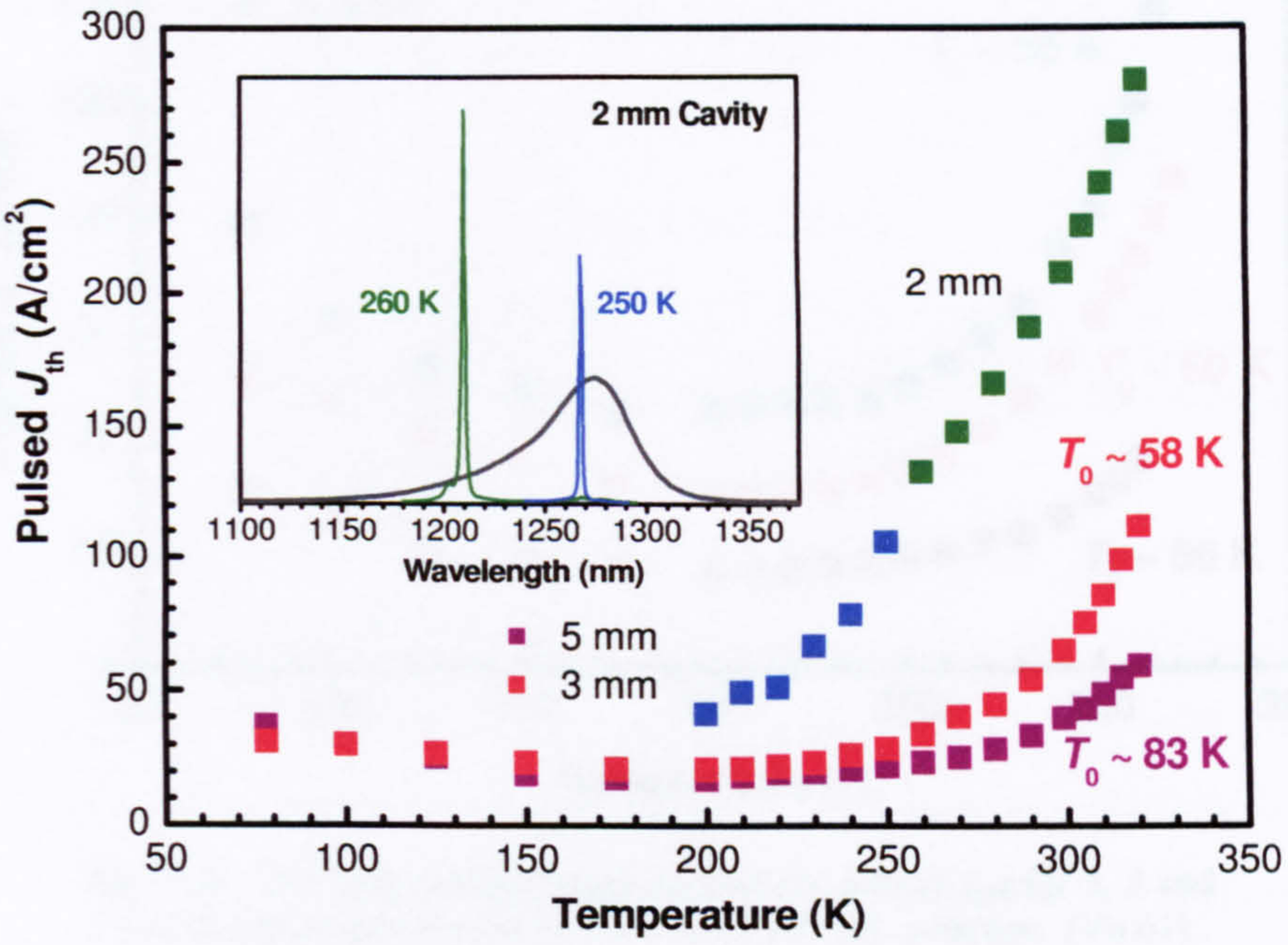

Fig. 3.23. Main part: the temperature dependence of the pulsed J_{th}s for 5, 3 and 2 mm cavity length devices of Vn 58. Inset shows the onset of excited state lasing above 250 K.

The slightly worse overall performance of the HGTSL structure with the *thinner* GaAs SLs separating the QD planes (Vn 58) is somewhat surprising, when its superior optical confinement factor is taken into account. A possible explanation would appear to be an increased effectiveness of the HGTSL process in a structure with thicker spacer layers. The validity of this explanation will be justified to some extent in chapter 4, section 4.2.

3.4.2.4 5-Layer HGTSL structure (50 nm spacer layers): Vn 61

Unlike the two previous 3-layer structures, a 2 mm cavity of this 5-layer version of Vn 58 is able to lase cw from the GS at room temperature. In addition, the T_0 is found to be less sensitive to cavity length (see Fig. 3.24). These features are a direct result of the increase in the saturated GS gain of the structure, due to the extra QD layers.

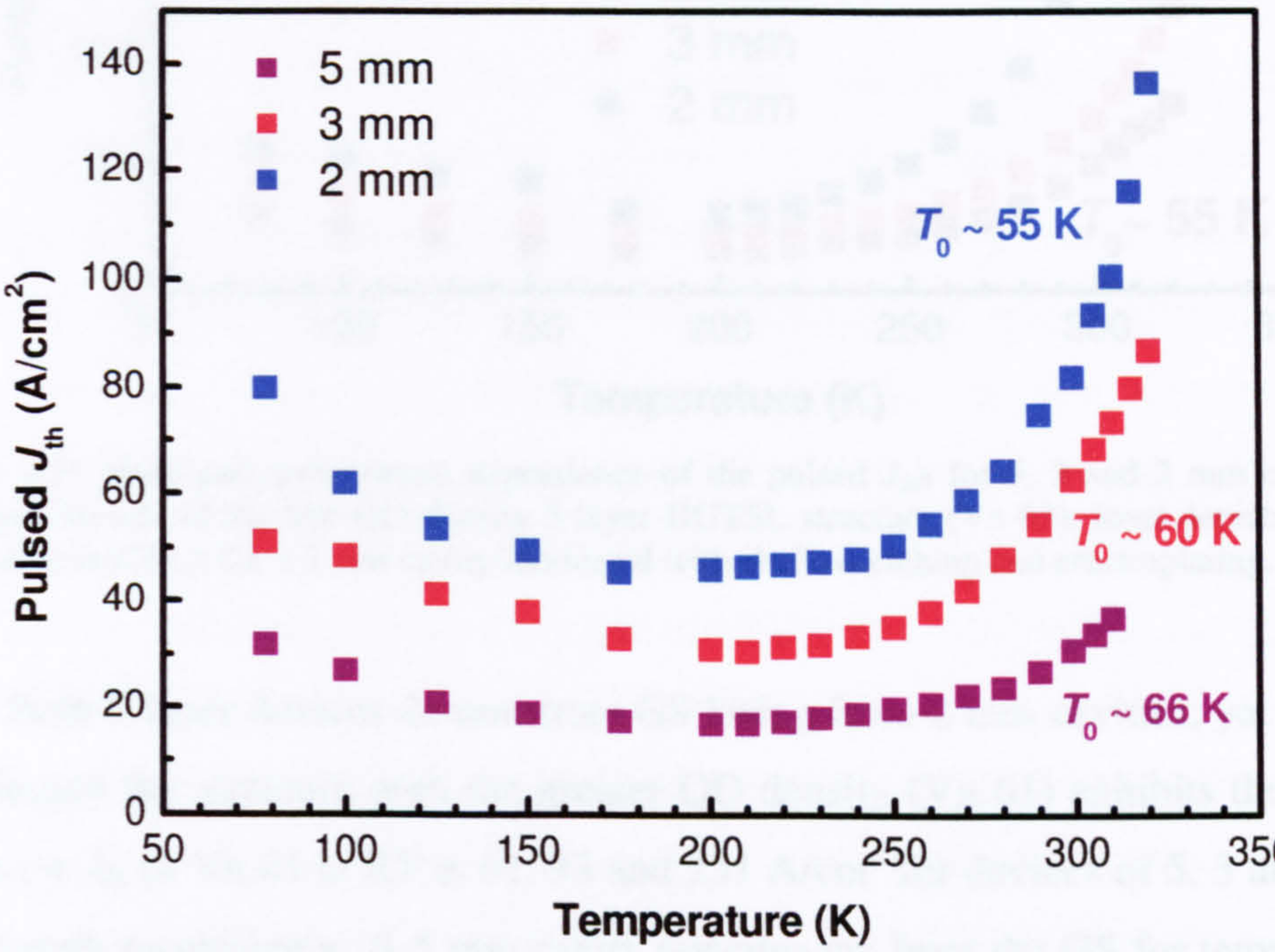

Fig. 3.24. The temperature dependence of the pulsed J_{th}s for 5, 3 and 2 mm cavity length devices of the 5-layer HGTSL structure. (Vn 61).

3.4.2.5 5-layer HGTSL structure (50 nm spacer layers) with a low QD density: Vn 63

By reducing the QD growth rate from 0.09 ML/s to 0.05 ML/s, the in-plane QD density could be decreased to ~2.5 x 10^{10} cm^{-2}, 1.6 times lower than that found in the other HGTSL structures Vn 57, 58 and 61. However, the laser characteristics of this structure are broadly similar to those of the structures with the higher QD density.

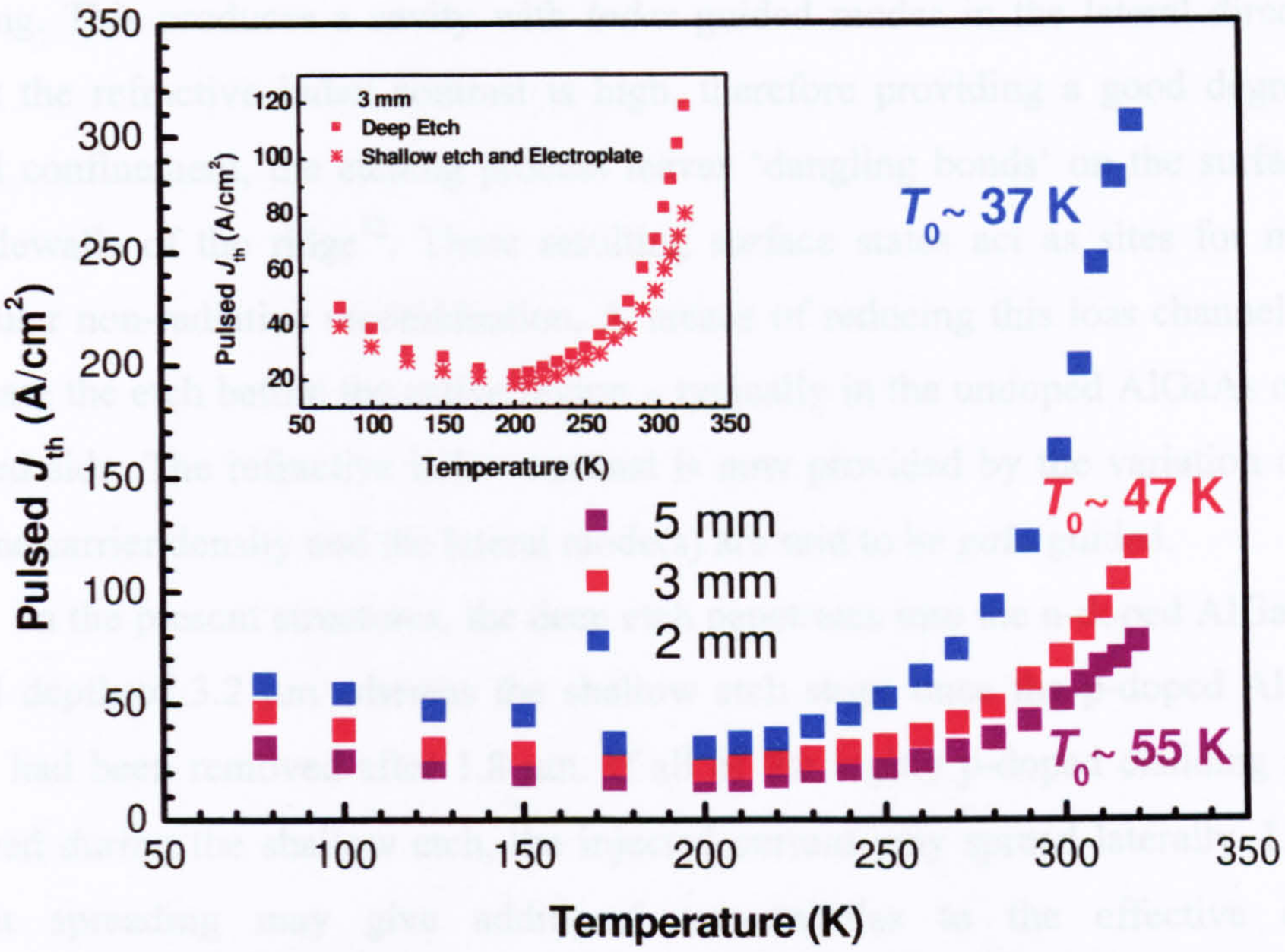

Fig. 3.25 Main par: temperature dependence of the pulsed J_{th}s for 5, 3 and 2 mm cavity length devices of the low QD density 5-layer HGTSL structure (Vn 63). Inset depicts this same dependence for a 3 mm cavity fabricated with shallow etching and electroplating.

Both 5-layer devices demonstrate GS lasing from 2 mm cavities, yet for each cavity length the structure with the greater QD density (Vn 61) exhibits the highest T_0. The cw J_{th} of Vn 61 at RT is 61, 93 and 231 A/cm^2 for devices of 5, 3 and 2 mm cavity length respectively. A 5 mm cavity operates cw from the GS for temperatures up to 85 °C. With the exception of the longer lasing wavelength, the relatively poorer performance of Vn 63, when compared to Vn 61, is probably a result of the reduced QD density producing a lower saturated GS gain. An additional cause that limits the available gain of this and the other samples in this series is the bimodal QD distribution, the effects of which will be discussed in section 3.5. It is immediately apparent that by reducing the QD density, no improvement is seen in the laser performance – in fact the opposite occurs. This observation provides confirmation that the higher QD densities found in the other HGTSL structures do not degrade the structure via the introduction of non-radiative centres. The inset of Fig. 3.25 compares the temperature dependence of the pulsed J_{th} for two 3 mm x 15 μm cavities of Vn 63 which differ only in the respective techniques used in the device fabrication. All the results presented so far are for devices with a deep etch step that passes through the active region, stopping in the n-type doped lower AlGaAs

cladding. This produces a cavity with *index* guided modes in the lateral direction. Whilst the refractive index contrast is high, therefore providing a good degree of optical confinement, the etching process leaves 'dangling bonds' on the surface of the sidewalls of the ridge[52]. These resulting surface states act as sites for mono-molecular non-radiative recombination. A means of reducing this loss channel is to terminate the etch before the active region – typically in the undoped AlGaAs on the p-doped side. The refractive index contrast is now provided by the variation of the in-plane carrier density and the lateral mode(s) are said to be *gain* guided.

In the present structures, the deep etch penetrates into the n-doped AlGaAs to a total depth of 3.2 μm whereas the shallow etch stops once the p-doped AlGaAs layers had been removed after 1.8 μm. If all of the highly p-doped cladding is not removed during the shallow etch, the injected current may spread laterally. Lateral current spreading may give additional uncertainties to the effective cavity dimensions. In addition, this current spreading may broaden the gain region, allowing indiscriminate lateral mode operation with consequently higher J_{th}[53].

Further improvements to the injection efficiency of the device can be made if thicker gold contact pads are used. Shallow etched ridges were selectively electroplated with 3 μm of gold, as opposed to the 250 nm applied by evaporation to the deep etched devices. These two alterations to the device fabrication reduce the losses even further, as reflected in the lower J_{th}s and their greater temperature stability in the re-processed device (see inset to Fig. 3.25). The change in the processing resulted in an increase of T_0 from 38 to 48 K. A more thorough study, conducted using temperatures up to 100 °C, attributes the enhanced performance to a combination of three factors: reduced optical and electrical loss from the etched ridge sidewalls and improved heat dissipation resulting from the use of thicker gold contacts[54].

3.5 Carrier redistribution effects in lasing and spontaneous emission characteristics of 1.3 μm In(Ga)As QD lasers

3.5.1 Bimodal QD ensembles

Fig. 3.26 shows EL at 78 K, recorded from mesa diodes at a low current density, where the carrier occupancy << 1 per QD. At this low temperature the

carriers populate the QDs randomly; hence for low injection levels the spectral distribution of the spontaneous emission spectrum represents the statistical distribution of QD shapes and sizes.

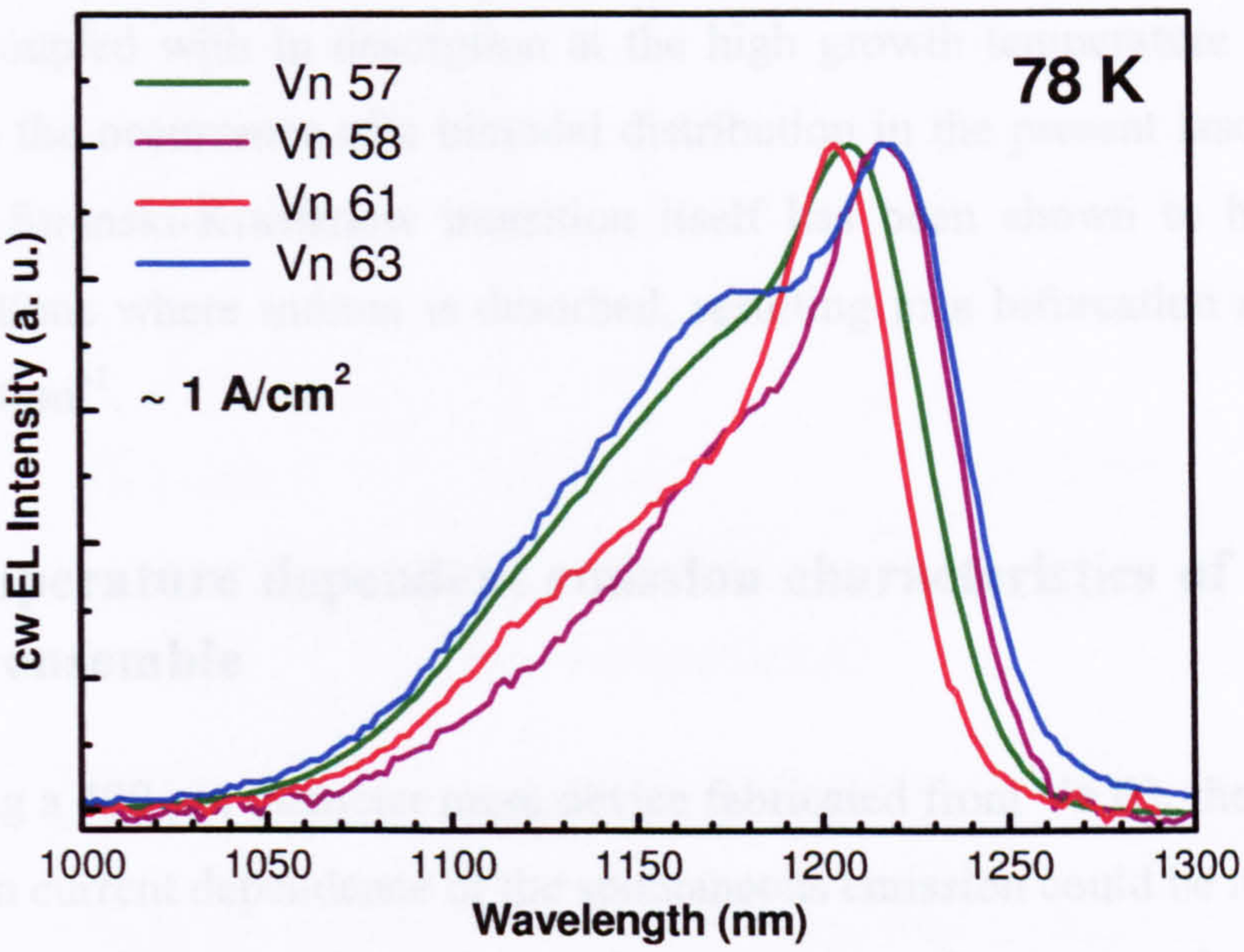

Fig. 3.26. Normalised, low temperature EL spectra of the HGTSL structures, obtained under low injection (~1 A/cm^2). The shoulder at ~1170 nm is a result of the bimodal QD size distribution.

These measurements are useful for assessing the uniformity of an ensemble of QDs. It can be assumed that, since the GaAs spacer layers are sufficiently thick in these samples ($\geq$ 50 nm), the uniformity of the QDs in successively grown layers is unaffected by this stacking process and that the variation in the QD size and shape exists mainly within the planes. The spectra of the four samples show similar features: broad emission (FWHM ~ 91 meV for Vn 63), with a peak between 1200 and 1217 nm and a shoulder at high energy centred at 1170 nm. This shoulder does not represent excited state recombination, as its intensity is independent of injection current. Instead it indicates the presence of a second subset of QDs having a Gaussian distribution peaked at higher energy. Collectively, the overall QD size distribution is said to be 'bimodal'. This wide distribution of GS energies leads to some interesting physics which is specific to QD systems. Commonly observed features such as quenching of the high energy shoulder and the interplay between the linewidths of each peak with increasing temperature[55] are seen in the present samples.

There is no single growth parameter that controls the development of a bimodal QD distribution, such a distribution has been observed to evolve as a function of InAs coverage[56, 57], substrate temperature[58] and post-growth annealing temperature[59]. As will be seen in chapter 4, section 4.4, the effects of post-growth annealing, coupled with In desorption at the high growth temperature of 510 °C[60] may explain the occurrence of a bimodal distribution in the present laser structures. Indeed, the Stranski-Krastanow transition itself has been shown to be reversible under conditions where indium is desorbed, resulting in a bifurcation of the island size distribution[61].

3.5.2 Temperature dependent emission characteristics of a bimodal QD ensemble

Using a 400 μm diameter mesa device fabricated from Vn 63, the temperature and injection current dependence of the spontaneous emission could be measured and related to the J_{th} of a 5 mm laser device fabricated from the same wafer. The current dependence of the spontaneous emission at 78 K confirms the bimodal nature of the QDs in this sample. Two features are observed at 1170 and 1215 nm, a ~40 meV separation, with a relative intensity which remains constant when the injection current is varied by two orders of magnitude (See Fig. 3.27a). This behaviour is consistent with the emission resulting from the GSs of two distinct subsets of QDs[62]. As the temperature is increased, the emission from the shorter wavelength subset of QDs is quenched and then at higher temperatures an excited state of the longer wavelength subset of QDs starts to emerge. This latter feature displays the expected increase in intensity with increasing current (Fig. 3.27 (b)). The separation between the peaks at high temperatures is ~58 meV, a typical sublevel splitting for 1.3 μm InAs QDs[63].

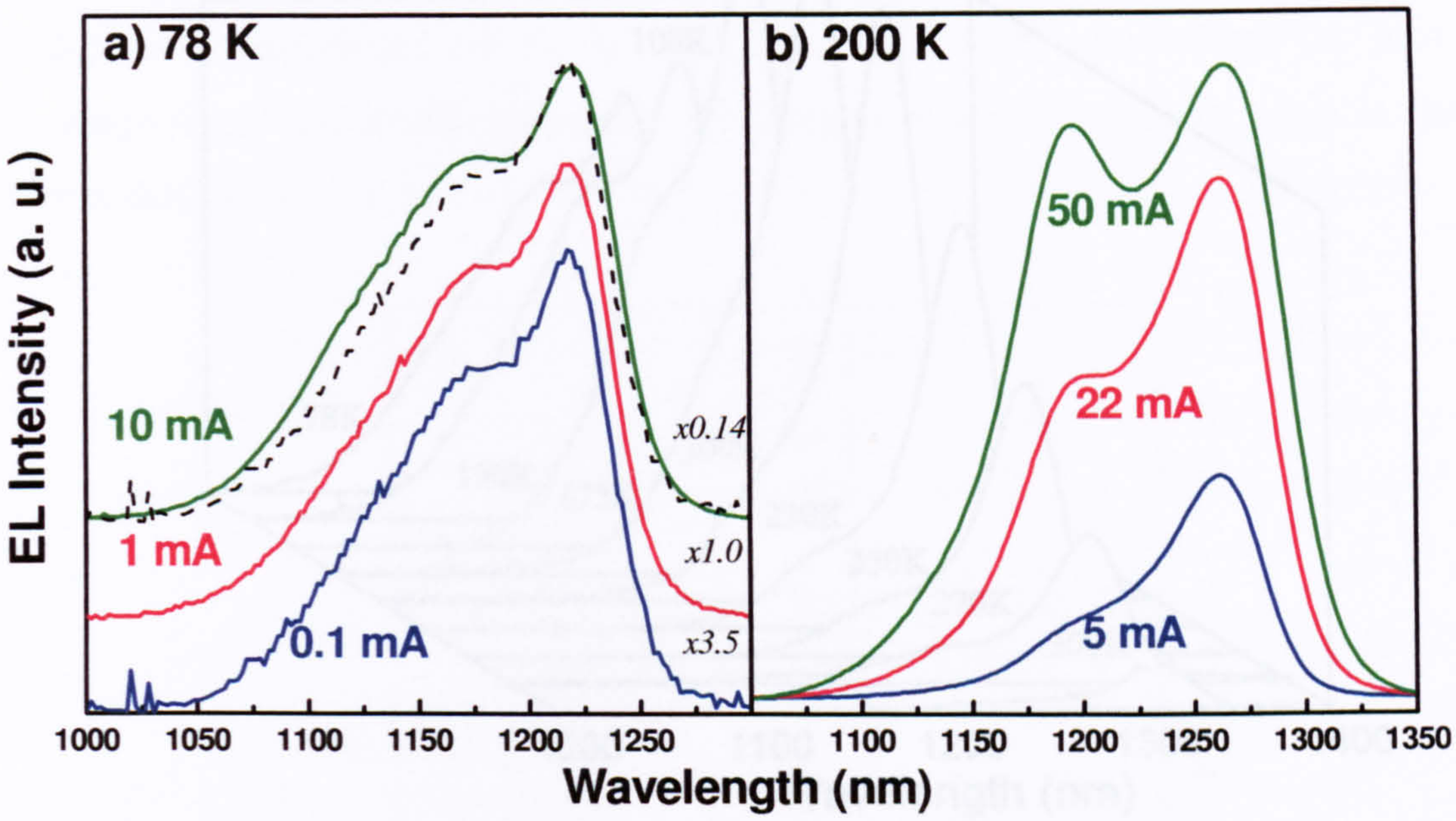

Fig. 3.27 (a) 77 K EL spectra of Vn 63, obtained under low injection conditions. Currents of 0.1, 1 and 10 mA correspond to current densities of 0.08, 0.8 and 8 A/cm^2. The spectral form of the emission is independent of current in this range. The dashed line is the 0.1 mA spectrum scaled and superimposed on the 10 mA spectra to show their very similar form. (b) 200 K EL showing clear filling of the first excited state as current is increased by an order of magnitude from 5 to 50 A/cm^2.

The temperature dependence of the bimodal QD emission is shown in more detail in Fig. 3.28. Between 78 and 175 K, the intensity of the peak at 1170 nm decreases with respect to the longer wavelength peak – the latter exhibiting an overall increase in intensity over this temperature range. This behaviour is consistent with the onset of a thermal equilibrium between carriers in different QDs and acts to redistribute carriers via the WL/InGaAs QW from smaller to larger QDs, thereby lowering the average GS exciton energy in the ensemble[64]. This increasing population of the large QDs has a pronounced effect on the performance of the laser device.

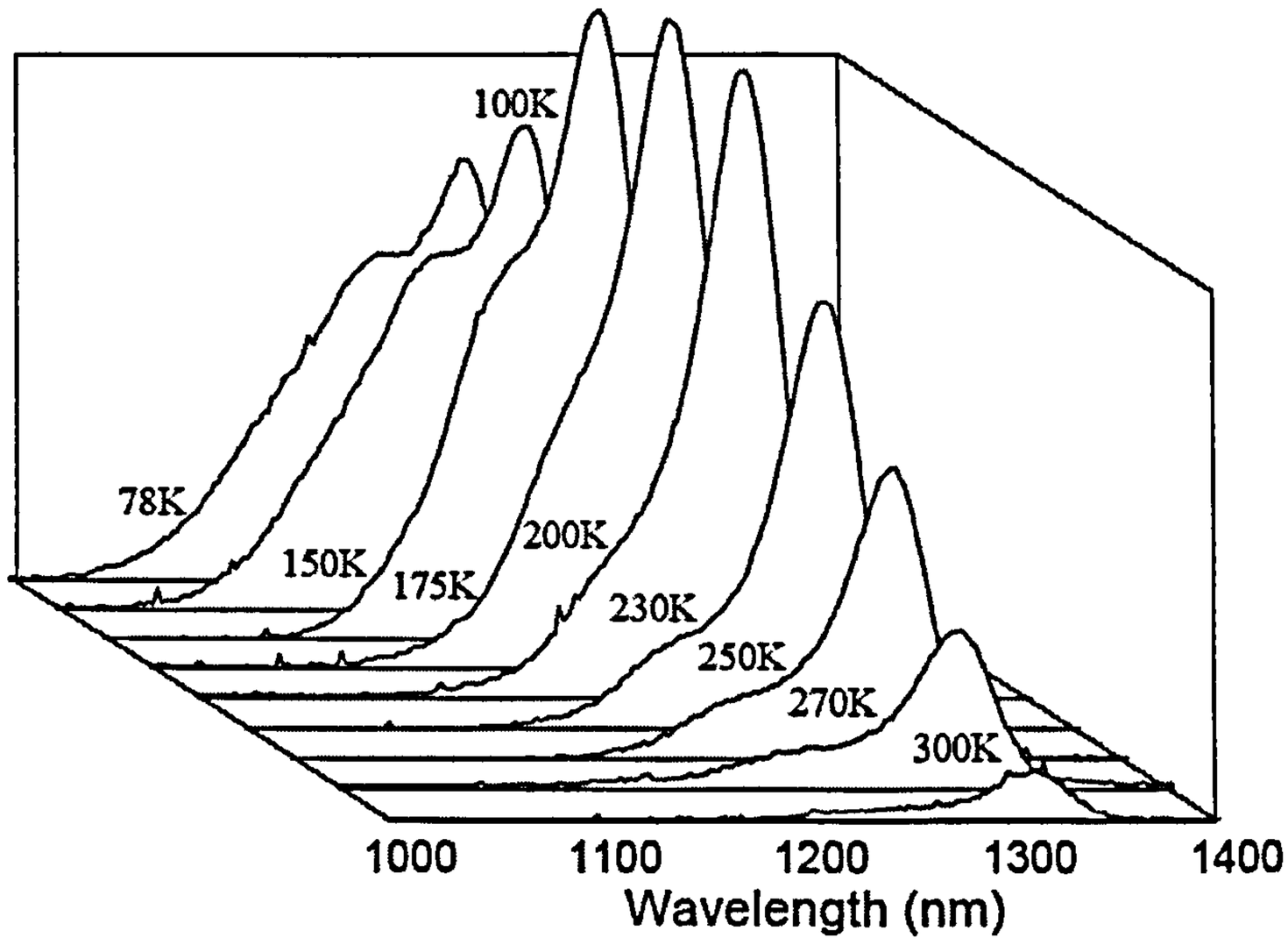

Fig. 3.28. EL spectra of Vn 63, measured at 1 A/cm^2, as a function of temperature, demonstrating the thermally induced redistribution of carriers from the high to low energy QDs

Plotted in Fig. 3.29 (a) is the peak EL intensity of the long wavelength subset of QDs and J_{th} as function of temperature. Above 78K J_{th} initially decreases with increasing temperature, reaching a minimum at 200K and then increases monotonically at higher temperatures. This low temperature decrease of J_{th} with increasing temperature is specific to QD lasers and is attributed to the transition from a non-equilibrium to equilibrium carrier distribution within the QD ensemble[65]. At low temperature, where thermally activated non-radiative processes can be ignored and carriers remain localised in the QDs in to which they are first captured, the value of the peak gain at a given injection level essentially reflects the extent of the inhomogeneous broadening in the QD ensemble. In other words, when the carrier distribution is non-thermal, a broader range of GS energy states is populated in more inhomogeneous samples and therefore, for a given injection level, the gain peak will be lower. Higher injection levels must be used to obtain threshold in such samples. As the temperature is raised, however, an equilibrium carrier distribution may be established, inducing a narrowing of the gain spectrum. Carriers injected into non-lasing QDs that previously would have been wasted are now able to take part in the lasing via this redistribution process. As a consequence, a lower injection current is required to reach threshold. This trend of decreasing J_{th} with increasing temperature

constitutes the regime of negative T_0. This carrier redistribution and its effect on the temperature dependence of J_{th} is expected to be more pronounced in more inhomogeneous (especially bimodal) QD samples and this is clearly seen in the present device(s).

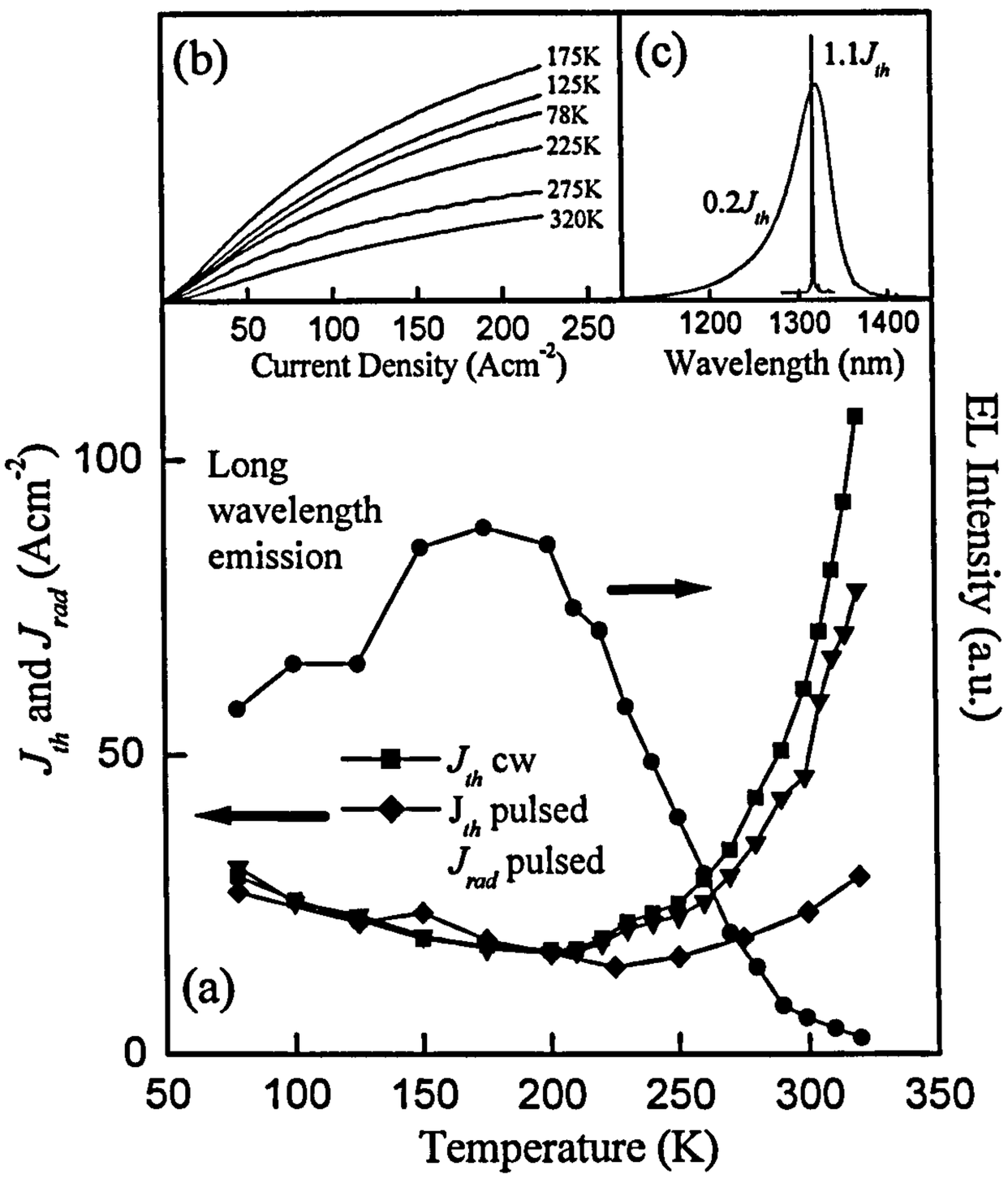

Fig. 3.29. (a): cw and pulsed J_{th} as a function of temperature for a 3 mm cavity of Vn 63. The radiative current density (J_{rad}) is proportional to the total spontaneous emission intensity at threshold, obtained from the LI curves shown in (b). The temperature variation of the integrated emission from the long wavelength sub-set of QDs is depicted by circles. (c): RT spontaneous emission and lasing spectra.

From Fig. 3.29 (a) it can be seen that the minimum value of J_{th} coincides with the maximum EL intensity of the longer wavelength subset of QDs. Lasing spectra taken throughout the investigated temperature range indicate that the lasing transition coincides with the peak of the emission from this subset, indicating that lasing always occurs from the same sub-set of QDs (See Fig. 3.29 (c)). A semi-quantitive analysis of the inter-dot carrier transfer can be made as follows. At 78 K ~70% of the total emission results from the smaller QDs, although only ~70% of this emission is spectrally separated from that of the larger QDs. If this fraction ($0.7^2 \approx 0.5$) of the

emission transfers to longer wavelengths then the intensity at the lasing wavelength would be expected to increase by a factor of ~2. This value is in reasonable agreement with the decrease of J_{th} between 78 and 200 K of 1.6, and the increase of the spontaneous emission at the lasing wavelength of ~1.5 over the same temperature range (Fig. 3.29 (a)).

A complication to this analysis is that the integrated emission from all the QDs increases between 78 and 150K, by a factor ~1.5 (between 78 and 200K the increase is ~1.2), and this increase in the radiative efficiency will also contribute to the decrease in J_{th}. The reason for this increase (the maximum efficiency occurs at 150K, slightly below the minimum for J_{th} at 200K) is unclear but may reflect reduced carrier diffusion to the surface of the device[66] or that the radiative efficiency of the larger QDs is greater than that of the smaller dots[67].

The variation of the integrated spontaneous emission with current at different temperatures is shown in Fig. 3.29 (b). This data can be used to obtain the temperature dependence of the spontaneous emission intensity at threshold, which is proportional to the radiative current density, (J_{rad})[68]. At 200K J_{rad} has been normalised to J_{th}, since below this temperature non-radiative processes are considered to be negligible. Between 78 and 200 K, J_{rad} and J_{th} follow a very similar trend, both decreasing with increasing temperature. As discussed previously, this decrease reflects the concentration of carriers in the lasing subset of QDs.

From 225 to 320 K J_{rad} increases by a factor of ~2.2, compared to an increase in J_{th} of ~4. At 320 K J_{rad} is 38% of J_{th}. This high-temperature increase of J_{rad} most likely reflects the excitation of carriers out of the lasing states to excited dot states. It has been shown that with increasing temperature the loss of carriers to excited QD states requires an increase in J_{rad} to maintain the ground state carrier density necessary to achieve the threshold gain. Spontaneous emission spectra at 300 K are similar to those at 200 K shown in Fig. 3.27 (b), with excited state emission observed for current densities comparable to J_{th}, consistent with significant carrier excitation out of the lasing ground state and into excited QD states. It is also possible that at high temperatures carriers are thermally excited into the subset of smaller QDs.

The fact that the integrated QD emission decreases with increasing temperature above 200 K however (Fig. 3.29 (b)), indicates that the corresponding increase in J_{th} is not entirely due to the thermal excitation of carriers into higher

energy, non-lasing dot states, as such a process would conserve the integrated dot emission. As the total dot emission is not conserved, carriers must either recombine non-radiatively in the dots or be lost from the dots. In the latter case they must subsequently recombine non-radiatively as negligible emission is observed from the regions (GaAs and InGaAs QW/WL) surrounding the quantum dots. The maximum integrated emission is obtained for a temperature ~150K. By 300K this intensity has decreased by a factor ~3. Assuming the QDs have a 100% quantum efficiency at low temperatures then at room temperature the radiative efficiency is at most ~30%. This result indicates the presence of significant non-radiative carrier recombination at high temperatures, even in high quality QD laser devices. Despite this evidence for non-radiative recombination, the nature of the underlying physical mechanism(s) is unclear.

For higher dimensionality systems, an analysis based on an assumed $L \propto n^2$ dependence, where L is the integrated emission and n is the carrier density has allowed the dominant carrier recombination process, expressed in terms of n^a, to be determined. However, the validity of this analysis for a QD system has been questioned[69]. For the present device and a current density $J \leq 60$ A/cm^2, a~1.5 which increases to >3 when J >200 A/cm^2, these values being approximately independent of temperature. In QW systems, a process with a>2 is associated with Auger recombination[68], but for QDs the validity of the $L \propto n^2$ model is not clear and other loss mechanisms, involving for example the loss of carriers from an excited state to a non-radiative centre outside the QD may also give a value of $a > 2$. The temperature dependence of the spectrally integrated emission at constant current (L), shown in Fig. 3.30, appears to be inconsistent with Auger recombination, which is expected to become more important at high temperatures and high currents in QDs[70]. The temperature sensitivity of L *decreases* with increasing injection current. From 200 to 320 K, L reduces by a factor of 15, 9, 7 and 5 relative to its normalised value at 200 K, for injection current densities of 0.8, 8, 24 and 80 A/cm^2 respectively. The pulsed J_{th} increases by a factor of ~4.5 over the same temperature range. This reduced temperature sensitivity of L is consistent with a saturation of defect states: as the injection current is raised, mono-molecular recombination involving defects (having a fixed concentration) will consume a smaller proportion of the injected carriers.

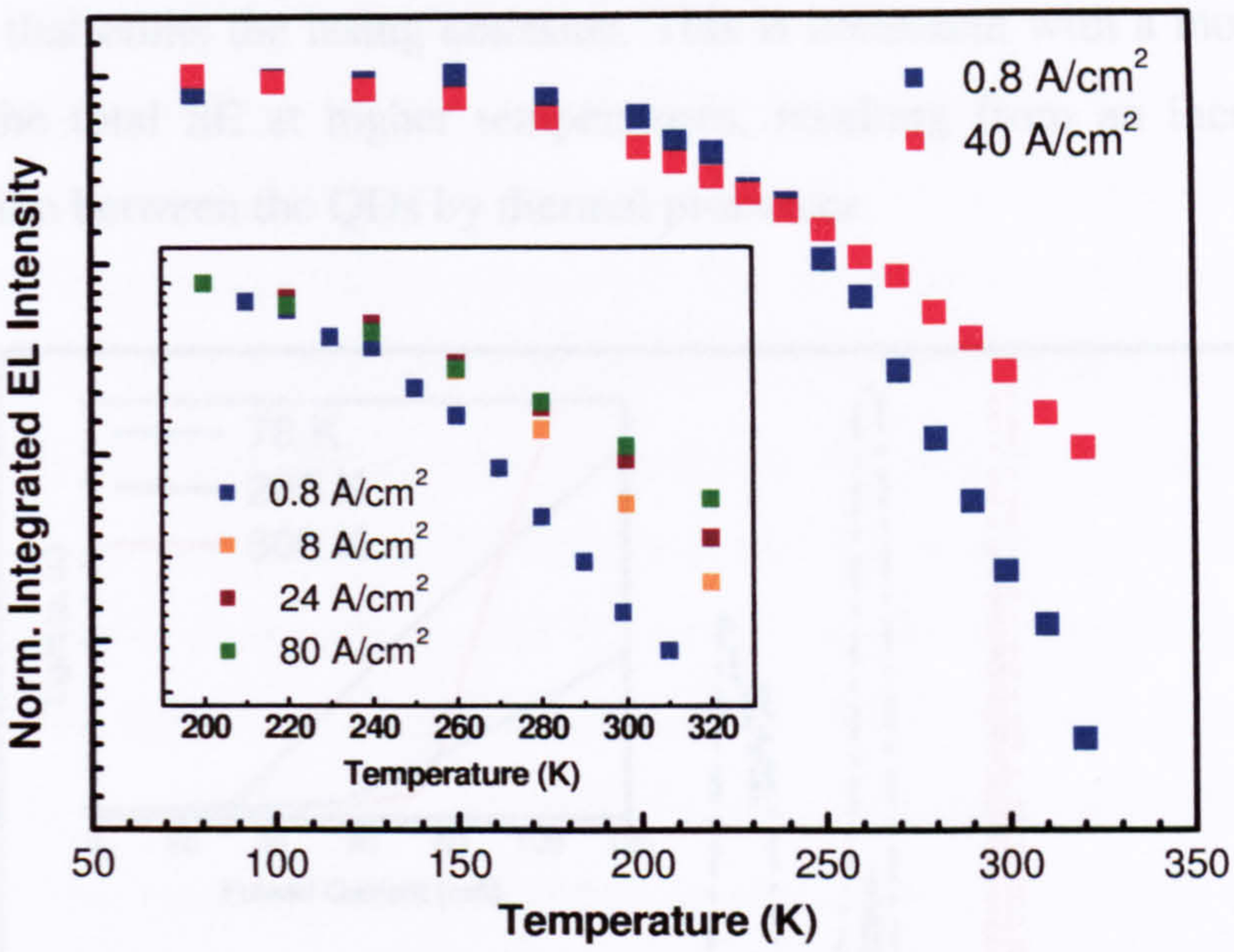

Fig. 3.30 Main part: temperature dependence of the integrated EL under an injection of 0.8 A/cm^2 (navy squares) and 40 A/cm^2 (red squares). The intensities are normalised to their 77 K values. Inset depicts the variation over a wider injection range, with intensities normalised to their 200 K values.

A direct comparison between the temperature dependence of the lasing and the spontaneous emission (SE) characteristics can be obtained from a laser device with small (50 μm) windows formed in the top contact. These windows allow the SE to be continued to be collected when the laser is operated close to and above threshold. It should be noted that due to the relatively large area of these windows and the focussing geometry of the optics, a small proportion of lasing light scattered from imperfections in the cavity will also be collected. The main part of Fig. 3.31 shows SE recorded at the lasing threshold J_{th} (solid lines) and at 1.5 x J_{th} (dashed lines) at 78, 205 and 300 K. The corresponding L-I characteristics, collected from the end facet, are shown in the inset.

If the temperature dependence of the emission spectra is considered initially, three important points can be made. First of all, there is an obvious narrowing of the scattered lasing emission at 1.5 x J_{th} as the temperature is increased. This has been attributed to either the effects of carrier redistribution processes combined with enhanced non-radiative recombination[71] or to a more effective energetic coupling of the discrete GS levels via their increased homogeneous linewidth at high temperature[46]. Second, the increase in the integrated intensity of the SE between J_{th} and 1.5 x J_{th} decreases as the temperature is raised, as determined by a 3 peak

Gaussian fit that omits the lasing emission. This is consistent with a more complete pinning of the total SE at higher temperatures, resulting from an increase in the communication between the QDs by thermal processes.

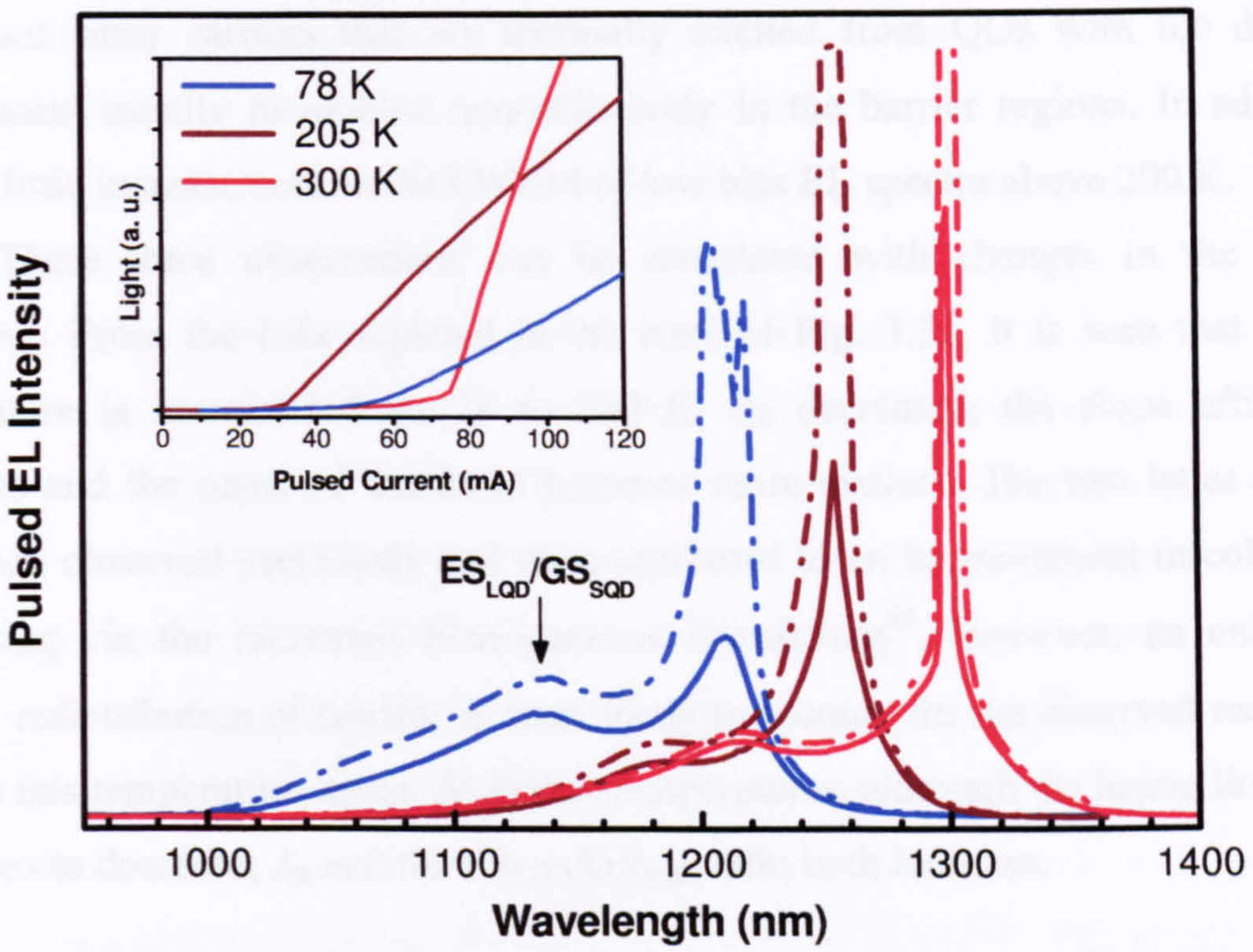

Fig. 3.31 Main part: Pulsed SE EL from a 3 mm cavity of Vn 61. Spectra taken at J_{th}, and 1.5 x J_{th} are indicated by solid and dash-dot lines respectively for each of the three temperatures (77, 205 and 300 K denoted by blue, maroon and red lines respectively). Inset shows the spectrally integrated L-I characteristics at 78, 205 and 300 K.

Finally, at J_{th}, the intensity of the higher energy emission peak (labelled ES_{LQD}/GS_{SQD} in the main part of Fig. 3.31) is observed to decrease with temperature (up to 200 K) relative to the SE originating from the lasing state. Above 200 K this trend is reversed. As discussed previously, it is assumed that the emission at higher energy is composed of both excited state emission from the larger sub-set of QDs and GS emission from the sub-set of smaller QDs. The fact that the relative intensities are seen to vary non-monotonically with temperature indicates the important role that both the inter- and intra – QD carrier distribution has in determining J_{th}. For example, even at room temperature, it is possible for the GS and ES carrier populations not to be in quasi-equilibrium with each other, yet for each to be described by individual Fermi-Dirac distributions[72].

Between 78 and 200 K the reduction in the relative intensity of the ES_{LQD}/GS_{SQD} peak can be accounted for by the carrier redistribution effect. For

temperatures above 200 K, the increase in ES_{LQD}/GS_{SQD} and also in J_{th} may, in principle, be explained by both an increase in the ES population of the lasing sub-set of QDs and in the thermal spreading of carriers to the GSs of QDs that lie outside the homogeneous linewidth of the lasing energy. The latter process is thought to be less significant since carriers that are thermally excited from QDs with the deepest confinement usually recombine non-radiatively in the barrier regions. In addition, there is little increase seen in the FWHM of low bias EL spectra above 200 K.

These three observations can be associated with changes in the lasing behaviour. From the L-Is depicted in the inset of Fig. 3.31, it is seen that as the temperature is increased from 78 to 200 K, J_{th} decreases, the slope efficiency increases and the onset of threshold becomes more distinct. The two latter effects have been observed previously and were attributed to an improvement in collective QD lasing via the increased homogeneous broadening[42]. However, an enhanced thermal redistribution of carriers is more likely to account for the observed reduction in J_{th} in this temperature range. At higher temperatures, although the lasing linewidth continues to decrease, J_{th} and the ES_{LQD}/GS_{SQD} ratio both increase.

3.6 Conclusions

The optical characteristics of InAs QD structures placed in $In_xGa_{1-x}As$ QWs (DWELL structures) have been studied. It was found that by increasing 'x' in the DWELL from 0 to 0.2, the QD room temperature emission wavelength could be tuned from 1.17 to 1.35 μm. An Indium fraction of 15% in the DWELL was found to be optimum for producing a high density of optically efficient QDs emitting at ~1.3 μm. A GS exciton confinement energy, independent of *x*, of ~310 meV was determined from a PLE study of these structures. This finding supports the assertion that the redshift of the QD emission with increasing '*x*' in the DWELL is primarily due to stimulated decomposition of the $In_xGa_{1-x}As$ QW surrounding the QDs and/or a reduction in the QD hydrostatic strain.

However, the performance of 3 and 5-layer laser structures incorporating the $In_{0.15}Ga_{0.85}As$ DWELLs was poor, with no RT lasing obtained from the 5 layer device. A TEM investigation of these structures revealed the presence of dislocated QD growth, originating in the second QD layer and propagated upwards through the

structures by threading dislocations in the GaAs spacer layers. An AFM study of the QD nucleation surface showed that the GaAs had not been sufficiently planarised during its growth, and had therefore promoted the formation of dislocated QDs in the subsequently grown layers. The low temperature (~510 °C) used to deposit the GaAs was attributed as the cause of the surface roughness, motivating the development of a new technique for GaAs spacer layer growth.

To increase the mobility of the Ga ad-atoms, and therefore increase the planarisation efficiency of the deposited GaAs, the upper 35 nm region of the spacer layer was grown at 580 °C. Spacer layers grown using this two-temperature technique were thereafter referred to as High Growth Temperature Spacer Layers (HGTSLs). A subsequent TEM investigation showed that the HGTSL procedure was able to reduce the dislocation density by over three orders of magnitude. The resultant improvements in the RT optical efficiency and reverse bias leakage currents of LED devices containing HGTSLs translated into a drastically improved laser performance. A 5-layer structure with 50 nm HGTSLs maintained cw GS lasing at room temperature down to a cavity length of 1.5 mm and a 5 mm cavity of the same structure operated cw from the GS at temperatures up to 85 °C. The elimination of defective QDs which, amongst other effects, results in a four-fold reduction in the internal cavity loss, yielded some of the lowest reported J_{th}s in the literature for 1.3 μm QD laser devices e.g. a double HR coated 1 mm cavity of a 3 layer structure with 70 nm HGTSLs lased cw at room temperature with a J_{th} = 19 A/cm^2. Despite this excellent cw performance, the highest T_0 achieved was only ~90 K for the 5 mm cavity of this structure, and this value represented the best for the series. Aside from measurements of the conventional laser parameters (J_{th}, T_0), characteristics unique to QD systems were investigated. In a 1 mm device that exhibited a switching of the lasing state from GS to ES1 with increasing drive current, the threshold current for this switch was found to decrease with increasing temperature. This behaviour was attributed to a temperature induced reduction in the saturated GS gain.

The spontaneous and lasing characteristics of a structure with a bimodal size distribution were studied as a function of temperature. It was found that the presence of a smaller sub-set of QDs with a higher GS energy than the main QD distribution enhanced the carrier redistribution effects common to all inhomogeneously broadened QD systems. As a result of the equilibration of the carrier population with

increasing temperature, a pronounced region of negative T_0 was observed between 78 and 200 K in these samples, attributed to a narrowing of the gain spectrum. Over a similar temperature range, an increase in the radiative efficiency of the QDs was observed which may account for some part of the reduction in J_{th}. Above ~220 K non-radiative processes are shown to contribute significantly to the increase in J_{th}. The nature of the non-radiative recombination is unclear, however the results of spontaneous emission measurements are consistent with a mechanism involving defects rather than Auger recombination.

A study of the spontaneous emission spectra above J_{th}, collected from windows formed in the top contact of a laser device, provided further confirmation of the important role played by the carrier distribution in determining the lasing characteristics. The temperature dependence of J_{th} followed that of the SE intensity originating from the high energy shoulder of the emission, suggesting the presence of a loss mechanism associated with excited QD states and/or smaller QDs. The SE intensity was shown to clamp more completely with increasing temperature over the investigated range (77 – 300 K).

References

1. Fariba Ferdos, Shumin Wang, Yongqiang Wei, Anders Larsson, Mahdad Sadeghi and Qingxiang Zhao, Appl. Phys. Lett. **81,** 1195 (2002)

2. M. V. Maximov, A. F. Tsatsul'nikov, B. V. Volovik, D. S. Sizov, Yu. M. Shernyakov, I. N. Kaiander, A. E. Zhukov, A. R. Kovsh, S. S. Mikhrin, V. M. Ustinov, and Zh. I. Alferov, R. Heitz, V. A. Shchukin, N. N. Ledentsov , and D. Bimberg, Yu. G. Musikhin and W. Neumann, Phys. Rev. B. **62,** 16671 (2000)

3. M. Grundmann, O. Stier, and D. Bimberg, Phys. Rev. B. **52,** 11969 (1995)

4. Kenichi Nishi, Hideaki Saito, Shigeo Sugou, Jeong-Sik Lee, Appl. Phys. Lett. **74,** 1111 (1999)

5. H. Y. Liu, X. D. Wang, J. Wu, B. Xu, Y. Q. Wei, W. H. Jiang, D. Ding, X. L. Ye, F. Lin, J. F. Zhang, J. B. Liang, and Z. G. Wang, J. Appl. Phys. **88,** 3392 (2000)

6. V. M. Ustinov, N. A. Maleev, A. E. Zhukov, A. R. Kovsh, A. Yu. Egorov, A. V. Lunev, B. V. Volovik, I. L. Krestnikov, Yu. G. Musikhin, N. A. Bert, P. S. Kop'ev, Zh. I. Alferov, N. N. Ledentsov, D. Bimberg, Appl. Phys. Lett. **74,** 2815 (1999)

7. G.T. Liu, A. Stintz, H. Li, K.J. Malloy, and L.F. Lester, Electron. Lett. **35,** (14) 1163 (1999)

8. H. Y. Liu and M. Hopkinson, Appl. Phys. Lett. **82,** 3644 (2003)

9. H. Y. Liu, M. Hopkinson, C. N. Harrison, M. J. Steer, R. Frith, I. R. Sellers, D. J. Mowbray, and M. S. Skolnick, J. Appl. Phys. **93,** 2931 (2003)

10. J. X. Chen, U. Oesterle, A. Fiore, R. P. Stanley, M. Ilegems and T. Todaro, Appl. Phys. Lett. **79,** 3681 (2001)

11. A. Ponchet, D. Lacombe, L. Durand, D. Alquier, and J.-M. Cardonna, Appl. Phys. Lett. **72,** 2984 (1998)

12. P. B. Joyce, T. J. Krzyzewski, G. R. Bell, T. S. Jones, E. C. Le Ru, and R. Murray, Phys. Rev. B. **64,** 235317 (2001)

13. F. Adler, M. Geiger, A. Bauknecht, D. Haase, P. Ernst, A. Dörnen, F. Scholz, and H. Schweizer, J. Appl. Phys. **83,** 1631 (1998)

14. R. Heitz, O. Stier, I. Mukhametzhanov, A. Madhukar, and D. Bimberg, Phys. Rev. B. **62,** 11017 (2000)

15. C. Wang, P.P. Chen, N.Y. Tang, T.X. Li, C.S. Xia, W. Lu, F.Z. Wang and Z.H. Chen, J. Cryst. Growth **289,** (2), 547 (2006)

16. F. Guffarth, R. Heitz, A. Schliwa, O. Stier, N. N. Ledentsov, A. R. Kovsh, V. M. Ustinov, and D. Bimberg, Phys. Rev. B. **64,** 85305 (2001)

17. M. J. Steer, D. J. Mowbray, W. R. Tribe, M. S. Skolnick, M. D. Sturge, M. Hopkinson, A. G. Cullis, C. R. Whitehouse, and R. Murray, Phys. Rev. B. **54,** 17738 (1996)

18. R. Heitz, M. Grundmann, N. N. Ledentsov, L. Eckey, M. Veit, D. Bimberg, V. M. Ustinov, A. Yu. Egorov, A. E. Zhukov, P. S. Kop'ev, and Zh. I. Alferov, Appl. Phys. Lett. **68,** 361 (1996)

19. R. Heitz, A. Kalburge, Q. Xie, M. Grundmann, P. Chen, A. Hoffmann, A. Madhukar, and D. Bimberg, Phys. Rev. B. **57,** 9050 (1998)

20. R. Heitz, I. Mukhametzhanov, O. Stier, A. Madhukar, and D. Bimberg, Phys. Rev. Lett. **83,** 4654 (1999)

21. Klopf, F.; Krebs, R.; Reithmaier, J.P.; Forchel, A. IEEE Photon. Technol. Lett. **13,** (8) 764 (2001)

22. O.G. Schmidt, N. Kirstaedter, N.N. Ledentsov, M.-H. Mao, D. Bimberg, V.M. Ustinov, A.Y. Egorov, A.E. Zhukov, M.V. Maximov, P.S. Kop'ev, and Z.I. Alferov, Electron. Lett. **32,** (14) 1302 (1996)

23. H. Y. Liu, I. R. Sellers, T. J. Badcock, D. J. Mowbray, M. S. Skolnick, K. M. Groom, M. Gutiérrez, M. Hopkinson, J. S. Ng, and J. P. R. David, Appl. Phys. Lett. **85,** 704 (2004)

24. Qianghua Xie, Anupam Madhukar, Ping Chen, and Nobuhiko P. Kobayashi, Phys. Rev. Lett. **75,** 2542 (1995)

25. H. Y. Liu, I. R. Sellers, M. Gutiérrez, K. M. Groom, W. M. Soong, M. Hopkinson, and J. P. R. David, J. Appl. Phys. **96,** 1988 (2004)

26. Wei-Sheng Liu, Holin Chang, Yu-Shen Liu, and Jen-Inn Chyi, J. Appl. Phys. **99,** 114514 (2006)

27. Q. Gong, R. Nötzel, G. J. Hamhuis, T. J. Eijkemans, and J. H. Wolter, Appl. Phys. Lett. **81,** 1887 (2002)

28. G. Costantini, A. Rastelli, C. Manzano, P. Acosta-Diaz, R. Songmuang, G. Katsaros, O. G. Schmidt, and K. Kern, Phys. Rev. Lett. **96,** 226106 (2006)

29. Q. Gong, P. Offermans, R. Nötzel, P. M. Koenraad, and J. H. Wolter, Appl. Phys. Lett. **85,** 5697 (2004)

30. P. B. Joyce, T. J. Krzyzewski, G. R. Bell, and T. S. Jones, Appl. Phys. Lett. **79,** 3615 (2001)

31. E. C. Le Ru, A. J. Bennett, C. Roberts, and R. Murray, J. Appl. Phys. **91,** 1365 (2002)

32. D. S. Sizov, M. V. Maksimov, A. F. Tsatsul'nikov, N. A. Cherkashin, N. V. Kryzhanovskaya, A. B. Zhukov, N. A. Maleev, S. S. Mikhrin, A. P. Vasil'ev, R. Selin, V. M. Ustinov, N. N. Ledentsov, D. Bimberg, and Zh. I. Alferov, Semiconductors **36,** (9) 1020 (2002)

33. H.Y. Liu, T.J. Badcock, I.R. Sellers, W.M. Soong, K.M. Groom, M. Hopkinson, D.J. Mowbray and M.S. Skolnick, Physica E **26,** (1-4) 129 (2005)

34. S. Sanguinetti, M. Padovani, M. Gurioli, E. Grilli, M. Guzzi, A. Vinattieri, M. Colocci, P. Frigeri and S. Franchi, Appl. Phys. Lett. **77,** 1307 (2000)

35. M. Gutiérrez, M. Hopkinson, H.Y. Liu, J.S. Ng, M. Herrera, D. González, R. Garcia and R. Beanland, Physica E **26,** 245 (2005)

36. Gyoungwon Park, O. B. Shchekin, D. G. Deppe, IEEE J. Quantum Electron. **36,** (9) 1065 (2000)

37. Mitsuru Sugawara, Kohki Mukai, and Yoshiaki Nakata, Appl. Phys. Lett. **75,** 656 (1999)

38. I. P Marko, A. D. Andreev, A. R. Adams, R. Krebs, J. P. Reithmaier, A. Forchel, IEEE J. Select. Topics Quantum Electron. **9,** (5) 1300 (2003)

39. Walker, C.L.; Sandall, I.C.; Smowton, P.M.; Sellers, I.R.; Mowbray, D.J.; Liu, H.Y.; Hopkinson, M., IEEE Photon. Technol. Lett. **17,** (10) 2011 (2005)

40. I. R. Sellers, PhD Thesis p113 University of Sheffield (2004)

41. H. Jiang and J. Singh, J. Appl. Phys. **85,** 7438 (1999)

42. Mitsuru Sugawara, Kohki Mukai, and Yoshiaki Nakata, Appl. Phys. Lett. **74,** 1561 (1999)

43. P. B. Joyce, T. J. Krzyzewski, G. R. Bell, B. A. Joyce, and T. S. Jones, Phys. Rev. B. **58,** 15981 (1999)

44. W. Langbein, P. Borri, U. Woggon, V. Stavarache, D. Reuter, and A. D. Wieck, Phys. Rev. B. **70,** 33301 (2004)

45. P. Borri, S. Schneider, W. Langbein, U. Woggon, A. E. Zhukov, V. M. Ustinov, N. N. Ledentsov, Zh. I. Alferov, D. Ouyang and D. Bimberg, Appl. Phys. Lett. **79,** 2633 (2001)

46. Mitsuru Sugawara, Kohki Mukai, Yoshiaki Nakata, Hiroshi Ishikawa, and Akira Sakamoto, Phys. Rev. B **61,** 7595 (2000)

47. M. Sugawara, N. Hatori, H. Ebe, M. Ishida, Y. Arakawa, T. Akiyama, K. Otsubo, and Y. Nakata, J. Appl. Phys. **97,** 043523 (2005)

48. F. Klopf, S. Deubert, J. P. Reithmaier, and A. Forchel, Appl. Phys. Lett. **81,** 217 (2002)

49. H.Y. Liu; D.T. Childs; T.J. Badcock; K.M. Groom; I.R. Sellers; M. Hopkinson; R.A. Hogg; D.J. Robbins; D.J. Mowbray; M.S. Skolnick; IEEE Photon. Technol. Lett. **17,** (6) 1139 (2005)

50. A. Markus, J. X. Chen, C. Paranthoën, A. Fiore, C. Platz and O. Gauthier-Lafaye, Appl. Phys. Lett. **82,** 1818 (2003)

51. A. Markus, M. Rossetti, V. Calligari, J. X. Chen, and A. Fiore, J. Appl. Phys. **98,** 104506 (2005)

52. S.A. Moore; L. O'Faolain; M.A. Cataluna; M.B. Flynn; M.V. Kotlyar; T.F. Krauss, IEEE Photon. Technol. Lett. **18,** (17) 1861 (2006)

53. Martin Achtenhagen and Amos Hardy, Appl. Phys. Lett. **74,** 1364 (1999)

54. S.K. Ray, K.M. Groom, R.A. Hogg, H.Y. Liu, M. Hopkinson, T. Badcock, D.J. Mowbray; M.S. Skolnick, IEEE Photon. Technol. Lett. **17,** (9) 1785 (2005)

55. H. S. Lee, J. Y. Lee and T. W. Kim, J. Cryst. Growth **258,** (3-4), 256 (2003)

56. S. J. Lee, S. K. Noh, J. W. Choe and E. K. Kim, J. Cryst. Growth **267,** (3-4), 405 (2004)

57. C. A. Duarte, E. C. F. da Silva, A. A. Quivy, M. J. da Silva, S. Martini, J. R. Leite, E. A. Meneses and E. Lauretto, J. Appl. Phys. **93,** 6279 (2003)

58. H. Kissel, U. Müller, C. Walther, W. T. Masselink, Yu. I. Mazur, G. G. Tarasov, and M. P. Lisitsa, Phys. Rev. B **62,** 7213 (2000)

59. Hao Lee, Roger Lowe-Webb, Thomas J. Johnson, Weidong Yang, and Peter C. Sercel, Appl. Phys. Lett. **73,** 3556 (1998)

60. S.I. Jung, H.Y. Yeo, I. Yun, J.Y. Leem, I.K. Han, J.S. Kim and J.I. Lee, Physica E **33,** (1) 280, (2006)

61. Hao Lee, Roger R. Lowe-Webb, Weidong Yang, and Peter C. Sercel, Appl. Phys. Lett. **71,** 2325 (1997)

62. H. L. Wang, D. Ning and S. L. Feng, J. Cryst. Growth **209,** (4), 630 (2000)

63. I. R. Sellers, D. J. Mowbray, T. J. Badcock, J.-P. R. Wells, P. J. Phillips, D. A. Carder, H. Y. Liu, K. M. Groom, and M. Hopkinson, Appl. Phys. Lett. **88,** 81108 (2006)

64. L. Brusaferri, S. Sanguinetti, E. Grilli, M. Guzzi, A. Bignazzi, F. Bogani, L. Carraresi, M. Colocci, A. Bosacchi, P. Frigeri, and S. FranchiAppl. Phys. Lett. **69,** 3354 (1996)

65. Alexey E. Zhukov, Victor M. Ustinov, Anton Yu. Egorov, Alexey R. Kovsh, Andrey F. Tsatsul`nikov, Nikolay N. Ledentsov, Sergey V. Zaitsev, Nikita Yu. Gordeev, Peter S. Kopèv and Zhores I. Alferov, Jpn. J. Appl. Phys. **36,** 4216 (1997)

66. P. Borri, W. Langbein, S. Schneider, U. Woggon, R. L. Sellin, D. Ouyang, D. Bimberg, IEEE J. Sel. Topics Quantum Electron. **8,** (5) 984 (2002)

67. Jeppe Johansen, Søren Stobbe, Ivan S. Nikolaev, Toke Lund-Hansen, Philip T. Kristensen, Jørn M. Hvam, Willem L. Vos, and Peter Lodahl, Phys. Rev. B 77, 073303 (2008)

68. A. F. Phillips, S. J. Sweeney, A. R. Adams, P. J. A Thijs, IEEE J. Sel. Topics Quantum Electron. **5,** (3) 401 (1999)

69. M. Grundmann, R. Heitz, D. Bimberg, J.H.H. Sandmann, J. Feldmann, phys. stat. sol. (b) **203,** (1) 121 (1997)

70. I. P. Marko, A. R. Adams, S. J. Sweeney, D. J. Mowbray, M. S. Skolnick, H. Y. Liu, K. M. Groom, IEEE J. Sel. Topics Quantum Electron. **11,** (5) 1041 (2005)

71. A. Patanè, A. Polimeni, M. Henini, L. Eaves, P. C. Main, and G. Hill, J. Appl. Phys. **85,** 625 (1999)

72. S. Osborne, P. Blood, P. Smowton, J. Lutti, Y. C. Xin, A. Stintz, D. Huffaker, L. F. Lester, IEEE J. Sel. Topics Quantum Electron. **40,** (12) 1639 (2004)

Chapter 4

Multilayer DWELL QD laser structures incorporating modified GaAs High Growth Temperature Spacer Layers (HGTSLs) or modified InGaAs capping layers

4.1 Re-grown multilayer QD laser structures containing HGTSLs

4.1.1 Introduction

As has now been established, the use of the High Growth Temperature Spacer Layer (HGTSL) step enables the coherent growth of high quality, 1.3μm emitting structures with up to 5-QD layers. The inclusion of additional QD layers is mainly of benefit at high temperature, where carriers thermally emitted from the QDs have a greater chance of recapture into a neighbouring DWELL if more DWELL layers are present. GS cw operation at > 100 °C and increased temperature stability are found for the high QD density 5-layer device (Vn 61), both characteristics are the direct result of the increased level of material gain, with little compensatory increase in the internal loss[1]. In light of these improvements, the HGTSL technique was applied to a new set of multilayer structures. The design of the active region in these new structures is nominally identical to the previous set (Vn 58 – 61), but now includes samples with 7 and 10 DWELL layers. The growth conditions used for the DWELLs and the 50 nm HGTSLs separating them were identical to those described in chapter 3, section 3.3.3.

4.1.2 Multilayer QD laser structures with a reduced thickness waveguide

The active regions of all the multilayer samples grown in this series were placed within a narrower waveguide, in an attempt to improve the modal gain of the devices further. The combined thickness of undoped $Al_{0.4}Ga_{0.6}As$ and GaAs in the

cladding was reduced from 250 nm to 120 nm i.e. an overall decrease of 43% in the thickness of the waveguide.

As part of this series, a control sample with a nominally identical structure to that of Vn 61 (5 layers, high QD density, old waveguide design) was grown. At room temperature (RT), a 3 mm cavity of this device (Vn 244) has a lasing wavelength of 1294 nm with a cw J_{th} of 64 A/cm^2. In comparison, the respective values for the same cavity length of Vn 61 are 1298 nm and 56 A/cm^2, verifying that a reasonable level of repeatability has been achieved between growth runs.

To determine the effect that narrowing the waveguide had on the lasing properties of the new 5 layer devices, the temperature dependence of J_{th} and RT spectra are compared for 3 mm cavities of Vn 244 and Vn 249 in Fig. 4.1. Vn 249 is a 5 layer structure, nominally identical to Vn 244, but with the redesigned, thinner waveguide.

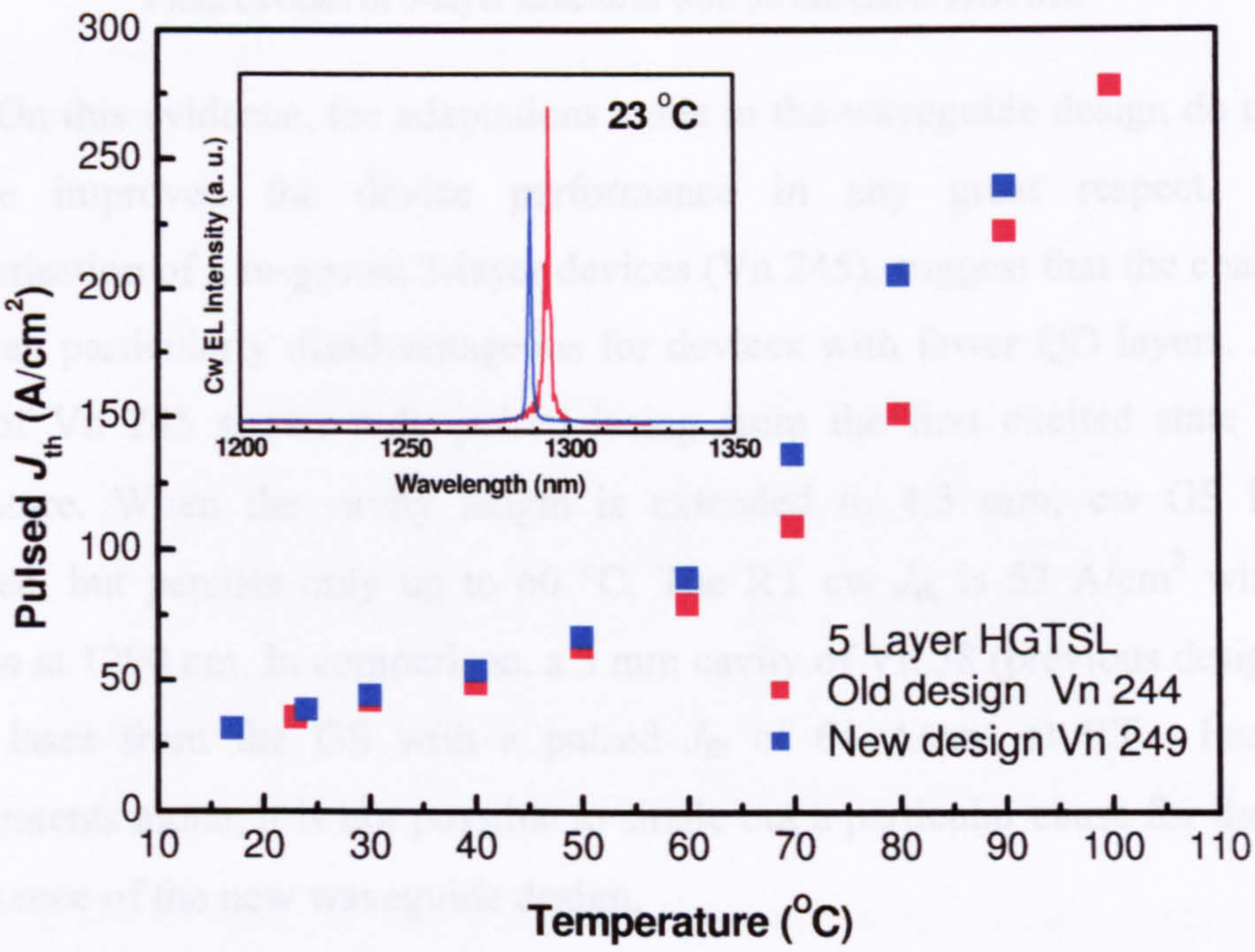

Fig. 4.1 main part: temperature variation of the pulsed J_{th}s between 17 and 100 °C for 3 mm cavities of two 5-layer samples. The active regions of each sample are nominally identical, but the thickness of the waveguide in Vn 249 is reduced. Inset shows the lasing emission at RT

The performance of the devices is similar. Vn 249 lases at a slightly shorter wavelength at RT (~1288 nm), but the pulsed J_{th}s are almost identical up to 60 °C, with a T_0 ~ 45 K. The cw J_{th} at room temperature is 76 A/cm^2 for Vn 249 (cf. 64 A/cm^2 for Vn 244) and lasing occurs up to 60 °C. Lasing above this temperature

could not be obtained due to the compliance limit being reached on the cw current source. GS pulsed lasing persists up to 90 °C. Vn 244 lases cw up to 70 °C, which is again compliance limited. Pulsed lasing from the GS is achieved for this sample up to 90 °C, with state switching to the first excited state (ES1) occurring at 100 °C. An overview of the laser performance characteristics is given in Table 4.2

Sample	Growth run	Waveguide design	Room Temperature		T_0 (K) [250-320 K]
			λ_{lasing} (nm)	cw J_{th} (A/cm^2)	
Vn 61	Old	Old	1298	56	60
Vn 244	New	Old	1294	64	40
Vn 249	New	New	1288	76	43

Table 4.2 Comparison of device characterisation parameters for 3 mm cavities of 5-layer structures with 50 nm GaAs HGTSLs

On this evidence, the adaptations made to the waveguide design do not seem to have improved the device performance in any great respect. In fact, characterisation of a re-grown 3-layer devices (Vn 245), suggest that the change may have been particularly disadvantageous for devices with fewer QD layers. A 3 mm cavity of Vn 245 shows only pulsed lasing from the first excited state at room temperature. When the cavity length is extended to 4.5 mm, cw GS lasing is recovered, but persists only up to 60 °C. The RT cw J_{th} is 53 A/cm^2 with lasing emission at 1290 nm. In comparison, a 3 mm cavity of Vn 58 (previous design, 3 QD layers) lases from the GS with a pulsed J_{th} of 64 A/cm^2 at RT. From these measurements alone, it is not possible to single out a particular cause for the inferior performance of the new waveguide design.

It is feasible that the internal loss (α_i) may be greater in structures with a narrower active region. In general, the total internal optical loss (α_i) of a confined mode in a laser structure is given by the sum of the weighted losses in the active layer (α_{ac}), the waveguide core (α_{wg}) and the cladding (α_{cl})^2. By reducing the thickness of the GaAs/AlGaAs waveguide, the highly doped cladding material is brought closer to the peak of the optical mode, whose tail may now penetrate further into these lossy layers, thereby increasing α_{cl} and hence α_i. The cladding loss in the

p-type material is expected to be particularly significant, due to its large free carrier absorption coefficient. Since the thickness of the waveguide is the same in all the re-grown multilayer structures, whereas that of the active region is not, the profile of the fundamental transverse optical mode will vary between each structure. To obtain a simple picture of how the intensity of this optical mode will differ between the doped and undoped AlGaAs, as a function of the number of QD layers in the active region, the entire structure was modeled as a N layer dielectric slab waveguide, as depicted in Fig. 4.3 with N = 1,2,3,4,5. The refractive indices (n) of the layers and their thicknesses (t) were entered as parameters into a program which computes the optical field pattern of guided modes in multilayer structures[3]. By inputting appropriate n_N and t_N values for each of the N layers, the intensity (E_y^2) of the fundamental TE mode could be plotted as a function of x, the distance along the growth direction. The outer layers 1 and 5 had the relevant n and t parameters for the $Al_{0.4}Ga_{0.6}As$ cladding; layers 2 and 4 those for $Al_{0.2}Ga_{0.8}As$ (average composition of $Al_{0.4}Ga_{0.6}As$/GaAs superlattice) and layer 3, the active region, was taken to be pure GaAs as the very thin QD and WLs make a negligible contribution to the refractive index of this region.

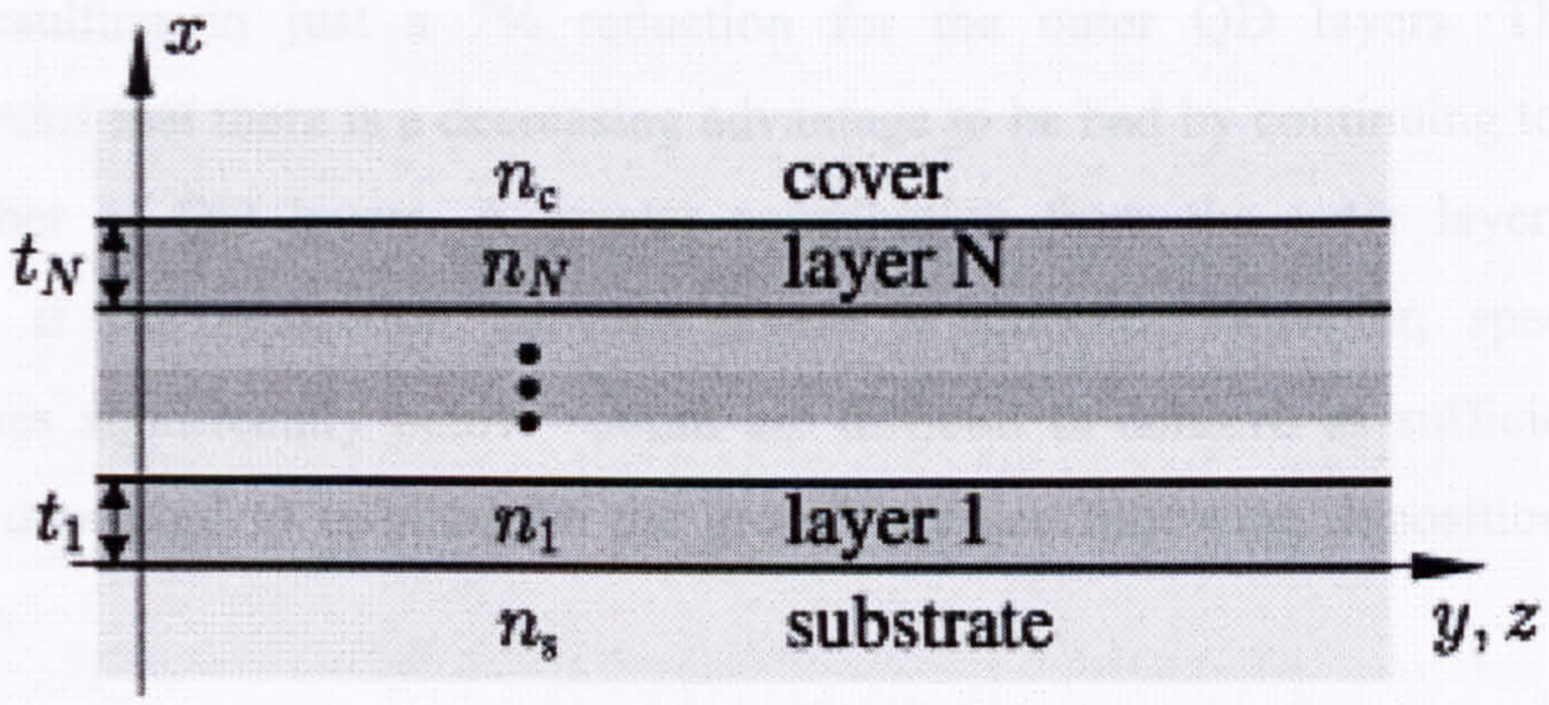

Fig. 4.3 Schematic diagram of the structure used in the multilayer dielectric slab waveguide model.

The results of this simulation suggest that for a 3-layer structure containing the redesigned thinner waveguide, the leakage of the optical mode into the doped cladding increases by approximately 25 % compared to the original design. The resulting additional loss may be enough to explain the inferior performance of the redesigned 3-layer structure, however, in the following section an alternative argument will be presented.

Before this however, it is interesting to note how the optical confinement factor (Γ_Z) *per QD layer* will vary depending on the position of an individual layer within a given structure. In structures with a greater number of QD layers there is an increased percentage variation in the intensity of the optical mode across the layers. This results in the outer QD layers of the active region contributing proportionately less to the total Γ_Z than those in the centre, and this proportional difference increases with the total number of layers in the structure. Percentage differences in the Γ_Z per layer for the central and outer QD layers are calculated for the new 3, 5, 7 and 10 layer structures, and are listed in Table 4.4.

3 QD Layers	5 QD Layers	7 QD Layers	10 QD Layers
$\Gamma_{Z,o} = 0.93 \times \Gamma_{Z,i}$	$\Gamma_{Z,o} = 0.8 \times \Gamma_{Z,i}$	$\Gamma_{Z,o} = 0.66 \times \Gamma_{Z,i}$	$\Gamma_{Z,o} = 0.51 \times \Gamma_{Z,i}$

Table 4.4. Proportional change in the optical confinement factor of the outer QD layers ($\Gamma_{Z,o}$) with respect to the value of the central QD layer(s) ($\Gamma_{Z,i}$) for 3, 5, 7 and 10 layer structures.

From these results it is seen that the outer QD layers in the 10 layer structure contribute only half as much to the total Γ_Z as those in the centre. In the 3 layer structure however, all the layers are relatively close to the maximum of the optical mode, resulting in just a 7% reduction for the outer QD layers. This result demonstrates that there is a decreasing advantage to be had by continuing to increase the number of QD layers. A greater contribution from the outer layers can be achieved if the separation between layers is reduced. However, spacer layer thicknesses significantly below ~50nm are difficult to achieve as sufficient GaAs must be deposited to re-planarise the growth surface following deposition of each QD layer.

4.1.3 Characterisation of the redesigned 3, 5, 7 and 10 layer HGTSL lasers

In order to ascertain whether any changes in Γ_Z, as described above, have significantly affected the lasing performance of the different multilayer structures, temperature dependent laser characterisation was performed on 3 mm x 13 μm cavity devices fabricated from each structure. A comparison of the temperature dependence

of devices with 5, 7 and 10 QD layers, separated by 50 nm HGTSL GaAs spacer layers is shown in Fig. 4.5

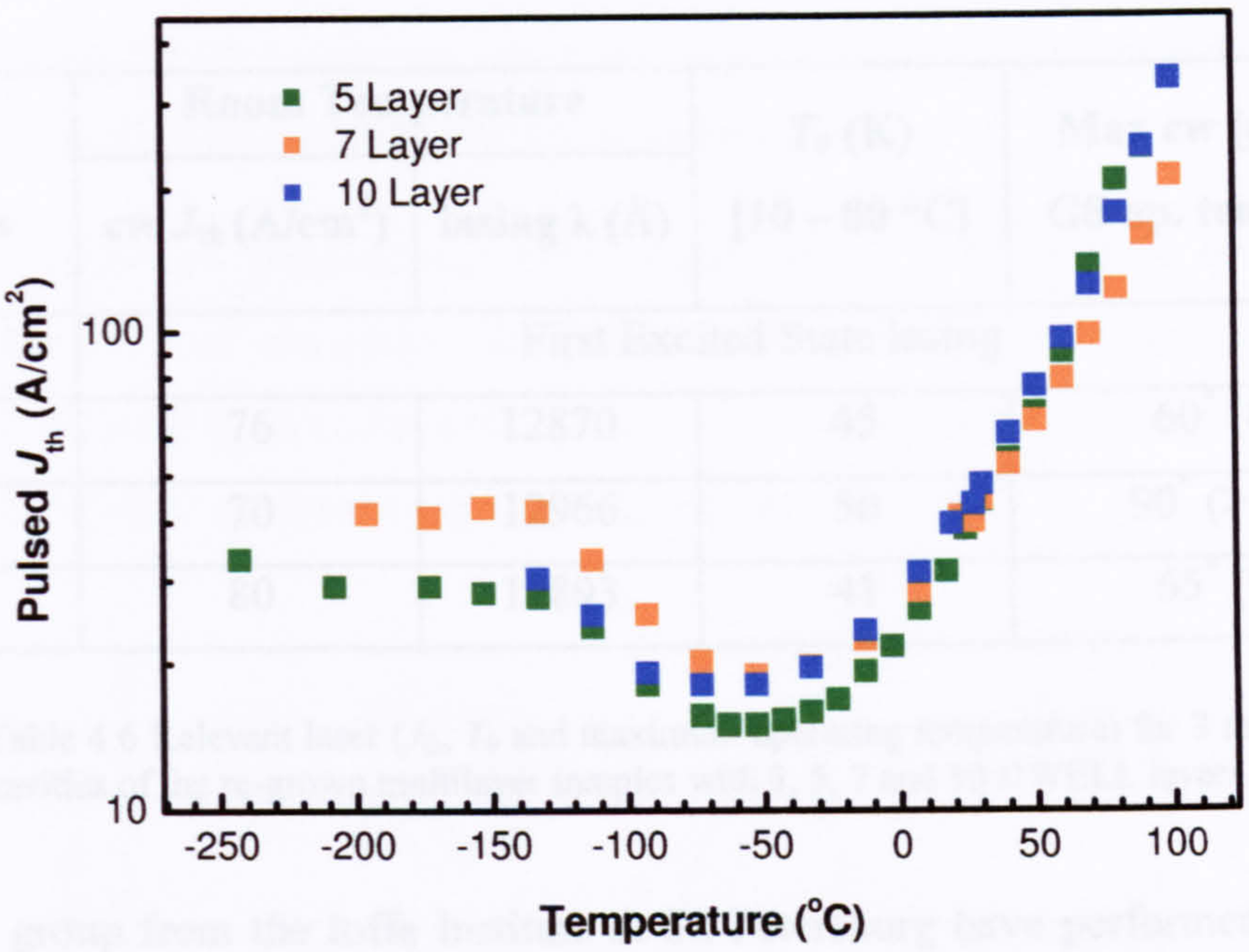

Fig. 4.5 Temperature variation of the pulsed J_{th}s between -250 and 100 °C for 3 mm cavities of the 5, 7 and 10 layer structures.

There is no clear difference in the trend observed in the J_{th} – temperature dependence between the different structures. All possess a negative T_0 between -150 and -50°C, as observed for the devices of the previous series, and in no device is there a significant reduction in the rapid rate of increase of J_{th} above room temperature, with T_0 values varying by only 5 K (see Table 4.6). Below room temperature there is no notable systematic increase of J_{th} with layer number, such as might be associated with a higher transparency current density. The 7-layer structure demonstrates the best performance, with emission at 1297 nm and a cw RT J_{th} of 70 A/cm^2. The T_0 of this device retains a value of 50 K between room temperature and 90 °C. Relevant parameters for the 3, 5 and 10-layer structures can be found in Table 4.6.

The apparent insensitivity of J_{th} and its temperature dependence to the number of QD layers suggests that any differences in Γ_Z for the structures has no significant effect on the lasing performance of these multilayer structures. It is likely that the observed differences are due to changes in the *material* gain of the structures. In the following section, a comparative analysis of the emission and absorption

properties of the samples suggests that the growth of each QD plane alters as the stacking proceeds. Before this study however, the parameters of similar multilayer structures grown elsewhere will be briefly reviewed.

QD Layers	Room Temperature		T_0 (K) [10 – 80 °C]	Max cw (pulsed) GS op. temp. (°C)
	cw J_{th} (A/cm^2)	lasing λ (Å)		
3	First Excited State lasing			
5	76	12870	45	60* (80)
7	70	12966	50	90* (>100)
10	80	12893	41	65* (90)

Table 4.6 Relevant laser (J_{th}, T_0 and maximum operating temperature) for 3 mm cavities of the re-grown multilayer samples with 3, 5, 7 and 10 DWELL layers.

A group from the Ioffe Institute in St. Petersburg have performed extensive characterisation studies of multilayer InGaAs capped 1.3 μm emitting QD lasers. They conclude that increasing the number of QD layers is an effective way of simultaneously increasing the external differential efficiency (η_D) and reducing the minimum cavity length that will sustain GS lasing (e.g. for a 0.6 mm cavity of a 10-layer device η_D = 88%). It is claimed that by increasing the total number of QDs in the structure, transparency may be reached at lower average QD occupation level. As a consequence, the number of carriers thermally excited out of QDs is predicted to decrease, leading to a lower population of states in the AlGaAs waveguide, which act to increase the internal loss[4]. For similar reasons, the calculated transparency current density per layer decreases with increasing layer number, reaching 6 A/cm^2 for 10-layers. However, the increase in layer number does not lead to a systematic increase in T_0: values of 140, 150 and 130 K between 20 and 50 °C are reported for 1.5 mm cavities with 2, 5 and 10-QD layers respectively. Although the structures studied in this chapter do not lase from the GS for cavity lengths of less than 1 mm and the T_0 parameter is typically less than 100 K, the RT lasing wavelength is routinely above 1.3 μm and the J_{th}s are competitive with the best reported values. For example, a pulsed J_{th} of 147 A/cm^2, obtained from a 1.5 mm 10-layer device grown at the Ioffe

institute[5] is comparable to the 150 A/cm^2 *cw* J_{th} from a 2 mm 10 layer Sheffield grown device.

4.1.4 Effect of QD layer number on the emission and absorption properties of multilayer structures.

EL, PLE and photocurrent (PC) spectroscopy were used to evaluate the relative emission and absorption strengths of the new multilayer structures. Low injection (0.8 A/cm^2), normalised EL spectra from 400 μm diameter mesa devices of the 3, 5 and 10-layer structures are shown in Fig. 4.7.

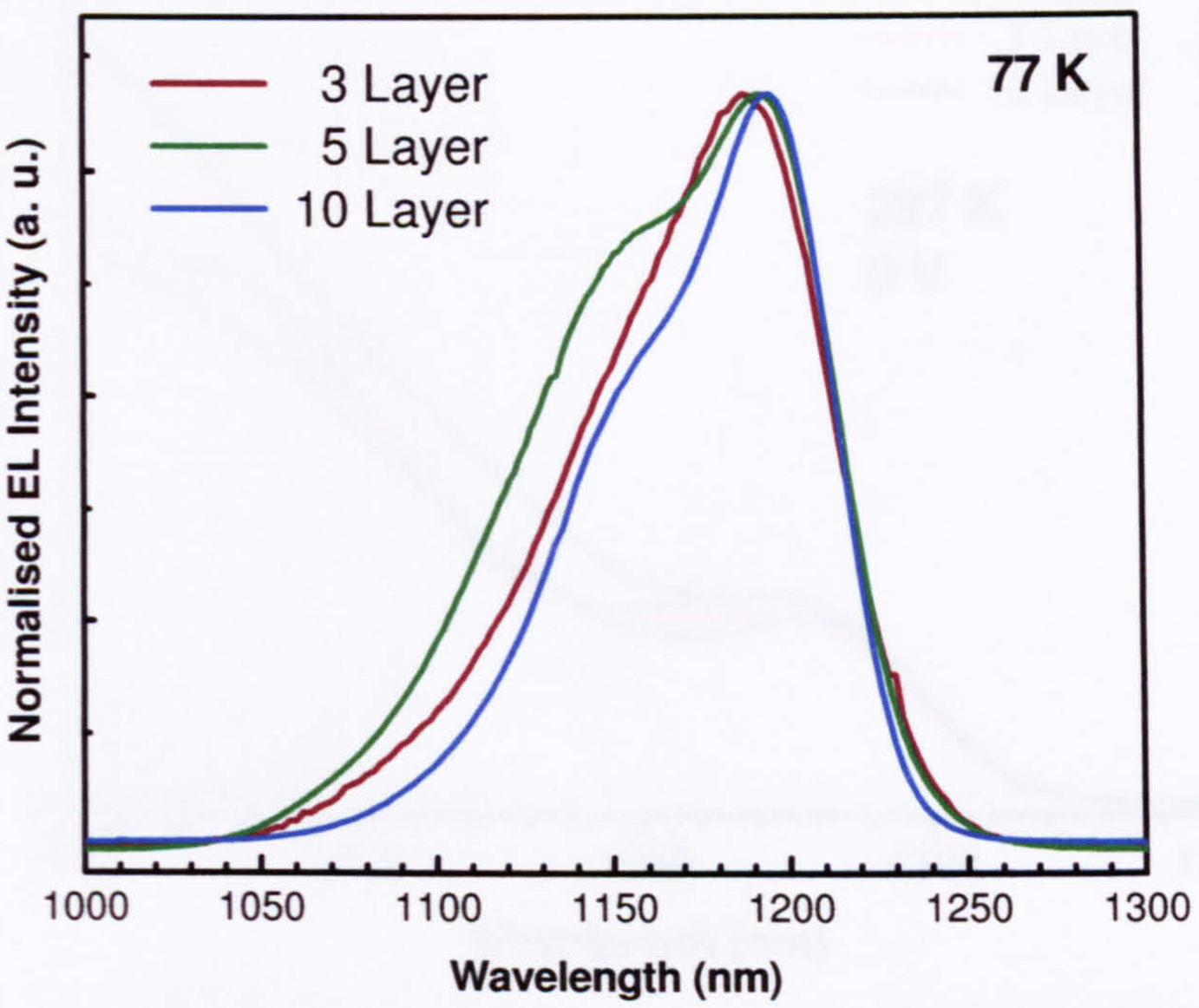

Fig. 4.7 Normalised, low temperature EL spectra obtained under low injection conditions (~0.8 A/cm^2) from 400 μm diameter mesas of the 3, 5 and 10-layer devices.

It is clear that the spectral forms of the 3 devices are fairly similar. All three devices exhibit a high energy shoulder to the main emission peak, with this being more intense in the 5-layer structure. Because of the low injection conditions used to excite these spectra this shoulder does not represent excited state emission but instead results from the presence of a bimodal QD distribution. The strength of this bimodal behaviour appears to be a very sensitive function of the growth conditions and exhibits a random variation between nominally identical structures.

The RT PC per QD layer is shown in Fig. 4.8. The PC was measured under zero applied bias, corresponding to a reverse bias of ~1.5 V, where it can be assumed that the majority of the photo-created carriers are able to thermally escape from the QDs before undergoing radiative recombination in the QDs[6]. As this process is expected to be dependent on the depth of the confinement potential it should be the same for each sample and hence the PC should reflect the intrinsic absorption strengths of the samples. However, any defect related non-radiative recombination will act to consume the carriers and results in a reduction of the PC signal.

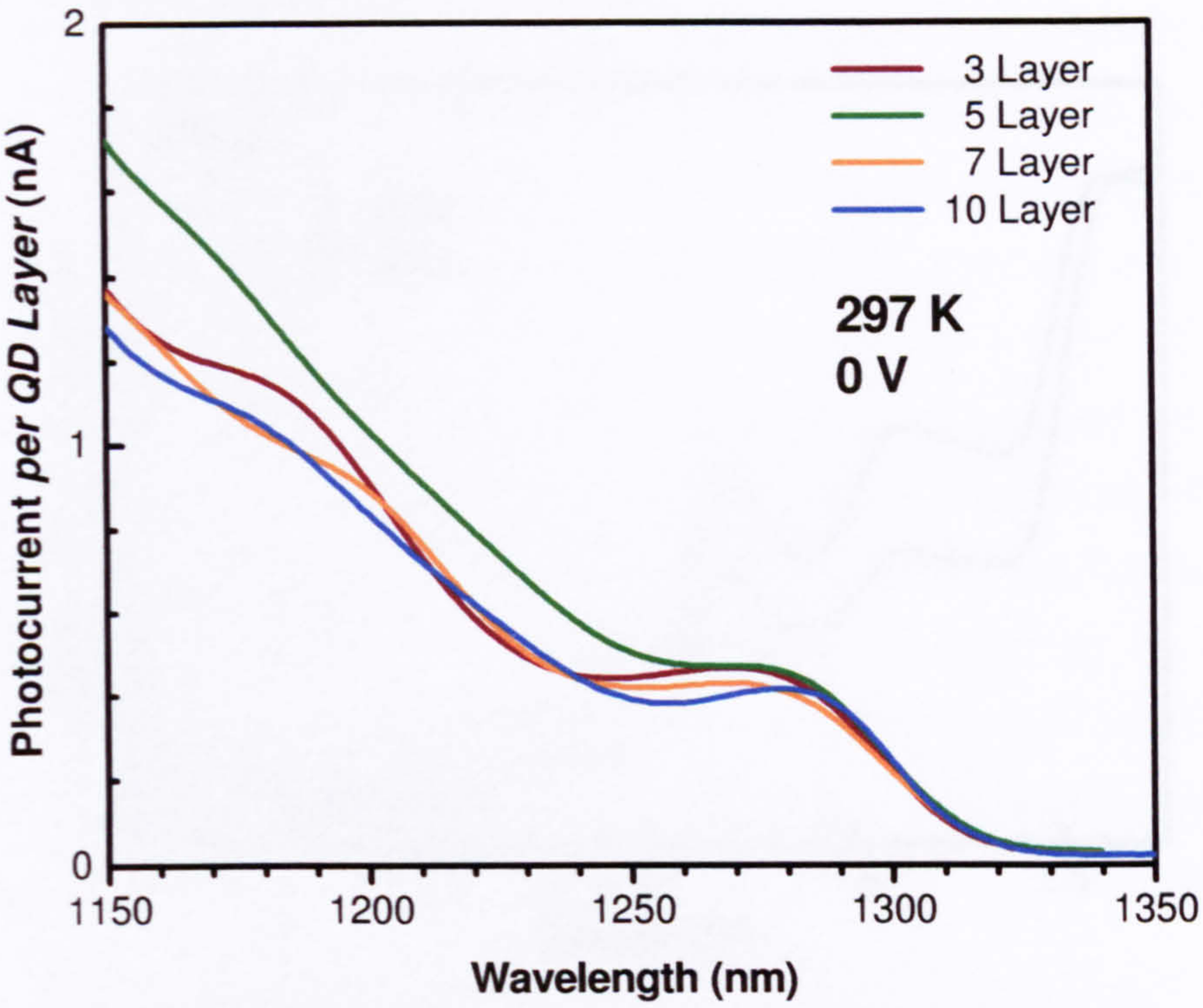

Fig. 4.8. RT photocurrent spectra, acquired with zero bias from 400 μm diameter mesas of the 3, 5, 7 and 10 layer samples. The strength of the PC has been scaled to the number of QD layers in the structure.

There are two features superposed on the background PC of each sample. The first clearly defined feature at ~1280 nm corresponds to absorption into the inhomogeneously broadened GS transition of the QDs. The magnitude of the absorption at this energy is seen to scale approximately with the total number of QD layers in the structure (it has a constant value in this figure due to the scaling to the QD layer number). The second broader feature, centred at ~1200 nm, is composed of the combined absorption into the first excited state of the larger QD subset and the GS transition of the smaller QD subset. The spectral form of this higher energy

PAGE

MISSING

IN

ORIGINAL

incorporated into large, dislocated QDs induced by the higher strain field surrounding these QDs, as has been seen in non-HGTSL multilayer structures[8]. If such dislocated QDs are present in the structure then it is reasonable to assume that their absolute number will increase with layer number, as defective QDs in one layer are likely to enhance the formation of similar QDs in subsequent layers. Therefore a higher level of non-radiative recombination, associated with the defective QDs, might be expected in structures with a higher layer number. This possibility can be probed by comparing the injection current dependence of the EL for structures with different numbers of QD layers.

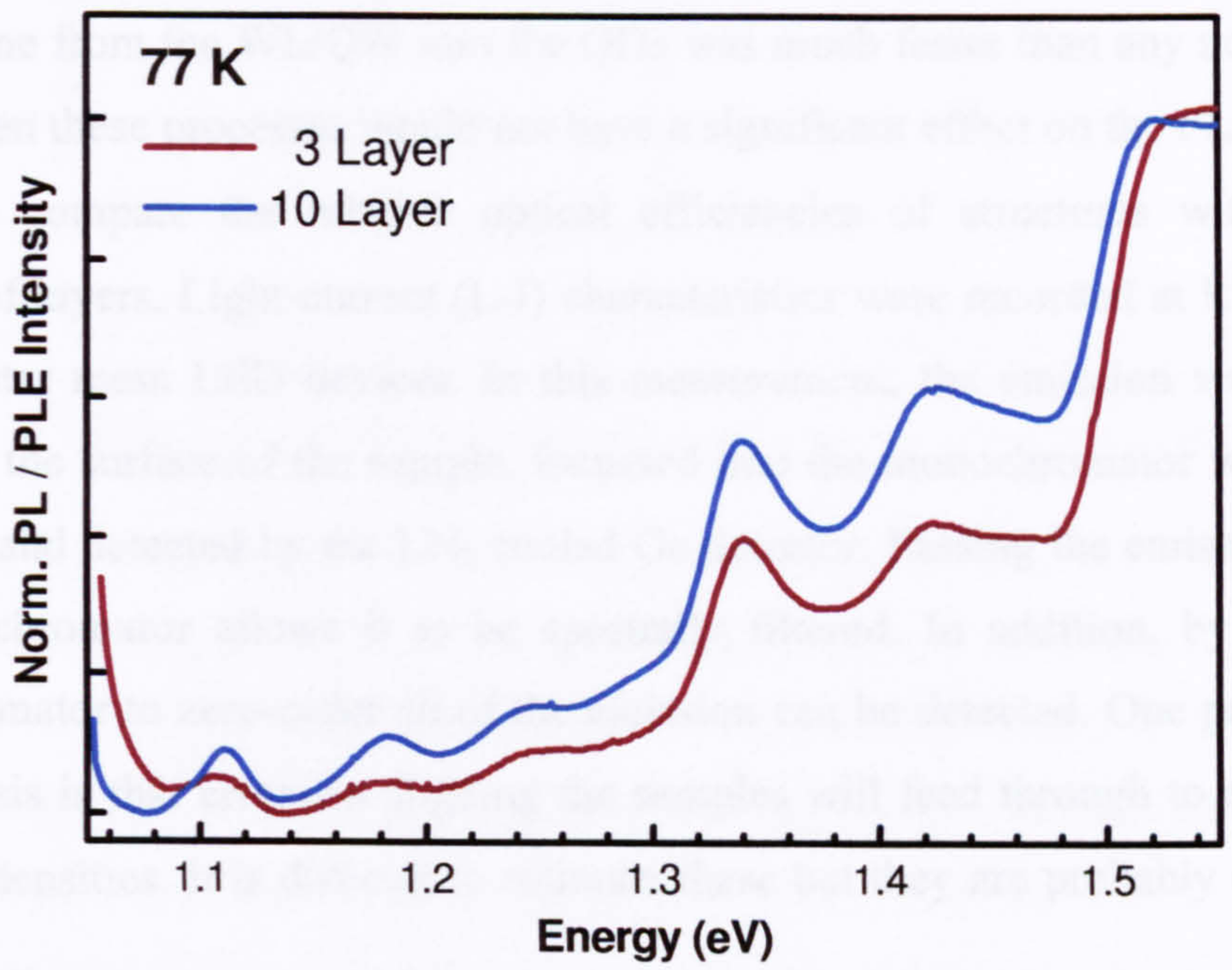

Fig. 4.9. 77 K PLE spectra, detected at the PL peak, of the 3 and 10 layer structures. Spectra have been normalised to the PLE intensity at 1.52 eV, the GaAs band edge.

Before this latter possibility is examined, it should be noted that there is no evidence for an increase in the dislocation density within the InGaAs WL/QW material with increasing layer number. Such an increase would be expected to affect the strength of the WL/QW signal observed in PLE as carriers initially created in this region would be more likely to recombine non-radiatively before being captured into the QDs. However by studying the relative intensity of the PLE of the WL/QW features for the 3 and 10-layer samples it appears possible to discount this possibility (Fig. 4.9). With respect to the absorption strength at the GaAs bandedge, where the PLE spectra have been normalised, there is a factor of 1.35 times more PLE signal

from the WL/QW of the 10 layer structure than that of the 3 layer structure. Denoting the total volumes of the InGaAs WL/QW and bulk GaAs material in the active region by V_{QW} and V_{GaAs} respectively, the ratio V_{QW}/ V_{GaAs} is 1.33 times greater in the 10 layer structure than in the 3 layer structure. This close agreement between the increases in the WL/QW PLE signal and material volume of the WL/QW suggests an equivalent degree of material quality for the WL/QW in the 10 and 3 layer structures, and hence that there is no degradation in higher layers due to a build up of strain. This analysis assumes that the GaAs PLE signal is not degraded by an increase in non-radiative centres within the GaAs or by similar centres in the WL/QW if carriers are captured from the GaAs into the QDs via the WL/QW. In addition, if the carrier capture time from the WL/QW into the QDs was much faster than any non-radiative process then these processes would not have a significant effect on the PLE signal.

To compare the relative optical efficiencies of structures with different numbers of layers, Light-current (L-I) characteristics were recorded at RT from 200 μm diameter mesa LED devices. In this measurement, the emission was collected normal to the surface of the sample, focussed into the monochromator with wide (3 mm) slits and detected by the LN_2 cooled Ge detector. Passing the emission through the monochromator allows it to be spectrally filtered. In addition, by setting the monochromator to zero-order all of the emission can be detected. One problem with this analysis is that errors in aligning the samples will feed through to errors in the relative intensities. It is difficult to estimate these but they are probably of the order 10%.

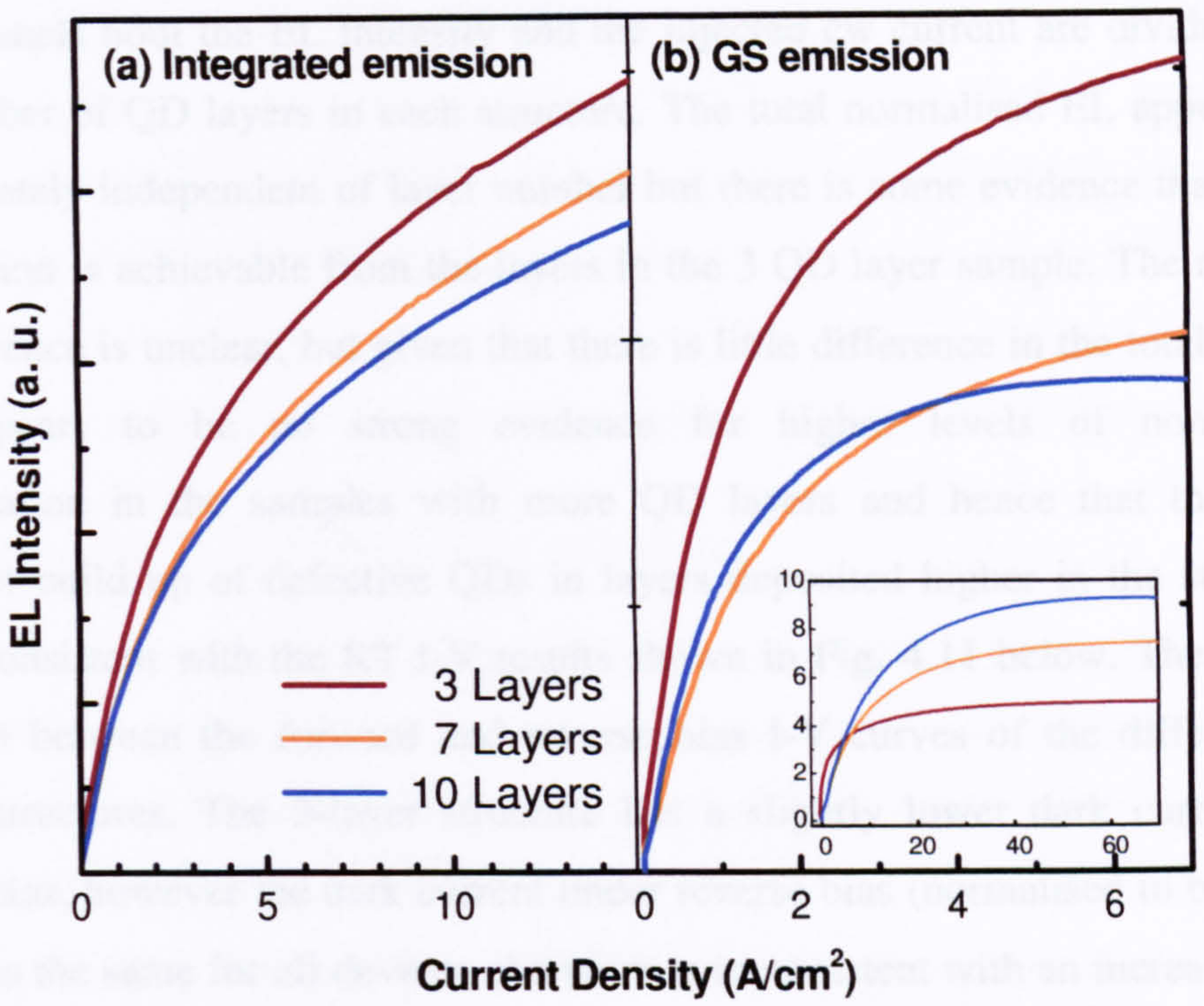

Fig. 4.10. Spectrally integrated (a) and GS (b) emission intensity, *per QD layer*, as a function of injection current *per QD layer* for the 3, 7 and 10-layer structures. Inset to (b) shows absolute GS emission intensity as a function of injection current for each structure.

The inset to Fig 4.10 (b) shows the GS emission as a function of current density for the 3, 5 and 7 layer samples. This data appears to show that at any current density the radiative efficiency increases with the number of layers. However this data is slightly misleading as the roll over with increasing current, observed for all samples, shows that the efficiency decreases with increasing current. This may reflect increasing carrier loss from excited states as these are populated or Auger processes. For example, in a 3 layer structure, a current density of 60 A/cm^2 corresponds to ~4 electron – hole pairs/QD. Whatever the mechanism, this acts to reduce the apparent overall efficiency of the samples with lower number of QD layers because, for a given injection current, the QDs in these samples will have a higher carrier occupancy. A better comparison is obtained by dividing both the horizontal (current density) and vertical (emission intensity) scales by the number of QD layers in each sample so that the intensity produced per layer for the current density injected into each layer is given. Such results are shown in the main part of Fig. 4.10, where in the right hand panel (b) the monochromator was set to 1300 (±3) nm to allow only GS emission from the large QD subset to be detected and in the left hand panel (a) the *total* emission (monochromator grating set to zero order) is shown.

In both panels both the EL intensity and the injected cw current are divided by the total number of QD layers in each structure. The total normalised EL appears to be approximately independent of layer number but there is some evidence that a larger GS emission is achievable from the layers in the 3 QD layer sample. The reason for this difference is unclear, but given that there is little difference in the total emission there appears to be no strong evidence for higher levels of non-radiative recombination in the samples with more QD layers and hence that there is no significant build up of defective QDs in layers deposited higher in the stack. This view is consistent with the RT I-V results shown in Fig. 4.11 below. There is little difference between the forward and reverse bias I-V curves of the different layer number structures. The 3-layer structure has a slightly lower dark current under forward bias, however the dark current under reverse bias (normalised to breakdown voltage) is the same for all devices, therefore is inconsistent with an increased defect density in the 3-layer structure.

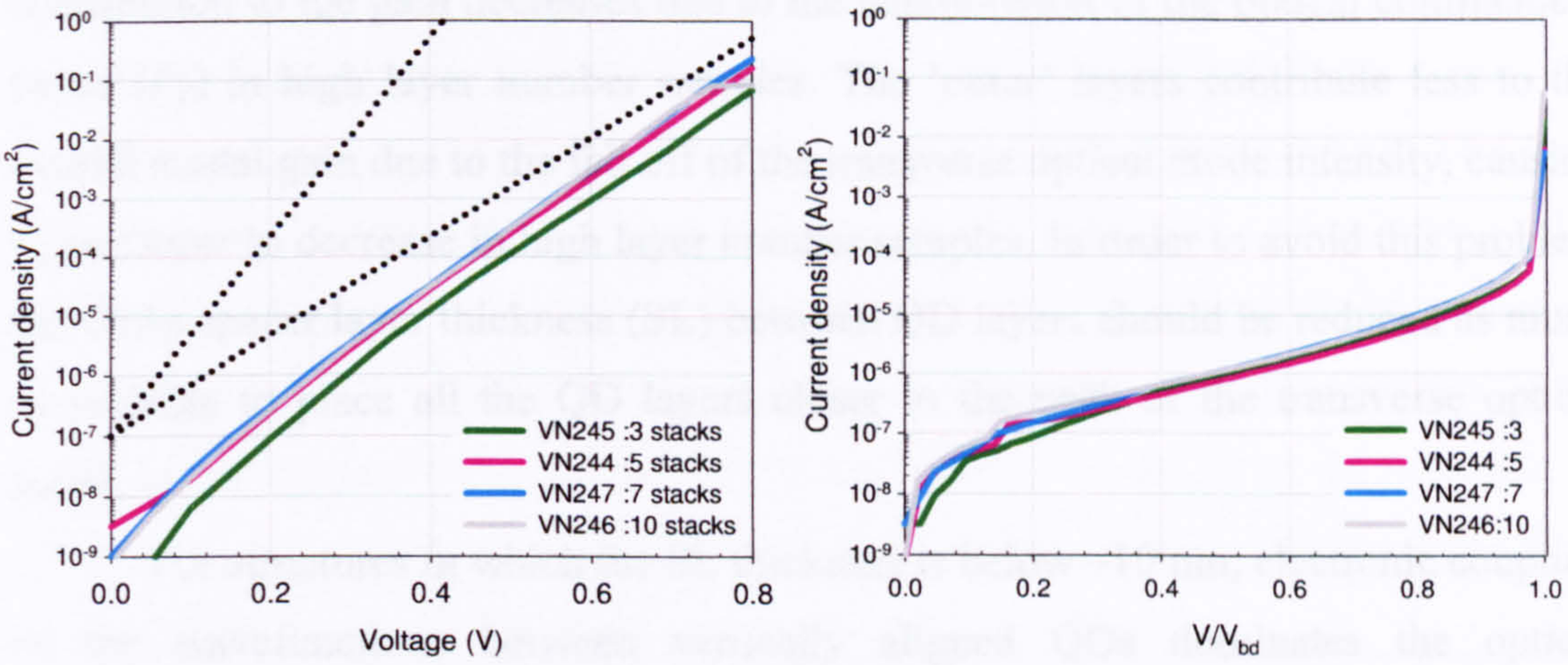

Fig. 4.11. RT I-V characteristics of the multilayer structures measured under forward bias (a) and reverse bias (b). The reverse bias I-Vs are normalised to the reverse breakdown voltage (V_{bd}) *Figure courtesy of Fadzlin Hasbullah*

Measurements of the peak modal gain per layer, radiative and non-radiative current density as functions of the quasi-Fermi level separation, performed at Cardiff University, provide some support for this conclusion. They reveal that, at low injection where the majority of the emission originates from the GS, the *per layer* peak modal gain and radiative current density per layer are approximately the same in all of the multilayer structures[7]. Another important outcome of the modal absorption measurements, especially with regard to the interpretation of the

discussion in section 4.1.2, is that the internal optical mode loss (α_i) does not increase with layer number, remaining constant at 3 (±2) cm^{-1} for all four samples. This implies that the change in waveguide design has not selectively damaged the performance of the narrower active region devices.

4.2 QD Laser structures incorporating 35 nm HGTSLs

4.2.1 Introduction and sample structures

The proportional increase in the GS absorption with layer number, as inferred from the PC spectra shown in Fig. 4.8, confirms that the HGTSL step is a viable method for stacking up to 10 QD-planes whilst avoiding catastrophic degradation to the structural and optical properties of QDs in latter deposited layers. To a certain extent, this important advance is reflected in the performance of the fabricated devices. However, as discussed in section 4.1.2, as more layers are added their contribution to the gain decreases due to the deterioration of the optical confinement factor (Γ_Z) in high layer number samples. The 'outer' layers contribute less to the overall modal gain due to the fall off of the transverse optical mode intensity, causing *Γ_Z per layer* to decrease in high layer number samples. In order to avoid this problem, the GaAs spacer layer thickness (SL) between QD layers should be reduced as much as possible to place all the QD layers closer to the peak of the transverse optical mode.

For structures in which the SL thickness is below ~10 nm, electronic coupling of the wavefunctions between vertically aligned QDs dominates the optical properties. Whilst the advantages of such structures have been predicted to include narrower lasing widths and higher output powers[9], practically these would be hard to achieve considering the high concentration of strained QD material present in the structures. Even when QD planes are separated by distances greater than the electronic coupling range, strain induced vertical ordering of 'columnar' QDs may persist for SL thicknesses up to ~20 nm, producing in-plane ensembles of QDs that increase in size as the stacking sequence is repeated[10]. It should be mentioned that such strain coupled QDs have demonstrated applications as gain media in laser structures[11, 12]. However both of these coupling mechanisms are undesirable if the

emission wavelength needs to be controlled with a small degree of tolerance, as is the case for 1.3 μm QD applications[13].

In order to investigate the possibility of using less material in the GaAs SLs, two new structures were grown, both containing 5 DWELL layers obtained under nominally identical conditions to those described in chapter 3, section 3.2, but with a reduced GaAs spacer layer thicknesses of 35 nm. The sample structures, summarised in Table 4.12, will now be described. Vn 505 has 35 nm GaAs SLs with the first 15 nm, after the DWELL growth, grown at the same temperature (510 °C) and the final 20 nm at 585 °C. This structure will be referred to as having a 'standard-HGTSL'. Vn 513 also has 35 nm SLs with the initial 15 nm of GaAs again deposited at 510 °C but with the final 20 nm of GaAs now grown at 620 °C. This latter structure will be labelled as having a 'super-HGTSL'. Standard ridge waveguide devices were processed and cleaved into 3, 2 and 1 mm cavity lengths.

In terms of laser performance there are two potential benefits of extending the original HGTSL technique in these new samples: it should potentially allow the growth of high quality multi-layer structures with a smaller QD layer spacing, increasing Γ_Z due to the more closely spaced QD planes (for a 5 layer structure, reducing the SL thickness to 35 nm increases Γ_Z by a factor of 1.05 relative to that for 50 nm SLs[14]); and should give a larger material gain caused by the improvement in the homogeneity of the ensemble due to the more effective planarisation of the GaAs growth surface produced by the higher growth temperature of the latter part of the SL.

Sample	Number of QD Layers	GaAs SL thickness (nm)	Initial 15 nm GaAs T_G (°C)	Final 20 nm GaAs T_G (°C)
Vn 505	5	35	510	585
Vn 513	5	35	510	620

Table 4.12 Growth parameters of the redesigned HGTSL structures.

4.2.2 Characterisation of QD laser structures with 35 nm HGTSLs

The difference in SL growth conditions has a profound effect on the laser performance of fabricated devices, as can be seen in Fig. 4.13. A 3 mm cavity of the 35 nm structure with the standard-HGTSL does not lase from the GS at RT. In contrast, the super-HGTSL structure exhibits a very low pulsed RT GS lasing with a J_{th} of 25 A/cm^2 – the lowest J_{th} obtained for any 3 mm cavity grown in Sheffield (see Table 3.16).

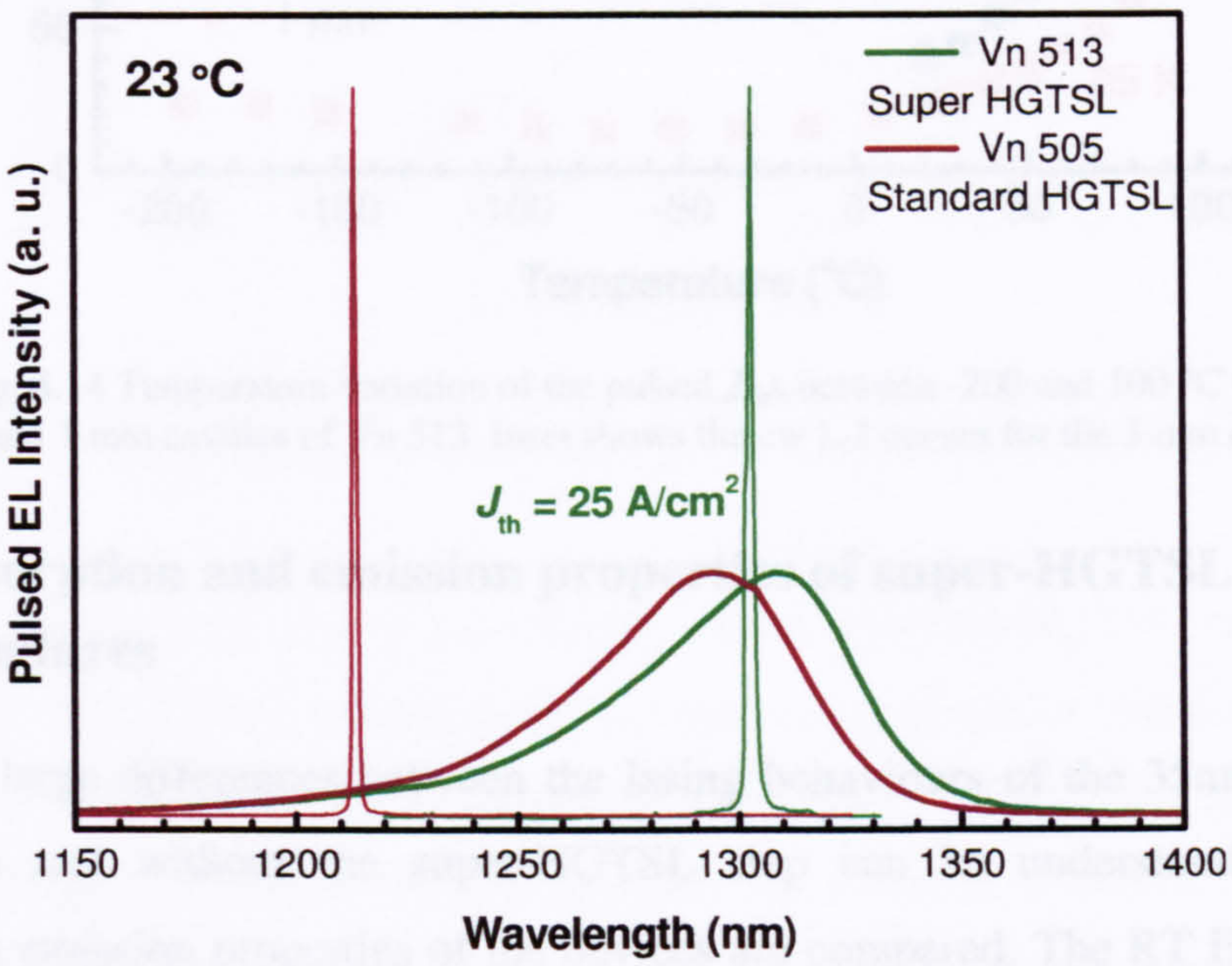

Fig. 4.13 Sub-threshold and lasing pulsed EL at RT for 3 mm cavities of the two 5 layer structures with 35 nm GaAs SLs grown at different temperatures.

In addition to their very low pulsed and cw J_{th}s, devices processed from the super-HGTSL structure possess a reduced J_{th} temperature sensitivity and shorter cavities are now able to operate at higher temperatures, as is shown in Fig. 4.14. The inset to this figure displays the above room temperature cw LI curves for the 3 mm device. Within experimental error, the slope efficiency is unchanged between 23 and 100 °C. Significantly, cw GS lasing (J_{th} = 217 A/cm^2) is now possible from a 1 mm as cleaved device. To date, this represents the shortest cavity length 1.3μm QD laser grown in Sheffield which is able to operate in cw mode from the GS.

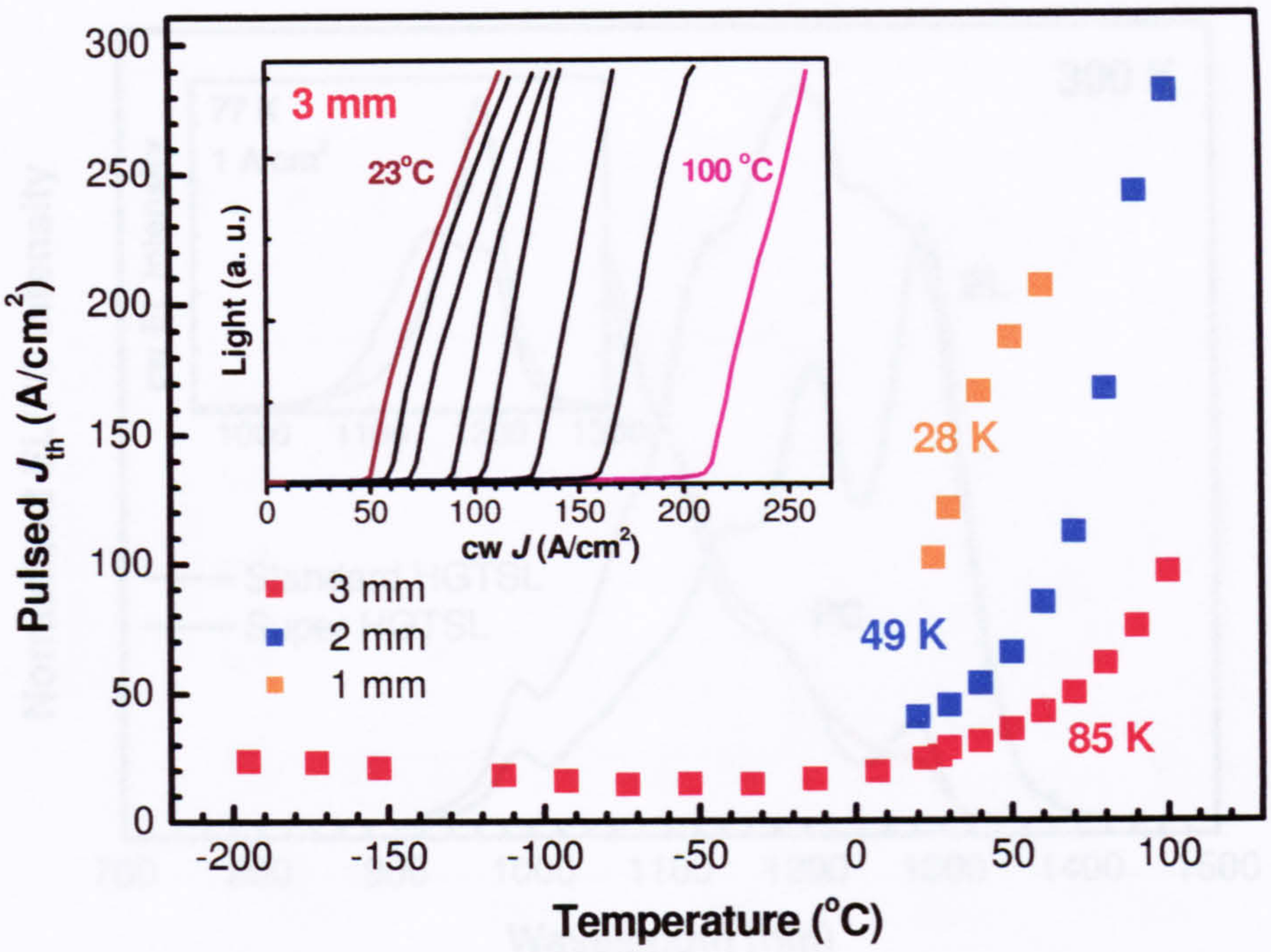

Fig. 4.14 Temperature variation of the pulsed J_{th}s between -200 and 100 °C for 3, 2 and 1 mm cavities of Vn 513. Inset shows the cw L-I curves for the 3 mm device

4.2.3 Absorption and emission properties of super-HGTSL structures

The large differences between the lasing behaviours of the 35nm structures grown with and without the super-HGTSL step can be understood when the spontaneous emission properties of the devices are compared. The RT EL, recorded under high pulsed bias (~ 320 A/cm^2) for each structure and shown in Fig. 4.14, reveals clear state filling effects in the super-HGTSL structure (Vn 513), in contrast to the poorly defined emission features of the standard-HGTSL structure (Vn 505). Correspondingly, the interband QD absorption features, as observed in PC spectra, are less distinct and weaker in the latter structure. These spectral differences between the samples closely resemble what was seen during the initial development of the HGTSL process based on 50 nm spacer layers and described in chapter 3, section 3.3.3, in which broadband emission and only low temperature lasing was obtained from a 5-layer structure without the HGTSL step, in contrast to the superior performance of a similar structure but with only 3-layers. Hence it appears that the normal HGTSL process may be unable to planarise the growth surface when the SL thickness is reduced to 35nm.

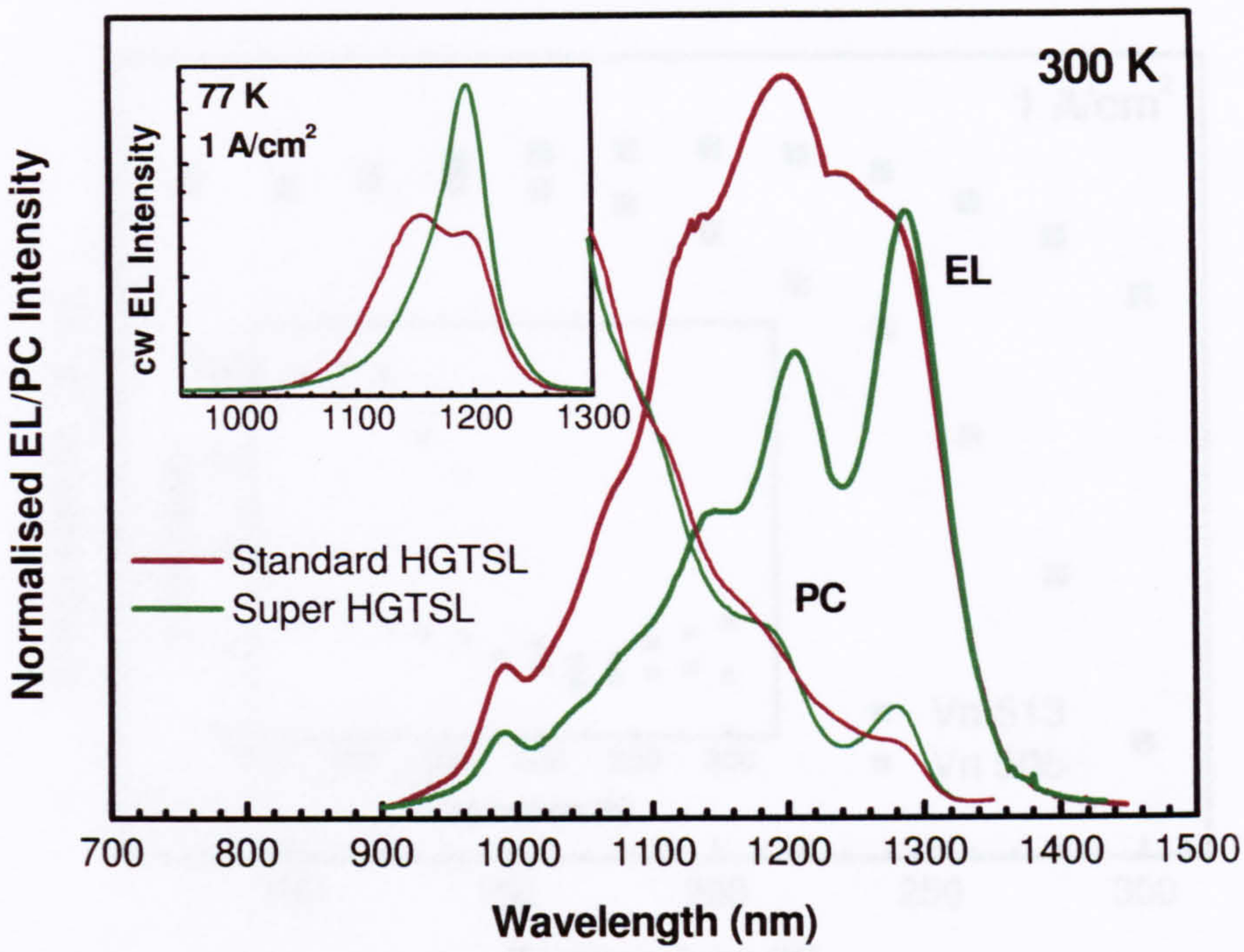

Fig. 4.15 main part: RT high bias (320 A/cm^2) normalised EL and PC for the standard and super-HGTSL 35 nm spacer layer structures. Inset shows a comparison of the 77 K low bias EL.

The weaker peak absorption strength of the standard-HGTSL structure (Vn 505), inferred from the PC, is consistent with the results of modal loss measurements, conducted at Cardiff University, using the segmented contact method[15]. The GS modal absorption of the super-HGTSL structure was found to be around twice that of the standard structure, indicating a factor of ~2 increase in the number of QDs contributing to the absorption at this energy[16]. It is clear from the low injection EL spectra at 77 K, shown in the inset to Fig. 4.15, that the spectral forms of the emission are very different. The low injection, low temperature EL depicted in the inset of Fig. 4.15 makes it clear that the standard-HGTSL structure is strongly bimodal, with a larger proportion of the QDs emitting at shorter wavelengths. In contrast, the super-HGTSL structure exhibits emission which is concentrated at long wavelengths. Interestingly however, the integrated emission intensities are approximately equal at this temperature, which may be related to the lack of evidence for defect formation in either structure, as observed in TEM images. However, it is also possible that any non-radiative processes are not active at this temperature and additional evidence, presented below, indicates a higher non-radiative recombination in the standard-HGTSL structure, particularly at high temperatures.

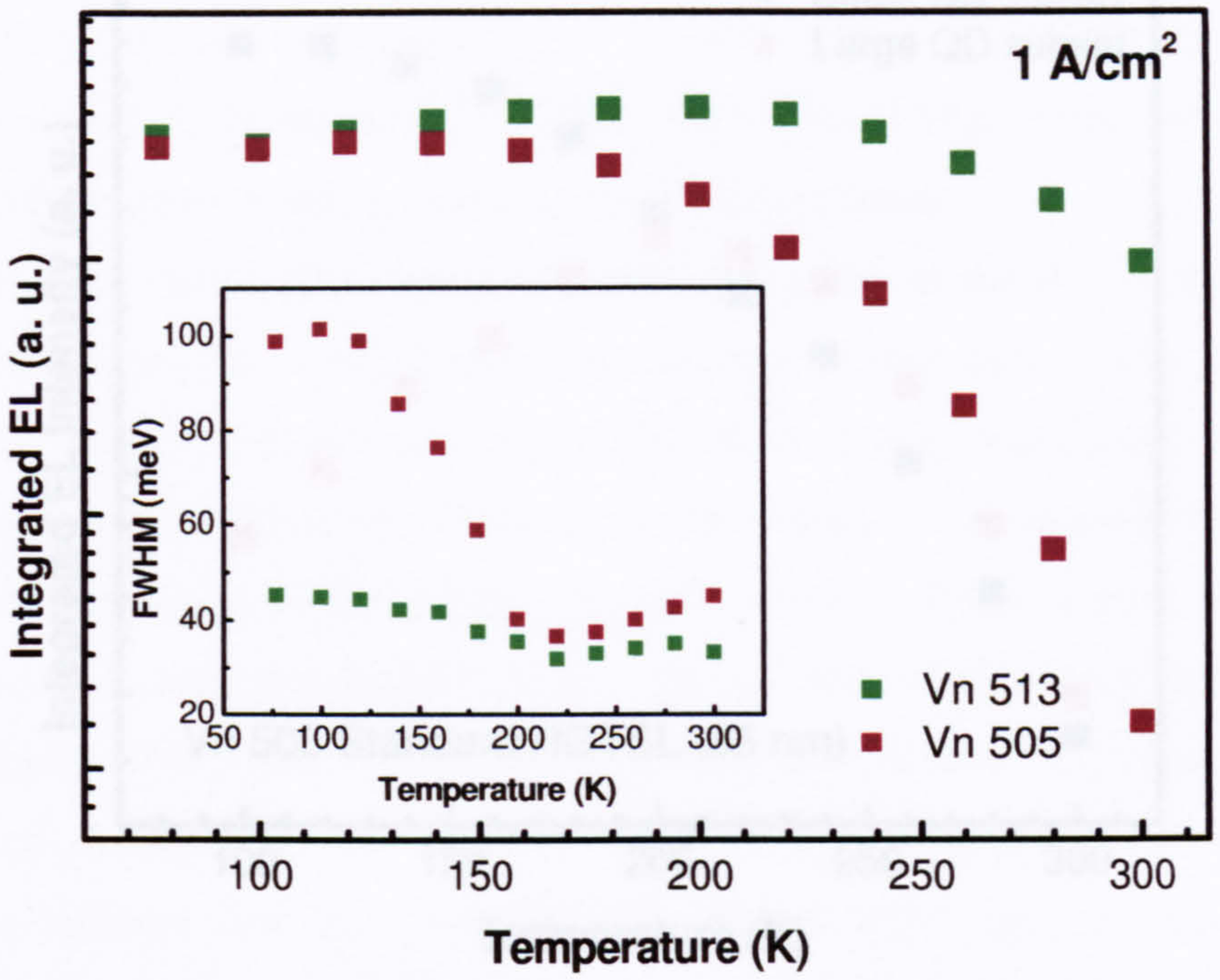

Fig. 4.16 Main part: Temperature dependence of the integrated emission intensity of the low injection EL for the standard and super HGTSL structures. The inset shows the respective variations of the FWHMs over the same temperature range.

Possibly associated with the less uniformly sized QDs or even defective QDs in the standard-HGTSL structure is the observed reduction in the high temperature radiative efficiency. The temperature dependencies of the integrated EL intensity of the two structures are shown in Fig. 4.16. Between 77 and 300 K, the integrated EL of the standard-HGTSL structure diminishes by an order of magnitude, whereas the corresponding decrease for the super-HGTSL structure is less than a factor of 2.

By fitting two Gaussian peaks to the emission spectrum of the standard-HGTSL structure at each temperature, the temperature dependence of the integrated EL intensity for each QD subset can be extracted. This is plotted in Fig. 4.17.

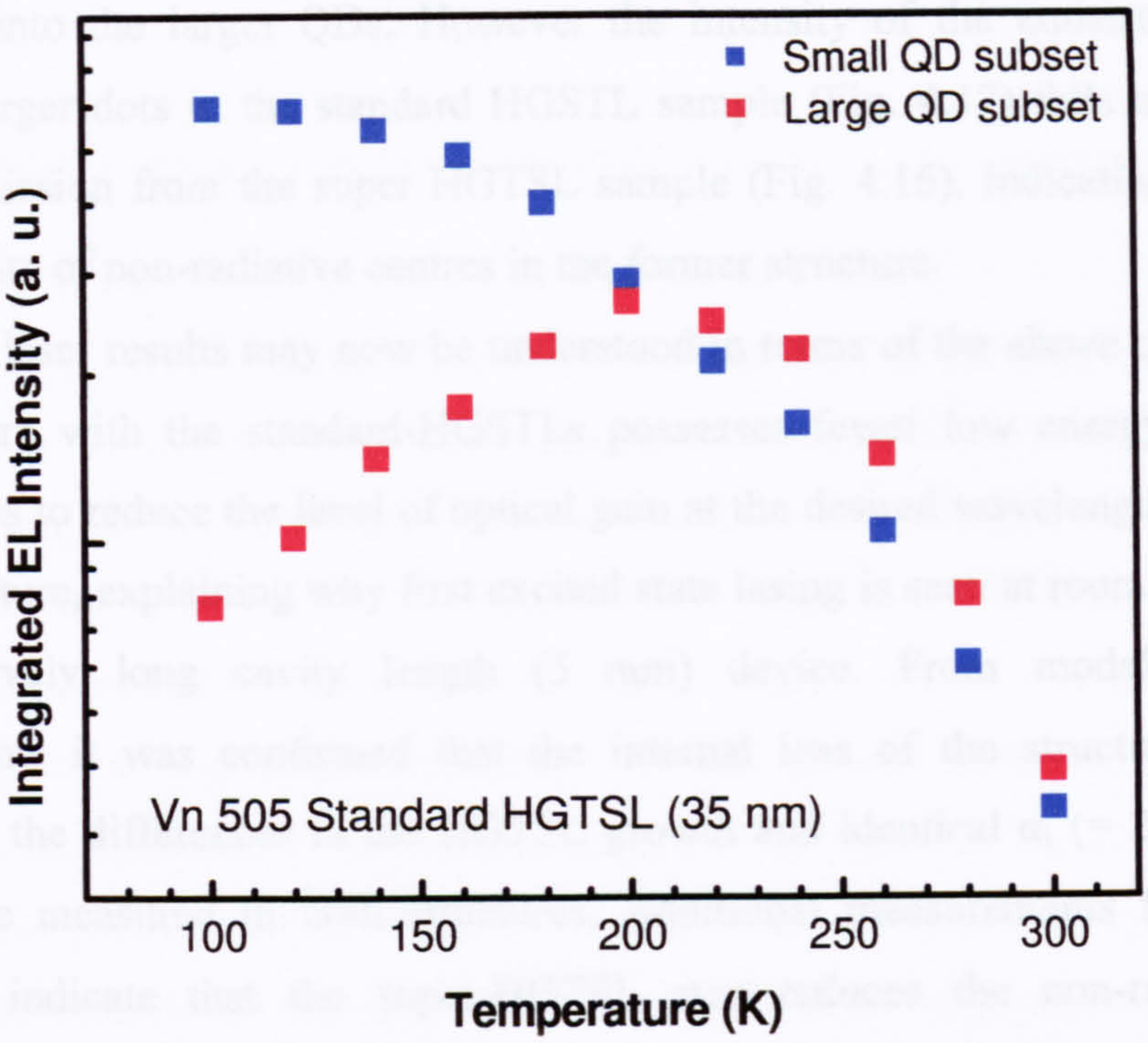

Fig. 4.17 Temperature dependent integrated EL intensities of the small, shorter wavelength QD subset (blue squares) and the large, longer wavelength QD subset (red squares) in the standard-HGTSL structure.

The effect of a temperature induced change in the equilibrium carrier redistribution between 77 and 200 K is clearly demonstrated by the opposite dependencies of the two integrated EL intensities. The shallower confinement potential of the smaller QDs allows carriers to escape at relatively low temperatures. If these thermally emitted carriers are then recaptured by the larger QDs before undergoing non-radiative recombination in the WL, then the emission spectrum will change shape without a reduction in the *total* integrated EL, which remains approximately constant between 77 and 200 K (see Fig. 4.16) Associated with the temperature induced change in the carrier distribution within the QD ensemble is the rapid reduction in FWHM, observed over the same temperature range and plotted in the inset of Fig. 4.16. Above 200 K, the integrated EL of the large QD subset begins to decrease, marking the onset of significant thermal carrier escape from the most deeply confined QD states in the ensemble Over this temperature range the total intensity of the standard HGTSL structure decreases more rapidly than that of the super HGTSL one (see Fig. 4.15). Some of this enhanced decrease may reflect the fact that carriers initially captured in the subset of smaller dots will spend some time in the WL, where they may undergo non-radiative recombination, before being

recaptured into the larger QDs. However the intensity of the emission from the subset of larger dots in the standard HGSTL sample (Fig. 4.17) falls more rapidly than the emission from the super HGTSL sample (Fig. 4.16), indicating a possible higher density of non-radiative centres in the former structure.

The laser results may now be understood in terms of the above observations. The structure with the standard-HGSTLs possesses fewer low energy QD states which serves to reduce the level of optical gain at the desired wavelength of ~1.3μm in this structure, explaining why first excited state lasing is seen at room temperature in a relatively long cavity length (3 mm) device. From modal absorption measurements it was confirmed that the internal loss of the structures was not affected by the differences in the HGTSL growth and identical α_i (= 2.2 ± 1 cm^{-1}) values were measured in both structures. Additional measurements from Cardiff University indicate that the super-HGTSL step reduces the non-radiative and increases the radiative current density at all injection levels in agreement with the data shown in Fig. 4.15. Hence the use of the super-HGTSL technique results in a greater number of larger, low energy emitting QDs and also improves the radiative efficiency of the structure.

However, the saturated GS gain of the super-HGTSL (~12 cm^{-1})[16] is still considerably lower than some of the values reported by other groups. It is desirable to maximise the saturated gain, since this will enable shorter cavities to lase from the GS. For example, recently a saturated GS gain of 41 cm^{-1} was reported for an MBE grown 7-layer DWELL device, operating at 1305 nm from a 320μm long cavity[17]. Previously the Ioffe Institute in St Petersburg achieved a saturated GS gain of 24 cm^{-1} using 33 nm thick SLs to separate 10 DWELL planes, with no noticeable degradation in the optical properties of the samples[4]. The deposition rate and growth temperature of the SLs remains, however, undisclosed. These results suggest that further improvements in the present devices are possible via further optimisation of the growth.

4.3 A QD laser with a Graded Strain Reducing Layer (GSRL)

4.3.1 Grading the In composition in the $In_xGa_{1-x}As$ capping layer

It is well known that the strain distribution surrounding InAs QDs is far from isotropic, due in part to the compositional inhomogeneity of the individual QDs but also reflecting relaxation of the lattice constant towards the InAs unstrained value with increasing height in the dot. Various studies have indicated that the Indium profile within the QDs tends to increase from QD base to tip[18]. When the QDs are capped with a material of a *fixed* composition and therefore lattice constant (a_0), this represents a potential problem since there will always be a difference between the cap-QD lattice mismatch at the top and bottom of the QD. An $In_{0.15}Ga_{0.85}As$ strain reducing layer (SRL) provides a partial solution, but a compositionally graded SRL would further reduce the strain contrast between the QD and surrounding matrix material. It was with this consideration in mind that a sample with a 6 nm $In_xGa_{1-x}As$ SRL of *graded In composition* was grown.

Above the QDs, the growth sequence of the compositionally graded InGaAs SRL consisted of 2 nm $In_{0.22}Ga_{0.78}As$, followed by 2 nm $In_{0.15}Ga_{0.85}As$ and finally 2 nm $In_{0.08}Ga_{0.92}As$. This sequence gives a high In composition immediately next to the QDs but minimises the total amount of strained material. Such a design will be referred to as a Graded SRLs (GSRLs). Aside from the change to the SRL, the design of the new sample containing GSRLs (Vn 248) was based on Vn 249 (i.e. 5 DWELL planes separated by 50 nm GaAs HGTSLs).

4.3.2 Comparison of emission characteristics: effect of the graded strain reducing layer (GSRL) on the QD size distribution

Fig. 4.18 compares the low temperature, low injection current mesa EL spectra of the two 5-layer structures grown with the standard SRL and the GSRL. Each spectrum is composed of two broad Gaussian peaks indicating a bimodal QD size distribution in each sample. Based on the relative emission intensities of the low and high energy QD sub-sets, there are a greater number of smaller QDs in the sample with the GSRL (Vn 248). The emission wavelength of the two subsets of QDs varies by only ~10 nm between samples.

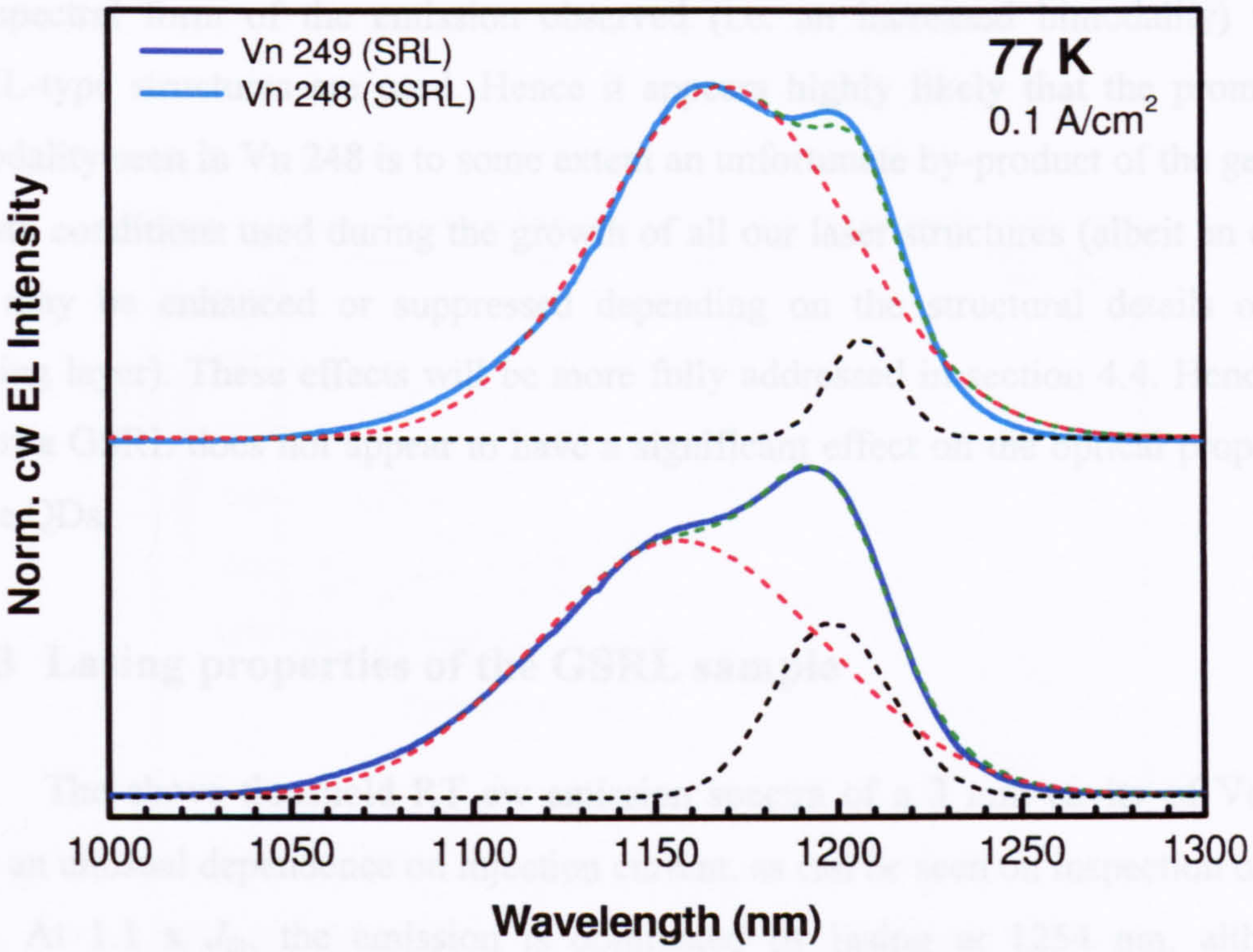

Fig. 4.18 Normalised, low injection cw EL spectra at 77 K of (lower trace) a five layer device with the standard ungraded $In_{0.15}Ga_{0.85}As$ capping layer – Vn 249 and (upper trace) the sample with the graded strain reducing InGaAs capping layer. Dotted lines are Gaussian fits to the spectra.

There have been a number of PL studies of capped QDs using composite In(Al)GaAs SRLs of varying In/Al composition, similar to that employed in Vn 248. Some reports cite the effects of mass transport during the overgrowth, which change the structural and therefore optical properties of the QDs[19]. Others rely on arguments based purely on strain modification[20]. For example, it has been proposed that the residual compressive strain near the bottom of the QDs has a greater effect on the emission wavelength than strain components near the QD tip due to the localisation of the GS electron wavefunction towards the base of the QDs[21].

The latter argument may be tested with respect to the present samples. For the GSRL sample (Vn 248), if it is assumed that the capping layer has the intended compositional variation and hasn't undergone significant intermixing during growth, the in-plane interface strain at the QD base and tip can be expected to be significantly different. However, the nearly identical PL peak positions (and their component Gaussians') of Vn 248/249 gives no evidence to support the claims of a systematic modification to the strain state of the QDs resulting from the use of a GSRL. To the

best of my knowledge, in none of the previous reports is any pronounced change to the spectral form of the emission observed (i.e. an increased bimodality) when GSRL-type structures are used. Hence it appears highly likely that the prominent bimodality seen in Vn 248 is to some extent an unfortunate by-product of the general growth conditions used during the growth of all our laser structures (albeit an effect that may be enhanced or suppressed depending on the structural details of the capping layer). These effects will be more fully addressed in section 4.4. Hence the use of a GSRL does not appear to have a significant effect on the optical properties of the QDs.

4.3.3 Lasing properties of the GSRL sample

The above threshold RT cw emission spectra of a 3 mm cavity of Vn 248 have an unusual dependence on injection current, as can be seen on inspection of Fig. 4.19. At 1.1 x J_{th}, the emission is dominated by lasing at 1254 nm, although subsidiary peaks occur at 1262 and 1284 nm. As the injection is increased to 1.2 x and 1.3 x J_{th}, the emission from these secondary peaks grows in intensity relative to the higher energy emission and eventually the emission at 1262 nm is quenched leaving a 30 nm separation between the lower and higher wavelength features. The spectral separation between the GS maxima of the low and high energy QD sub-set was measured to be 40 nm at 77 K, therefore it seems reasonable to attribute the emission at high injection to lasing via the GSs of both QD sub-sets. The single lasing wavelength of 1290 nm observed from a 4 mm cavity is consistent with this explanation, since the lower threshold gain required can be attained under lower injection such that the GS of the smaller QD subset is not significantly populated

Further anomalous behaviour for the GSRL structure is seen in the temperature dependence of the lasing wavelength (recorded for pulsed injection at 1.1 x J_{th}) for the 3 mm cavity of Vn 248 and Vn 247, shown in the inset to Fig 4.19. The presence of additional lasing lines in Vn 248 blurs the pure dependence, but the overall trend is not obscured. It is seen that the rate at which the lasing wavelength shifts with temperature is reduced by a factor of ~4, from 0.44 nm/K in the sample with conventional SRLs (Vn 247) to 0.12 nm/K in the GSRL structure (Vn 248).

Over a similar temperature range, coefficients of 0.48 nm/K[22] and 0.41 nm/K[23] have been measured in other 1.3 μm In(Ga)As QD laser structures.

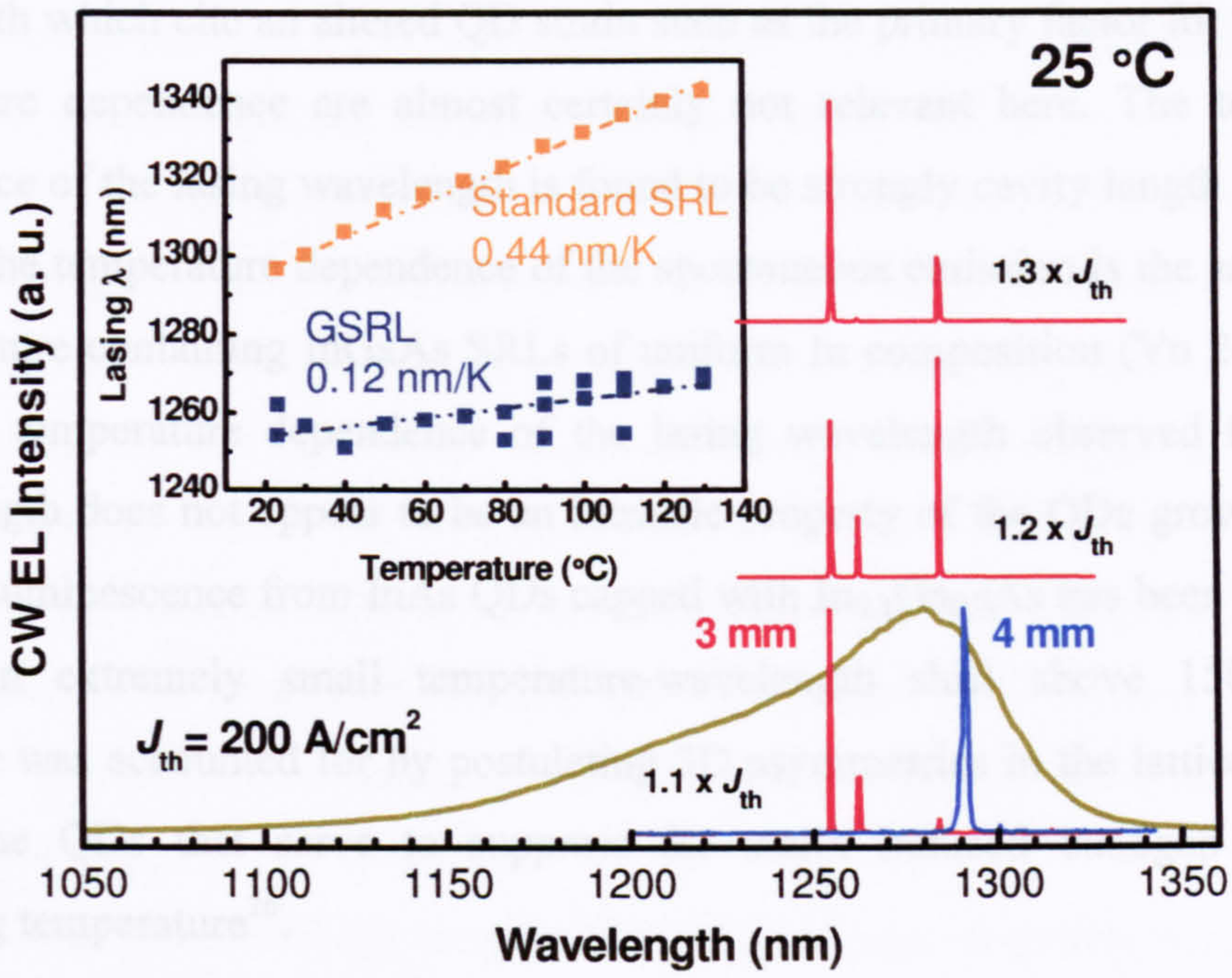

Fig. 4.19 RT cw lasing spectra for 3 and 4 mm cavities of the GSRL structure (Vn 248). Inset shows the temperature dependence of the lasing wavelength at 1.1 x J_{th} for a 3 mm cavity of Vn 248 (navy dots) and a structure with an InGaAs SRL of uniform In composition (Vn 247 – orange dots).

Compared to QW lasers, QD lasers have previously been observed to possess a weaker temperature dependence of the lasing wavelength ($d\lambda/dT$) due to the temperature insensitivity of the peak gain (G)[24]. This somewhat fortuitous result relies on the energy distribution of the QD states, as determined by the inhomogeneous broadening, matching the thermal spread of the Fermi functions for a given value of G. A similar study concluded that energies (E), where dE/dG is a minimum, also correspond to a minimum in $d\lambda/dT$[25]. These conditions are most likely to be met in shorter devices that are operated closer to their saturated gain, where a greater proportion of higher energy states are populated – as is observed for the 3 mm cavity in Fig. 4.19. A 4 mm cavity of Vn 248 did not exhibit the same $d\lambda/dT$ dependence as the 3 mm cavity, since the weak $d\lambda/dT$ sensitivity of the latter results from a specific gain spectrum determined by the cavity length and state population. Hence the observed relatively temperature insensitive emission of the 3mm cavity of the GSRL structure does not appear to be an intrinsic property but

may be enhanced by the presence of a larger bimodal distribution of QD sizes present in this sample (Fig. 4.18) which appears to give a slightly flatter emission and hence possibly flatter gain spectrum.

Alternative arguments for the weaker temperature dependence of the lasing wavelength which cite an altered QD strain state as the primary factor for the weaker temperature dependence are almost certainly not relevant here. The temperature dependence of the lasing wavelength is found to be strongly cavity length dependent, whereas the temperature dependence of the spontaneous emission is the same as that of a structure containing InGaAs SRLs of uniform In composition (Vn 249). Hence the weak temperature dependence of the lasing wavelength observed for a 3mm cavity length does not appear to be an intrinsic property of the QDs grown with the GSRL. Luminescence from InAs QDs capped with $In_{0.3}Ga_{0.7}As$ has been reported to exhibit an extremely small temperature-wavelength shift above 150 K. This behaviour was accounted for by postulating 3D asymmetries in the lattice distortion around the QDs that serve to suppress the strain induced bandgap shift with increasing temperature[26].

4.4 The effect of post-growth heat treatment on the optical and electronic properties of DWELL structures

4.4.1 Introduction: low temperature emission comparison of laser and test structures

The application of *in situ* or *ex situ* heat treatment to QD structures is a comparatively simple way of producing often drastic changes to their optical properties. Usually, small portions of wafer (~1 cm^2) are placed in a Rapid Thermal Annealing (RTA) machine under nitrogen ambient and then, for a specified duration, undergo an annealing process at a fixed temperature. Such temperatures typically fall between 650 and 900 °C and are applied for times lasting from a few seconds up to 30 minutes. With respect to QD laser optimization, the study of annealed QD ensembles is of relevance, as shall be explained.

High quality (low defect density) AlGaAs, as required in all GaAs-AlGaAs heterostructure devices, must be grown using substrate temperatures in excess of 600 °C. Due to the quantity of cladding material that must be grown in a typical laser

structure (~1.5 μm), the sample may be subjected to these temperatures for 1 – 2 hours. During the growth of the upper cladding this can have the effect of changing the structural or compositional properties of the active region, particularly the pre-grown QDs, via a kind of *in situ* annealing process that promotes atomic interdiffusion. A process of this type may be invoked to explain the results shown in Fig 4.20. In the main part of the figure, the normalised, low power PL from two 5 layer DWELL structures is displayed for temperatures of 77 and 300 K. One of the structures was grown as a test structure prior to the growth of the series of multilayer lasers (Vn 245 – 249) and does not contain AlGaAs cladding layers. The other structure is the Vn 244 laser wafer, discussed in section 4.2, with the p^+ doped top AlGaAs cladding etched off to allow photo-excitation of the QDs. With the exception of the AlGaAs/GaAs layers comprising the cladding/waveguide in Vn 244, the two samples are nominally identical and so any differences in their spectra can reasonably be attributed to unintentional processes that occur during the growth in Vn 244 of the upper AlGaAs cladding.

At both low and high temperature the two main emission peaks of both samples are coincident with a noticeable shoulder at ~50 nm to shorter wavelength present in each samples. As described earlier, this shoulder indicates the presence of a bimodal QD distribution in the samples. This is confirmed at low temperatures by its continued presence even when the excitation power is reduced to very low levels.

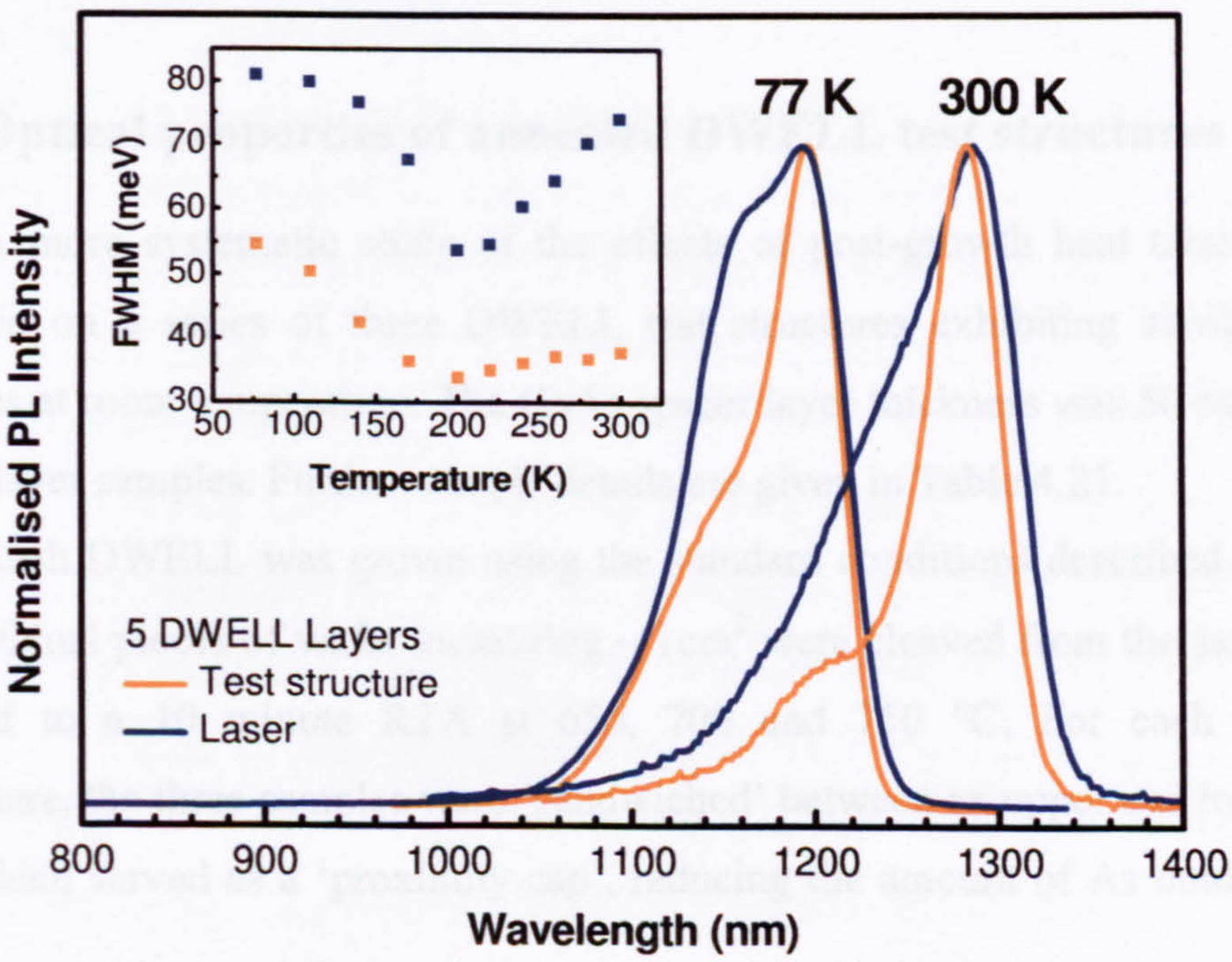

Fig. 4.20 Normalised, low power PL spectra taken at 77 K and 300 K from a five layer test structure and laser structure (Vn 244). Inset shows the temperature variation of the FWHM for both structures.

At high temperatures study of this behaviour is complicated by the presence of emission from the excited state of the larger QDs. If the low temperature emission is taken as representing the true distribution of QD sizes then it is seen that in the laser structure the number of smaller QDs is almost twice as large as in the test structure. This difference is also reflected in the considerably broader FWHM of the full laser structure emission. The inset in Fig 4.20 plots the FWHM as a function of temperature between 78 and 300 K for both samples. For both structures the FWHM decreases between 78 and 200K as carriers are concentrated in the subset of larger dots. Above 200K the FWHM increases as the first excited state of the larger dot is populated with a possible contribution from the repopulation of the smaller dots. The variation in the FWHM for the laser structure in both temperature regimes is larger than in the test structure, a consequence of the stronger bimodal distribution.

It appears that a post-growth change in the QD size distribution has occurred in the laser structure, which is attributed to the high temperature growth used during the deposition of the AlGaAs waveguide/cladding layers. The effects of cladding layer growth temperature on the performance of QD lasers has been reported previously[27]. However, in this study, only a pronounced blueshift of ~50 nm in the peak of the spontaneous emission was observed with increasing AlGaAs growth temperature and little difference was seen in the spectral distribution of the emission. However the response to this annealing is likely to be a sensitive function of the amount of InAs deposited to form the QDs.

4.4.2 Optical properties of annealed DWELL test structures

A more systematic study of the effects of post-growth heat treatment was performed on a series of three DWELL test structures exhibiting similar optical properties at room temperature. The GaAs spacer layer thickness was 50 nm for each of the 5 layer samples. Further sample details are given in Table 4.21.

Each DWELL was grown using the standard conditions described in section 3.2 Individual pieces of wafer measuring ~ 1cm^2 were cleaved from the samples and subjected to a 10 minute RTA at 650, 700 and 750 °C. For each annealing temperature, the three samples were 'sandwiched' between an upper and lower GaAs wafer which served as a 'proximity cap', reducing the amount of As outdiffusion[28].

Low power (~0.5 mW) and high power (~20 mW) PL measurements were performed at 77 K as well as temperature dependent low power PL.

Sample	No. QD Layers	HGTSL ?	RT PL peak (Å)	RT FWHM (meV)
Vn 137	1	n/a	12858	41
Vn 134	5	yes	12841	36
Vn 136	5	no	12837	38

Table 4.21 Structural details of the 3 DWELL test samples, used for the annealing studies.

Studies of annealed InAs/GaAs QDs are fairly numerous, as are the arguments used to explain the observed changes in their optical and structural properties. Typically, the PL emission is seen to blueshift with an accompanying reduction in the FWHM as the annealing temperature is increased. In general, an enhanced interdiffusion rate of In and Ga between the QD and matrix at higher annealing temperatures is invoked to explain this simultaneous change in the mean GS energy of the QDs and its variation within the ensemble[29]. However, more detailed descriptions of this process, involving diffusion coefficients, rely heavily on specific QD geometries and growth conditions – both of which influence the defect densities and strain distribution surrounding the QDs and therefore affect the interdiffusion[30].

The normalised, low temperature PL spectra of the three annealed samples, shown in Fig. 4.22, highlight what has just been described: the PL peak blueshifting and FWHM narrowing with increasing annealing temperature. Systematic differences in the integrated PL intensities between samples of different annealing temperature (T_A) are hard to establish with certainty in the present study. For all three samples, the low temperature PL intensity remained fairly constant up to $T_A \sim 700$ °C, above which it decreased slightly.

The as-grown samples are similar in their emission properties. At low T_A (~650 °C) the annealing promotes an increase in the intensity of the shorter wavelength sub-set of QDs with respect to the longer wavelength subset for *all* of the samples. The extent of this modification is greatest in the single layer sample (Vn 137) and weakest in the 5 layer HGTSL sample (Vn 134). Likewise, the overall blueshift between the as-grown and $T_A = 750$ °C sample is largest for the single layer

sample (164 meV) and smallest for the 5 layer HGTSL sample (90 meV), suggesting that the effect of annealing is greatest for the single layer sample.

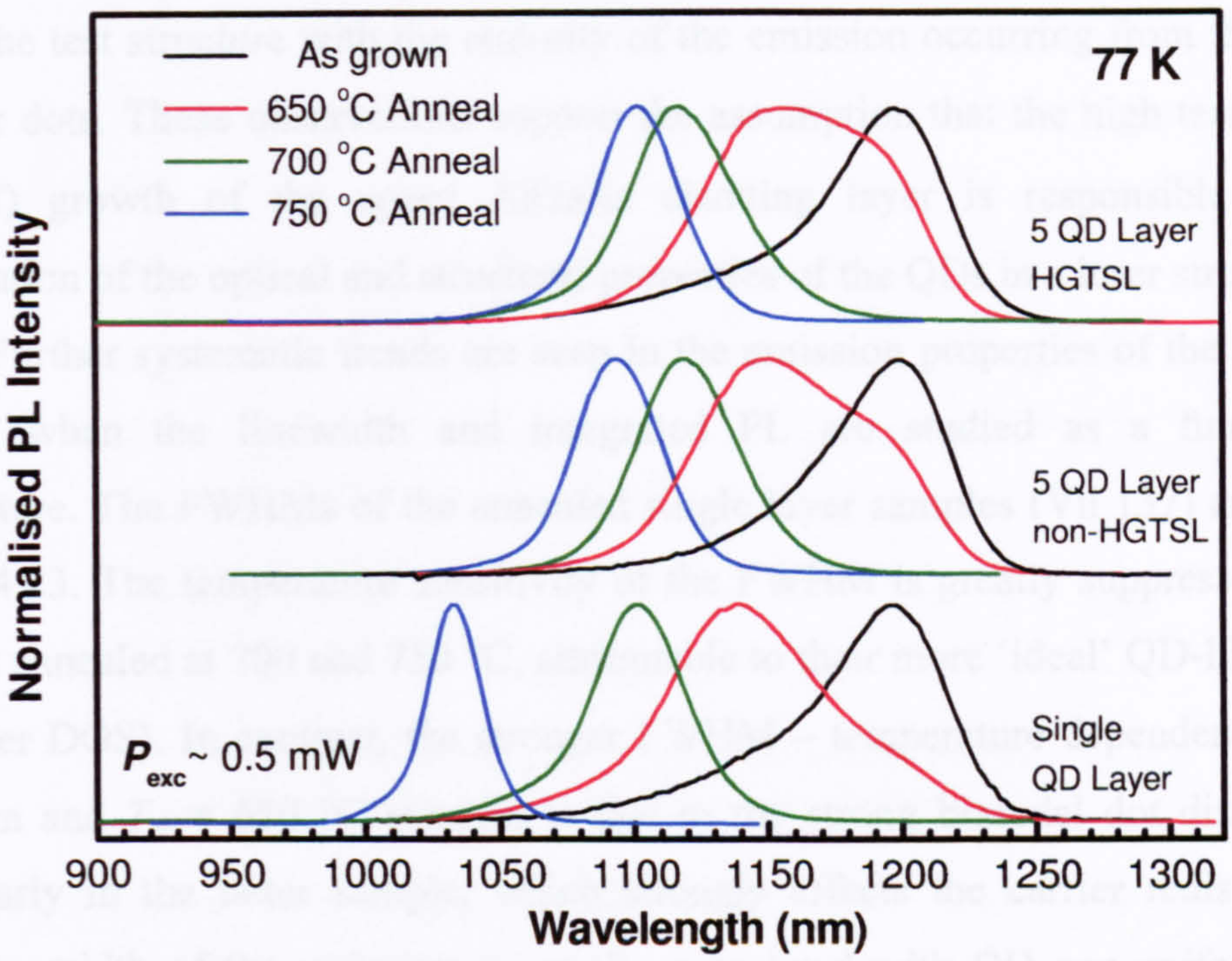

Fig. 4.22 Normalised low power PL spectra at 77 K for the 3 DWELL samples listed in Table 4.21. Individual pieces from each sample were annealed at 650, 700 and 750 °C for 10 mins. The PL from the as-grown wafer is shown for reference.

This agrees with what has been found in studies of multilayer MOCVD grown samples, where the reduction in the blueshift for samples with a greater number of QD layers was attributed to a suppression of In interdiffusion under the strain field of nearby QDs[31]. The presence of dislocations may also influence the extent of the annealing induced effects. It is highly likely that there are a significant proportion of large, optically inactive QDs in the present DWELL structures which, whilst not overly degrading the optical efficiency of as-grown structures, could influence some of the kinetic processes during RTA. Indeed, structural studies have suggested that RTA acts as a kind of 'size filter' for the coherent islands in a QD ensemble, possibly eliminating a bimodal distribution in the as-grown sample[32]. A comparison of the different spectral forms of the PL in the as-grown, T_A = 650 and 700 °C samples may support this claim.

As T_A increases over this range there is a clear shift in the weight of the PL emission to the shorter wavelength side of the PL peak, indicating a relative decrease

in the number of large QDs. In terms of QD laser growth, the spectra of the T_A = 650 °C samples are of great interest. They closely resemble that of Vn 244 in Fig. 4.20 with a strong bimodal form. In contrast the emission of the as-grown samples reflects that of the test structure with the majority of the emission occurring from the subset of larger dots. These observations support the assumption that the high temperature (~680°C) growth of the upper AlGaAs cladding layer is responsible for the modification of the optical and structural properties of the QDs in a laser structure.

Further systematic trends are seen in the emission properties of the annealed samples when the linewidth and integrated PL are studied as a function of temperature. The FWHMs of the annealed single layer samples (Vn 137) are shown in Fig. 4.23. The temperature sensitivity of the FWHM is greatly suppressed in the samples annealed at 700 and 750 °C, attributable to their more 'ideal' QD-like nature (narrower DOS). In contrast, the stronger FWHM – temperature dependence of the as-grown and T_A = 650 °C samples is due to the strong bimodal dot distribution, particularly in the latter sample, which strongly affects the carrier redistribution. Since the width of the emission is usually associated with QD non-uniformity, its reduction has been attributed to a reduction in size and strain inhomogeneities as the degree of intermixing increases. However, a theoretical study has indicated that only a reduction in the QD height fluctuations within the ensemble can account for the observed FWHM narrowing of *all* QD transitions[33]. This conclusion was reached under the assumption that the diffusion proceeds isotropically, with the fractional changes in QD dimension being more effective in the growth direction due to its smaller extent. Although the evolution of the first excited state (ES1) FWHM with T_A cannot be determined exactly in the present samples (due to the bimodal distribution of the as-grown sample) its behaviour does not seem inconsistent with the previous proposition: the PL presented in Fig. 4.25 suggests that the GS and ES1 FWHMs are comparable.

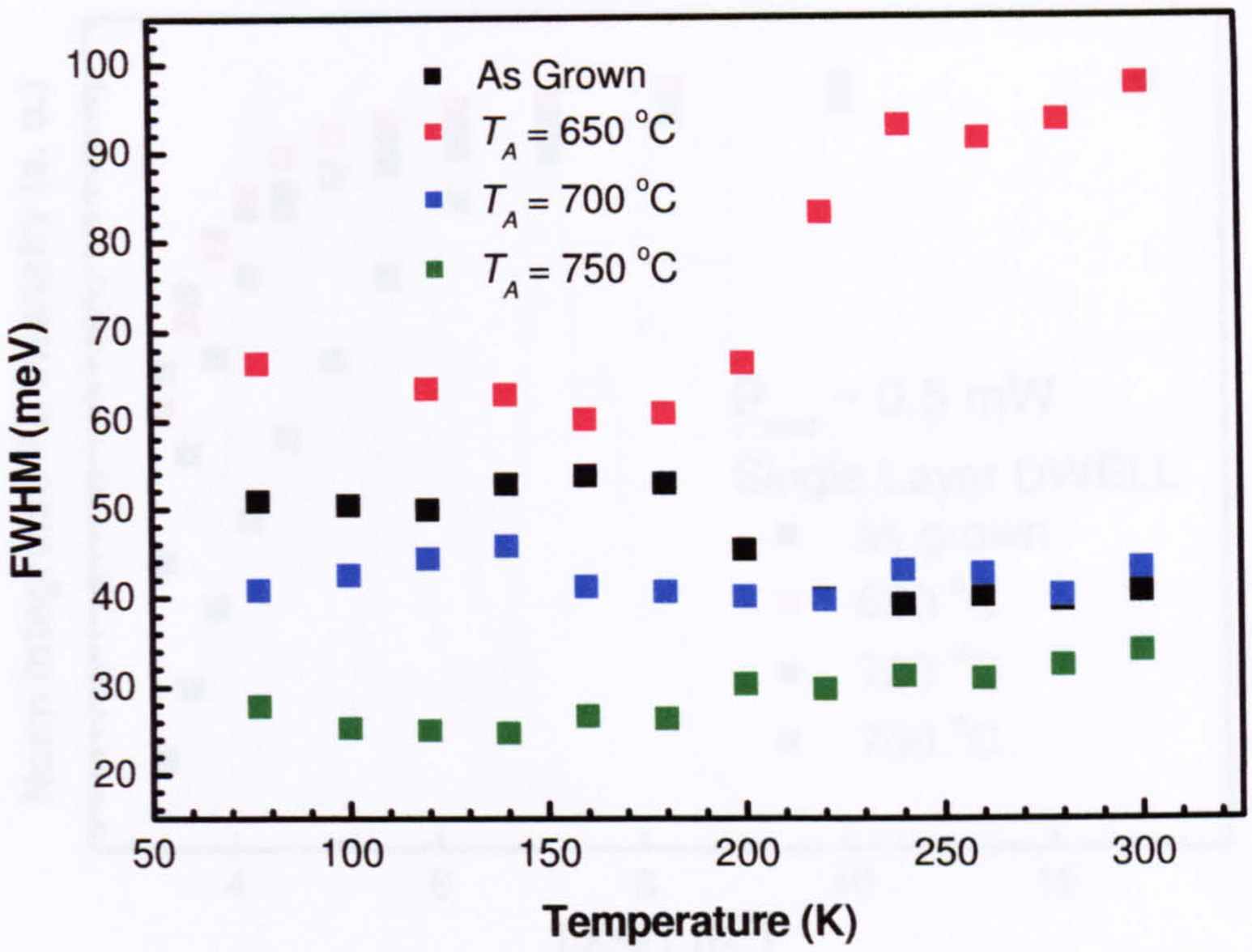

Fig. 4.23 Temperature variation of the emission FWHM in annealed pieces of the single layer sample (Vn 137).

Fig. 4.24 shows the temperature dependence of the normalised integrated PL intensity (IPL) for the as-grown and different annealing temperatures of the single layer sample. For all T_A, there are three regimes of IPL temperature dependence. i) A 'low temperature range', over which the integrated PL intensity (IPL) remains constant. This is narrower for higher T_A. ii) A 'strong thermal quenching range' at high temperatures, where the IPL decreases exponentially with an Arrhenius dependence [$\propto \exp(E_a/k_BT)$], and iii) an 'intermediate quenching' regime that exists for temperatures between regions i) and ii).

The onset of the intermediate regime is seen to occur at lower temperatures and exist for a larger temperature range as T_A increases. Activation energies (E_a) extracted from the strong quenching regime are found to reduce with increasing T_A: decreasing from 280 meV in the unannealed sample to 125 meV for T_A = 750 °C. These values correspond closely to the respective interband energy separations between the peak of the GS emission and the lowest confined state in the WL/QW, as determined from PLE. This represents the thermally activated escape of *both* an electron and hole from a QD to a final non-radiative state in the WL.

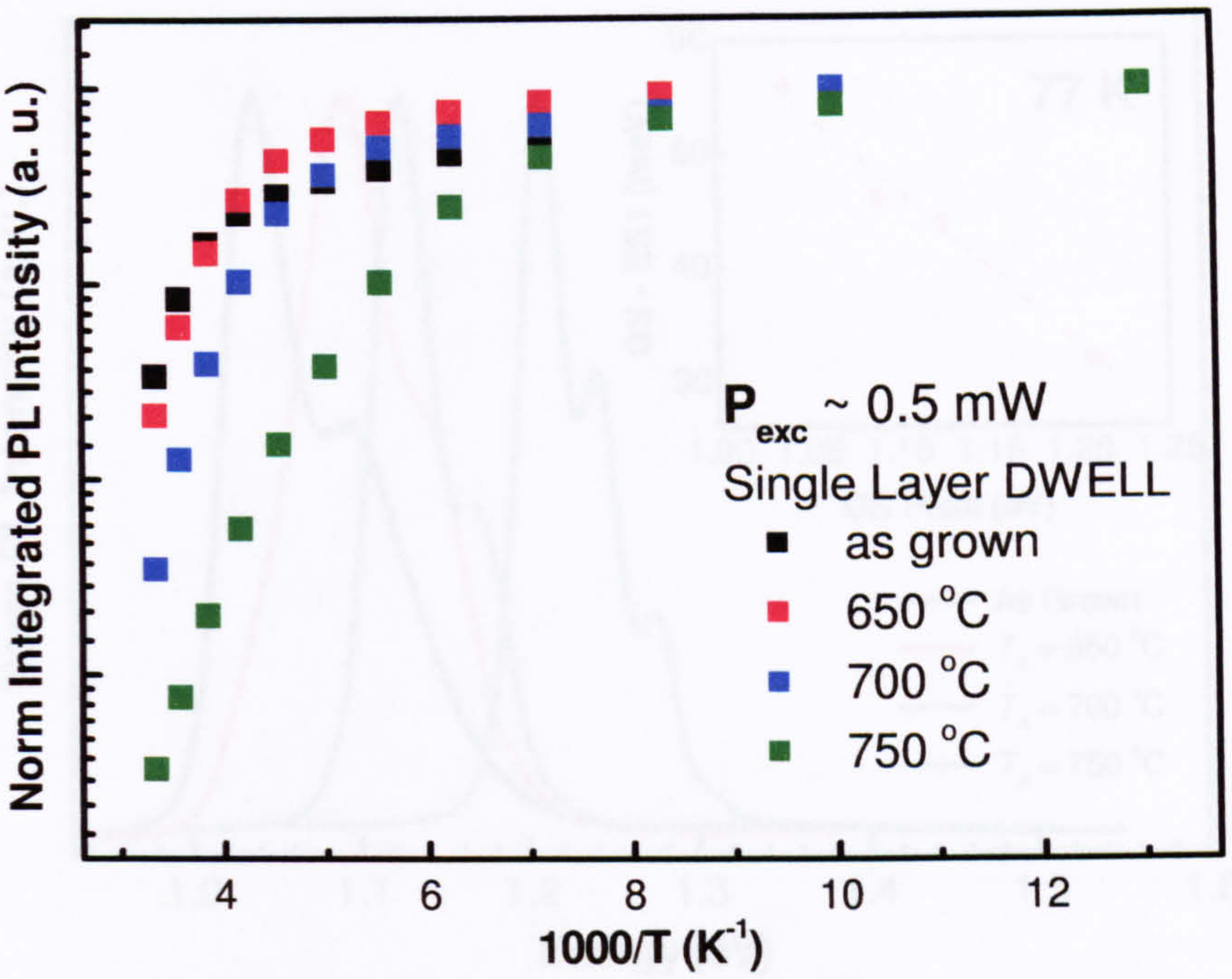

Fig. 4.24 Temperature variation of the normalised integrated PL intensity (IPL) for annealed pieces of the single layer sample.

The variation of the IPL with incident power and temperature has been studied previously for annealed InAs QDs[34]. A superlinear power dependence of the IPL was found for temperatures $\geq$ 100 K, corresponding to the onset of the 'intermediate' quenching regime. In turn, this was interpreted as being due to the independent escape of electrons and holes from the QDs. This can be understood qualitatively with reference to Fig. 4.24: as T_A increases, the respective confinement of electrons and holes is diminished by the enhanced In - Ga interdiffusion between the QD and the barrier. Hence, the decreasing 'onset' temperature of the weak IPL quenching with increasing T_A can be attributed to the lower activation energy of the more weakly confined carrier (the hole).

Concomitant with a reduction in the confinement of the QD states should be a reduction in their inter-sublevel splitting. High power PL measurements (~20 mW), carried out at 77K, allow an approximate determination of the separation between the GS and first excited state for each T_A of the single layer sample. The resolution of the ES1 emission improves considerably as T_A increases – a consequence of the narrowing FWHM. The energy separation between the GS and ES1 is plotted as a function of the GS peak energy in the inset of Fig. 4.25

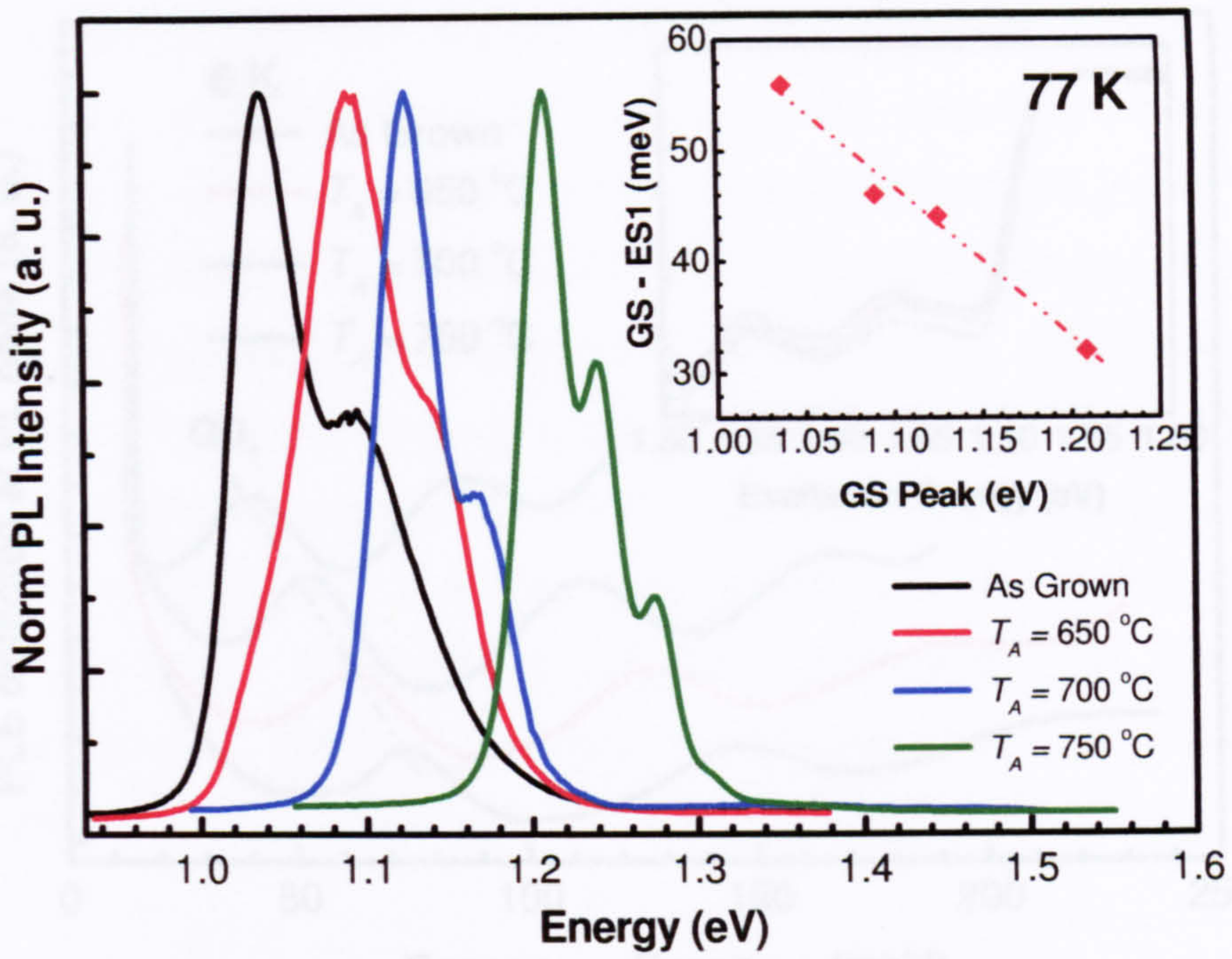

Fig. 4.25 main part: low temperature normalised high power PL spectra of the annealed single layer sample. Inset shows the variation of the GS-to-first-excited-state energy separation, as a function of GS energy.

The linear relationship between these two quantities has been observed previously, but there is no consensus as to the underlying cause. Both a flattening of the QD aspect ratio[35, 36] and a reduction in the barrier potential[37] with increasing T_A have been cited as possible explanations. Unfortunately, the only existing TEM study of annealed (non-DWELL) InAs/GaAs QDs grown in Sheffield does not reveal any particularly significant features, save an annealing-induced gradual dissolution of the QD into the surrounding matrix. This makes speculation difficult as to a possible mechanism responsible for the systematic shifts observed in the present samples.

As has been shown, RTA significantly alters the QD transition energies via the assumed interfacial In-Ga interdiffusion between the QD and the InGaAs QW that encapsulates the QDs. Therefore, it is not unreasonable to expect that there may be some related shift in the absorption features of the InGaAs QW, and possibly GaAs absorption edge. To investigate this possibility, low temperature PLE measurements were performed for each T_A of the single layer sample, typical spectra are shown in Fig. 4.26.

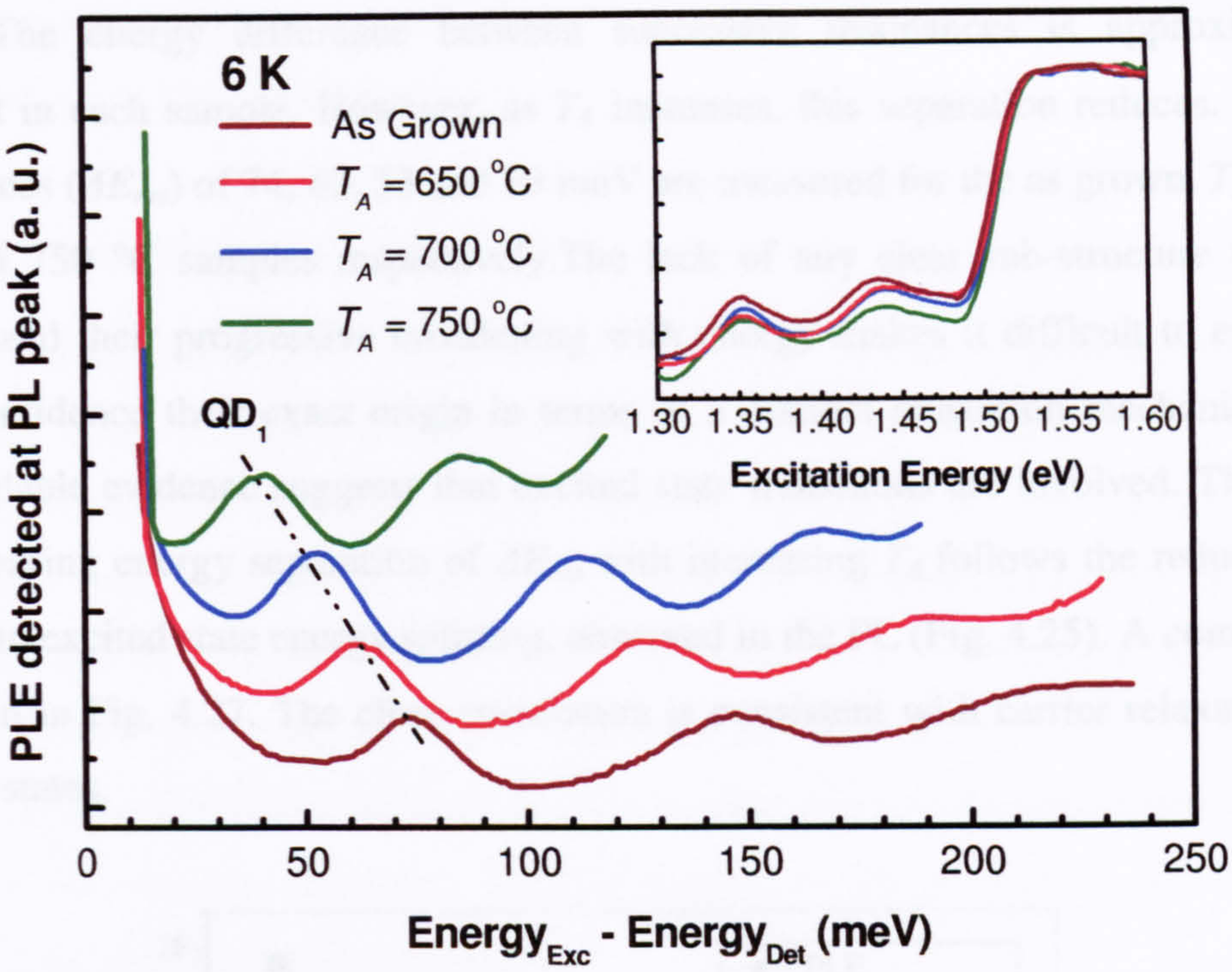

Fig. 4.26 main part: PLE spectra, detected at the PL peak, plotted with respect to the detection energy for each of the annealed pieces of the single layer sample. Inset shows the PLE of the barrier region plotted as a function of excitation energy.

On inspection of the high energy portion of the spectra (see inset of Fig. 4.26), it is clear that the annealing procedure has had little impact on the relative positions of these features. Although this result is initially unexpected, it is more reasonable when considering the large difference in the volume : interdiffusion 'contact area' ratio for the QD/2D/bulk regions.. As an aside though, it is interesting to note that a small redshift (~ 5 meV) with T_A is observed for the lowest confined QW/WL state in the non-HGTSL 5-layer sample (Vn 136). In this case, a proportion of point defects, resulting from the non-optimised growth, may be enhancing the interdiffusion of group III species, possibly resulting in a higher In composition in the Strain Reducing Layer following annealing.

When the excitation energy range is tuned below that of the QW/WL region, three broad resonances are observed for each T_A (the lowest energy one QD_1 is marked in Fig. 4.26). As the detection energy is stepped across the PL peak, these resonances shift rigidly and can therefore be related to carrier relaxation steps within the sub-set of QDs probed. The presence of such features in PLE spectra has been used to confirm the continued existence of QDs in structures that have been annealed at temperatures as high as 900 °C[38].

The energy difference between successive resonances is approximately constant in each sample. However, as T_A increases, this separation reduces. Energy differences (ΔE_{res}) of 74, 62, 53 and 39 meV are measured for the as grown, T_A = 650, 700 and 750 °C samples respectively.The lack of any clear sub-structure to each feature and their progressive broadening with energy makes it difficult to establish with confidence their exact origin in terms of a distinct relaxation mechanism, but the available evidence suggests that excited state transitions are involved. The trend in decreasing energy separation of ΔE_{res} with increasing T_A follows the reduction in the GS to excited state energy splitting, observed in the PL (Fig. 4.25). A comparison is shown in Fig. 4.27. The close correlation is consistent with carrier relaxation via excited states.

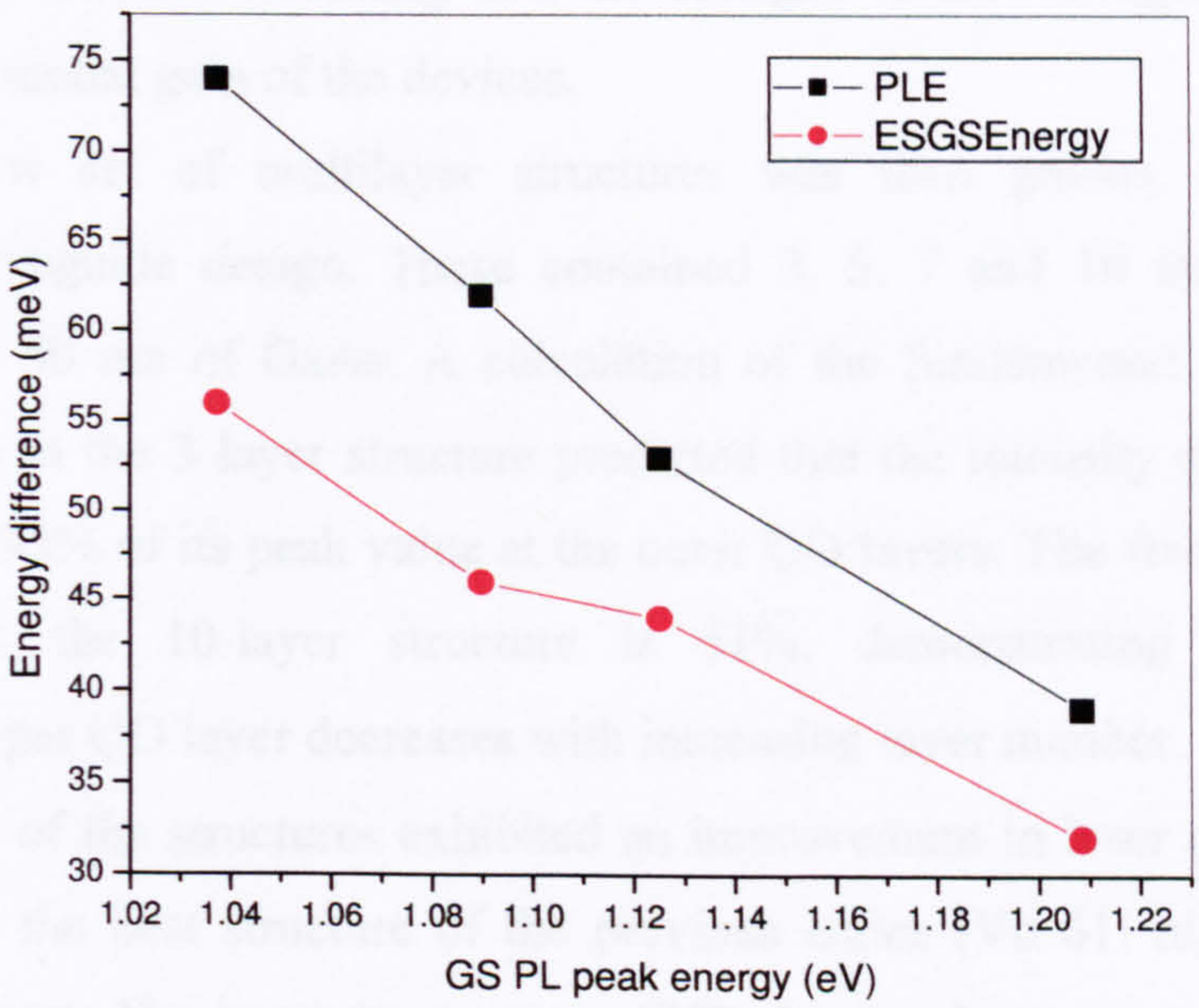

Fig. 4.27 Energy difference between resonances observed in the PLE (black symbols) and the PL GS to first excited state separation shown as a function of GS PL peak energy for the annealed samples.

A purely LO phonon-mediated relaxation channel within the QDs is unlikely, since $In_xGa_{1-x}As$ LO phonon energies *decrease* with increasing x, opposite to the observed behaviour if it is assumed that annealing increases the Ga content of the QDs. The broader nature of the higher energy features is consistent with a process involving excited states, as these are more sensitive to the size and shape fluctuations in the QD ensemble than is the GS. Likewise, the reduction in FWHM of the ES1 transition, determined from the high power PL, for increasing T_A may be reflected in

the slight (~5 meV) narrowing of the lowest energy (QD_1) feature between the as-grown and T_A = 750 °C sample.

4.5 Conclusions

The present chapter begins with a comparison of the lasing properties of two structures, each containing 5 DWELL layers separated by 50 nm of GaAs, but with different waveguide designs. In one structure, the design of the waveguide was unchanged from that used in the previous series of In(Ga)As/GaAs DWELL lasers and described in Chapter 3. In the other, the thickness of the undoped AlGaAs and GaAs adjacent to the active region was reduced, with the aim of increasing the inherently low optical confinement factor. However, the temperature dependencies of J_{th} were very similar, indicating that the changes to the waveguide had had little effect on the modal gain of the devices.

A new set of multilayer structures was then grown, incorporating the modified waveguide design. These contained 3, 5, 7 and 10 layers of DWELLs separated by 50 nm of GaAs. A calculation of the fundamental transverse optical mode profile in the 3 layer structure predicted that the intensity of the optical field decreases to 93% of its peak value at the outer QD layers. The fractional decrease in intensity for the 10-layer structure is 51%, demonstrating that the optical confinement per QD layer decreases with increasing layer number.

None of the structures exhibited an improvement in laser performance when compared to the best structure of the previous series (Vn 61: high QD density; 5 DWELL layers). The room temperature (RT) J_{th}s for the measured 3 mm x 15 μm cavities were similar, as were the temperature dependencies. The 7-layer structure exhibited the best overall performance. The fact that the lasing performance was found to be relatively insensitive to the number of DWELL layers suggested that the modal gain was being determined primarily by the material gain. In photocurrent measurements, the GS absorption strength was found to scale in proportion to the number of QD layers in the structure. There is some evidence for a decrease in the density of smaller QDs in samples with a greater number of QD layers but the degree of non-radiative recombination appears to be independent of layer number.

To highlight the effect of the GaAs spacer layer (SL) growth conditions on the optical properties of the QDs, two new laser structures with 35 nm SLs were grown and characterised. In one sample the HGTSLs were grown using the same parameters as before – initial 15 nm GaAs at 510 °C, remaining section at 585 °C – whereas in the other, the temperature of the final 20 nm of GaAs was raised to 620 °C. The former structure displayed poor lasing performance, with ES1 lasing at RT from a 3 mm cavity, in contrast to the GS lasing obtained from a 1 mm as-cleaved cavity of the structure containing HGTSLs grown at the higher temperature. This marked improvement in the lasing performance of the structure with higher growth temperature HGTSLs was attributed to a reduction in the inhomogeneous distribution of the QDs and a reduction in the amount of non-radiative recombination. The mechanism responsible for the greater QD homogeneity in this sample was thought to be the same as that found in the initial development of the HGTSL step (see chapter 3, section 3.3.3) i.e. a smoother nucleation surface for the QDs.

An anomalous structure, containing an InGaAs capping layer with a vertically graded In composition, was then studied. The purpose of this design was to relieve the in-plane components of QD strain that serve to increase the GS energy of the QDs. However, no significant effect on the electronic properties of the QDs was found. The resultant broadening of the GS energy levels produced a very temperature insensitive lasing wavelength in a 3 mm cavity length device, attributed to a flat gain profile but this did not appear to be an intrinsic effect of the graded capping layer.

The final section of the chapter focussed on the effect of post-growth annealing on the optical properties of DWELL structures. Annealing at a relatively low temperature (~650 °C) resulted in the enhancement of the characteristic bimodal emission i.e. the proportion of the emission from the short-wavelength QD subset increased in intensity relative to that of the longer wavelength emitting subset. However, little change in the relative peak positions of the two QD sub-sets was observed. This difference in spectral form was reflected in the comparison of the low temperature emission spectra of test and laser structures, indicating that the growth of the AlGaAs cladding at ~680 °C acts as a kind of *in situ* annealing process for the QDs within the structure. When annealed at higher temperatures the PL emission peak progressively blueshifted and narrowed (to a single Gaussian) with increasing annealing temperature. Along with the blueshift and narrowing, the ground-to-first-

excited-state separation decreased from 56 to 32 meV between as-grown and 750 °C annealed samples. This systematic reduction may be related to the decreasing separation of the intra-QD relaxation resonances observed in the PLE.

References

1. Walker, C.L.; Sandall, I.C.; Smowton, P.M.; Sellers, I.R.; Mowbray, D.J.; Liu, H.Y.; Hopkinson, M., IEEE Photon. Technol. Lett. **17**, (10) 2011 (2005)

2. B. S. Ryvkin and E. A. Avrutin J. Appl. Phys. **97**, 123103 (2005)

3. http://wwwhome.math.utwente.nl/~hammerm/oms.html

4. A. R. Kovsh, N. A. Maleev, A. E. Zhukov, S. S. Mikhrin, A. P. Vasil'ev, E. A. Semenova, Yu. M. Shernyakov, M. V. Maximov, D. A. Livshits, V. M. Ustinov, N. N. Ledentsov, D. Bimberg and Zh. I. Alferov, J. Cryst. Growth **251**, (1-4), 729 (2003)

5. A.R. Kovsh, N.A. Maleev, A.E. Zhukov, S.S. Mikhrin, A.P. Vasil'ev, Yu.M. Shernyakov, M.V. Maximov, D.A. Livshits, V.M. Ustinov, Zh.I. Alferov, N.N. Ledentsov, and D. Bimberg, Electron. Lett. **38**, (19) 1104 (2002)

6. P. W. Fry, I. E. Itskevich, S. R. Parnell, J. J. Finley, L. R. Wilson, K. L. Schumacher, D. J. Mowbray, M. S. Skolnick, M. Al-Khafaji, A. G. Cullis, M. Hopkinson, J. C. Clark, and G. Hill, Phys. Rev. B **62**, 16784 (2000)

7. Sandall, I.C.; Smowton, P.M.; Hui-Yun Liu; Hopkinson, M.; IEEE J. Quantum Electron. **43**, (8) 698 (2007)

8. H. Y. Liu, I. R. Sellers, M. Gutiérrez, K. M. Groom, W. M. Soong, M. Hopkinson, and J. P. R. David, J. Appl. Phys. **96**, 1988 (2004)

9. B. Shi and Y. H. Xie, Appl. Phys. Lett. **82**, 4788 (2003)

10. Sugawara, M.; Mukai, K.; Nakata, Y.; Otsubo, K.; Ishilkawa, H.; IEEE J. Select. Topics Quantum Electron. **6**, (3) 462 (2000)

11. Mukai, K.; Nakata, Y.; Shoji, H.; Sugawara, M.; Ohtsubo, K.; Yokoyama, N.; Ishikawa, H.; Electron. Lett. **34**, (16) 1588 (1998)

12. N. N. Ledentsov, V. A. Shchukin, M. Grundmann, N. Kirstaedter, J. Böhrer, O. Schmidt, D. Bimberg, V. M. Ustinov, A. Yu. Egorov, A. E. Zhukov, P. S. Kop'ev, S. V. Zaitsev, N. Yu. Gordeev, Zh. I. Alferov, A. I. Borovkov, A. O. Kosogov, S. S. Ruvimov, P. Werner, U. Gösele, and J. Heydenreich, Phys. Rev. B **54**, 8743 (1996)

13. Mitsubishi Laser Diode data sheet http://www.fti-optronic.com/pdfs/ml7xx8.pdf

14. P M Smowton (Private communication)

15. Blood, P.; Lewis, G.M.; Smowton, P.M.; Summers, H.; Thomson, J.; Lutti, J.; IEEE J. Select. Topics Quantum Electron. **9**, (5) 1275 (2003)

16. Walker, C.L.; Sandall, I.C.; Smowton, P.M.; Mowbray, D.J.; Liu, H.Y.; Liew, S.L.; Hopkinson, M.; IEEE Photon. Technol. Lett. **18**, (14) 1557 (2006)

17. A. Salhi; L. Martiradonna; G. Visimberga; V. Tasco; L. Fortunato; M.T. Todaro; R. Cingolani; A. Passaseo; M. De Vittorio, IEEE Photon. Technol. Lett. **18,** (16) 1735 (2006)

18. M. A. Migliorato, A. G. Cullis, M. Fearn, and J. H. Jefferson, Phys. Rev. B **65,** 115316 (2002)

19. Jin Soo Kim, Jin Hong Lee, Sung Ui Hong, Won Seok Han, Ho-Sang Kwack, and Dae Kon Oh, Appl. Phys. Lett. **83,** 3785 (2003)

20. N.-T. Yeh, T.-E. Nee, J.-I. Chyi, T. M. Hsu and C. C. Huang, Appl. Phys. Lett. **76,** 1567 (2000)

21. Eui-Tae Kim, Zhonghui Chen, and Anupam Madhukar, Appl. Phys. Lett. **81,** 3473 (2002)

22. A. E. Zhukov, A. R. Kovsh, N. A. Maleev, S. S. Mikhrin, V. M. Ustinov, A. F. Tsatsul'nikov, M. V. Maximov, B. V. Volovik, D. A. Bedarev, Yu. M. Shernyakov, P. S. Kop'ev, and Zh. I. Alferov, Appl. Phys. Lett. **75,** 1926 (1999)

23 V. Tokranov, M. Yakimov, A. Katsnelson, M. Lamberti, and S. Oktyabrsky, Appl. Phys. Lett. **83,** 833 (2003)

24 J. D. Thomson, H. D. Summers, P. M. Smowton, E. Herrmann, P. Blood, and M. Hopkinson, J. Appl. Phys. **90,** 4859 (2001)

25 F. Klopf, S. Deubert, J. P. Reithmaier, and A. Forchel, Appl. Phys. Lett. **81,** 217 (2002)

26 Kohki Mukai and Mitsuru Sugawara, Appl. Phys. Lett. **74,** 3963 (1999)

27 F. Schäfer, J. P. Reithmaier, and A. Forchel, Appl. Phys. Lett. **74,** 2915 (1999)

28 Adam Babiński, J. Jasiński, R. Bożek, A. Szepielow, and J. M. Baranowski, Appl. Phys. Lett. **79,** 2576 (2001)

29 R. Leon, Yong Kim, and C. Jagadish, M. Gal, J. Zou and D. J. H. Cockayne, Appl. Phys. Lett. **69,** 1888 (1996)

30 O. Gunawan, H. S. Djie and B. S. Ooi, Phys. Rev. B **71,** 205319 (2005)

31 Jun Tatebayashi, Yasuhiko Arakawa, Nobuaki Hatori, Hiroji Ebe, Mitsuru Sugawara, Hisao Sudo and Akito Kuramata, Appl. Phys. Lett. **85,** 1024 (2004)

32 Q. W. Mo, T. W. Fan, Q. Gong, J. Wu, Z. G. Wang and Y. Q. Bai, Appl. Phys. Lett. **73,** 3518 (1998)

33 Nathalie Perret, Denis Morris, Loic Franchomme-Fossé, René Côté, Simon Fafard, Vincent Aimez, and Jacques Beauvais, Phys. Rev. B **62,** 5092 (2000)

34 E. C. Le Ru, J. Fack, and R. Murray, Phys. Rev. B **67,** 245318 (2003)

35 X. C. Wang, S. J. Xu, S. J. Chua and Z. H. Zhang, J. Appl. Phys. **86,** 2687 (1999)

36 L. Wang, A. Rastelli, and O. G. Schmidt, J. Appl. Phys. **76,** 691 (2000)

37 T. M. Hsu, Y. S. Lan, W.-H. Chang, N. T. Yeh and J.-I. Chyi, Appl. Phys. Lett. **76,** 691 (2000)

38 Surama Malik, Christine Roberts, Ray Murray and Malcolm Pate, Appl. Phys. Lett. **71,** 1987 (1997)

Chapter 5

Optical properties of *p*-type modulation doped Quantum Dot laser structures

5.1 Introduction

5.1.1 Motivation

In the previous two chapters, it has been shown that by using the High Growth Temperature Spacer Layer (HGTSL) step, multilayer QD lasers may be grown with ultra-low continuous wave threshold current densities (J_{th}s) and room temperature (RT) operation at wavelengths at or slightly above 1.3μm. Although these characteristics represent a significant achievement, the strong temperature sensitivity of J_{th} above RT remains a problem. The temperature sensitivity is can be represented by a T_0 parameter, where a higher T_0 value represents increased temperature stability. In practise T_0 varies with temperature and hence the relevant temperature range should be quoted when stating a T_0 value. Ideal quantum dot lasers have a T_0 of infinity but real QD lasers are found to have T_0 values above room RT which are only comparable to those of quantum well lasers. Commercial lasers are required to operate to 90 or even 110 °C and this generally requires the use of thermoelectric cooling which increases the power consumption and system complexity. There is hence a significant need for temperature insensitive lasers.

As noted previously, there is little consensus in the literature as to the dominant cause of the rapid increase in J_{th} observed for all QD lasers, which typically begins between -50 °C and RT and generally becomes relatively rapid and comparable to that of quantum well lasers above ~40-50°C. The thermal excitation of carriers out of the lasing states, to higher dot states or states external to the dots, may contribute and theoretical work has suggested that it may be possible to improve T_0 by increasing the energy separation between the Ground (GS) and Excited State (ES) transitions in the QDs[1]. However, whilst the inter-level spacing for electrons may exceed $3k_BT$ for In(Al)GaAs capped InAs QDs at RT and above, the valance states typically lie within ~10 meV of each other. This small energy spacing allows injected holes to become thermally distributed between these states, even at relatively low

temperatures (~200 K), profoundly affecting the lasing characteristics of the devices. At a sufficiently high temperatures, the thermally induced depopulation of the hole GS causes an effective saturation of the gain at approximately one third of its maximum value[2]. This effect is likely to contribute significantly to the rapid rise in J_{th} above RT, observed in QD lasers. In addition, the reduction in differential gain and hence also in modulation speed, with increasing temperature is detrimental for applications requiring high bit-rate data transmission.

In 2002, O. B. Shchekin and D. G. Deppe[3] proposed the use of *p*-type modulation doping of the QDs as a means of counteracting these negative effects associated with the thermal excitation of holes. A significant number of extrinsic holes, supplied by a thin layer of acceptors (typically Beryllium or Carbon atoms) placed a few nm above or below the QDs, may be captured into the QDs ensuring that the lowest energy hole states in the QDs remain occupied up to high temperatures. In QW lasers, *p*-type modulation doping has been shown to increase the gain at a given injection level, due to a shift in both quasi-Fermi levels towards the valence states[4]. This applies equally to QD lasers, yet the impact can be expected to be greater in QD-based devices, due to the relative magnitudes in the density of electronic states between QWs and QDs. Because of the potential advantages offered by *p*-type modulation doping, there is currently much research activity geared toward achieving an understanding of the underlying processes that affect the behaviour of *p*-type modulation doped QD laser structures. The work presented in this chapter forms part of this study.

5.1.2 Recent landmarks in *p*-type doped QD laser performance

The first reported study of the effect of *p*-type modulation doping on the J_{th} characteristics of QD lasers was performed by the same group which proposed the technique (Deppe et al., University of Texas). A systematic increase in the RT T_0 parameter was found with increasing Be dopant concentration: undoped, 26 and 52 acceptor/QD devices of 3 mm cavity length exhibited T_0's of 85, 145 and 161 K respectively[5]. However, the absolute values of J_{th} also increased with increasing doping level, possibly due in part to an increase in the internal optical loss (α_i) and a small decrease in the internal efficiency (η_i). Subsequently, the same group

demonstrated that by increasing the number of QD layers from 2 to 5, the T_0 value could be increased to ~230 K in a 1 mm cavity[6]. Further theoretical work by the same group has indicated that *p*-type doping may be able to increase the maximum modulation speed to ~30 GHz[7]. Although significant, the frequency modulation properties of QD devices will not be discussed in this chapter. The results of work performed by other groups are broadly consistent with the findings of Deppe et al. For example, a *p*-type doped 10 layer device with a 500 μm cavity length exhibited a RT T_0 of 420 K up to 70°C[8]. A similar structure demonstrated an infinite T_0 up to 75 °C[9]. In other work a 10 layer *p*-type doped structures exhibited a high modal gain (up to 23 cm^{-1}) and a very low transparency current density per QD layer (6 A/cm^2)[10].

Complementary to studies of the modulation and J_{th} characteristics in *p*-type doped devices are those that focus on the current and temperature dependence of the gain. Work conducted at Cardiff University and the University of Surrey indicates that *p*-type doping affects both the temperature and current dependence of the peak modal gain. Simulations and experimental work performed by the former group indicate that the population inversion factor ($f_c - f_v$), ie. the difference in occupation probability of the electron and hole GSs, systematically increases with increasing doping concentration for a given quasi-Fermi level separation[11]. Therefore the gain available at a given photon energy should increase with doping level, assuming the optical matrix element is unaffected by the doping. Consistent with these predictions are the findings from Surrey that confirm that *p*-type doping successfully reduces the gain saturation at the expense of higher J_{th}s[12]. The multi-section devices that were studied in Cardiff were fabricated from identical material to that studied in this chapter, enabling direct comparisons to be made between their work and the results presented below.

5.2 Sample Structures

Two series of *p*-type modulation doped structures are studied in this chapter. The first series was grown in the same growth run as the set of multilayer HGTSL samples Vn 245-249 that were discussed in chapter 4 and contained structures incorporating 5 DWELL layers. The second series was grown approximately one year later and contained structures with 7 DWELL layers. All of the structures in

both series contained 50 nm GaAs spacer layers (SLs) grown with the HGTSL technique described in chapter3, section 3.3.3, ie. the final 35 nm of the GaAs SL was deposited at 580 ºC, with a nominally unchanged waveguide. For the growth of the modulation doped portion of each structure, it was decided to follow the approach of Deppe *et al*. In each structure, the *p*-type dopant (Beryllium) was contained in a 60 Å thick region of GaAs placed 90 Å below each DWELL. The sample details for the first and second series are summarised in Table 5.1. The doping concentration required to give the appropriate number of electrons/holes per QD was calculated based on an assumed in-plane QD density of 3 x 10^{10} cm^{-2}, as measured by AFM on uncapped test structures. A single acceptor per QD corresponds to an extrinsic hole density of 1.9 x 10^{-16} cm^{-3}.

Sample	**Number of QD Layers**	**doping**	**Number of acceptors per QD**
Vn 249	5	undoped	0
Vn 251	5	*p*	15
Vn 250	5	*p*	50
Vn 517	7	undoped	0
Vn 518	7	*p*	6
Vn 519	7	*p*	12
Vn 520	7	*p*	18

Table 5.1 Structural details of the samples studied in this chapter. Black typeface denotes those grown in series 1, blue typeface corresponds to those grown in series 2.

5.3 Overview of the lasing properties of the *p*-type doped structures

The temperature dependence of J_{th} for 3 mm x 15 µm cavities of all samples is presented initially. It will become clear that although the respective lasing and spontaneous emission properties of the individual sample sets can be correlated to a certain extent, there is a greater consistency within the spontaneous emission results as a whole.

Shown in Fig 5.2 is the temperature dependence of the pulsed J_{th} for the two *p*-type doped and one undoped 5 layer structures grown in series 1. The relevant laser characterisation parameters are listed in Table 5.3

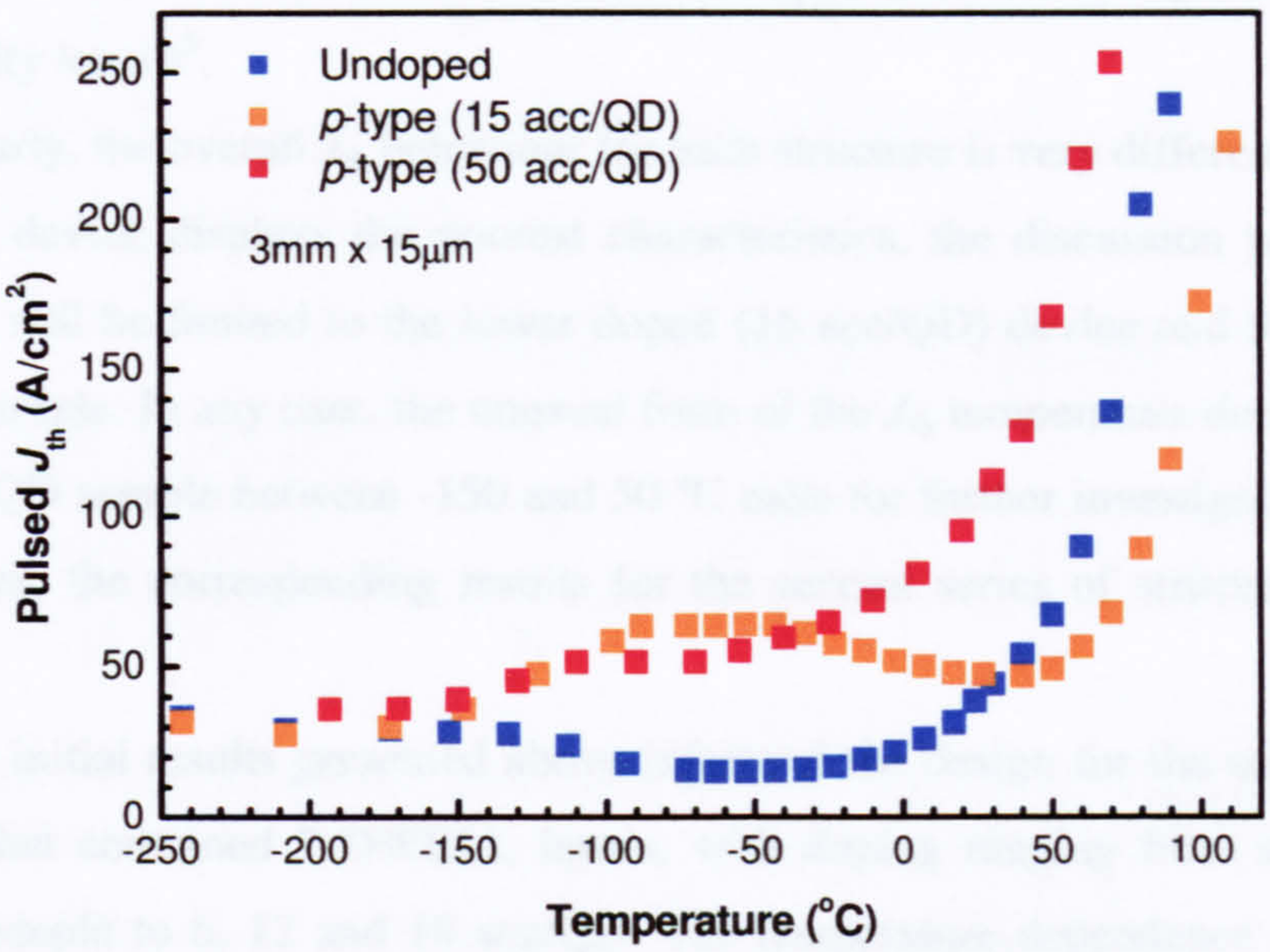

Fig. 5.2 Temperature dependence of the pulsed J_{th} for 3 mm cavity length *p*-type doped and undoped devices grown in series 1

	Undoped	**15 acc/QD**	**50 acc/QD**
RT pulsed J_{th} (A/cm^2)	38	47	105
RT Lasing λ (nm)	1289	1303	1300
T_0 (K) [0 - 70 °C]	43	~ ∞	54

Table 5.3 RT laser characterisation parameters for the *p*-type doped and undoped structures grown in series 1. The values are obtained for 3 mm x 15 μm cavities.

Below -150 ºC all devices have a similar and approximately constant J_{th}. However, above -150 ºC, J_{th} for the doped devices increases whilst that of the undoped device decreases. The latter reaches a minimum at ~ -60 ºC, consistent with typical QD laser behaviour, above which it starts to increase. For the device with 50 acceptors per QD (acc/QD), apart from the initial region below -150 ºC, only between -115 and -70 ºC is J_{th} temperature insensitive and above ~ -70 ºC J_{th} increases strongly with temperature. In stark contrast, between -50 and 40 ºC, J_{th} *decreases* with temperature for the 15 acc/QD device to give a negative T_0

behaviour. Above ~70 °C, the temperature sensitivity of J_{th} for the undoped and 15 acc/QD devices is virtually identical. The larger J_{th} of the 50 acc/QD device, observed close to RT (~20 °C), is consistent with a previous report in which the RT J_{th} increased from 35 to 80 A/cm^2 between undoped and ~50 acc/QD devices of a similar cavity length[5].

Clearly, the overall J_{th} behaviour for each structure is very different. Since the 50 acc/QD device displays the poorest characteristics, the discussion presented in section 5.4 will be limited to the lower doped (15 acc/QD) device and the undoped reference sample. In any case, the unusual form of the J_{th} temperature dependence of the 15 acc/QD sample between -150 and 50 °C calls for further investigation. Before this however, the corresponding results for the second series of structures will be presented.

The initial results presented above informed the design for the second set of structures that contained 7 DWELL layers, with doping ranging from an undoped reference sample to 6, 12 and 18 acc/QD. The temperature dependence of J_{th} for 3 mm cavities of the structures in this second series is shown in Fig. 5.4. As for series 1, the relevant laser characterisation parameters are listed in Table 5.5

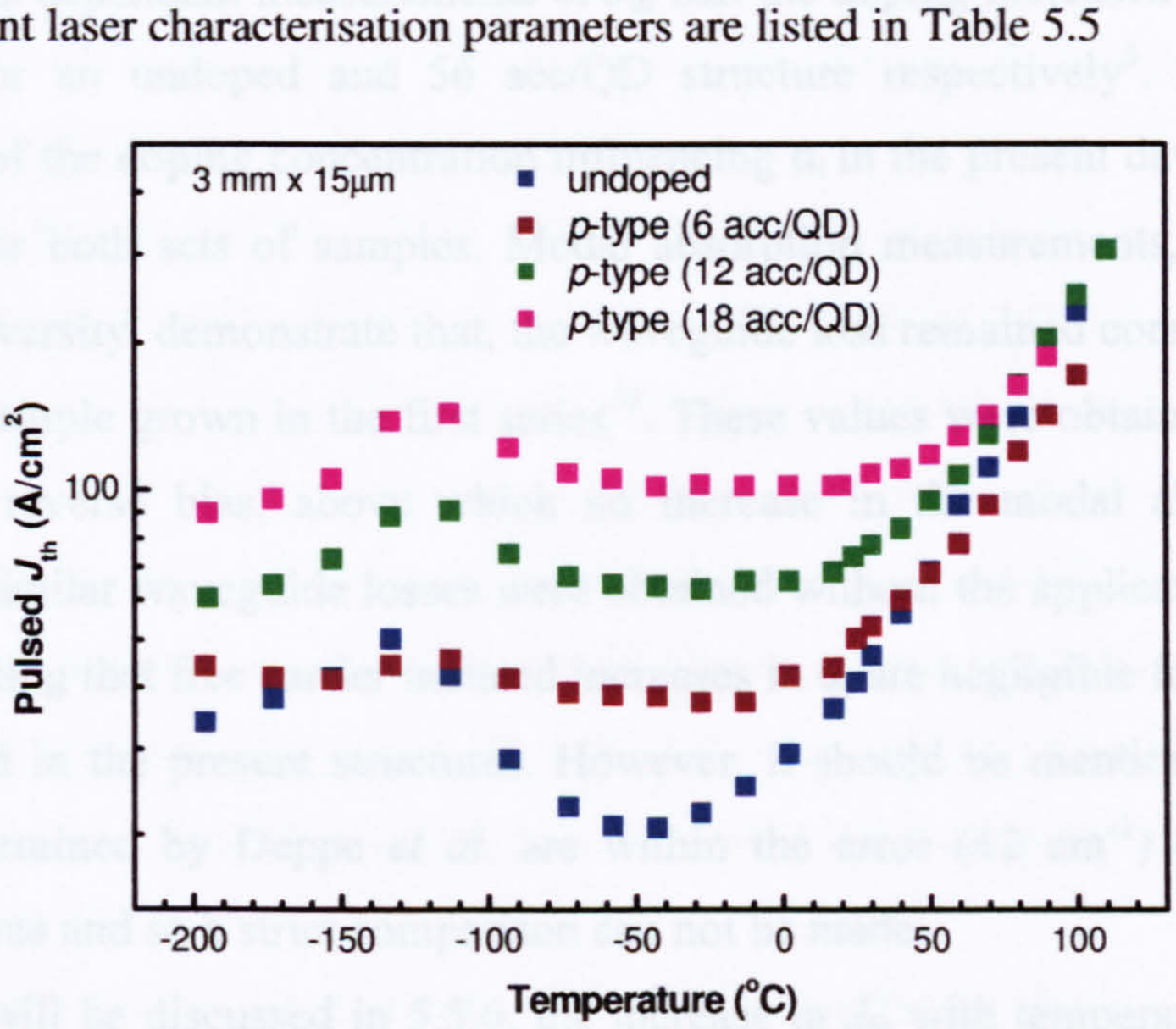

Fig. 5.4 Temperature dependence of the pulsed J_{th} for 3 mm cavity length *p*-type doped and undoped devices grown in series 2

Although the form of the temperature behaviour of J_{th} is different to that observed in Fig. 5.2, there are trends in the temperature dependence that vary more

systematically with doping level. For example, unlike the structures grown in series 1, the T_0 values above RT increase monotonically with doping density (see Table 5.1) and the region of quasi-infinite T_0 above -100 °C extends to higher temperatures as the doping level increases. Likewise, the doping level dependence of J_{th} below RT is different to what is seen for the first series of structures, and would initially seem consistent with the idea that the dopants or extrinsic holes serve to increase the internal loss (α_i) of the structures.

	Undoped	6 acc/QD	12 acc/QD	18 acc/QD
RT Pulsed J_{th} (A/cm^2)	90	79	126	155
RT lasing λ (nm)	1312	1316	1315	1314
T_0 (K) [0 - 70°C]	46	60	61	71

Table 5.5 RT laser characterisation parameters for the *p*-type doped and undoped structures grown in series 2. The values are obtained for 3 mm x 15 μm cavities.

In the original work of O. B. Shchekin and D. G. Deppe, it was inferred from cavity length dependent measurements of J_{th} that the doping increased α_i from 1.8 to 2.9 cm^{-1} for an undoped and 56 acc/QD structure respectively[5]. However, the possibility of the doping concentration influencing α_i in the present devices has been ruled out for both sets of samples. Modal absorption measurements, performed at Cardiff University, demonstrate that, the waveguide loss remained constant at ~2 cm^{-1} for each sample grown in the first series[13]. These values were obtained under -2 V of applied reverse bias, above which no increase in the modal absorption was observed. Similar waveguide losses were obtained without the application of reverse bias, indicating that free carrier induced increases in α_i are negligible for the levels of doping used in the present structures. However, it should be mentioned that the α_i values determined by Deppe *et al.* are within the error (±2 cm^{-1}) of the Cardiff measurements and so a strict comparison can not be made.

As will be discussed in 5.5.6, the increase in J_{th} with temperature between -200 and -100 °C may be related to thermally induced changes in the intra-QD carrier distribution. What is apparent from Fig. 5.3 is that the strong temperature sensitivity of J_{th} between -150 and 0 °C, observed in all undoped QD lasers and attributed to carrier redistribution effects, is greatly suppressed in devices doped with as few as 6

acceptors/QD. This stability is highlighted by the logarithmic J_{th} scale used in Fig. 5.3 and correlates nicely with the EL properties presented in sections below.

5.4 Temperature dependence of J_{th} in the 15 acc/QD device

Although the *p*-type doping may compensate for the thermal excitation of holes from the lasing state and therefore enhance the temperature stability of J_{th}, this alone cannot account for either the increase in J_{th} between -150 and -90 °C or the negative T_0 around RT exhibited by the 15 acceptor/QD device (see Fig. 5.2). This behaviour will be discussed in more detail in section 5.6, in which the details of a new physical model are outlined.

Work from other groups suggests that differences in the temperature dependencies of the Auger recombination rate in *p*-type doped and undoped devices determines the overall form of the J_{th} – temperature dependence. Specifically, the infinite T_0 observed between 5 and 75 °C in a 10 layer *p*-type doped device was accounted for by invoking opposing temperature dependencies of different non-radiative processes over this temperature range[9]. Above RT, the increase in non-radiative recombination involving states in the barrier is compensated by a significant reduction in Auger recombination.

In a similar *p*-type doped structure, grown by the same company (NL Semiconductors, now Innolume), the positive and negative regions of T_0 observed from -220 to -115 °C, and -75 to 10 °C respectively, were explained by assuming a combination of increasing Auger recombination rates at low temperatures coupled with a delayed onset of the inter-QD carrier thermalisation[14]. The electrostatic attraction due to the high concentration of holes in or near the QDs in *p*-type doped structures is proposed to increase the effective confinement potential of the bound electrons, therefore requiring higher temperatures before thermal escape, followed by recapture, becomes possible.

Neither the results obtained in Sheffield, nor those of our collaborators at Cardiff University, support the claims of increased Auger recombination in *p*-type modulation doped samples at high temperatures. There is, however, considerable evidence that the doping of the QDs affects the carrier distribution between the QD states in the ensemble (see section 5.5.6). In the following sections the physical

processes occurring in doped and undoped QD lasers are probed using a range of optical spectroscopic techniques.

5.5 Spontaneous emission properties of *p*-type doped QD devices

5.5.1 Low temperature EL spectra measured under low injection

Normalised 77 K spontaneous emission spectra, collected from 400 μm diameter mesa devices under low cw injection, are shown in Fig. 5.6 (a) and (b) for the first and second series of structures respectively. It is clear that the average GS energy of the QDs, determined by the peak emission wavelength, is approximately the same for all samples. This suggests that the structural properties, i.e. the size and shape of the *individual* QDs are unaffected by the doping process. The small variations in peak position (<2 meV) observed in the present samples are negligible compared to the 50 meV blueshift observed in other 1.3 μm *p* type doped QDs[15]. This blueshift has been suggested to result from an enhancement of the interdiffusion between the QD and surrounding matrix material due to the presence of excess holes during the growth[16]. No evidence for similar effects is seen in the present samples.

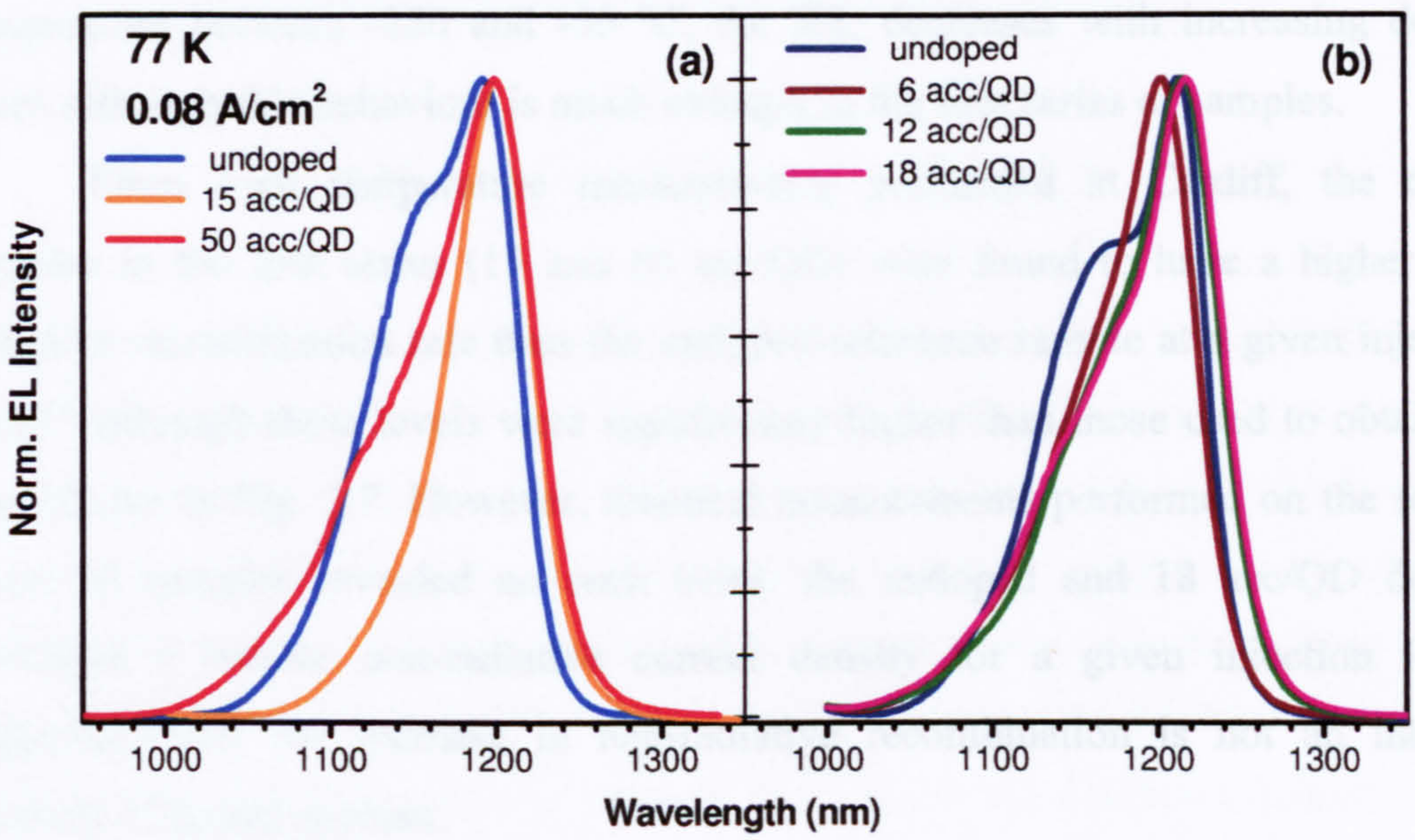

Fig. 5.6. Normalised low cw injection EL spectra, measured at 77 K, for series 1 structures (left hand panel) and series 2 structures (right hand panel)

However, it is possible that the dopants affect the growth kinetics at the WL surface and are therefore able to influence the QD size *distribution* within the

ensemble. High concentrations of Be dopants are known to diffuse easily in GaAs via their repulsive Coulombic interactions[17, 18]. This may explain why the bimodal shoulder at shorter wavelengths is seen to be somewhat 'smeared' in the spectra of all the doped samples. In the first sample series, the linewidth of the low temperature emission varies non-systematically with doping level, being narrowest for the 15 acc/QD sample (54 meV) and broadest for the undoped structure (87 meV). In the second series, again the undoped structure has the broadest emission (91 meV), but this narrows only slightly for the doped structures – all have a FWHM of ~ 75 meV.

5.5.2 Temperature dependence of the integrated EL under constant current injection

Fig. 5.7 shows the temperature variation of the integrated EL (IEL) for all the *p*-type doped samples under very low injection levels corresponding to ~0.004 electron-hole pairs/QD[♣]. Data for the two reference undoped samples is also included in this figure. There are several points to note about the behaviour shown. If the change in IEL with doping level at a given temperature is considered, it is clear that below ~ -50 °C the undoped structures emit most strongly. In fact, for any temperature between -250 and -50 °C, the IEL decreases with increasing doping level, although this behaviour is much stronger in the first series of samples.

From high temperature measurements performed at Cardiff, the doped samples in the first series (15 and 50 acc/QD) were found to have a higher non-radiative recombination rate than the undoped reference sample at a given injection level[13] although these levels were significantly higher than those used to obtain the data shown in Fig. 5.7. However, identical measurements performed on the second series of samples revealed no such trend: the undoped and 18 acc/QD devices exhibited a similar non-radiative current density for a given injection level[19] suggesting that the increase in non-radiative recombination is not an intrinsic property of doped devices.

♣ No. carriers per QD $= \frac{J\tau_{rad}}{N_L e \rho_{QD}}$ where J is the current density (0.08 A/cm^2), τ_{rad} is the GS exciton radiative lifetime (~1 ns in undoped structures), N_L is the no. of QD layers (5), e is the electron charge and ρ_{QD} is the area QD density (3 x 10^{10} cm^{-2}).

The results in Fig. 5.7 are consistent with the finding that non-radiative effects appear to be more important in the first series of samples. However again it is important to note that the injection levels used in the Cardiff work were much higher than those used to record the data of Fig. 5.7. As will be shown, the difference between the undoped and doped samples is much smaller for higher injection levels. At high temperatures the behaviour observed at low temperatures is reversed, with the doped sample having a slightly higher intensity than the undoped sample.

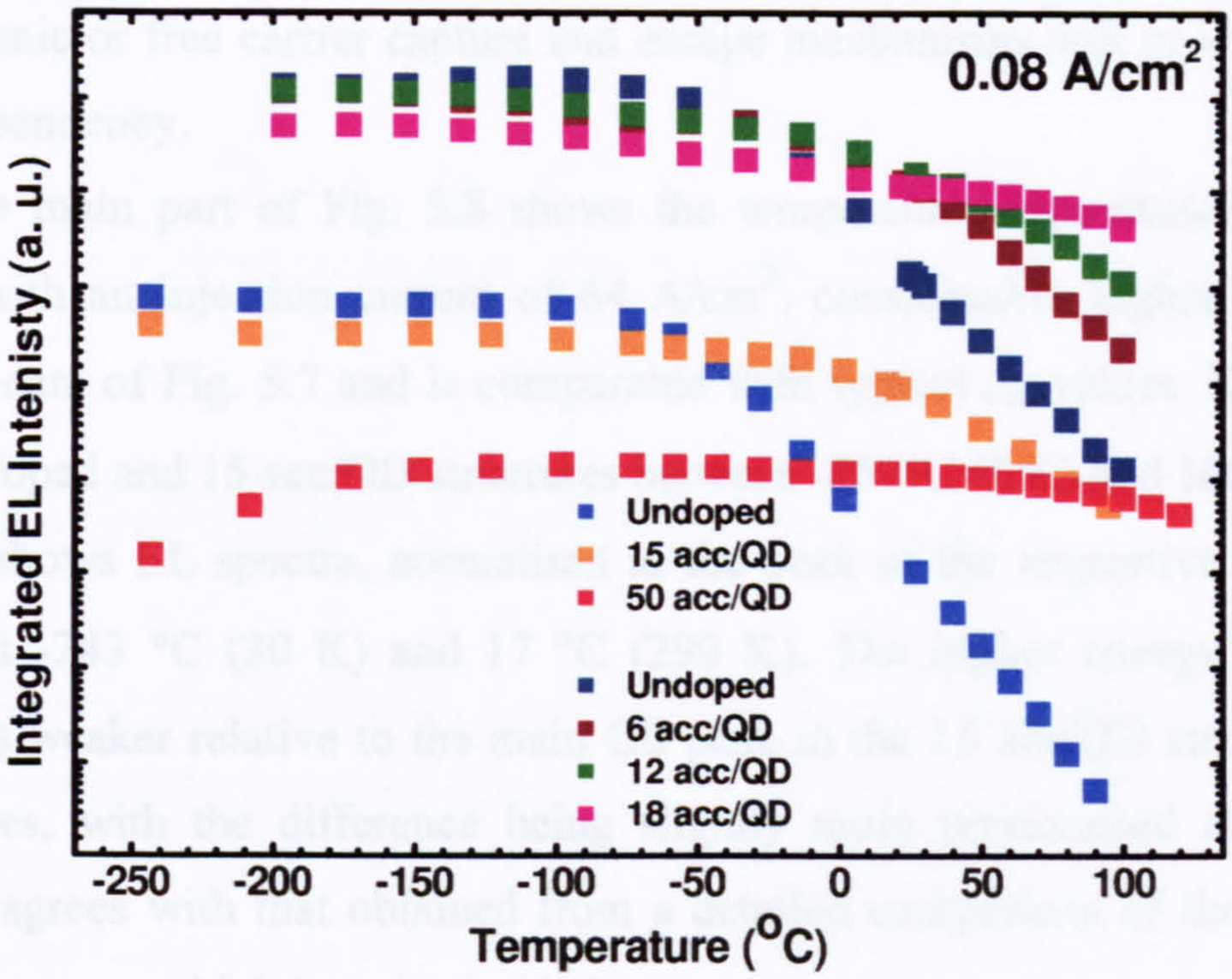

Fig. 5.7 Integrated EL, acquired at low injection, as a function of temperature for all of the doped samples.

The second point to note in Fig. 5.7, is that above RT the stability of the IEL improves considerably with increasing doping concentration, in the present regime of low injection current density. This trend may be understood if it is assumed that the GS hole occupation probability increases in proportion to the doping concentration. At low temperature, electrically, and therefore non-resonantly generated carriers, are captured randomly into the QDs where the characteristic time for thermal escape (τ_{esc}) greatly exceeds the radiative lifetime (τ_{rad}): $\tau_{esc} >> \tau_{rad}$. Carriers captured non-geminately into a QD remain there until a carrier of opposite charge is captured into the same dot and recombination can occur. At higher temperatures, this is not the case: carrier escape is able to compete with recombination ($\tau_{esc} \sim \tau_{rad}$) and hence the PL intensity is quenched if the carriers are able to recombine non-radiatively when

they are outside of the QDs. However, carrier escape at high temperatures can be made less probable if the time that the injected carriers spend unaccompanied in the QD GS can be reduced. Such a situation may exist if one species of carrier is built-in to the QDs via modulation doping. This effectively increases the proportion of injected carriers that are captured into a QD already containing a carrier of the opposite charge, thereby increasing the radiative efficiency of the sample. An interesting consequence of $\tau_{esc} >> \tau_{rad}$ at low temperature is that the nature of the carrier capture and escape processes is effectively 'masked' in an EL measurement: both excitonic or free carrier capture and escape mechanisms will produce the same IEL - J dependency.

The main part of Fig. 5.8 shows the temperature dependence of the IEL, obtained with an injection current of 64 A/cm^2, considerably higher than used to obtain the data of Fig. 5.7 and is comparable with typical J_{th} values. Data is shown for the undoped and 15 acc/QD structures between -267°C (6 K) and 100 °C (373 K). The inset shows EL spectra, normalised to the peak of the respective GS emission intensity at -243 °C (30 K) and 17 °C (290 K). The higher energy excited state emission is weaker relative to the main GS peak in the 15 acc/QD structure at both temperatures, with the difference being slightly more pronounced at 30 K. This behaviour agrees with that obtained from a detailed comparison of the temperature dependent spectra which is presented below.

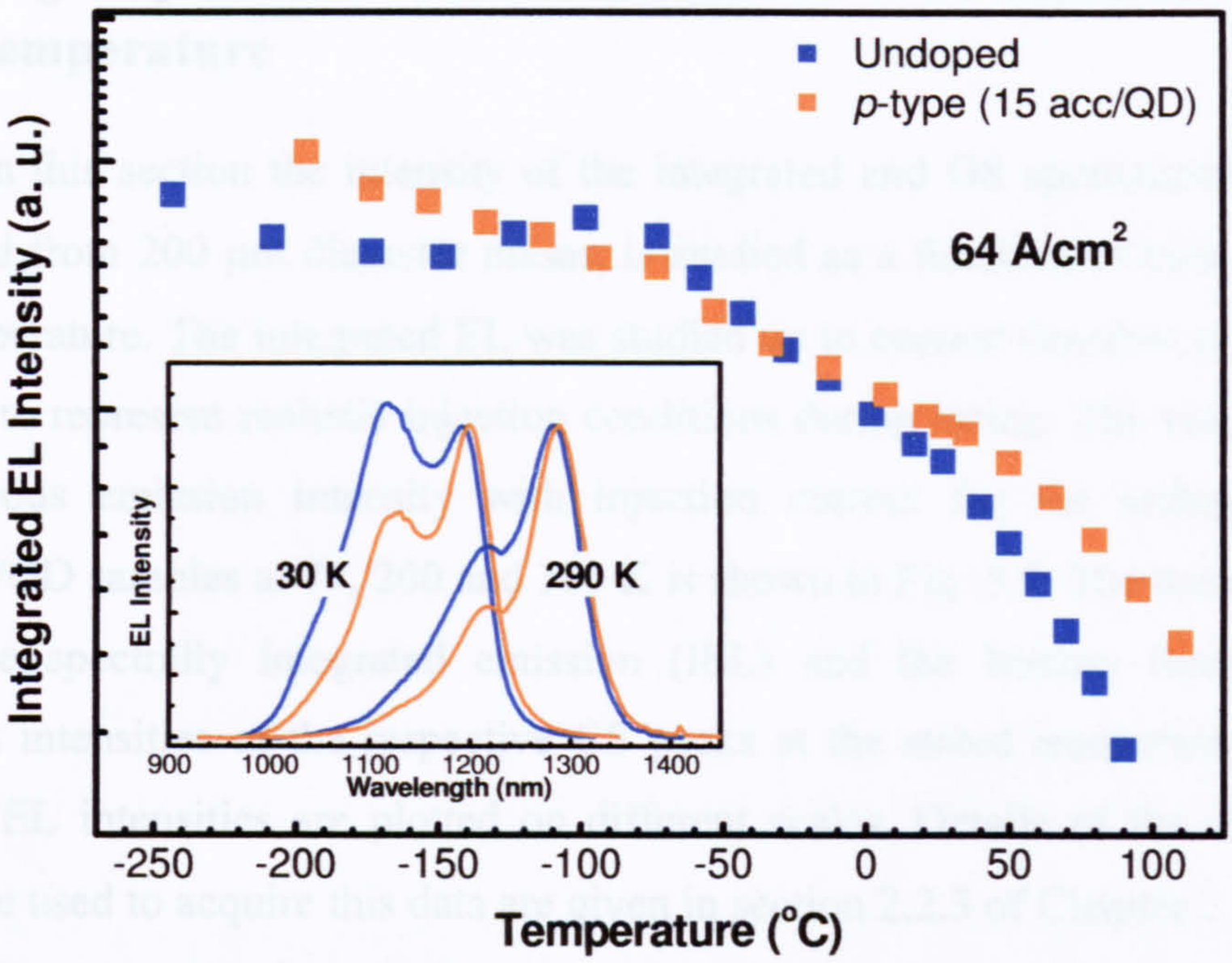

Fig. 5.8 Integrated EL, acquired at high injection, as a function of temperature for the 15acc/QD and undoped reference sample grown in series 1.

In both structures, the IEL decreases by less than two orders of magnitude over the investigated temperature range. Overall, the temperature stability of the IEL is slightly greater in the 15 acc/QD device, but the dependencies are similar with the RT IEL values being within ~20 % of each other. The relative intensities of the two structures are much more comparable than is the case for the lower level injection data shown in Fig. 5.7 above. The local maximum in the IEL observed for the undoped structure at ~200 K (-80 °C) is not observed in the 15 acc/QD structure. The physical origin of this feature is unclear. It may be due to carriers, localised in trap centres in the wetting layer at low temperatures, being re-emitted and captured into the QDs as the temperature is increased[20]. Local maxima in the IEL at ~200 K have been observed for other undoped structures (e.g. see Fig 4.15, chapter 4) but it is notable that such features are far less pronounced in the IEL of doped structures, perhaps indicating that the extrinsic holes are able to saturate traps in the wetting layer.

5.5.3 High injection EL studies as function of current and temperature

In this section the intensity of the integrated and GS spontaneous emission, measured from 200 μm diameter mesas, is studied as a function of injection current and temperature. The integrated EL was studied up to current densities of 250 A/cm^2 in order to represent realistic injection conditions during lasing. The variation of the spontaneous emission intensity with injection current for the undoped and 15 acceptor/QD samples at 77, 200 and 300 K is shown in Fig. 5.9. The three top panels show the spectrally integrated emission (IEL) and the bottom three show the emission intensities of the respective GS peaks at the stated temperature. The IEL and GS EL intensities are plotted on different scales. Details of the experimental technique used to acquire this data are given in section 2.2.3 of Chapter 2.

The presence of non-radiative recombination pathways in both structures can be inferred from the sub-linear 'roll-over' of the IEL observed at high current densities for all temperatures. A somewhat different behaviour is seen for the GS emission however, which saturates at much lower current densities. Even in the absence of non-radiative processes saturation of the GS emission with increasing current is expected as the GS can only accommodate a maximum of two electrons and two holes. However, the fact that the saturation level decreases with increasing temperature indicates that non-radiative effects contribute to this saturation. The IEL should increase linearly with current in a system without non-radiative processes; the observed roll-over at high currents again indicates the presence of significant non-radiative recombination in the present lasers. As expected, the apparent saturation of the total integrated EL occurs at higher currents than for the GS, as the former contains contributions from the excited QD transitions and possibly radiative transitions external to the QDs.

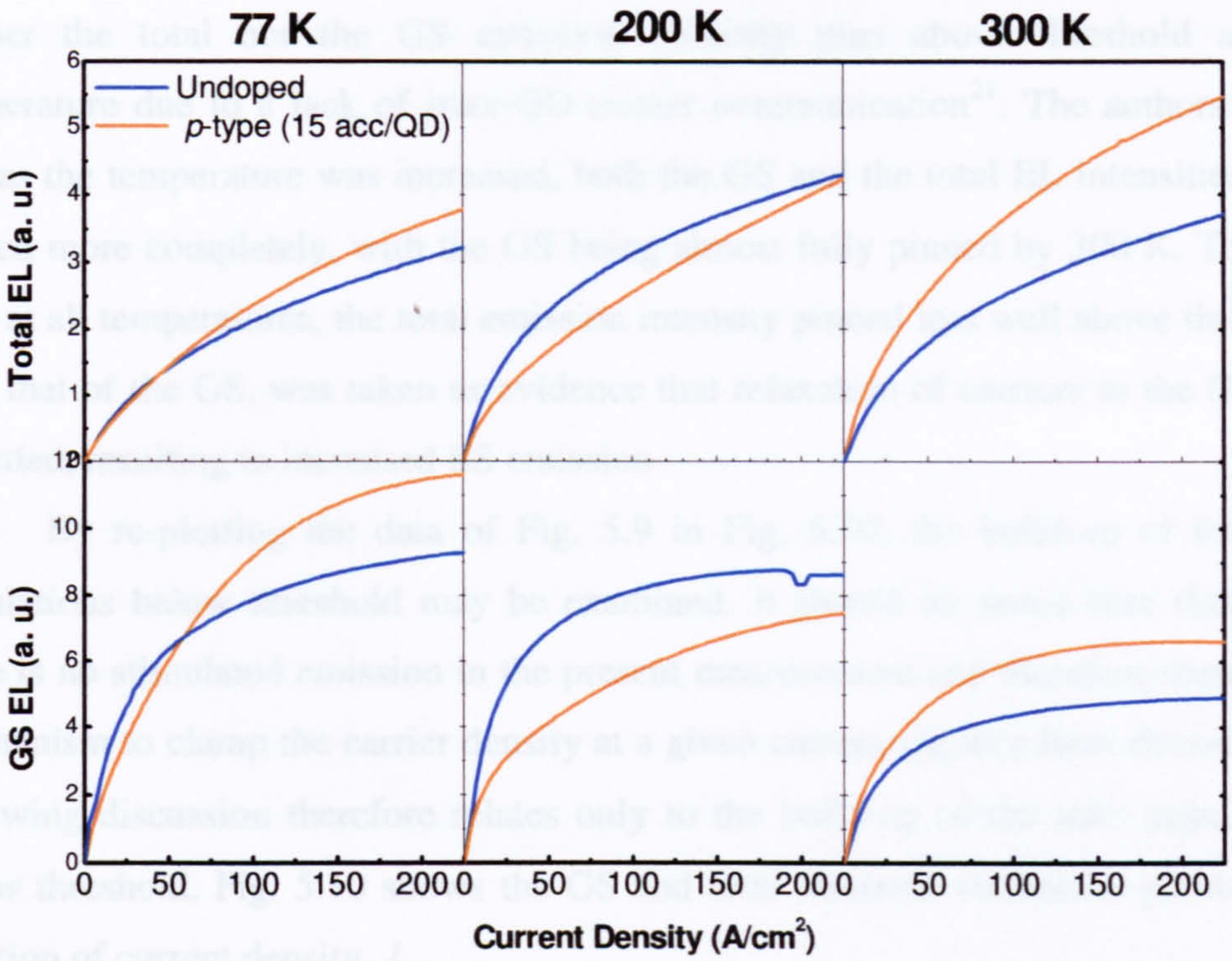

Fig. 5.9 Integrated total emission intensity (top panels) and GS emission intensity (bottom panels) as a function of injection current density for 200μm diameter mesa devices of the undoped and 15 acc/QD samples at 77, 200 and 300 K.

With increasing temperature, the saturation of the GS emission for both structures has a sharper form and occurs at a progressively lower current density. Eventually there is a negligible change with further increase in temperature. For the undoped structure the almost constant form is reached by 200 K. In contrast, for the doped structure a temperature significantly above 200K must be reached. As noted above, the saturation level decreases with increasing temperature. Although part of this effect may represent the influence of non-radiative recombination, inter-QD carrier thermalisation within the ensemble and intra-QD carrier relaxation to the GS may also contribute. For example, saturation at a lower current density is expected if only a sub-set of the QDs is populated, this is expected to occur at high temperatures. The present results suggest that the attainment of a thermal equilibrium population of carriers within the QD ensemble may occur at higher temperatures in the doped sample, possibly due to an increase in the electron confinement potential as a result of the extrinsic hole population of the QDs. This may be one reason why the saturation of the GS emission is delayed to higher temperatures in the doped device.

Unamplified spontaneous emission versus current measurements, obtained from holes milled in the substrate of undoped QD laser devices, have shown that

neither the total nor the GS emission intensity pins above threshold at low temperature due to a lack of inter-QD carrier communication[21]. The authors found that as the temperature was increased, both the GS and the total EL intensities were pinned more completely, with the GS being almost fully pinned by 300 K. The fact that, at all temperatures, the total emission intensity pinned less well above threshold than that of the GS, was taken as evidence that relaxation of carriers to the GS was impeded, resulting in increased ES emission.

By re-plotting the data of Fig. 5.9 in Fig. 5.10, the build-up of the state populations below threshold may be examined. It should be noted here that since there is no stimulated emission in the present measurement and therefore there is no mechanism to clamp the carrier density at a given current (J_{th} in a laser device). The following discussion therefore relates only to the build-up of the state populations *below* threshold. Fig. 5.10 shows the GS and total emission intensities plotted as a function of current density, J.

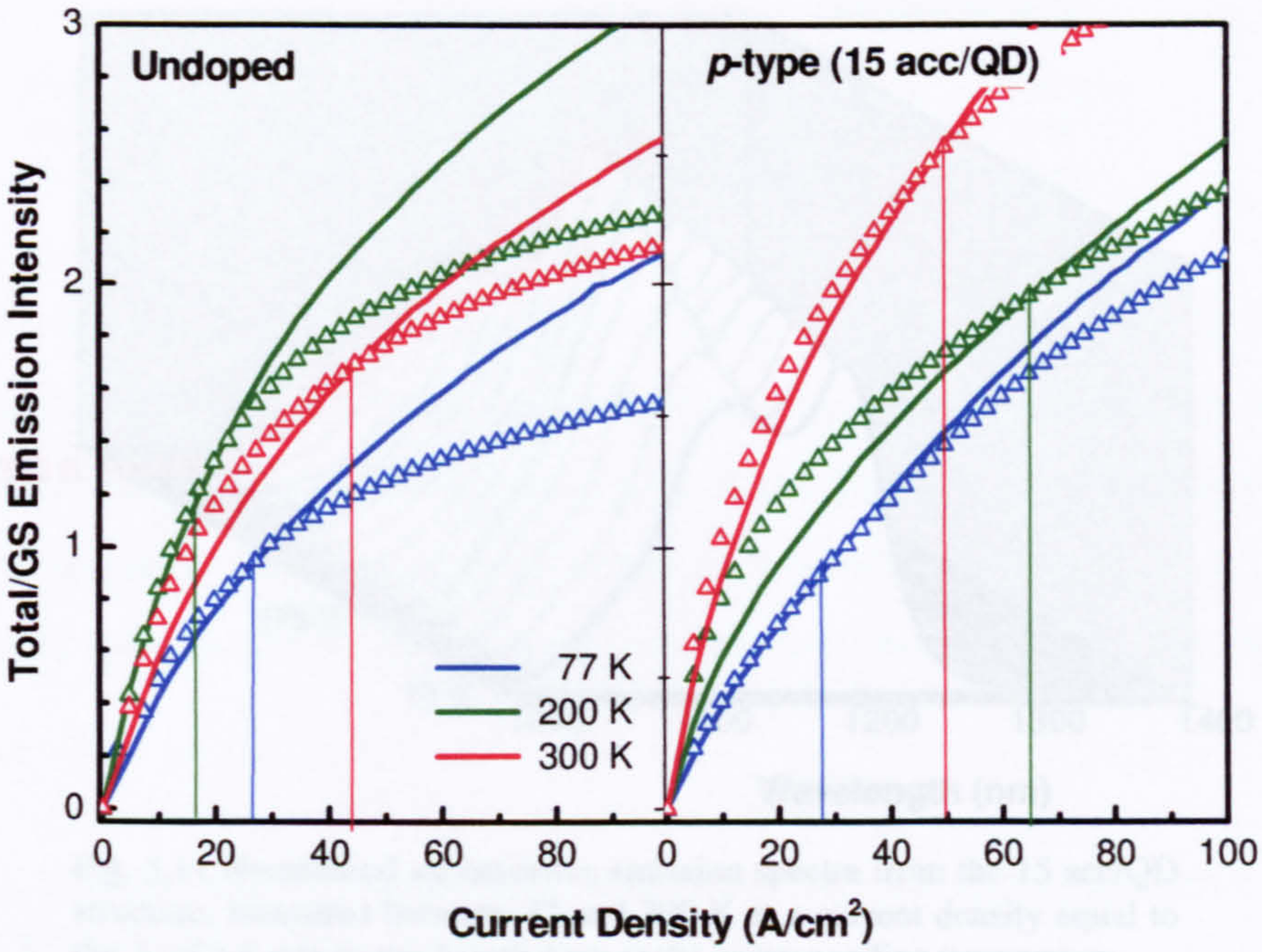

Fig. 5.10 Integrated emission intensity (lines) and GS emission intensity (triangles) as a function of injection current density for 200μm diameter mesa devices of the undoped and 15 acc/QD samples at 77, 200 and 300 K. At each temperature, the GS emission intensity has been normalised to the integrated emission intensity at a current density corresponding to the J_{th} for a 3 mm cavity.

The GS emission intensity is normalised to the intensity of the IEL at a current density corresponding to J_{th} of a 3 mm device at the same temperature. At 77 K, the current dependence of the GS emission follows that of the IEL up to J_{th} for

both structures, demonstrating that the majority of the recombination occurs from the GS. This behaviour persists up to 200 K in the undoped device. However, at 200 K in the *p*-type doped structure, the emission efficiency of the IEL decreases relative to that of the GS emission for $J < J_{th}$. Clearly, between 77 and 200 K, an additional component to the radiative recombination is present in the *p*-type doped structure.

Normalised spontaneous emission spectra, measured between 77 and 300K at a current density equal to J_{th} in a 3 mm cavity at the corresponding temperature, are shown in Fig. 5.11 for the 15 acc/QD device. Equivalent measurements for the undoped structure are shown in Fig. 5.12. As discussed in section 5.5.1, both of the samples studied in this section possess a bimodal QD size distribution. However for the relatively high injection levels used for the present measurements, the higher energy EL peak is predominantly due to the filling of the first excited state of the large QD subset.

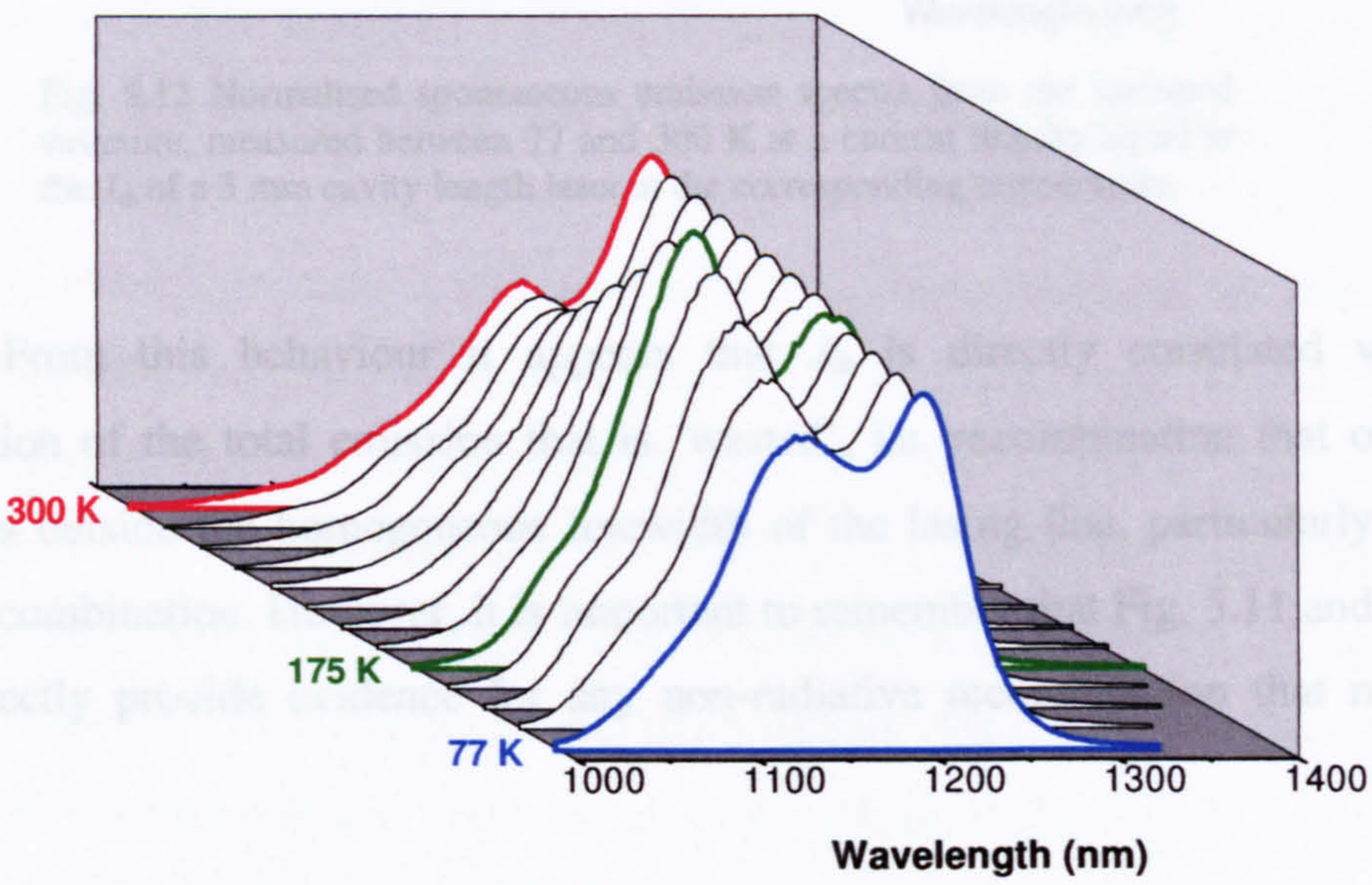

Fig. 5.11 Normalised spontaneous emission spectra from the 15 acc/QD structure, measured between 77 and 300 K at a current density equal to the J_{th} of a 3 mm cavity length laser at the corresponding temperature.

For the doped structure it is clear that at threshold the emission from the first ES increases in intensity relative to the GS peak, between 77 and 175 K. This follows the increase in J_{th} between 77 and ~200 K (Fig. 5.2). Between 200 and 300 K, the ES emission decreases with respect to that of the GS. For the undoped structure the opposite behaviour is seen but in general, the temperature dependence of the ES/GS emission intensity ratio reflects that of the J_{th} in each structure. The

temperature dependence of the ES/GS emission intensity ratio is determined by the relative rates of radiative recombination in the GS, thermal excitation to the excited states for both electrons and holes and carrier relaxation between the QD states.

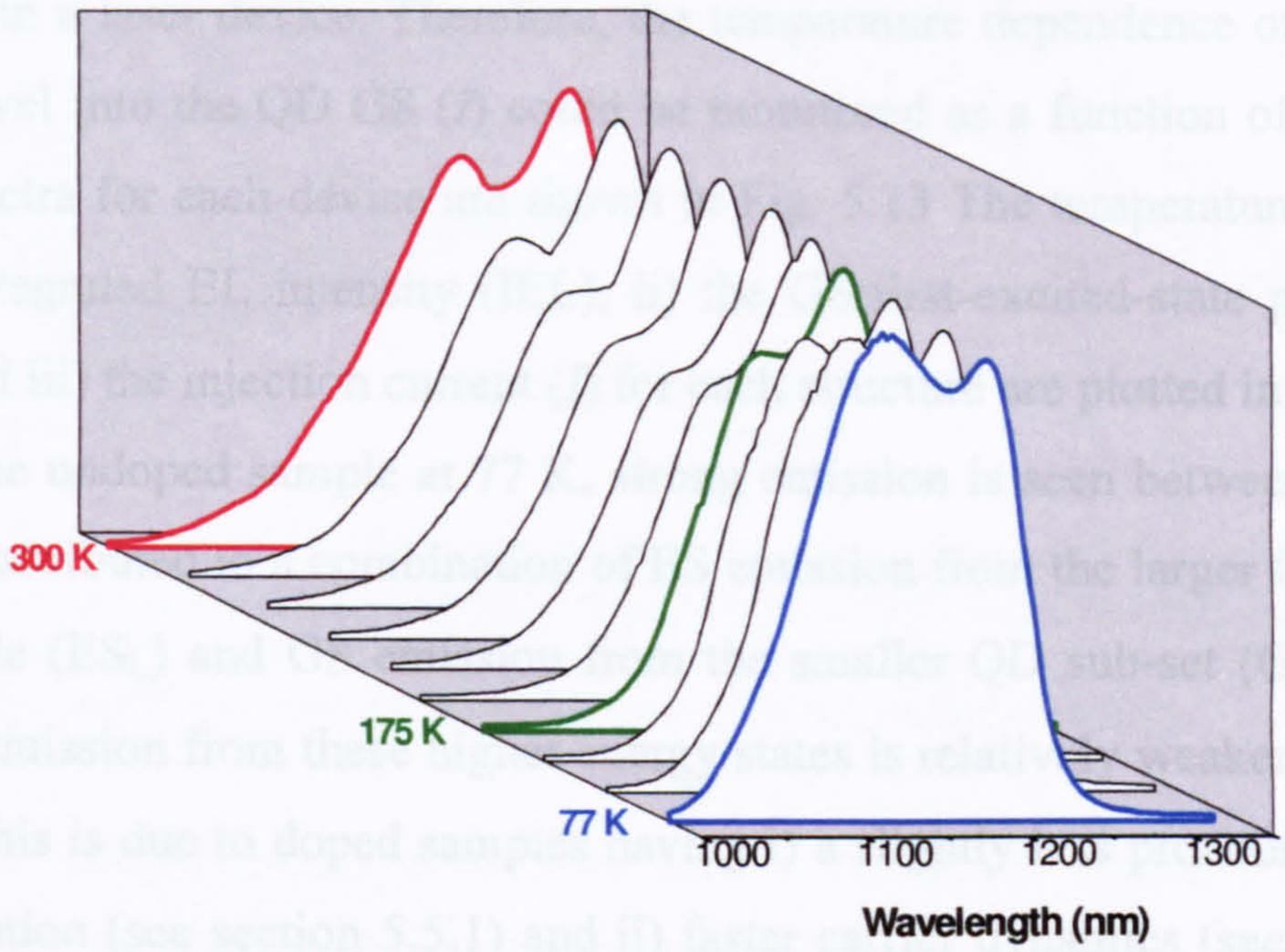

Fig. 5.12 Normalised spontaneous emission spectra from the undoped structure, measured between 77 and 300 K at a current density equal to the J_{th} of a 3 mm cavity length laser at the corresponding temperature.

From this behaviour it appears that J_{th} is directly correlated with the proportion of the total emission that is 'wasted', i.e. recombination that occurs at energies outside the homogeneous linewidth of the lasing line, particularly excited state recombination. However, it is important to remember that Fig. 5.11 and 5.12 do not directly provide evidence for any non-radiative recombination that may also occur.

5.5.4 A temperature dependent study of carrier injection into the QD GS: the effect of *p*-type doping

Individual sets of temperature and injection dependent EL spectra will now be presented. These measurements were performed on 200μm diameter mesa devices of the undoped and 18 acc/QD samples that were grown in the second series. In the first set of measurements, a single EL spectrum per device was recorded under cw injection at temperatures between 77 and 290 K, using 20-30 K intervals. At 77 K, the cw current density was chosen to be 125 A/cm^2 for both devices, which was

above the corresponding J_{th} for a 3 mm cavity. As the temperature was increased, the injection current (I) was adjusted such that the peak GS emission remained at a constant intensity. The 'normalisation' of the peak GS emission intensity was intended to fix the degree of GS population inversion ($f_c - f_v$), which is proportional to the gain in a laser device. Therefore, the temperature dependence of the *effective* injection level into the QD GS (I) could be monitored as a function of fixed 'gain'. The EL spectra for each device are shown in Fig. 5.13 The temperature dependence of i) the integrated EL intensity (IEL), ii) the GS:first-excited-state peak intensity ratio (R) and iii) the injection current (I) for each structure are plotted in Fig. 5.14.

In the undoped sample at 77 K, strong emission is seen between 1.1 and 1.2 eV. This is attributed to a combination of ES emission from the larger QD sub-set in the ensemble (ES_L) and GS emission from the smaller QD sub-set (GS_S) (see Fig. 5.14). The emission from these higher energy states is relatively weaker in the doped structure. This is due to doped samples having i) a slightly less pronounced bimodal size distribution (see section 5.5.1) and ii) faster carrier dynamics (see section 5.7), resulting in weaker ES emission (see section 5.5.5). This difference can also be seen in the inset to Fig. 5.8.

As the temperature is increased to 200 K, the intensity of the higher energy emission feature becomes weaker relative to the main GS peak in both structures, predominantly due to the carrier redistribution effect within the QD ensembles. As a consequence of this more effective population of the GS in the larger, lower energy QDs, the required injection level (I) is reduced by a factor of ~4 in the undoped structure (see Fig. 5.14). In the 18 acc/QD structure, I is reduced by only a factor of ~1.5. This difference is also reflected, to some extent, in the different behaviours of J_{th} over this temperature range (Fig. 5.4) where J_{th} for the undoped device decreases but increases for the doped device.

It is interesting to note that the minimum value of R occurs at a higher temperature in the doped structure (~260 K) than for the undoped structure (~235 K) in line with the claim that a non-thermal carrier distribution still exists in doped structures below ~250 K[19]. This observation also agrees with studies of the EL FWHM as a function of temperature and doping level, presented in section 5.5.6

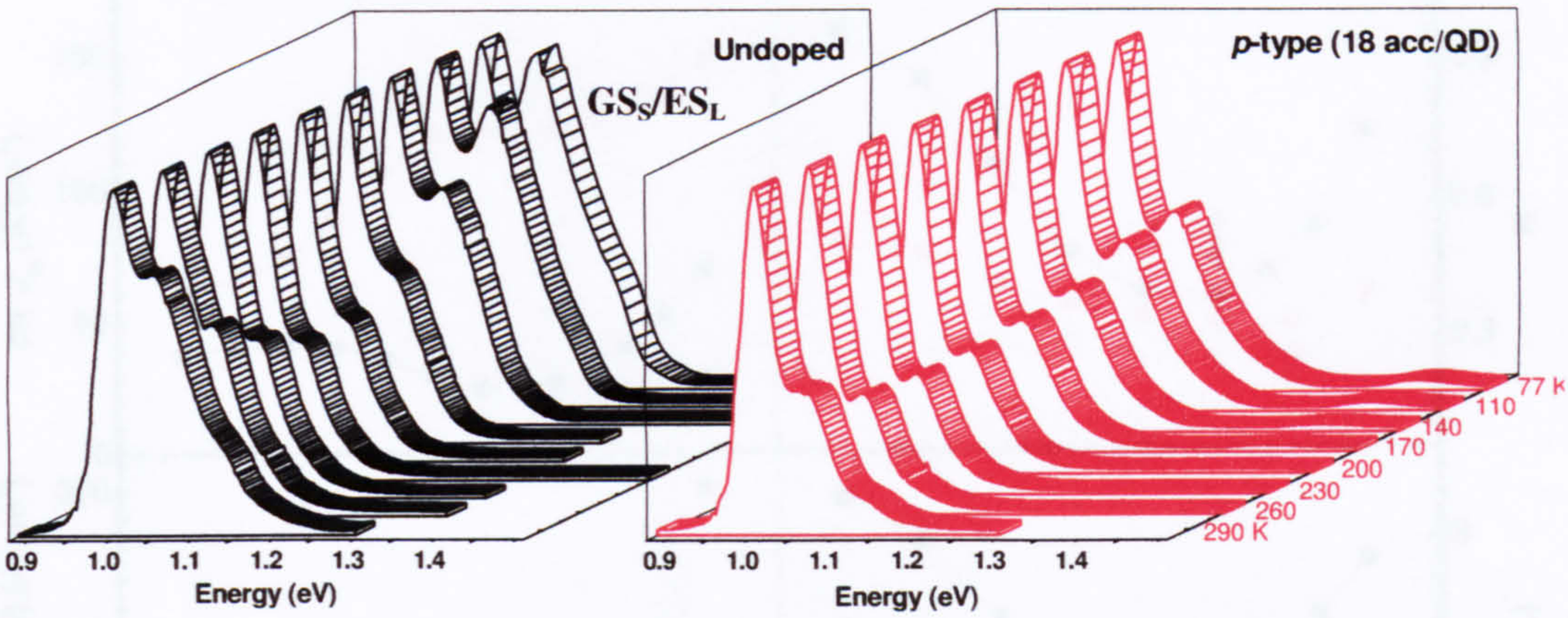

Fig. 5.13 Left hand side: EL as a function of temperature between 77 and 300 K for the undoped structure (left hand side) and 18 acc/QD structure (right hand side) in series 2. For each measurement the injection current I was adjusted independently in order to maintain a constant peak GS emission intensity.

As the temperature is raised from 200 to 290 K, the current I required to maintain a constant gain increases in each sample. However, this increase is much more pronounced in the undoped structure: between 200 and 290 K I has to be increased by a factor of 9.2 in the undoped structure whereas the increase is only 1.9 in the 18 acc/QD sample (see Fig. 5.14). Again this correlates to some extent with the observed weaker temperature behaviour of J_{th} for the doped sample over this temperature range. Over the same temperature range, the increase in the IEL is less than that observed for I in both structures, confirming that non-radiative processes become increasingly important in both structures over this temperature range. The origin of this non-radiative recombination may be associated with carriers occupying excited QD states[22] from which they can be more easily be lost to non-radiative centres, which is consistent with the observed increase in R with increasing temperature above 200 K. This effect is seen to be particularly strong in the undoped structure.

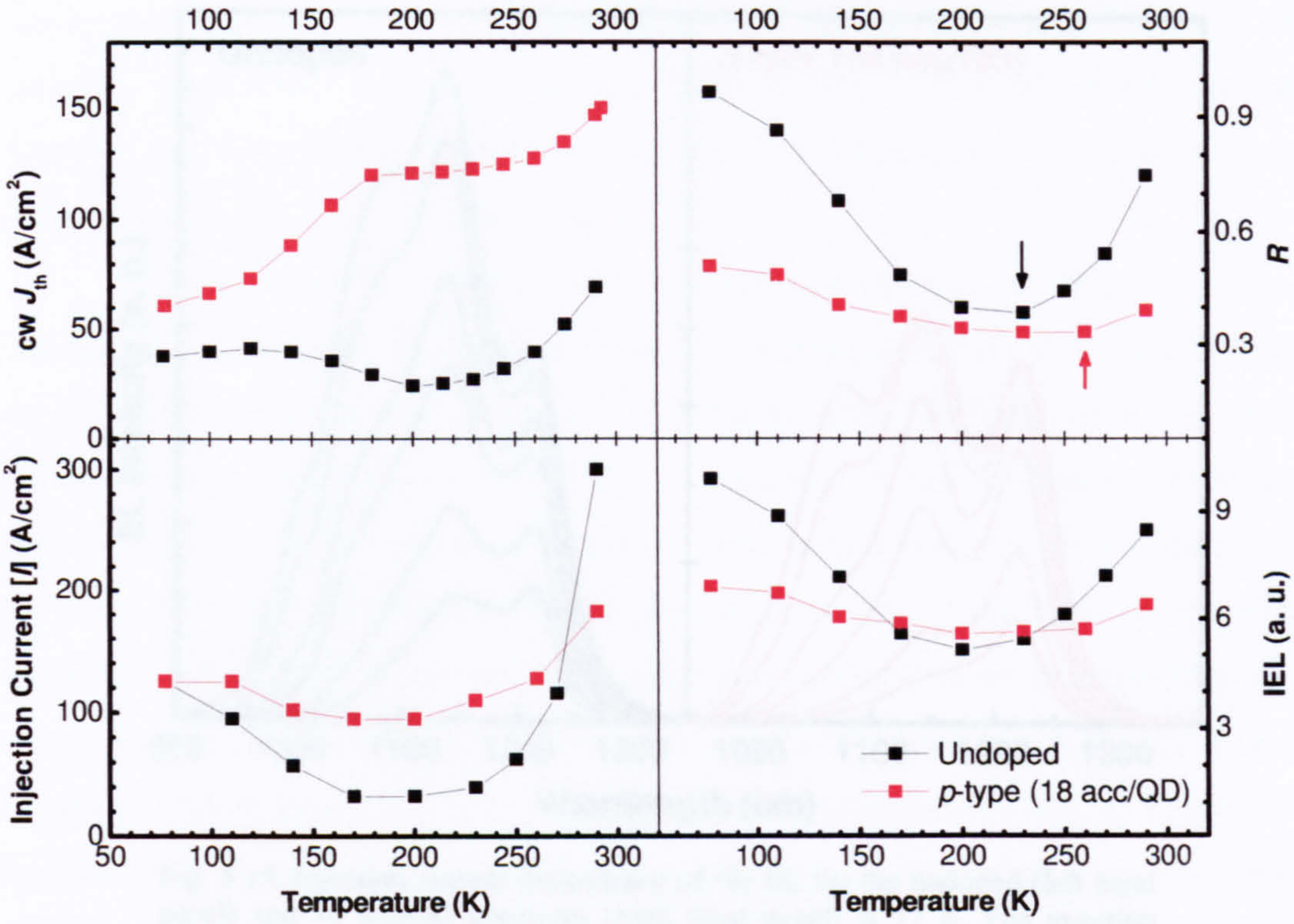

Fig. 5.14 Temperature dependence of *I*, IEL and *R* for the undoped and 18 acc/QD structures. The arrows correspond to the temperature at which *R* is a minimum in the respective structure.

5.5.5 Characteristics of state filling behaviour in *p*-type doped QDs

Direct spectral evidence has now been shown indicating that *p*-type doping suppresses the increase of the ES emission with increasing injection current density at all temperatures. This relative reduction of the ES emission with increasing carrier injection is a general property of all doped QD structures and will now be investigated in more detail for the undoped and doped structures at low temperature.

EL spectra, recorded at 77 K for various injection levels from both undoped and 18 acc/QD mesa devices, are shown in Fig. 5.15 Two important differences can be distinguished, which are attributed to the intrinsic effects caused by the *p*-type doping of the structure. First, the QD state filling is seen to occur in a more sequential manner in the doped structure, i.e. the GS is closer to saturation before a significant ES population builds up. Second, the relative saturated intensity of the first ES emission is substantially lower in the doped structure than in the undoped structure.

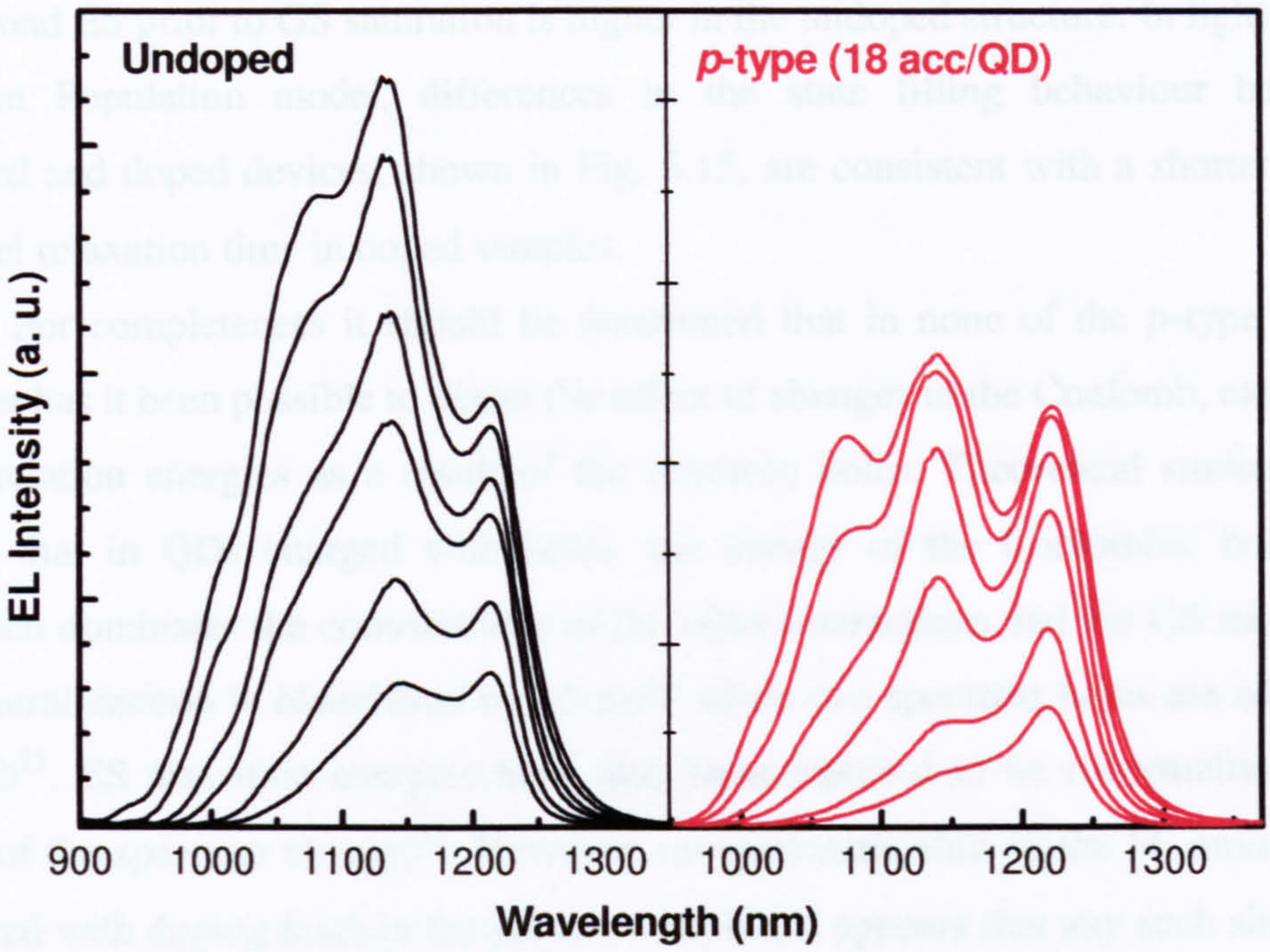

Fig. 5.15. Injection current dependence of the EL for the undoped (left hand panel) and 18 acc/QD structures (right hand panel) at 77 K. The injection levels used correspond to current densities of 16, 31, 78, 125, 219, 313 A/cm^2.

At low temperatures, when the carrier capture can be considered to be a random process and thermal reemission negligible, modulation doping the QDs can modify the evolution of the state-filling behaviour in a number of ways. Doping induced increases in the characteristic rates of carrier capture, intraband relaxation and the GS recombination can all act to ensure that the GS is replenished at a higher rate and hence carriers spend a reduced amount of time in the higher energy states, therefore suppressing the emission from these states. Independent of the direct measurement of such parameters, the results of Fig. 5.15 can be compared with the predictions of a statistical model for the QD carrier population level at low temperatures. This applies when it is inappropriate to describe the population of the QD states by a unique Fermi level as is adopted in the more conventional rate equation formalisms[23]. One of the key results of the so-called 'Random Population' model is the prediction of significant emission from the *second* ES prior to the saturation of the GS[24]. The presence of this higher energy emission prior to GS saturation is interpreted as a 'fingerprint' of a finite inter sub-level relaxation rate. From an inspection of Fig. 5.15, it is clear that the state filling proceeds in a more sequential manner in the doped structure and that the relative emission intensity of

the second ES prior to GS saturation is higher in the undoped structure. In light of the Random Population model, differences in the state filling behaviour between undoped and doped devices, shown in Fig. 5.15, are consistent with a shorter inter-sublevel relaxation time in doped samples.

For completeness it should be mentioned that in none of the *p*-type doped samples has it been possible to detect the effect of changes in the Coulomb, exchange or correlation energies as a result of the extrinsic holes. Theoretical studies have shown that in QDs charged with holes, the energy of the Coulombic hole-hole repulsion dominates the contributions of the other interactions and the GS energy of the neutral exciton is *blueshifted* by ~5 meV when two spectator holes are added to the QD[25]. ES transition energies have also been reported to be renormalised as a result of the spectator charges[26]. However, no systematic shift in the PL emission is observed with doping level in the present samples. It appears that any such shifts are too small to observe against sample to sample growth fluctuations and the broad inhomogeneous linewidth.

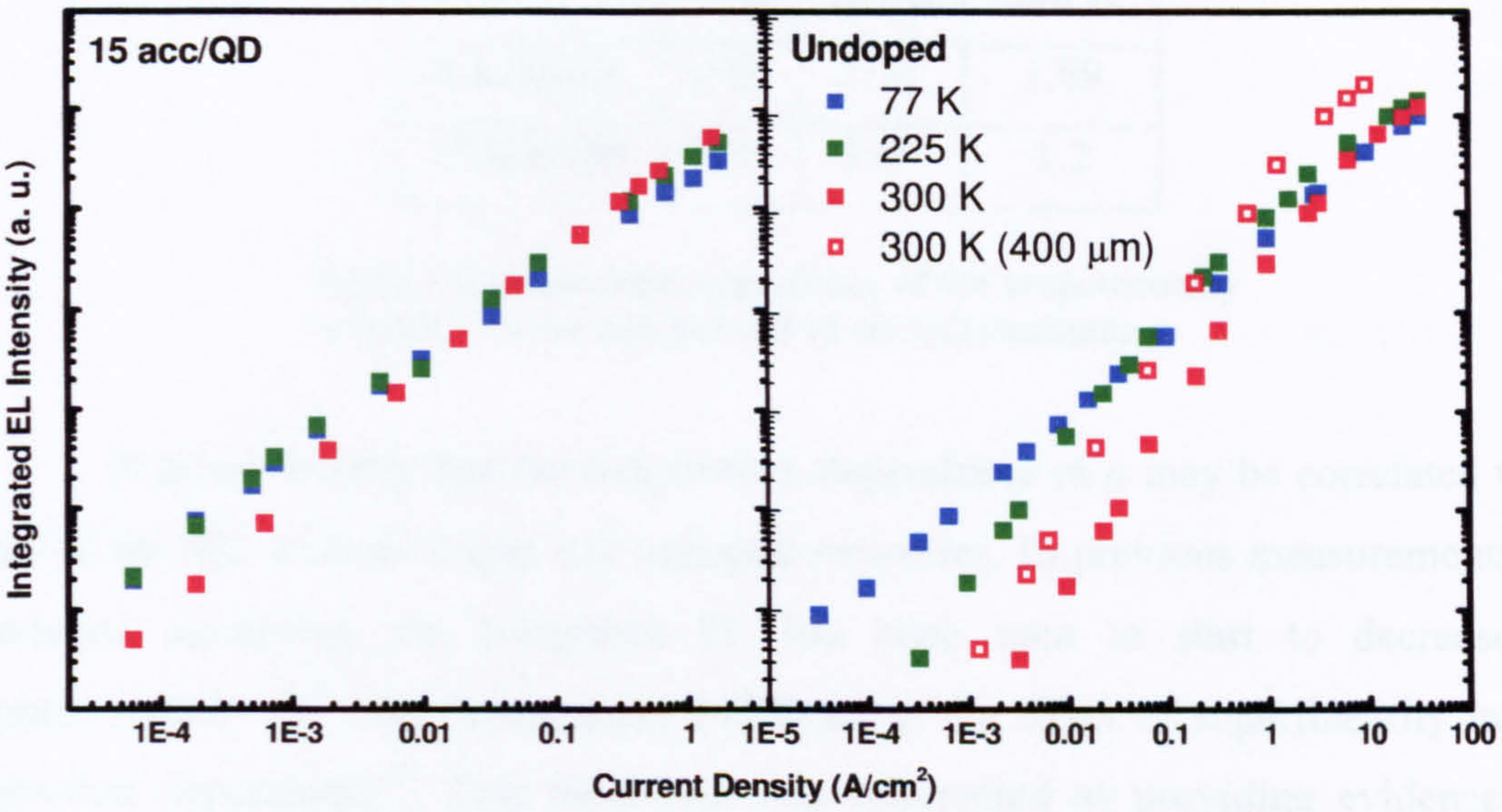

Fig. 5.16. Log-Log plot of the IEL as a function of current density for the 15 acc/QD device (left hand panel) and undoped structure (right hand panel) at 77, 225 and 300 K.

Fig. 5.16 shows the dependence of the IEL on injected current density (J), over a range of relatively low current densities from 10^{-4} to 10 A/cm^2, for the undoped and 15 acc/QD sample at 77, 225 and 300 K. The IEL *vs* J dependence can be fitted using a power law expression, $IEL = \gamma J^{\alpha}$, where γ is a constant

proportional to the collection efficiency and the internal quantum efficiency, J is the current density injected into the mesa and α is dependent on the dominant carrier recombination process. In bulk or quantum wells a value of α=1 implies radiative recombination and values of α<1 and α>1 imply Auger and defect recombination respectively. When α<1, the injection dependence is said to be sublinear and a value above unity implies superlinearity. However the applicability of this analysis to quantum dots with discrete energy states has been questioned and in the following only differences in the α values for the doped and undoped samples and their temperature behaviours are considered. Values of α were extracted from the data plotted in Fig. 5.16 with an associated error of ± 1% and are listed in Table 5.17. In the doped structure α is weakly temperature dependent and has a value close to unity at all temperatures, with possibly a small increase at high temperatures. In the undoped device, however, α increases from 0.9 at 77 K to 1.7 at 300 K.

	α values		
	77 K	**225 K**	**300 K**
Undoped	0.89	1.51	1.69
15 acc/QD	1.05	1.04	1.2

Table 5.17 temperature dependence of the proportionality constant α for the undoped and 15 acc/QD structures.

It is noteworthy that the temperature dependence of α may be correlated with that of the IEL in both doped and undoped structures. In previous measurements on undoped structures, the integrated PL has been seen to start to decrease at approximately the same temperature (~200 K) as the onset of superlinearity in the injection dependence[27]. This behaviour was interpreted as providing evidence for uncorrelated carrier escape from states in the QDs to non-radiative centres in the wetting layer. If applicable for the present samples this would imply stronger defect recombination in the undoped structure at room temperature. However given that J_{th} for the undoped device is less than that for the doped device at 300 K it seems unlikely that there can be significantly stronger non-radiative recombination in the former device at this temperature. In general there appears to be no correlation

between the temperature variation of α and J_{th} for both samples and hence the reason for the different α values for the undoped and doped samples is unclear.

5.5.6 Temperature dependence of the carrier redistribution process in *p*-type doped QDs

It is well established that the emission linewidth of InAs/GaAs QD ensembles exhibits a pronounced narrowing as the temperature increases from cryogenic temperatures, typically reaching a minimum between 100 and 200 K[28]. This effect is ubiquitously attributed to the initially randomly captured carriers, distributed uniformly throughout the ensemble, being preferentially concentrated in the more deeply confined, lower energy localised states of the larger QDs as a result of their thermal emission from the smaller QDs. As has been mentioned previously, the presence of extrinsic holes in the QDs may have the effect of increasing the confinement potential seen by the electrons, due to the electrostatic interaction between the electrically injected electrons and the 'spectator' holes. Fig. 5.18, which shows the temperature dependence of the full-width at half-maximum (FWHM), obtained from the low injection EL spectra of the first series of samples, provides evidence supporting this picture.

The emission linewidth of the undoped structure decreases with increasing temperature between -240 °C (77 K) and -40 C° (230 K), reaching a minimum value of 38 meV at 230 K. This is also the temperature at which J_{th} (in a 3 mm cavity) is a minimum (see Fig. 5.2). The temperature at which the FWHM reaches a minimum is seen to increase for the 15 acc/QD device. Here the minimum FWHM occurs at ~300 K, which is also the temperature of the local minima in J_{th} for this structure. Hence these observations support the view that changes in the carrier redistribution are at least partly responsible for the more stable T_0 at RT, reported for many *p*-type modulation doped QD lasers.

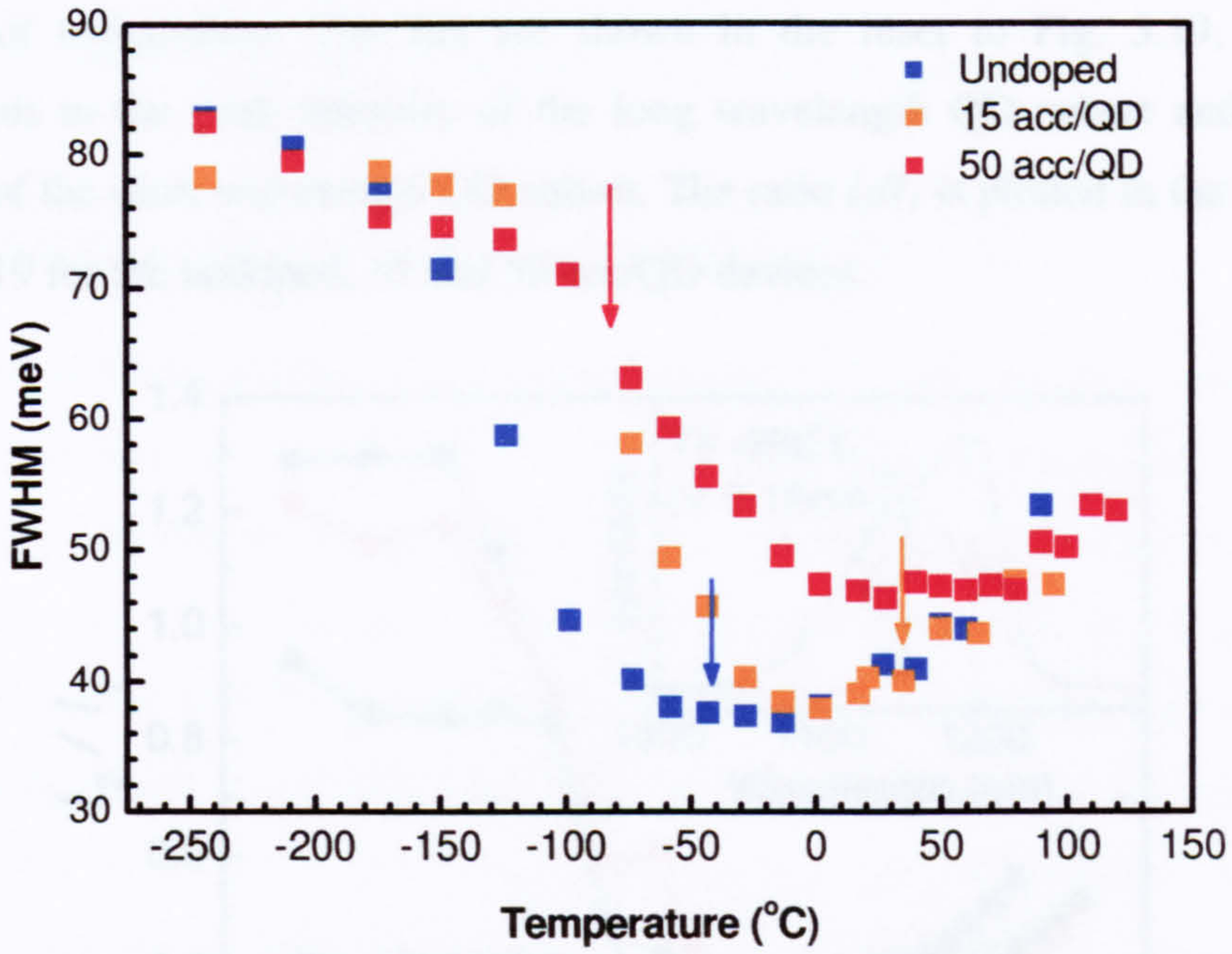

Fig. 5.18. FWHM of the low injection (0.08 A/cm^2) EL spectra as a function of temperature for the doped structures grown in series 1. Arrows mark the corresponding minima in J_{th} for 3 mm laser structures.

Essentially, the minimum in J_{th} which is observed in undoped devices (see Figs. 5.2 and 5.4) is shifted to higher temperatures when the QDs are p-type modulation doped. The increase in linewidth observed at higher temperatures in Fig. 5.18 is attributed to the thermal re-population of higher energy QDs and/or excited QD states.

Although the present measurements are recorded for injection levels which are significantly lower than those typically required to reach lasing it has been shown that the minimum in the FWHM for the undoped and 15 acc/QD samples occur at the same temperatures for injection levels comparable to J_{th}[29], further verifying the connection between the minimum in the linewidth and the minimum of J_{th}. For the 50 acc/QD structure, as shown in Fig. 5.18, the minima in the FWHM and J_{th} do not occur at the same temperature. This observation suggests that carrier redistribution amongst the QD states is not the principle determinant of J_{th} in more highly doped structures.

An alternative way to study any redistribution of carriers within the QD ensemble is provided by the bimodal QD distribution present in the current samples. The same EL spectra used to obtain the data shown in Fig. 5.18 have been fitted with Gaussians, allowing the peak intensities of the two QD sub-sets to be studied as a

function of temperature. The fits are shown in the inset to Fig. 5.19, where I_1 corresponds to the peak intensity of the long wavelength QD subset and I_2 is the intensity of the short wavelength QD subset. The ratio I_2/I_1 is plotted in the main part of Fig. 5.19 for the undoped, 15 and 50 acc/QD devices.

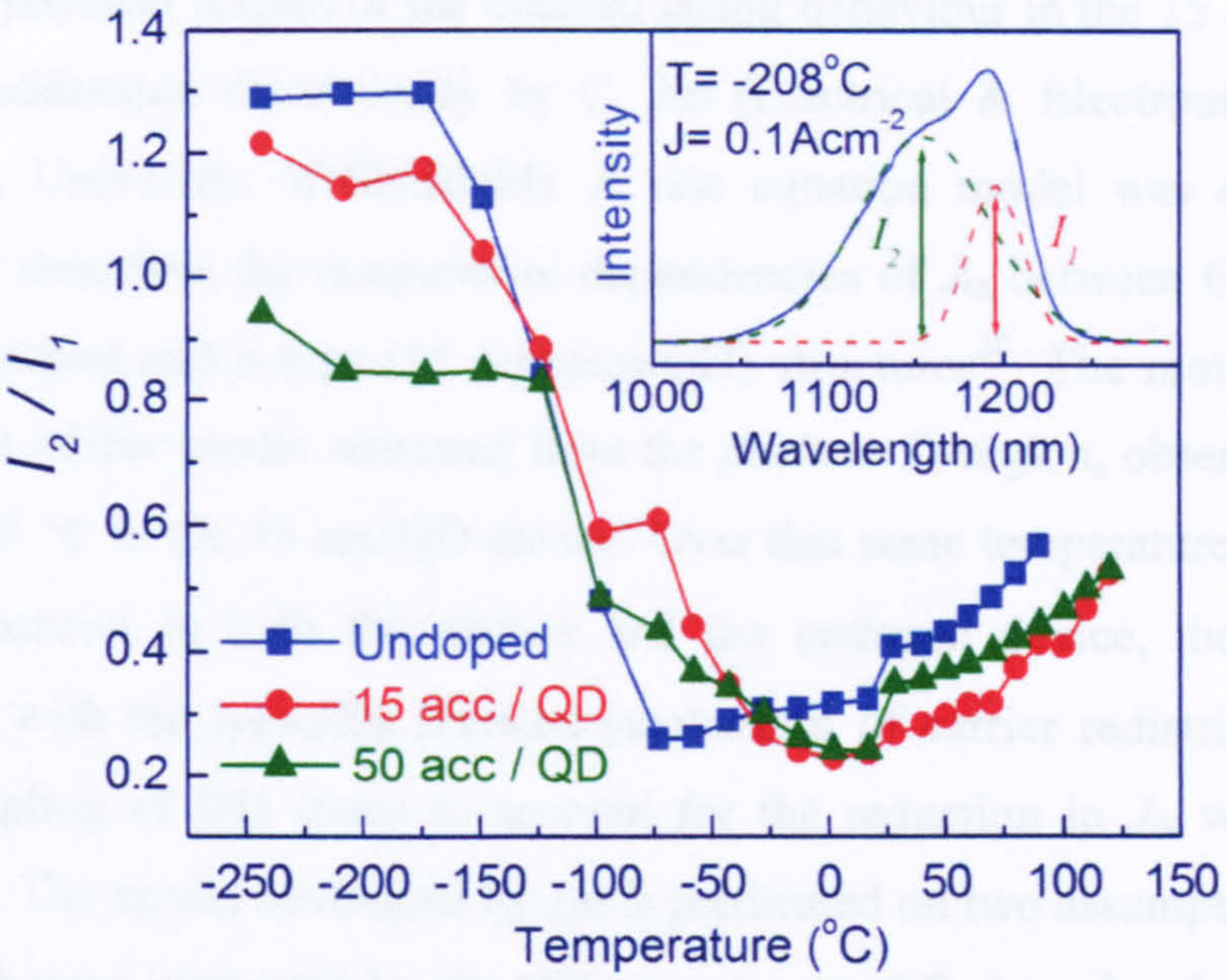

Fig. 5.19 Spontaneous emission intensity ratio for the two subsets of quantum dots. The inset shows a typical spectrum of the undoped device with two Gaussians fitted to the experimental data.

For all devices, the relative intensity due to the subset of smaller QDs decreases above −150 °C. However, while a minimum intensity ratio for the undoped device is reached at −75 °C, correlating closely with the minimum J_{th} for this device at −60 °C, the minima for the doped devices are not reached until the higher temperature of 0 °C. This behavior is consistent with full electron thermalisation occurring at a higher temperature in the *p*-type doped devices due to an increased depth of the conduction band potential well, a result of Coulomb attraction by the confined holes. The increasing ratio above 0 °C for all three samples again reflects a thermal population of the excited electron state, which affects the fitting procedure applied to extract the intensity ratio. This complication prevents an accurate determination of the temperature at which the intensity ratio reaches a minimum for the doped devices.

Hence, both the relative emission intensities of the two subsets of QDs and the EL linewidth suggest that p-type doping of the QDs delays the attainment of a

thermal electron population to higher temperatures, resulting in more temperature stable operation of p-type doped lasers around room temperature.

5.6 Photon coupling of spatially isolated QD states

The physical origins of the unusual lasing behaviour in the 15 acc/QD device have been addressed theoretically by C. Jin (Electrical & Electronic Engineering Department, University of Sheffield). A rate equation model was developed that successfully describes the temperature dependencies of J_{th} between 6 and 300 K in both the undoped and *p*-type (15 acceptor/QD) structures[30]. The motivation for the development of this model stemmed from the *positive* T_0 region, observed between -200 and -100 °C in the 15 acc/QD device. Over this same temperature range, the PL linewidth narrows in both this device and the undoped device, thereby possibly inconsistent with the typically invoked mechanism of carrier redistribution via the thermal coupling of QD states to account for the reduction in J_{th} with increasing temperature. The model developed by Jin is predicated on two assumptions:

(i) Photons generated by the QDs may be amplified or absorbed by both GS and ES transitions due to the distribution of QD sizes within the ensemble. For example, photons emitted by the GS's of smaller QDs may be absorbed by the (unoccupied) ES's of larger QDs. A photon coupling mechanism (PCM) can therefore occur between GS and ES transitions which are separated in energy by less than the homogeneous broadening. In this way the carrier population of the GS at threshold depends on the ES population. The PCM and its effect on the gain spectrum are illustrated schematically in Fig. 5.20

(ii) The thermal excitation of GS holes to higher energy states occurs at lower temperatures than for electrons. It is assumed that there is a critical temperature for carrier thermal excitation to higher energy states within the QDs. The onset temperature for hole (electron) escape is T_h (T_e) and it is assumed that $T_h < T_e$, a result of the smaller hole state separation.

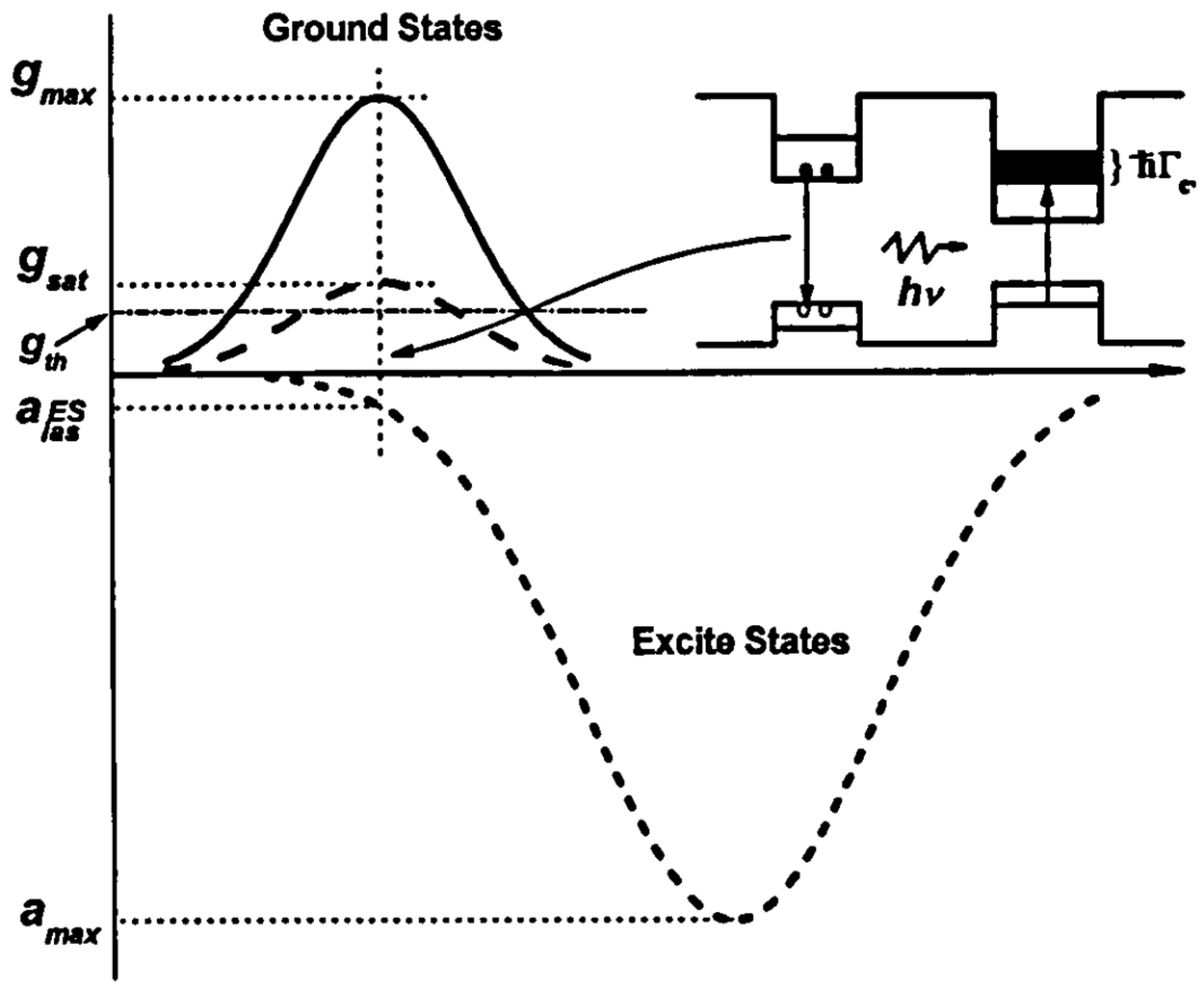

Fig. 5.20 Schematic illustration of the photon coupling mechanism (PCM)

For temperatures above T_h, the ES hole population increases in an undoped laser, producing a corresponding reduction in the ES absorption via state blocking, and hence resulting in a decrease in J_{th}. In contrast, for the doped laser, the hole ES is fully occupied at low temperature and any thermal excitation results in an un-blocking of the holes states and subsequent increase in the ES absorption and hence in J_{th}. When the temperature exceeds T_e, electron excitation starts to occur and the excited electron states become increasingly blocked in the doped device, resulting in a decreasing J_{th} between T_e and RT, due to the reduction in ES absorption. A rapid increase in non-radiative recombination above RT causes J_{th} to increase abruptly in both devices.

According to the PCM, the total gain spectrum and its temperature dependence are determined by the distribution of GS and ES energies, which depend sensitively on the overall QD size distribution. Therefore the exact form of the temperature dependence of J_{th} is intimately linked with the inhomogeneity of the QD ensemble. This may explain the range of reported T_0 values at RT both within the present chapter and by other groups. In bimodal QD ensembles, where the effect of the PCM is shown to be particularly pronounced[30], the predicted T_0 is indeed negative for the 15 acc/QD device, as is observed in Fig. 5.2

In addition to the variation in the temperature dependent J_{th} behaviour, there are differences in the temperature dependence of the lasing wavelength between the

doped and undoped devices. Lasing and spontaneous emission spectra, recorded for an injection level of 1.1 x J_{th} and 1 mA respectively, for 3 mm cavities of the undoped and *p*-type doped structures are shown in Fig. 5.21 at temperatures of 77, 180 and 300 K.

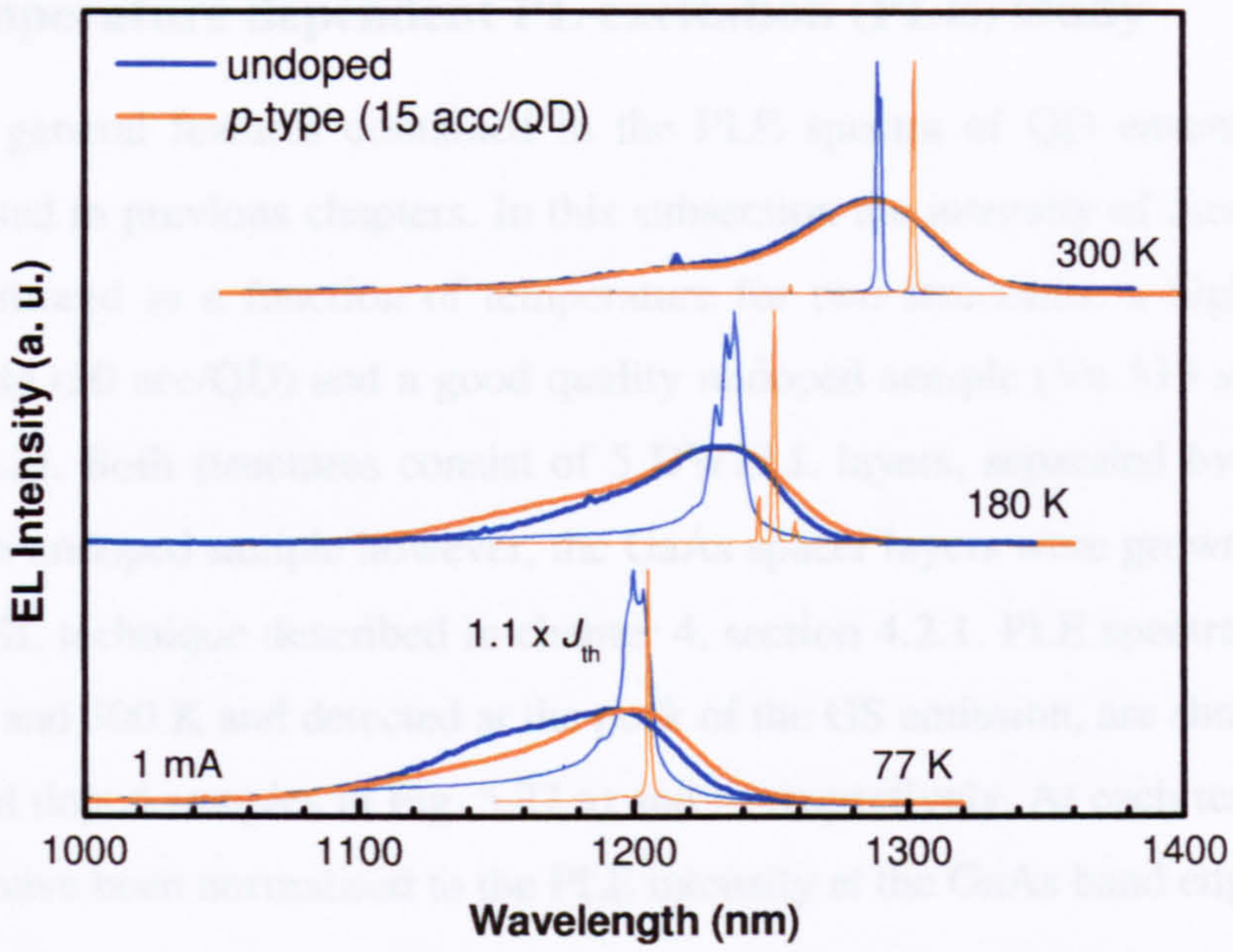

Fig. 5.21 Spontaneous emission (1 mA) and lasing (1.1 x J_{th}) spectra for 3 mm cavities of the 15 acc/QD and undoped structure at 77, 180 and 300 K.

There are two features to note. First, the low temperature (<180 K) lasing emission appears to be narrower in the *p*-type doped structure, which is possibly a result of the extrinsic holes increasing the dephasing rate and correspondingly the homogeneous broadening[31, 32]. Second, the peak emission wavelength of the *p*-type doped structure undergoes a significant redshift (~10 nm) between 77 and 180 K relative to both that of the undoped sample and the peak of the spontaneous emission. This is attributed to the same effect causing the temperature dependence of J_{th} to diverge for the doped and undoped devices; the ES absorption being respectively unblocked and blocked in the *p*-type doped and undoped structures over this temperature range, therefore shifting the peak GS gain to longer wavelength in the *p*-type doped device via the PCM[33]. Hence the photon coupling model is able to explain the very different behaviours of the doped and undoped lasers. However, as was discussed above, a modified temperature induced carrier redistribution within the QD ensemble can also explain the experimentally observed behaviour. What

remains unclear is the relative strengths of these two processes on the behaviour of the doped and undoped lasers.

5.7 Carrier dynamics in modulation doped QDs

5.7.1 Temperature dependent PL excitation (PLE) study

The general features contained in the PLE spectra of QD ensembles have been discussed in previous chapters. In this subsection the intensity of these features will be monitored as a function of temperature for two structures: a highly *p*-type doped sample (50 acc/QD) and a good quality undoped sample (Vn 513 see chapter 4, section 4.2). Both structures consist of 5 DWELL layers, separated by 50 nm of GaAs. In the undoped sample however, the GaAs spacer layers were grown using the super-HGTSL technique described in chapter 4, section 4.2.1. PLE spectra, recorded between 77 and 300 K and detected at the peak of the GS emission, are shown for the undoped and doped samples in Fig. 5.22 a) and b) respectively. At each temperature, the spectra have been normalised to the PLE intensity at the GaAs band edge.

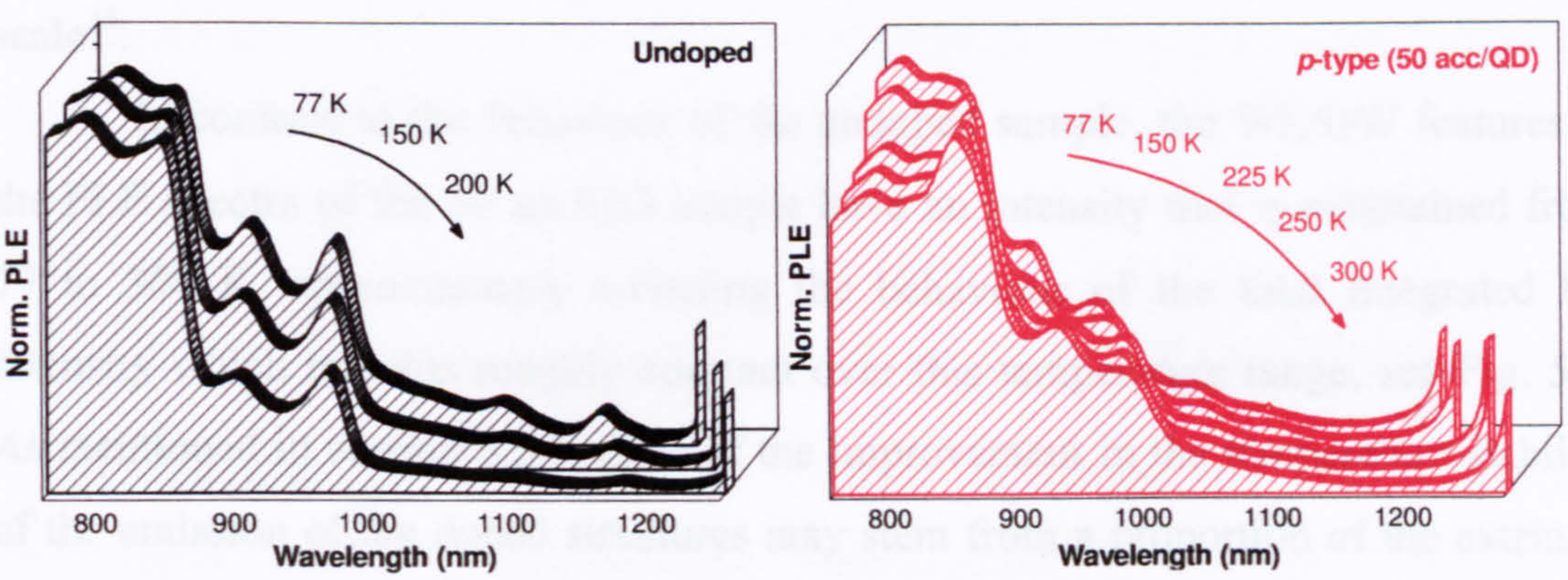

Fig. 5.22 Temperature dependent PLE for an undoped structure (Vn 513) (left hand panel (a)) and *p*-type doped (50 acc/QD) structure grown in series 1. At each temperature, the excitation spectra were recorded at the peak emission wavelength.

Considering the undoped sample initially, between 77 and 200 K a negligible decrease in the EL intensity is seen (cf. Fig. 4.15, chapter 4, section 4.2.3). In fact, over this limited range, a slight increase in the intensity occurs. In contrast, over the same temperature range, both the two WL/QW peaks between 900 and 1000 nm and the intra-QD features > 1050 nm are quenched with increasing temperature. Since the

form of the PLE spectra is intimately related to the carrier capture and relaxation processes within the QDs[34], it should be possible to correlate the temperature dependent changes observed in Fig. 5.22 with the carrier dynamics. The decreasing intensity of the WL/QW absorption features with increasing temperature indicates that for carriers photo-generated in this region, the carrier capture and transfer process to the QD GS becomes less efficient with increasing temperature. However the fact that the EL remains approximately constant over this temperature range suggests that carriers in the GaAs may bypass the WL/QW and possibly the excited QD states. PL up-conversion measurements have indicated that hot carriers in the GaAs cool down directly *and simultaneously* transfer to the lower energy QD states[35] – the overall process being mediated by Auger processes involving continuum states and possibly 'crossed' transitions between QD states and the WL[36]. The presence of periodic oscillations in the PLE above the GaAs bandedge in Fig. 5.22 supports this conclusion and provides an indication of the timescale for the capture process. These features demonstrate that hot-electron relaxation processes, leading to the formation of low mobility free excitons near the Γ point, are competing with carrier capture into the QDs, which places the capture and relaxation process on a ~5 ps time-scale[34].

In contrast to the behaviour of the undoped sample, the WL/QW features in the PLE spectra of the 50 acc/QD sample have an intensity that is maintained from 77 to 300 K, approximately reflecting the behaviour of the total integrated EL intensity which remains roughly constant over this temperature range, see Fig. 5.7. As mentioned in section 5.5.1 some of the improvement in the temperature stability of the emission of the doped structures may stem from a proportion of the extrinsic carriers saturating defect states in the matrix material[20]. This would be consistent with the retention in the PLE intensity, which for the doped structure is independent of the carrier injection loci. It should also be mentioned that faster carrier relaxation processes in the doped structure would also serve to reduce the sensitivity of the emission intensity to non-radiative recombination.

The temperature induced reduction in the definition of the features attributed to the discrete carrier relaxation steps within the QD states (features observed beyond ~1000 nm) and mediated by a combination of LO phonon emission, possibly coupled with absorption into excited QD states, suggests that carrier-carrier scattering

processes become more important at high temperature. These features are seen to be less distinct in the doped sample, even at 77 K, supporting the view that carrier relaxation to the GS is not dominated by LO phonon emission in doped samples. In PLE measurements of charge-tuneable QDs a similar dependence on the free carrier density in the QDs was observed ie. a 'washing out' of the intra-QD resonances with increasing carrier occupancy of the QDs[37].

The low temperature carrier relaxation time for the present structures has been measured using an inter-band pump – intra-band probe technique. The rise time of the differential transmission signal was found to be ~5 ps in the undoped structure, reducing to ~0.5 ps in the 18 acc/QD structure. In another reported study, a carrier relaxation time as short as 0.42 ps at 6 K was reported for *p*-type QDs doped at a similar level (20 acc/QD), which was attributed to an enhancement of the electron-hole scattering rate[15]. A slightly longer relaxation time of ~1.5 ps was reported in a study of less highly doped QDs (~1 hole/QD)[38]. This latter report claimed that the presence of extrinsic holes within the QDs induced vibrating polarisation fields that served to accelerate the capture and relaxation of photoexcited carriers. In conclusion, both the findings of the time resolved and excitation spectroscopy studies are consistent, indicating that the carrier dynamics in *p*-type doped QDs are significantly faster than in undoped samples.

5.7.2 Time resolved PL studies of *p*-type doped QD structures

Obtaining knowledge of the relative timescales for carrier capture, intersublevel relaxation and radiative recombination in QDs is of paramount importance if QD lasers are to be optimised to fulfil their potential as a medium for ultra-high bit-rate data transmission. In the following subsection the carrier lifetime of the QD GS transition (τ_{rec}), obtained from time resolved (TR) PL measurements, is studied as a function of doping density and temperature. These measurements were performed as part of a collaboration with Y Jang of Chungnam University, South Korea.

Optical excitation was provided by a mode-locked Ti:Sapphire laser with a repetition rate of 76 MHz and pulse-width of ~180 fs. Carriers were created above the GaAs band-edge at 1.676 eV, with an excitation power density of 0.74 W/cm^2,

low enough such that no change was seen in the form of the PL transient with further reduction in excitation power. The estimated photo-excited electron-hole number is significantly less than one per QD. The transient PL signal was detected at the peak of the ground state emission by a streak camera having an intrinsic resolution of 4 ps and with a spectral band-pass filter of width 10 nm. The actual time resolution was 76 ps, in order to achieve a good signal-to-noise ratio. The samples studied are those grown in the second series with the addition of a higher doped 30 acc/QD sample

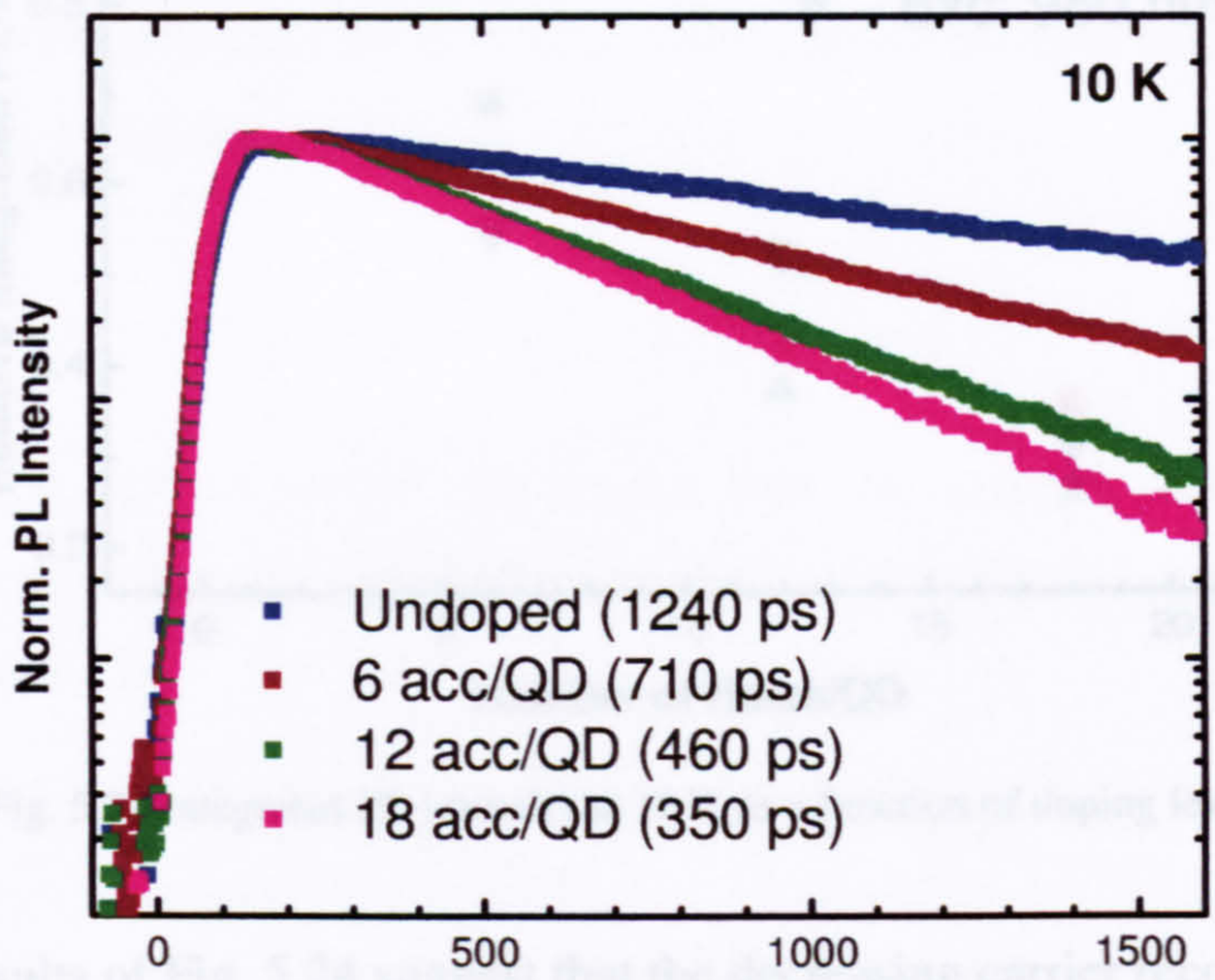

Fig. 5.23 10 K PL decay transients, measured at the PL peak, for the series 2 doped samples.

The time resolved (TR) PL decay transients for samples of different doping concentration are shown in Fig. 5.23 As the p-type modulation doping level increases, the measured decay time (τ_{rec}) decreases monotonically, by a factor of ~4 from 1.24 ns in the undoped sample to 350 ps in a sample with 18 acc/QD. τ_{rec} is listed for each sample in the legend of Fig. 5.23.

As the carrier decay time may contain contributions from both radiative and non-radiative recombination it is necessary to determine which of these makes the main contribution to the behaviour displayed in Fig. 5.23. Figure 5.24 plots the doping dependence of the ratio of the low temperature integrated PL intensity relative to that of the undoped sample for different excitation wavelengths. Squares (515 nm-excitation) and circles (750 nm-excitation) represent excitation far above and close to the band-gap of GaAs (~ 820 nm at low temperature), respectively. Data is also shown for excitation into the WL (triangles) and QDs (inverted triangles).

Figure 5.24 shows that the integrated PL-intensity decreases with increasing doping level but that this decrease is independent of the excitation wavelength. Hence any non-radiative processes must involve carriers within the QDs and does not occur as carriers migrate to, or are captured into, the QDs.

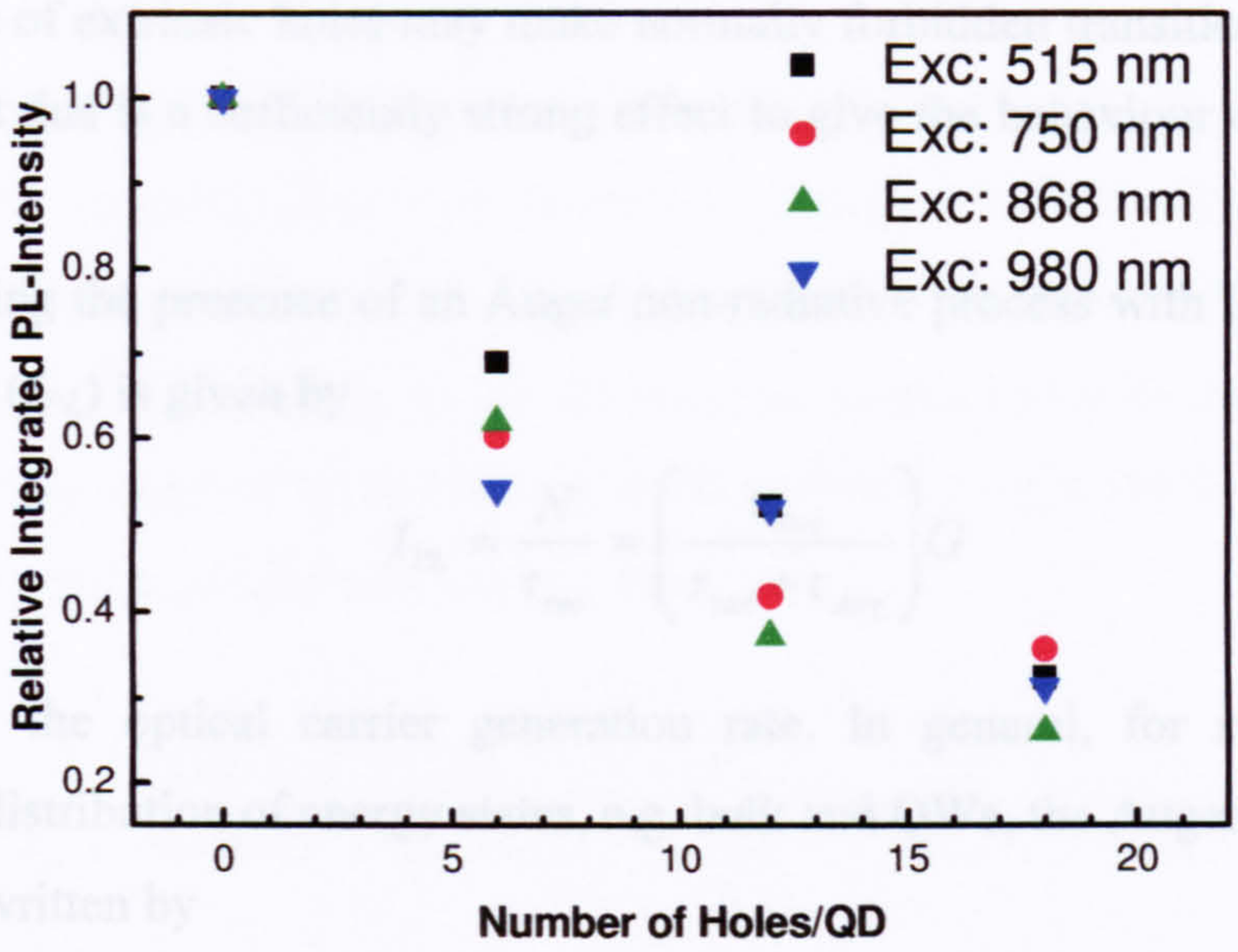

Fig. 5.24 Integrated PL intensity at 10 K as a function of doping level

The results of Fig. 5.24 suggest that the decreasing carrier recombination time with increasing p-type doping results from the presence of a non-radiative process, the strength of which increases with increasing doping level. As will be shown below the most likely explanation for this is an Auger process, the strength of which is enhanced by the extrinsic holes. However before discussing this process the possibility of a doping level dependent radiative lifetime will be discussed.

In QW and bulk systems, the radiative recombination rate increases in proportion to the product of the electron and hole densities[39] and a decreasing radiative recombination lifetime with increasing doping has been observed. However, a similar effect in QDs may be much weaker or not possible at all. Because of their discrete density of states and resultant optical transition selection rules, electrons in the GS may only be able to recombine with holes in the GS. As the GS degeneracy is two, the addition of one or two holes/QD may decrease τ_{rad} but additional holes will reside in excited hole states via which recombination with GS electrons may not be possible. Hence it appears that a further decrease of τ_{rad} for

greater than two holes/QD is only possible if nominally forbidden transitions between the electron GS (n=1) and excited holes states ($m\neq1$) are allowed. Unfortunately, there have been no calculations of the transition oscillator strength in doped QDs.

Although it is possible that modifications to the carrier wavefunctions due to the presence of extrinsic holes may make normally forbidden transitions allowed it is unlikely that this is a sufficiently strong effect to give the behaviour observed in Fig 5.23.

Assuming the presence of an Auger non-radiative process with lifetime τ_{Aug} the PL intensity (I_{PL}) is given by

$$I_{PL} = \frac{N}{\tau_{rec}} = \left(\frac{\tau_{Aug}}{\tau_{rad} + \tau_{Aug}} \right) G \qquad \text{(Eq. 5.1)}$$

where G is the optical carrier generation rate. In general, for systems with a continuous distribution of energy states, e.g. bulk and QWs, the Auger recombination rate (R_A) is written by

$$R_A = \frac{N}{\tau_{Aug}} = C_n N^2 P + C_p N P^2 . \qquad \text{(Eq. 5.2)}$$

For a *p*-type doped system the Auger recombination rate can be approximated as $1/\tau_{Aug} = C_p P^2$ where C_p and P are the Auger coefficient and hole density, respectively. However, for QDs the Auger recombination rate may not vary as the square of the hole density since the oscillator strength for transitions between excited hole states and the ground electron state is expected to be significantly weaker than that of the electron-hole ground state transition. In the case of the excited hole to ground electron transitions having zero oscillator strength the Auger rate will vary linearly with hole density. In the following calculations the Auger recombination rate in the *p*-type doped QDs was set to $1/\tau_{Aug} = C_p P^n$, with the exponent (n) determined below from a fitting to the experimental data.

The hole density is divided into contributions from the optically generated carriers and the doping, with $P^n = (\Delta p + \Delta p_e)^n$ where Δp and Δp_e represent the number of holes produced by optical excitation and doping per QD, respectively. Here it is assumed that Δp equals 1, a result of the low excitation power used for the lifetime measurements. The quantum efficiency of the undoped QDs at low

temperatures is assumed to be 1, with the consequence that the PL intensity of the undoped QDs is equal to *G*. With these assumptions, Eq. (5.1) can be rewritten as

$$I_{PL} = \frac{\dot{I}_{PL}^{Undoped}}{1+\tau_{rec}C_p(1+\Delta p_e)^n} \qquad \text{(Eq. 5.3)}$$

For the present samples, Δp_e varies from 0 to 18. Eq. (5.3) predicts a decreasing PL intensity (I_{PL}) with increasing doping level. In addition to this decrease the PL decay time (τ_{rec}) will also decrease with increasing Δp_e since this is given by $1/\tau_{rec} = 1/\tau_{rad} + 1/\tau_{Aug}$. Using the previous results and with the assumption that there is only radiative recombination in the undoped sample, the lifetime ratio *R* (defined as $\tau_{rec}(p)/\tau_{rec}(Undoped)$) can be written as

$$\frac{\tau_{rec}(p)}{\tau_{rec}(Undoped)} = \frac{\tau_{Aug}}{\tau_{Aug}+\tau_{rad}} = \frac{1}{1+\frac{\tau_{rad}}{\tau_{Aug}}} = \frac{1}{1+\tau_{rad}C_p(1+\Delta P_e)^n} \qquad \text{(Eq. 5.4)}$$

Hence both the PL intensity and carrier lifetime are predicted to decrease with increasing doping level.

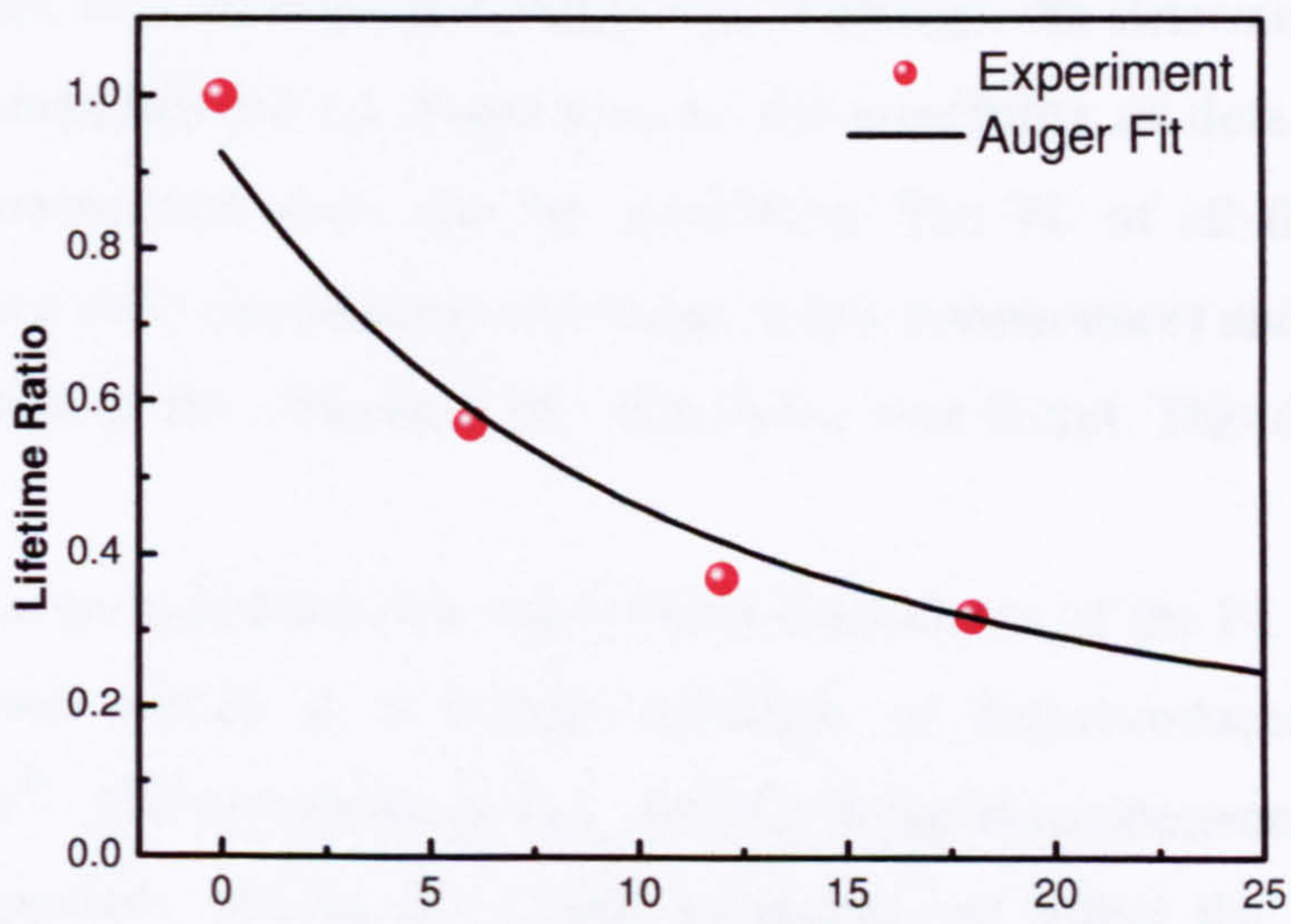

Fig. 5.25 Decay time ratio [$\tau_{rec}(p)/\tau_{rec}(Undoped)$] at 10 K as a function doping level

In Fig. 5.25 the doping level variation of the decay time ratio has been fitted to Eq. (5.4) with the best fit depicted by the solid line and solid-circles representing

the experimentally determined ratio R of the doped:undoped carrier lifetime. Eq. (5.2) provides a good fit to the experimental data and gives values for the exponent (n) and Auger coefficient (C_p) of 1.1 ± 0.2 and (1.6±0.8)x10^8 s^{-1}, respectively. As expected the strength of the Auger process in the QDs does not follow the square of the hole density (exponent of two) but instead has a value close to that of a linear dependence. This indicates that transitions between excited hole states and the ground electron state are at most only very weakly allowed. The value determined for the Auger coefficient is difficult to compare with the limited number of previously published values as these quote an effective bulk value with units cm^6s^{-1}. For example Ghosh et al determine a temperature dependent Auger coefficient, the value of which decreases from ~8x10^{-29} cm^6s^{-1} at 100 K to ~4x10^{-29} cm^6s^{-1} at 300 K[40]. It is not clear from their work why an effective bulk value is extracted for a 0D system and their method used to determine the Auger coefficient is open to significant criticism as it is based on an $An + Bn^2 + Cn^3$ analysis of the turn–on dynamics of a QD laser. It is generally believed that this latter equation is not applicable to a 0D system[41].

The data presented above provides strong evidence for the presence of a non-radiative process operating in the doped QDs at low temperature, the strength of which increases with increasing doping level. Although the determined exponent is close to that expected for an Auger process the possibility of defect-induced non-radiative recombination must also be considered. The PL of all the samples was measured over a wide excitation power range at low temperatures and for all samples a linear variation of the integrated PL with power was found. This data is shown in Fig. 5.26.

There is no indication of a super-linear dependence of the PL intensity on the excitation power which is a typical signature of defect-induced non-radiative recombination[42]. The maximum power used for these measurements gave a photo-excited electron-hole density of ~1/QD so should not affect the Auger process. Hence there is no evidence from these measurements of significant defect-related non-radiative recombination. In addition, from the observation of the wavelength independent relative PL intensities (Fig. 5.24) any defects would have to be either in or very close to the QDs. Hence, Auger recombination appears to be the dominant

non-radiative process at low temperatures, resulting in the decrease of both the PL intensity and recombination time with increasing p-type doping level.

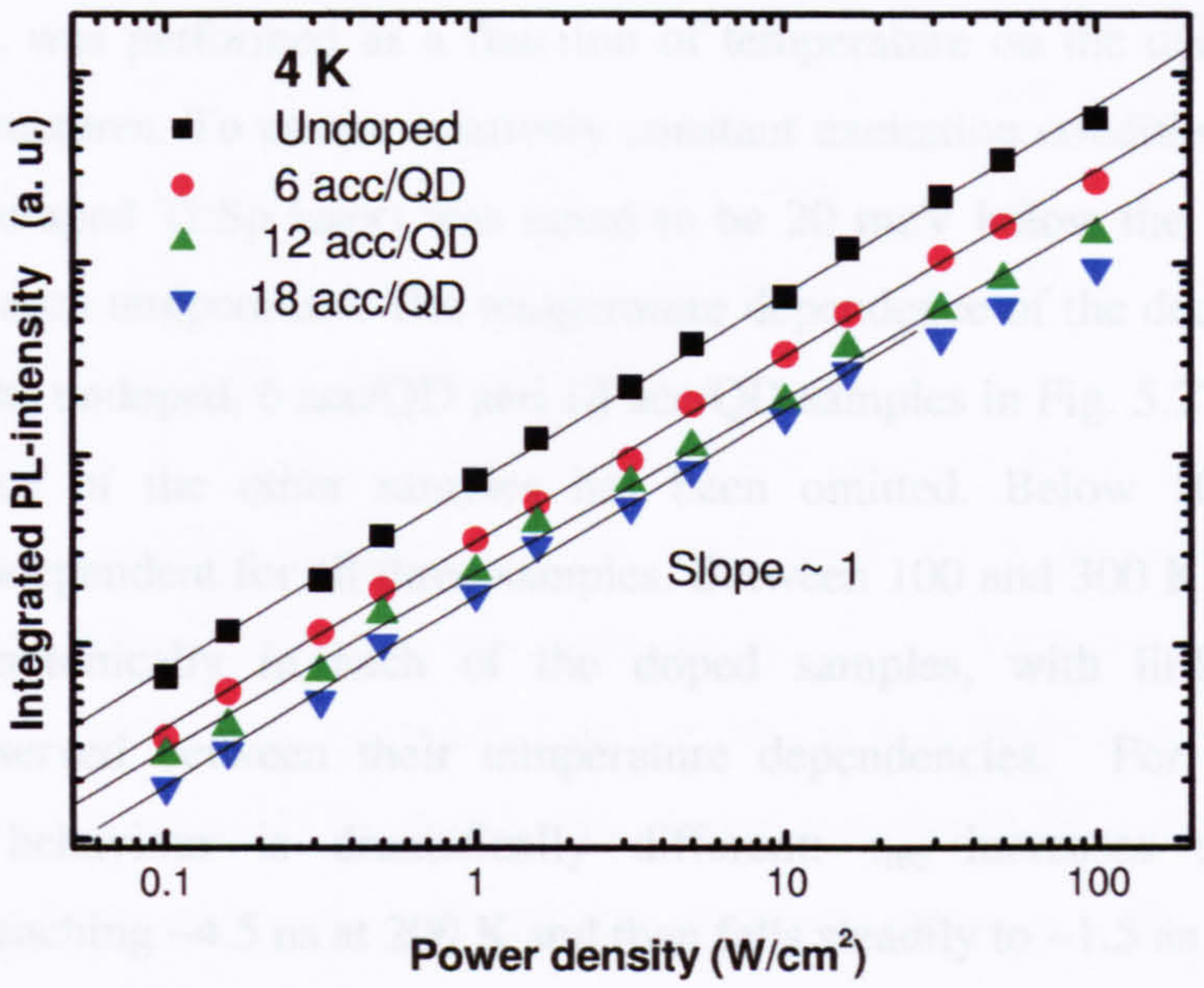

Fig. 5.26 Variation of integrated PL with laser excitation density at 4 K for the doped samples in series 2

The only other report of the τ_{rad} dependence with doping concentration is a study of similar long wavelength emitting InAs QDs at 80 K, where lifetimes of 1.1 ns and 192 ps were measured for undoped and p-type doped (~100 acc/QD) samples respectively[43]. In this case, the lifetimes measured in the doped samples were stated to be insensitive to the doping level, which suggested non-radiative recombination pathways such as interstitial defects associated with the dopants[16] were dominating the lifetime in the doped structures, yet this claim was not supported by an analysis of the relative PL efficiencies.

One important question is that if doping increases the strength of the Auger recombination then why is it possible to achieve laser devices with excellent characteristics based on relatively highly doped structures? One significant difference between the present time resolved measurements and conditions used to achieve lasing is the injected carrier density. For the former a value <<1 e-h pair /QD is used whereas for a laser lasing via the GS a value > 1 e-h pair /QD is required. Comparing Figs 5.7 and 5.8 it can be seen that the relative efficiencies of the doped and undoped structures is a function of the level of carrier injection and hence that

the differences between doped and undoped structures may become less at high injection. In addition there is evidence that the strength of the Auger process becomes weaker as the temperature is raised.

TR PL was performed as a function of temperature on the undoped and p-type doped structures. To ensure relatively constant excitation conditions, the pump source (Ar^+ pumped Ti:Sp laser) was tuned to be 20 meV below the band-edge of bulk GaAs at each temperature. The temperature dependence of the decay time (τ_{rec}) is shown for the undoped, 6 acc/QD and 18 acc/QD samples in Fig. 5.27. For clarity, the dependence of the other samples has been omitted. Below 100 K, τ_{rec} is temperature independent for all three samples. Between 100 and 300 K however, τ_{rec} increases monotonically in each of the doped samples, with little systematic difference observed between their temperature dependencies. For the undoped sample, the behaviour is dramatically different: τ_{rec} increases sharply with temperature, reaching ~4.5 ns at 200 K and then falls steadily to ~1.5 ns at 300 K.

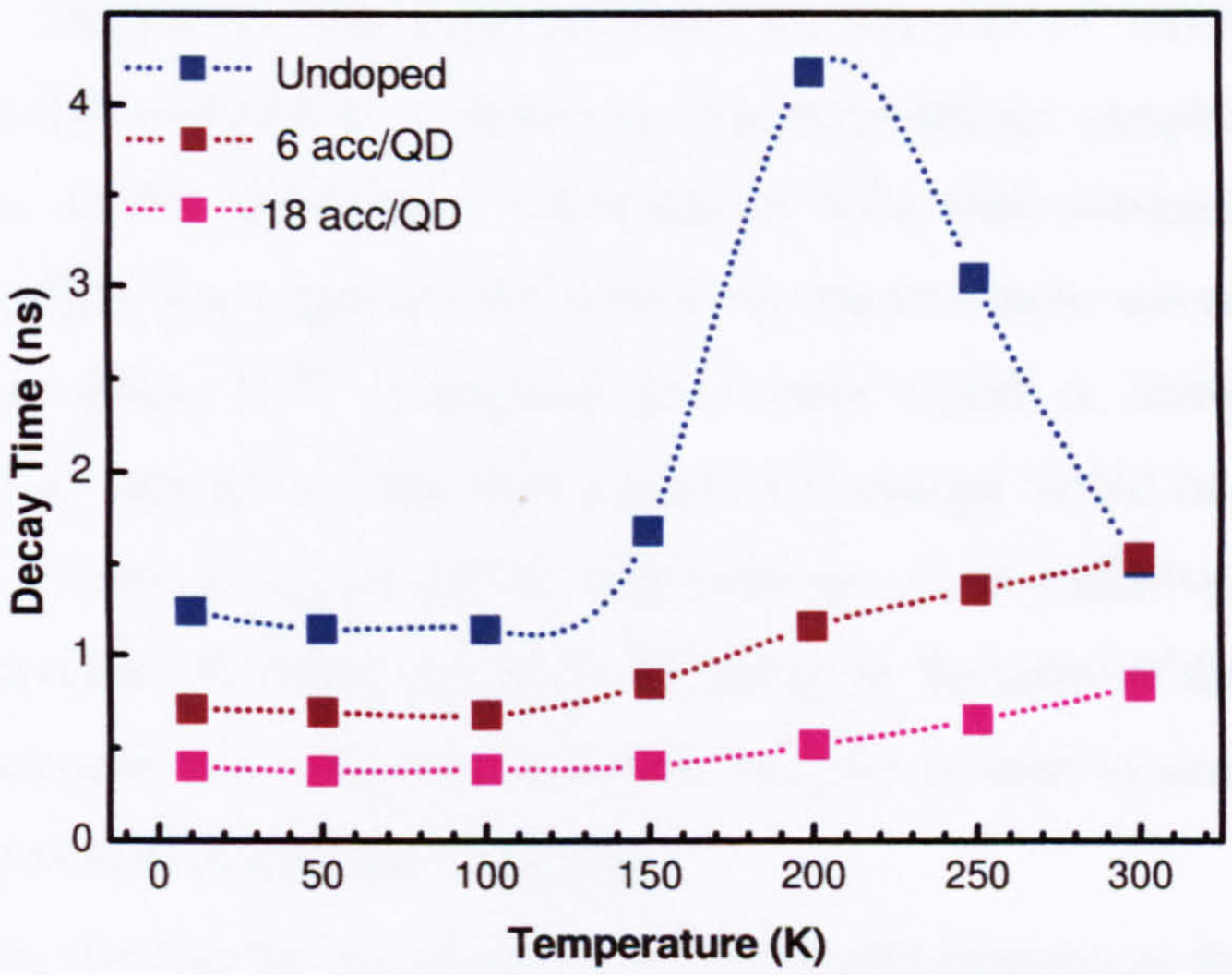

Fig. 5.27 Temperature dependence of the PL decay time (τ_{rec}) for the doped structures grown in series 2.

Similar temperature dependent τ_{rec} behaviour has been reported previously for undoped GaAs capped InAs QDs and In(Ga)As DWELL structures[44]. In the former work, τ_{rec} increased two-fold from 1.2 ns between 80 and 150 K and then decreased slightly at higher temperatures[45]. Additionally, the form of the decay transient was also seen to change from a mono-exponential to bi-exponential in this intermediate

temperature range, eventually returning to a mono-exponential form at RT. However, for the present series of samples there is no indication of a significant change in the form of the decay with increasing temperature. Nonetheless, it is possible that the increase of τ_{rec} in the intermediate temperature range and the change in the form of the decay reported in other work both result from the thermal population of excited QD states that have lower interband transition rates[46, 47]. The thermal population of optically 'dark' exciton states has also been invoked to account for the increase in τ_{rec} with increasing temperature in undoped QDs[48]. The built-in hole population in doped QDs should ensure the continual occupation of the hole GS up to high temperatures and is therefore consistent with the reduced temperature sensitivity of τ_{rec}.

Alternatively, the more pronounced change in τ_{rec} between 10 and 300 K in the undoped structure may be related to the stronger carrier redistribution effects observed in its EL, relative to that of the doped structures. However, it is unclear whether there is a systematic GS energy dependence of τ_{rec}. TR PL studies of bimodal QD ensembles indicate that smaller QDs have a shorter τ_{rec}[49]. Conversely, the opposite dependence has been observed for samples of In(Ga)As QDs with different peak GS energies, ie. a shorter τ_{rec} was recorded for samples with lower PL peak energies. In the latter report, lower energy QDs were assumed to have lower aspect ratios which was suggested to increase the electron-hole wavefunction overlap and therefore reduce τ_{rec}[50]. Assuming the former report is correct; the thermal redistribution of carriers to QDs with a lower GS energy would be consistent with the sudden increase in τ_{rec} at 200 K, followed by a non-radiative contribution at higher temperatures. However, the large difference in the scale of the increase in τ_{rec} at ~200 K between the undoped and doped samples is hard to account for if only carrier redistribution effects are considered.

Finally, the fact the τ_{rec} increases for the doped samples as the temperature is raised suggests that the strength of the proposed Auger process decreases with increasing temperature. The reason for this is unclear but could reflect the excitation of holes out of the GS. This possible decrease in the strength of the Auger process may also explain why p-type doped lasers are able to exhibit excellent performance around room temperature.

5.8 Photocurrent spectroscopy of *p*-type doped QD structures

5.8.1 State blocking effects in *p*-type doped QD structures

In undoped InAs/GaAs QD structures, photocurrent (PC) spectroscopy has been shown to be an effective probe of the intrinsic absorption properties of the QD states both in single and multilayer structures[51]. Extensive studies of the GS PC as a function of temperature and bias have confirmed the relative importance of thermal and tunnelling escape mechanisms in these structures[52]. At low temperatures, thermal escape is negligible and a sufficient electric field must be applied to produce a tunnelling rate greater than the recombination rate. At RT the thermal carrier escape rate from the QD or WL/QW states exceeds the tunnelling rate under flat band conditions and is comparable to the recombination rate. Hence to good approximation, the PC at RT is proportional to the absorption strength of the transition[53]. Fig. 5.28 shows the room temperature PC of the GS transition for the undoped, 15 and 50 acc/QD structures grown in the first sample series, as a function of bias.

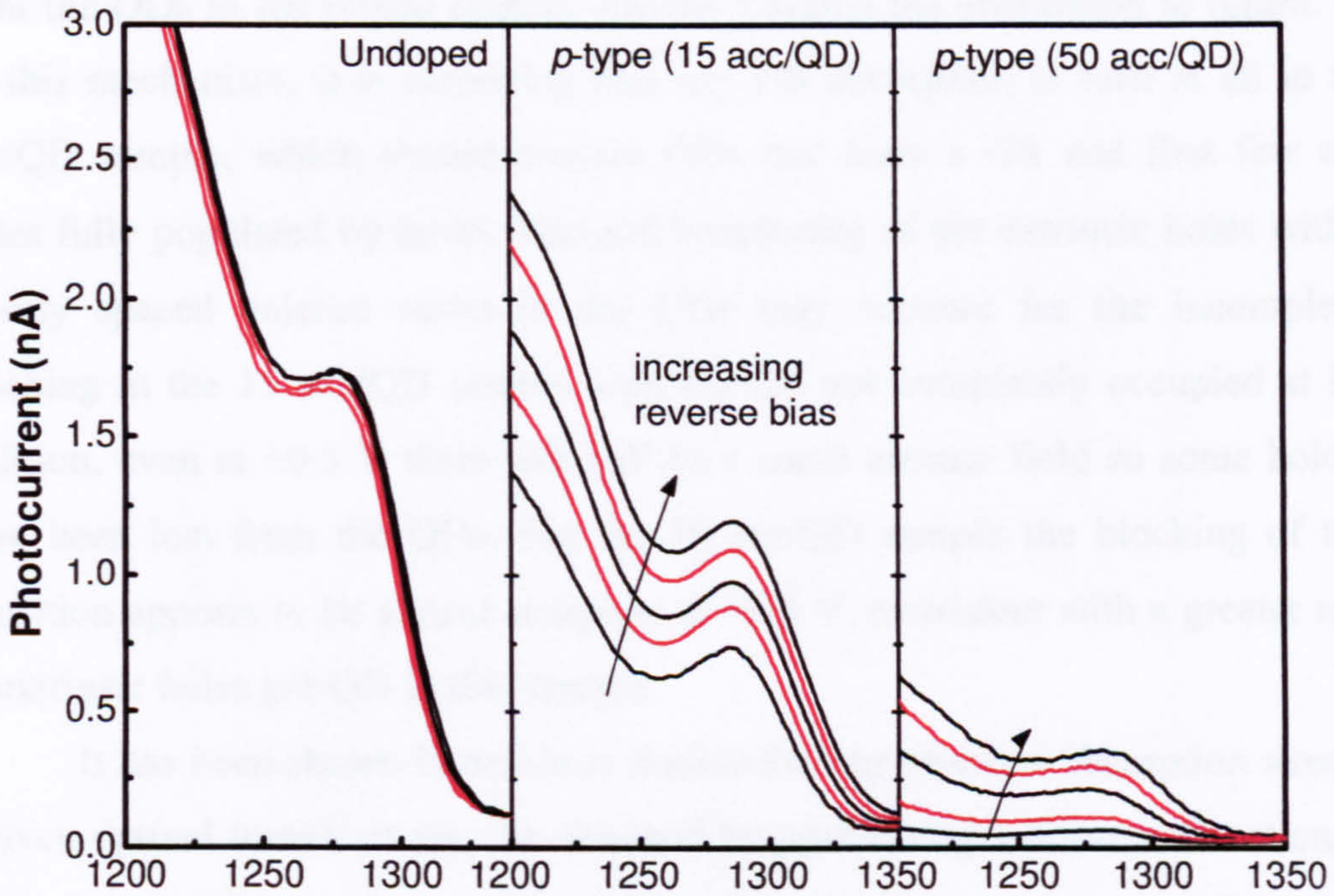

Fig. 5.28 RT PC spectra, recorded with biases of +0.5, 0, -0.5, -1, and -1.5 V, for the first series of doped structures. Only the GS transition is shown for clarity.

In Fig. 5.28 the bias was increased in increments of 0.5 V, from 0 to -1.5 V, denoted by the alternating line colour. Clearly, there are systematic differences between the bias dependencies of each sample. As expected, for small reverse biases, the GS PC peak of the undoped sample displays little sensitivity to the applied electric field at RT. This is because the majority of the photo-generated carriers created in the QD GS may escape via thermal excitation and the Quantum Confined Stark Effect, discussed in section 5.8.4, does not significantly reduce the electron – hole wavefunction overlap at these relatively low electric fields. However, this insensitivity is not seen in the case of the doped samples. For a given reverse bias, the PC decreases with increasing doping density and the sensitivity of the PC to the bias increases with increasing doping.

The observation of a reduced PC for a more highly doped structure is to be expected, to some extent, due to the existence of 'state blocking'. The occupation of the lower energy hole states with extrinsic carriers prior to optical excitation, will prevent interband transitions involving these states from being observed under flat band conditions. When the reverse bias is increased, the extrinsic holes may tunnel from the QDs to the *p*-type contact, thereby causing the absorption to return. Based on this mechanism, it is surprising that any GS absorption is seen at all in the 15 acc/QD sample, which should contain QDs that have a GS and first few excited states fully populated by holes. Thermal broadening of the extrinsic holes within the closely spaced valence states in the QDs may account for the incomplete GS blocking in the 15 acc/QD sample with the GS not completely occupied at RT. In addition, even at +0.5 V there will still be a small electric field so some holes may have been lost from the QDs. For the 50 acc/QD sample the blocking of the GS transition appears to be almost complete at +0.5 V, consistent with a greater number of extrinsic holes per QD in this sample.

It has been shown in previous studies that the absolute absorption strength of a given optical transition may be obtained by performing a linear subtraction of the background PC[51] over the spectral width of the transition resulting in a Gaussian-like peak. This approach has been adopted, in order to study the temperature and bias dependencies of the GS absorption of the doped samples.

5.8.2 Temperature dependence of the PC in *p*-type doped structures

Each measurement was performed for zero bias and the GS transition portion of the spectra was extracted. It is important to note that in one respect these measurements are not strictly comparable. Since there is strong evidence for the existence of additional built-in electric fields in the doped samples (see section 5.8.3), which have a significant effect on the carrier transport processes and hence PC signal, the use of zero bias conditions for each sample does not provide a truly equal 'confinement' environment for the photo-generated carriers. In spite of this, there are clear trends that can be ascertained for each sample which closely reflect those observed in emission.

Fig. 5.29 shows the temperature dependence of the GS PC intensity for zero bias. Data is shown for an undoped reference sample and three samples from series 2 doped with 6, 12 and 18 acc /QD. As a general comment, it is obvious from Fig. 5.29 that the GS PC of the undoped structure is more sensitive to temperature than that of any of the doped structures. Furthermore, at any temperature, the magnitude of the PC is larger in the undoped structure.

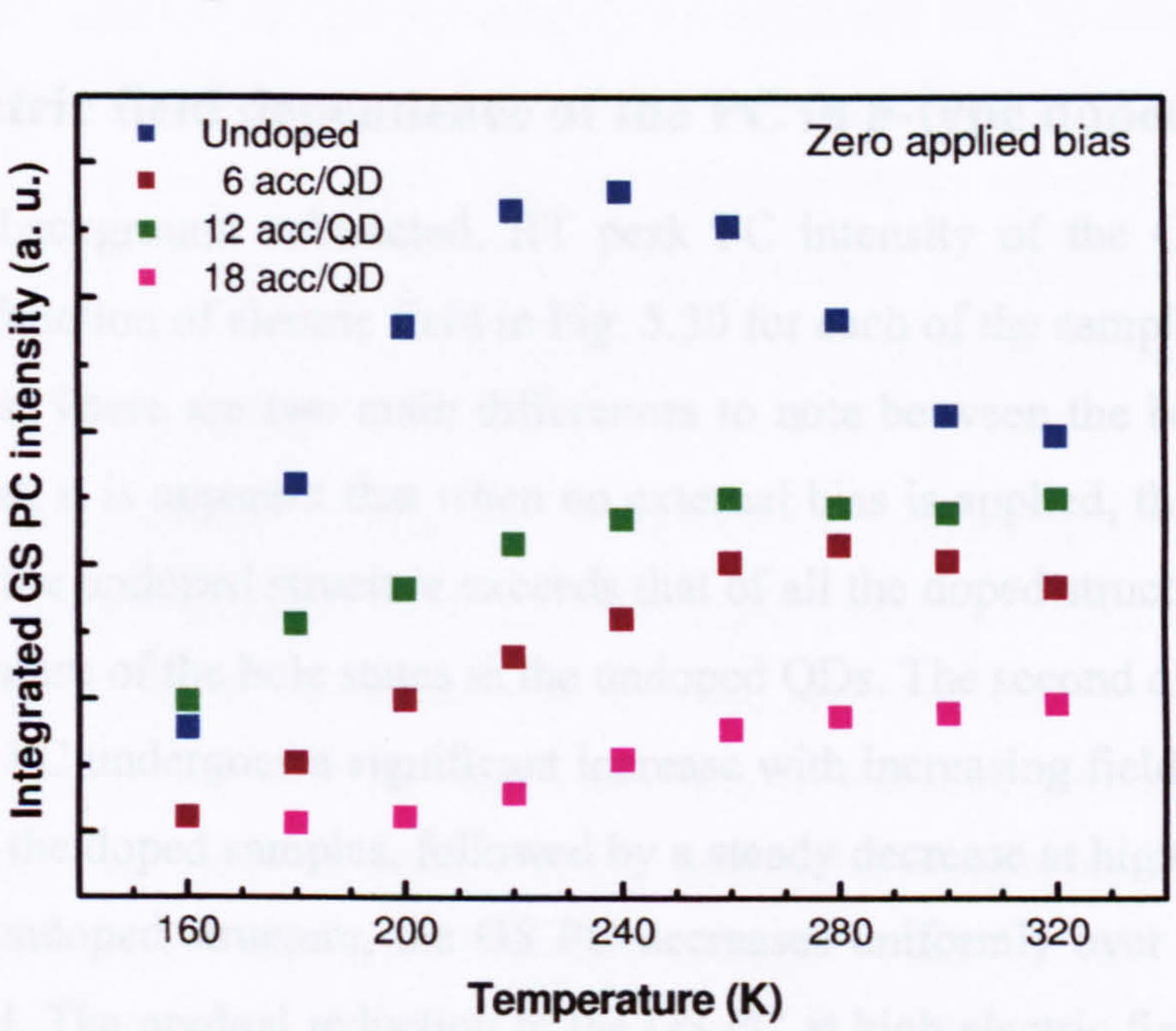

Fig. 5.29 Temperature dependence of the GS PC intensity, measured with no applied bias for the doped structures in series 2.

The weaker PC at all temperatures with increasing doping level is consistent with more efficient state blocking of the transition. In the undoped sample there is a

strong increase in the PC between 160 and 240 K (by a factor of ~5) followed by a more gentle reduction between 240 and 320 K. The rapid rise in the PC between 160 and 240 K is due to the increasing thermal escape rate for the confined carriers, which is able to better compete with the radiative recombination rate. Above 240 K, after escape from the QDs the carriers may recombine at non-radiative sites, reducing the collected current; as conjectured in similar temperature dependent studies of the PC in InAs/GaAs QDs[54].

By comparison, the increase of the PC in the doped samples with increasing temperature is suppressed and the temperature at which the maximum PC is recorded increases with increasing doping concentration. For the 12 and 18 acc/QD samples, the PC has not reached its peak value even by room temperature. This weaker temperature induced increase of the PC signal may reflect a reduced electron emission from the doped samples, a result of an increased confinement potential due to the Coulomb attraction by the extrinsic holes. This process is suggested to account for the different temperature behaviours of the emission linewidths and indirectly for the temperature dependence of J_{th}.

5.8.3 Electric field dependence of the PC in *p*-type doped structures

The background subtracted, RT peak PC intensity of the GS transition is plotted as a function of electric field in Fig. 5.30 for each of the samples grown in the second series. There are two main differences to note between the behaviour of the samples. First, it is apparent that when no external bias is applied, the PC of the GS transition in the undoped structure exceeds that of all the doped structures, due to the unblocked nature of the hole states in the undoped QDs. The second difference is that the peak GS PC undergoes a significant increase with increasing field between 0 and 70 kV/cm in the doped samples, followed by a steady decrease at higher fields. In the case of the undoped structure, the GS PC decreases uniformly over the entire field range studied. The gradual reduction in the GS PC at high electric fields is the result of the field induced separation of the electron and hole wavefunctions, which reduces their overlap integral and consequently decreases the oscillator strength of the transition[55]. The initial increase in the PC for the doped samples is attributed to the tunnelling of the extrinsic holes from the QDs, thereby unblocking the GS absorption.

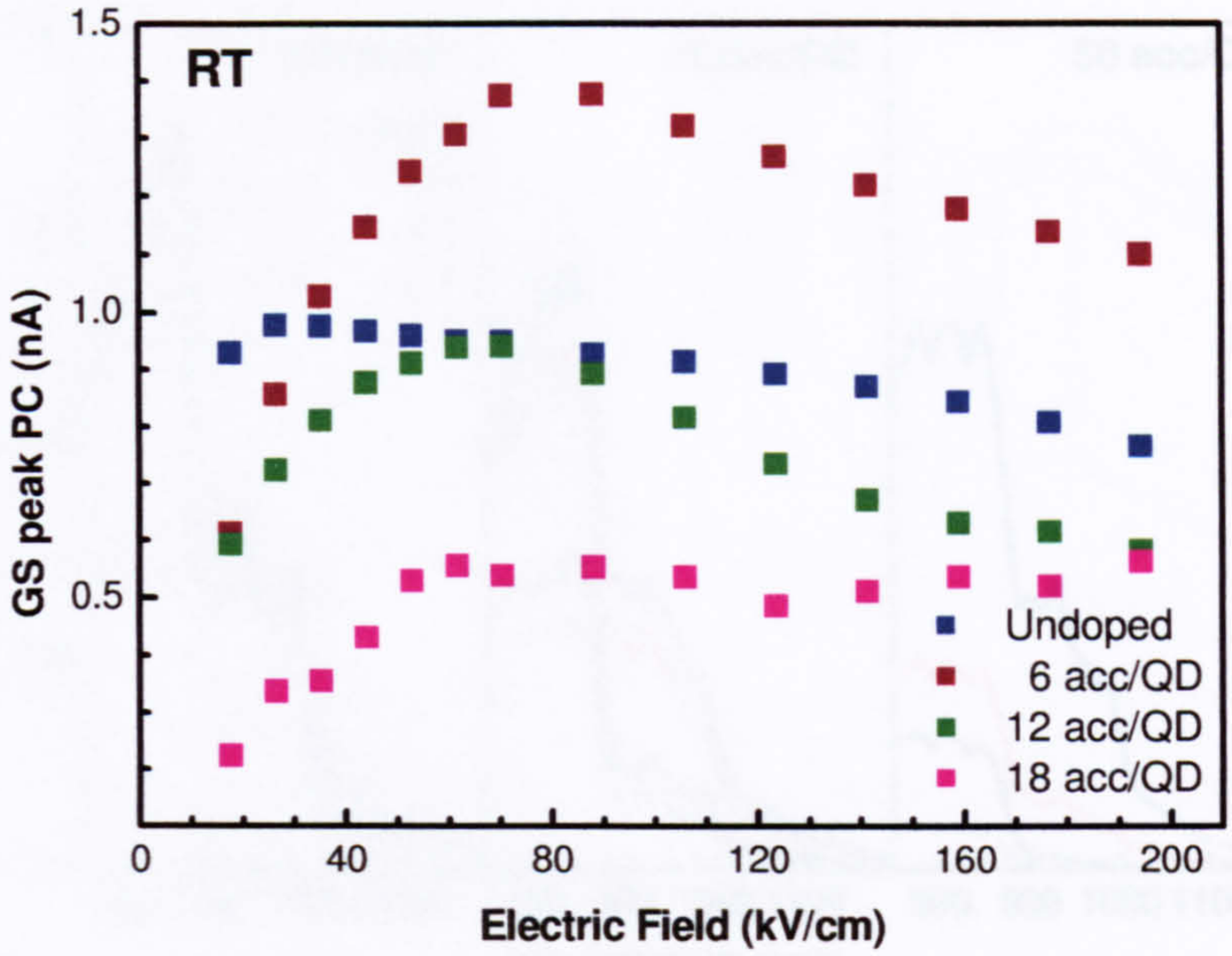

Fig. 5.30 Electric field dependence of the GS PC intensity, measured at RT, for the doped structures grown in series 2.

By noting that the carrier tunnelling rate and the extent of the wavefunction overlap have opposite electric field dependencies, it is not surprising that the maximum PC observed in each structure is not equal and that the field required to obtain this maximum it does not 'scale' with the nominal doping level. In addition, there is some evidence to suggest that the intrinsic dipole moment at zero field, which determines the electric field dependence of the wavefunction overlap, is systematically changed by the incorporation of modulation doping. These results will be presented in section 5.8.4.

In addition to, and independent of, the QD state blocking effect, there is a second mechanism that reduces the PC of the doped structures, under the conditions of zero applied bias. Bias dependent PC spectra, recorded at RT, for the series 1 samples are shown in Fig. 5.31. These spectra were recorded over a wider energy range to include the GaAs and WL/QW regions. For each structure, four values of bias were used, +0.5, 0, -4 and -8 V, corresponding to electric fields of -12, 24, 96 and 193 kV/cm respectively.

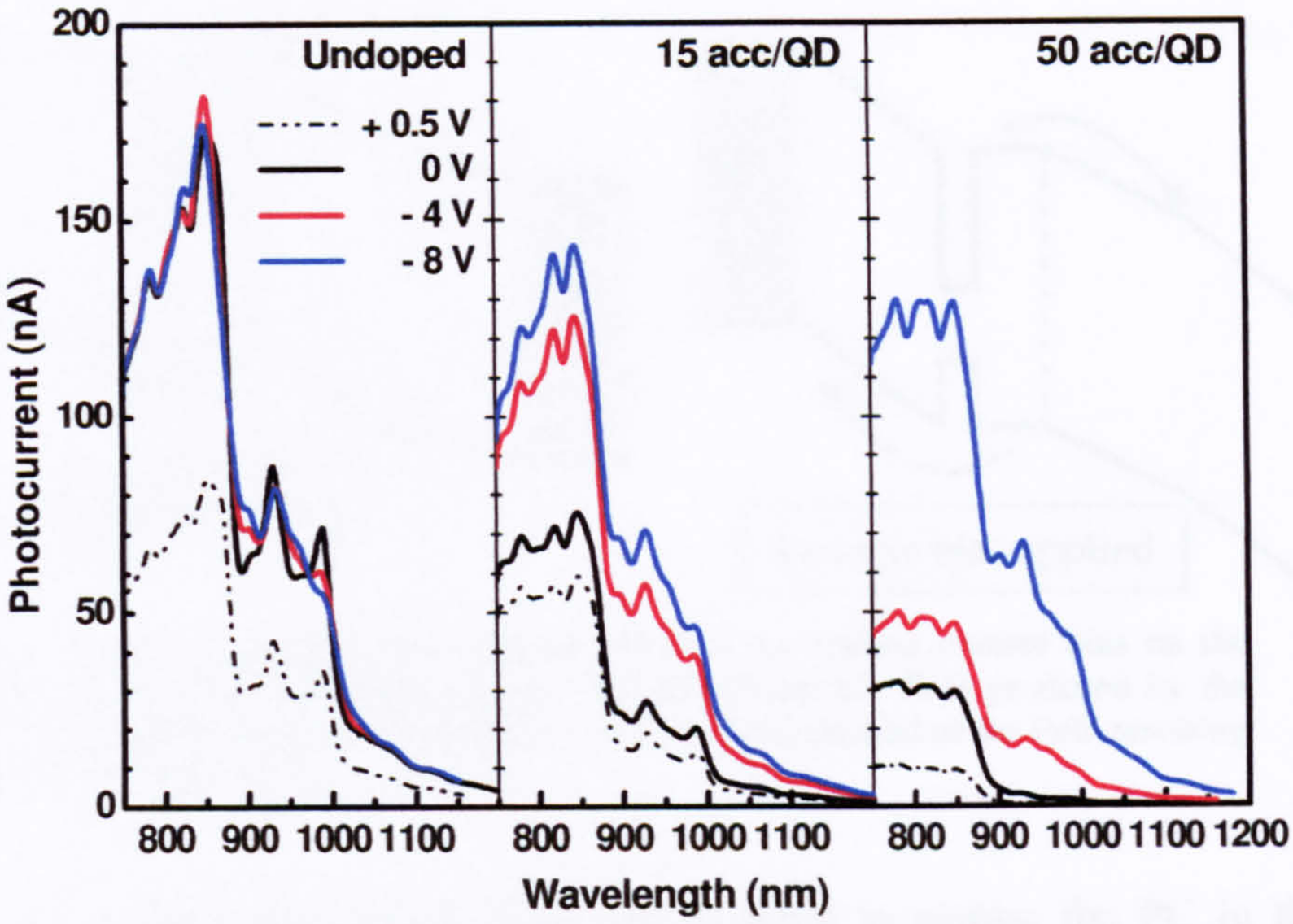

Fig. 5.31 Electric field dependence of the RT PC, including the WL and GaAs regions, for the doped samples grown in series 1.

In the undoped sample, an increase in reverse bias causes no significant change in the magnitude of the PC for excitation into either the GaAs or the WL/QW, as is also the case for the QD GS transition. However in the doped samples, the PC at these higher spectral energies displays a strong sensitivity to the bias. Even if it is assumed that the acceptors are fully ionised and that any extrinsic holes that are not located in the QDs occupy the lowest energy hole states in the WL/QW, the far greater degeneracy of the 2D/bulk states should make state blocking negligible. Instead, it appears that there are local electric fields within each layer of the active region, created between the planes of Be acceptors and the extrinsic holes in the DWELLs. These will tilt the band edges of the WL/QW and GaAs in the vicinity of the QDs, increasing the ionisation barrier and inhibiting the thermal escape of electron-hole pairs photogenerated in these regions. By applying an electric field in the opposite direction (a reverse bias) to counteract the effect of these built-in fields, the magnitude of the PC intensity can be regained, such that it almost equals that of the undoped sample at -8 V (193 kV/cm). The effect of increasing reverse bias on the electric field profile close to the DWELL in a single layer structure is shown schematically in Fig. 5.32. The ionisation barrier for thermal carrier escape is reduced with the application of a reverse bias, hence increasing the PC intensity.

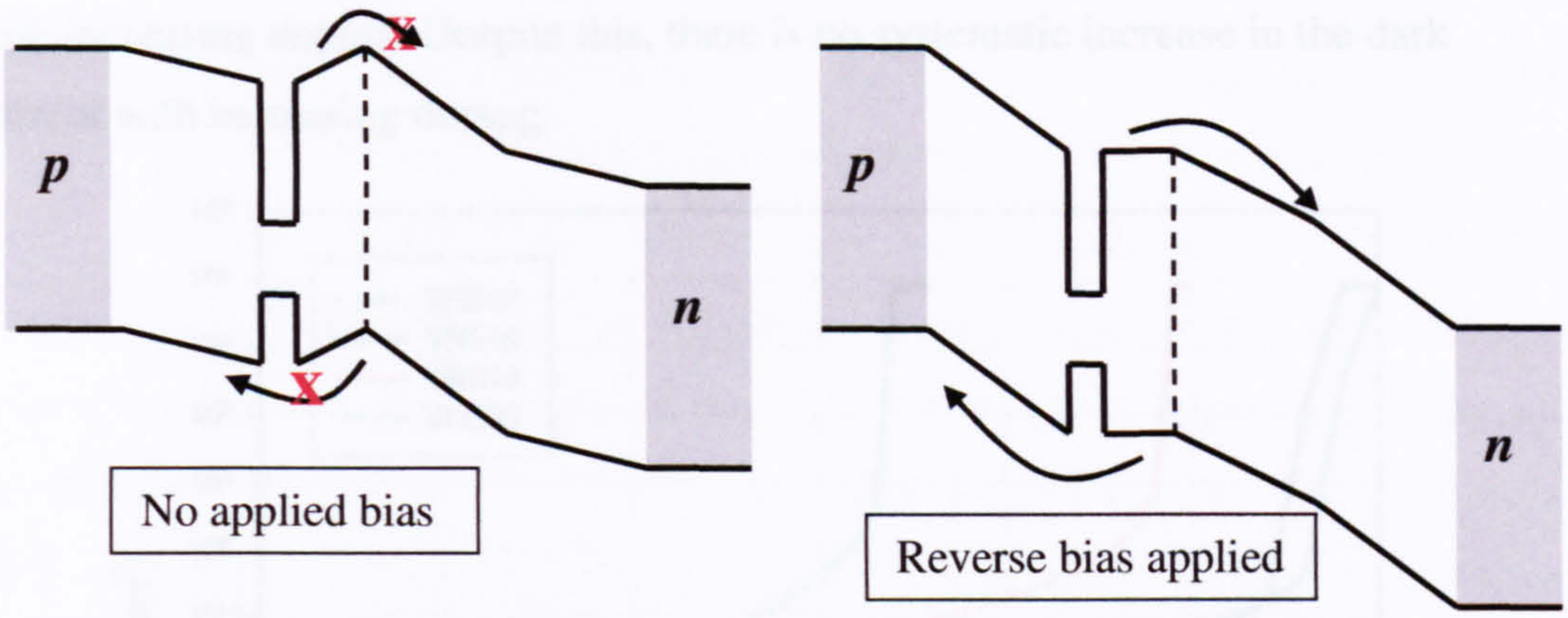

Fig. 5.32 Schematic diagram depicting the effect of an applied reverse bias on the band-edges of the WL and GaAs region. The in-built electric field produced by the planes of Be dopants and holes in the QDs is directed anti-parallel to the field resulting from the *p-i-n* diode.

It is evident that higher fields are required to restore the PC in the more highly doped 50 acc/QD sample, consistent with the built-in field being greater in this structure. In the samples grown in the second series, a similar trend is seen (Fig. 5.33): with increasing doping level, the PC measured under zero bias is systematically suppressed.

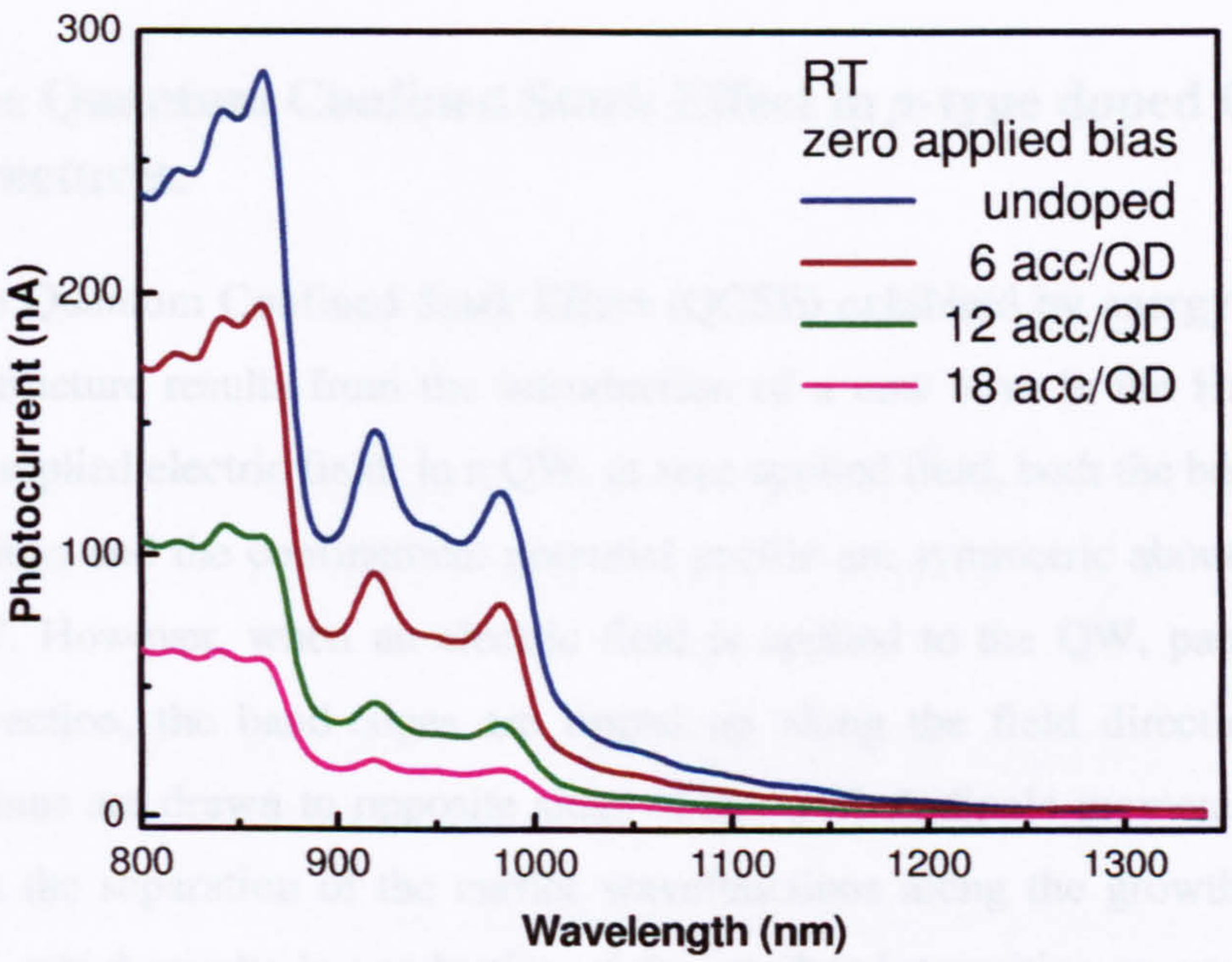

Fig. 5.33 RT PC spectra for the series 2 doped structures

The presence of local electric fields in the DWELL region may be the cause of the reduced breakdown voltage (V_{bd}) observed in the reverse bias I-V characteristics of the doped devices shown in Fig. 5.34, where V_{bd} is seen to reduce

with increasing doping. Despite this, there is no systematic increase in the dark current with increasing doping

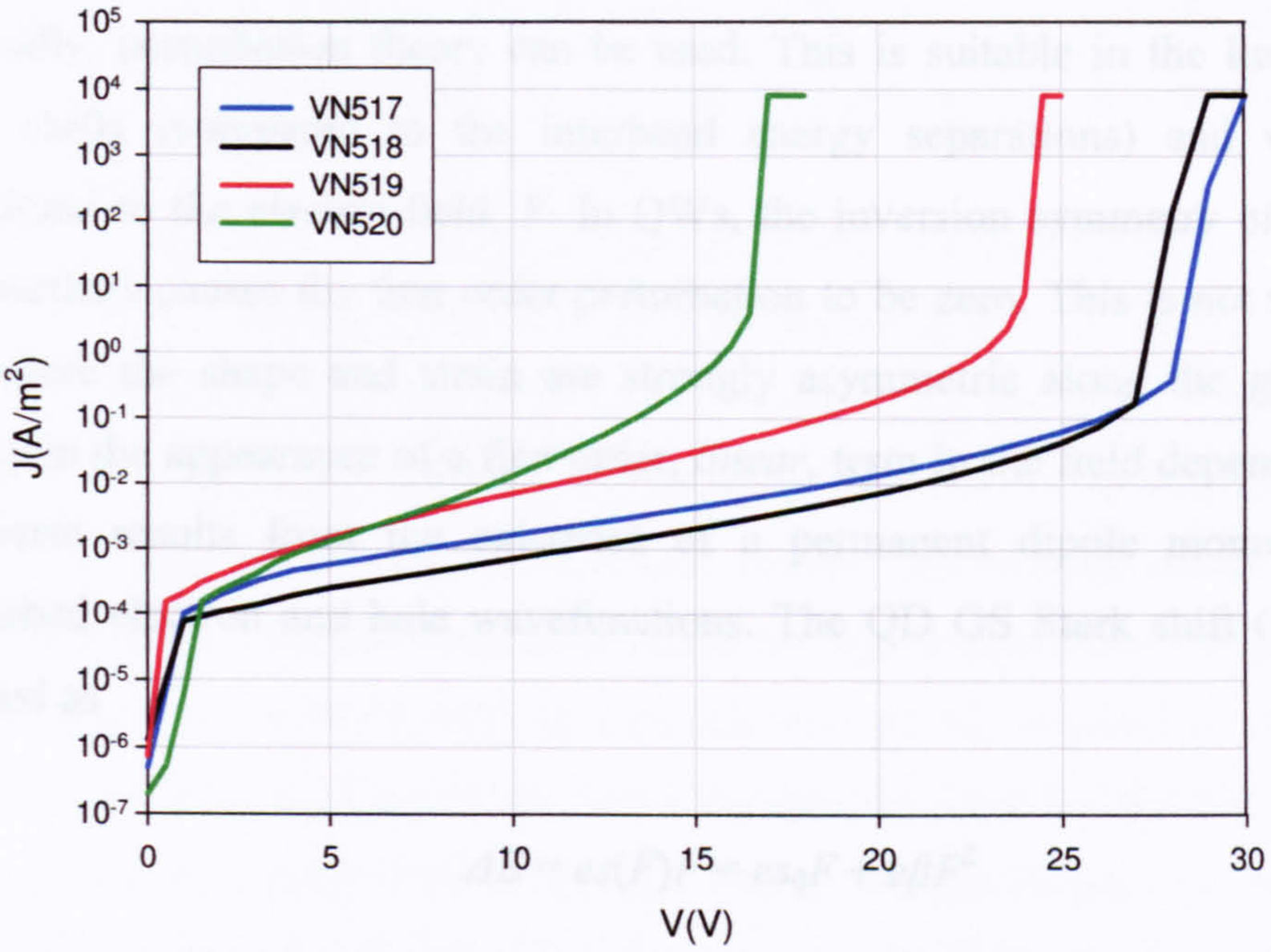

Fig. 5.34. RT reverse bias I-V characteristics of the series 2 doped structures The corresponding doping level of each sample is listed in table 5.1 *Figure courtesy of Fadzlin Hasbullah*

5.8.4 The Quantum Confined Stark Effect in *p*-type doped QD structures.

The Quantum Confined Stark Effect (QCSE) exhibited by energy states in a quantum structure results from the introduction of a new term in the Hamiltonian, due to the applied electric field. In a QW, at zero applied field, both the bound carrier wavefunctions and the confinement potential profile are symmetric about the centre of the QW. However, when an electric field is applied to the QW, parallel to the growth direction, the band-edges are tipped up along the field direction and the wavefunctions are drawn to opposite sides of the QW. A dipole moment, $\boldsymbol{p}$ (= e.**d**, where **d** is the separation of the carrier wavefunctions along the growth direction) now exists, which results in a reduction of the interband transition energy (the Stark Shift) and a reduction in the oscillator strength of the transitions. Because of the removal of mirror symmetry from the well, optical selection rules are broken and previously forbidden transitions may become allowed.

In order to calculate the exact variation of the energy levels with electric field, appropriate approximations have to be made. Under the assumption of an infinite QW confining potential, containing energy levels that may be calculated analytically, perturbation theory can be used. This is suitable in the limit of small energy shifts (compared to the interband energy separations) and where ***p*** is proportional to the electric field, *F*. In QWs, the inversion symmetry of the carrier wavefunctions causes the first order perturbation to be zero. This is not the case for QDs, where the shape and strain are strongly asymmetric along the growth axis, resulting in the appearance of a first order, *linear*, term in the field dependence. This linear term results from the existence of a permanent dipole moment for the unperturbed electron and hole wavefunctions. The QD GS Stark shift (ΔE) can be expressed as

$$\Delta E = es(F)F = es_0F + e\beta F^2 \qquad \text{(Eq. 5.5)}$$

where $s(F)$ is the separation of the electron and hole at electric field F, s_0 is the electron-hole separation at F=0 and β is the sum of the polarisabilities for the electron and hole wavefunctions. The polarisability reflects the response of the position of the wavefunction to the applied field. From (5.5) the transition energy, $E_T(F)$, at field F, is given by

$$E_T(F) = E_T(0) + es_0F + e\beta F^2 \qquad \text{(Eq. 5.6)}$$

where $E_T(0)$ is the transition energy at F=0. Hence, from (5.6), the linear contribution to the Stark shift results explicitly from the zero field dipole moment of the electron and hole, es_0.

Prior to the publication of work performed in Sheffield in 2000[56], the theoretical consensus was that for InAs/GaAs QDs, the GS electron wavefunction should lie above that of the hole, due to the in-equivalence of their effective masses and the strain-induced form of the valence band edge profile (the strain localises the holes in the widest region of the QDs)[57]. In this case s_0 will be positive. However, PC measurements revealed the direction of the zero-field dipole to be aligned *anti*-parallel to the growth direction and hence that the hole lies above the electron in the QD. The results of subsequent modelling indicated that in order to explain this

inverted dipole the QDs were required to have a truncated pyramidal shape and to have a graded Indium composition profile, with a larger In content toward the apex of the QDs[58]. These findings will be shown to be consistent with the PC results presented in this section, despite the different structure of the QDs investigated in this chapter (InAs QDs in an InGaAs QW).

PC spectra were recorded as a function of bias (between +0.5 and -20 V) for each of the doped samples (except 18 acc/QD) grown in the second series. It was decided not to include the 18 acc/QD sample in the study; due to its very weak PC signal at 220 K (see Fig. 5.30) The measurements were performed at a temperature of 220 K in order to achieve a compromise between the thermal escape rate and reverse breakdown voltages. Despite this relatively high temperature, it is clear from Fig. 5.30 and that electric field(s) of a certain strength are required to extract the extrinsic holes from the QDs in the doped samples in order for the GS PC to be measured. The PC spectra of the undoped, 6 and 12 acc/QD samples are shown as a function of increasing reverse bias (in increments of -2 V) in Fig. 5.35

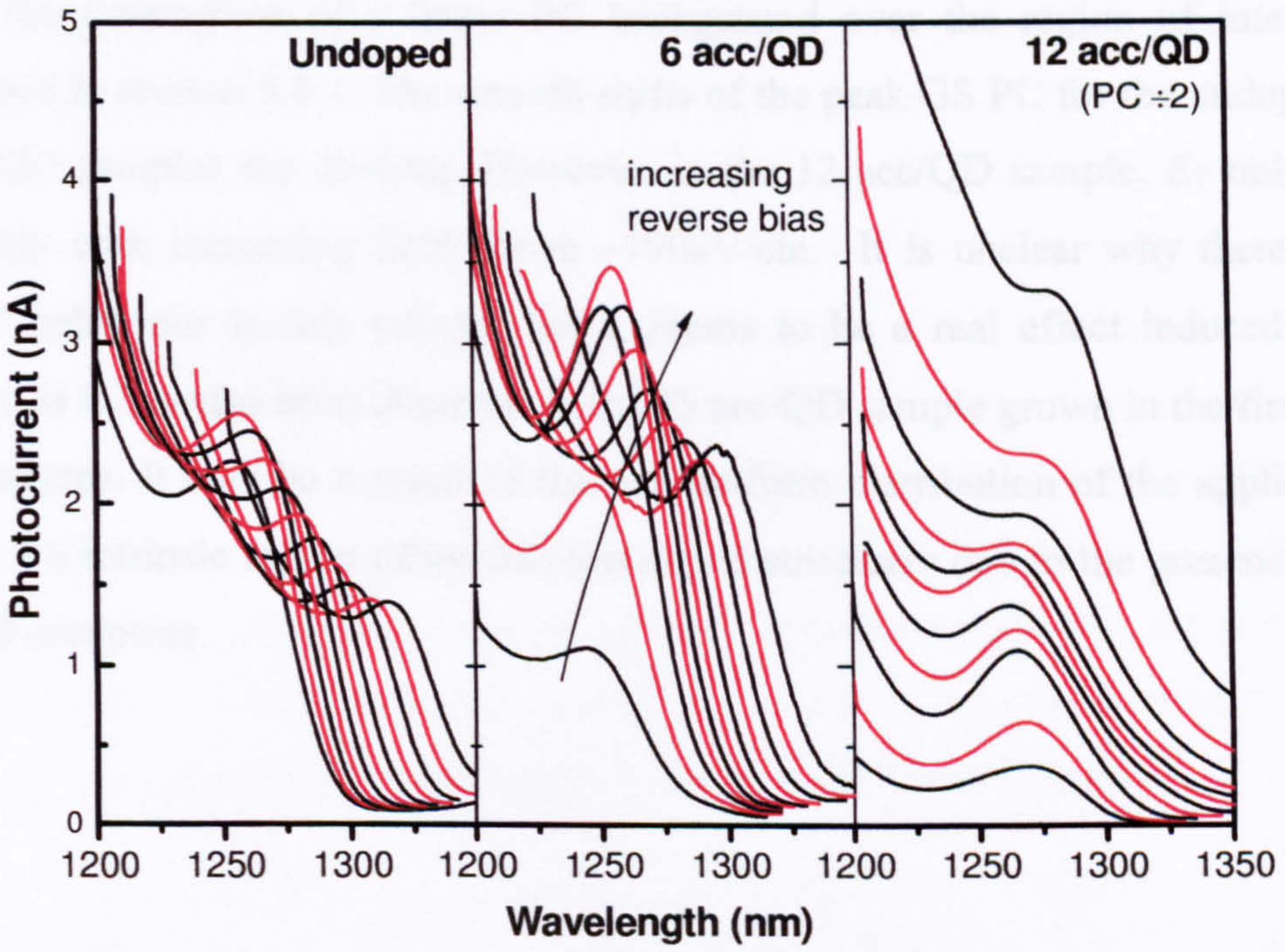

Fig. 5.35 Bias dependent PC spectra, measured at 220 K and recorded over the GS transition for the series 2 doped structures. The bias was varied between +0.5 and -20 V in increments of 2 V.

The undoped sample displays a characteristically smooth reduction in both the GS transition energy and PC signal with increasing reverse bias, confirming that carrier tunnelling is not the dominant escape mechanism in this structure at 220 K.

The character of the GS peak shift in the 6 acc/QD sample is similar to that of the undoped sample, but between 0 and -5 V the peak PC increases strongly, due to the unblocking of the GS hole states as discussed above. Above -5 V, the PC decreases slowly in a similar fashion to the undoped sample as a result of the increasing electric field induced separation of the electron and hole wavefunctions.

Aside from the increase in the GS peak intensity between 0 and -5 V, qualitatively different behaviour is seen in the field dependence of the PC for the 12 acc/QD sample. In particular, the GS peak energy does not redshift with increasing field until reverse biases in excess of ~10 V are reached. Furthermore, at high fields the GS transition becomes harder to resolve due to a combination of the rise in the intensity of the background PC and the increased inhomogeneous absorption linewidth of the GS, the origin of which will be discussed shortly. This increase in the background PC also serves to obscure the field dependence of the GS PC signal.

To make these trends clearer, the GS PC peak energy for each sample (E_T) is plotted as a function of electric field in Fig. 5.36. The peak energies were extracted using the assumption of a linear PC background over the region of interest, as described in section 5.8.1. The smooth shifts of the peak GS PC for the undoped and 6 acc/QD samples are obvious. However, in the 12 acc/QD sample, E_T only shifts smoothly with increasing field above ~190kV/cm. It is unclear why there is this 'onset' behaviour in this sample, but it seems to be a real effect induced by the doping, as it has also been observed in the 15 acc/QD sample grown in the first series of structures. It may be a result of the non-uniform distribution of the applied field across the intrinsic region of modulation doped structures due to the presence of the ionised acceptors.

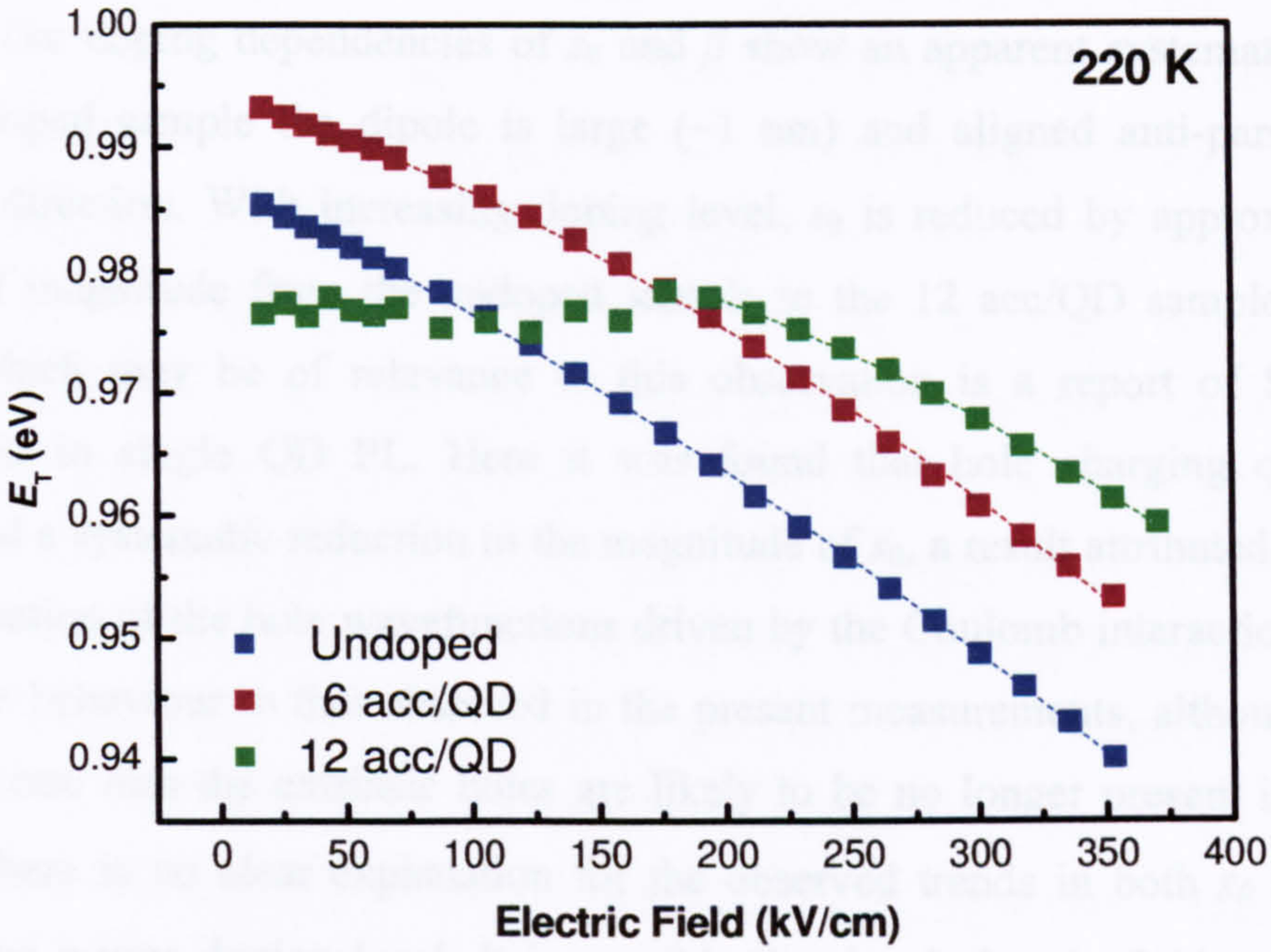

Fig. 5.36 Electric field dependence of the GS peak energy (E_T), extracted from the background subtracted PC spectra at 220 K for the series 2 doped structures. A fit using Eq. 5.6 is superposed for each sample

Despite this possible non-uniformity at low fields the energy shift of the GS transition can still be described by a parabolic field dependence (Eq. 5.6). A good fit is obtained for all of the investigated samples for fields above ~175 kV/cm, as indicted by the dashed lines in Fig. 5.35. From these fits it is possible to extract values for the electron-hole dipole separation at zero field (s_0) and the polarisability (β), these are listed in Table 5.36. The value for s_0 for the undoped sample is approximately twice as large but of the same sign as that determined for undoped InAs/GaAs QDs grown and studied previously in Sheffield[51]. A large value for s_0 is probably not unsurprising for the present large InGaAs capped QDs. An s_0 of ~0.4 nm was obtained from measurements of the Stark shift of low temperature (460 °C) grown InAs/GaAs QDs, obtained using an electro-reflectance technique[59].

Sample	s_0 (Å) (±0.01 Å)	β x10^{-7} (eVkV^{-2}cm^2) (±6 x 10^{-9} eVkV^{-2}cm^2)
Undoped	10.2	-1.0
6 acc/QD	5.2	-2.0
12 acc/QD	1.5	-2.2

Fig. 5.36 Extracted s_0 and β parameters using the fitted data shown in Fig. 5.35 for the undoped, 6 and 12 acc/QD structures.

The doping dependencies of s_0 and β show an apparent systematic trend. In the undoped sample the dipole is large (~1 nm) and aligned anti-parallel to the growth direction. With increasing doping level, s_0 is reduced by approximately an order of magnitude from the undoped sample to the 12 acc/QD sample. The only work which may be of relevance to this observation is a report of Stark shifts measured in single QD PL. Here it was found that hole charging of the QDs produced a systematic reduction in the magnitude of s_0, a result attributed to a spatial redistribution of the hole wavefunctions driven by the Coulomb interaction[60]. This is a similar behaviour to that observed in the present measurements, although here for high reverse bias the extrinsic holes are likely to be no longer present in the QDs. Hence there is no clear explanation for the observed trends in both s_0 and β with increasing *p*-type doping level. It is possible that local electric fields which result from the doping perturb both these quantities or, alternatively, that the physical structure of the QDs is perturbed by the doping. The latter seems unlikely as the emission energy of the QDs is not affected significantly by the doping.

5.8 Conclusions

p-type modulation doping has been applied to 1.3μm quantum dot lasers in order to improve their temperature stability at and above room temperature. In agreement with previously published work, the absolute values of J_{th} are found to increase with doping level but the temperature stability can also be improved. For a device doped with 15 acceptors/QD both a low J_{th} (less than 50 A cm^{-2} at room temperature) and a negative characteristic temperature between -50 and 45°C is obtained.

A detailed study of the optical properties of samples doped with different amounts of acceptors has been presented. There is no evidence that the doping (placed ~10nm below each QD layer) affects the physical structure of the QDs. In addition no charging induced shifts of the emission energy are observed for doping levels up to 50 acceptors / QD.

Electroluminescence measurements as a function of temperature and for very low current injection indicate that the optical efficiency at low temperatures decreases as the doping level is increased. At high temperatures the opposite trend is

found. Similar measurements performed for high injection levels reveal much less difference between the doped and undoped structures. The decreasing optical efficiency with increasing doping level at low temperatures is also seen in PL measurements and correlates with a decreasing PL lifetime with increasing doping. An analysis suggests that this behaviour results from an Auger process which is enhanced by the extrinsic holes. However the dependence of this process on the hole density is weaker than in higher dimensionality system, a result of the discrete energy states and resultant optical transition selection rules in QDs. As the temperature is increased there is evidence that this Auger process weakens.

Further studies of the EL suggest that there is some correlation between J_{th} and the emission from 'wasted' carriers in excited QD states. The temperature variation of the excited state emission is found to be significantly different in the doped and undoped structures. There is also evidence for faster carrier relaxation between the QD states in doped structure and that carriers may be lost from excited states to non-radiative centres at high temperatures. The power law relationship between injected current and integrated EL is found to be different in doped and undoped samples, the reason for this difference is unclear.

Studies of the temperature dependence of the EL linewidth and the relative populations of the two subsets of QDs suggest that the attainment of a thermal carrier distribution within the QD ensemble is delayed in doped structures. This may be a result of a deeper potential confinement for electrons in the doped QDs due to the Coulomb attraction by the extrinsic holes. This has the effect of shifting the region of negative T_0, typically observed in undoped QD lasers around ~ 200K, to room temperature in p-type doped QD lasers; hence explaining the improved temperature stability of the latter at and above room temperature. In addition, a photon coupling model which relies on the interaction between ground and excited states in an inhomogeneously broadened QD ensemble is able to fully explain the different temperature behaviours of J_{th} in doped and undoped devices. The relative contributions of this process and the thermal redistribution of carriers within the ensemble are unclear.

PLE measurements provide evidence for faster QD carrier capture and relaxation in doped samples. This behaviour is supported by more direct pump-probe time resolved measurements.

Finally, photocurrent spectroscopy demonstrates the hole state blocking of the lower energy QD transitions in the doped structures. With increasing applied electric field holes are swept out of the QDs and the transitions become unblocked. Quantum confined stark effect (QCSE) measurements reveal an unusual non-parabolic dependence on electric field at low fields for a highly doped structure. As the doping is increased from 0 to 6 to 12 acceptors / QD the permanent dipole moment reduces and the polarisability increases.

References

1. G. Park, O.B. Shchekin, D. G. Deppe, IEEE J. Quantum Electron. **36,** (9) 1065 (2000)
2. S. Osborne, P. Blood, P. Smowton, J. Lutti, Y. C Xin, A. Stintz, D. Huffaker, L. F. Lester, IEEE J. Sel. Topics Quantum Electron. **40,** (12) 1639 (2004)
3. O. B. Shchekin and D. G. Deppe, Appl. Phys. Lett. **80,** 2758 (2002)
4. Kerry J. Vahala and C. E. Zah, Appl. Phys. Lett. **52,** 1945 (1988)
5. O. B. Shchekin and D. G. Deppe, Appl. Phys. Lett. **80,** 3277 (2002)
6. O.B. Shchekin, J. Ahn, and D.G. Deppe, Electron. Lett. **38,** (14) 712 (2002)
7. Deppe, D.G.; Huang, H.; Shchekin, O.B., IEEE J. Quantum Electron. **38,** (12) 1587 (2002)
8. Koji Otsubo, Nobuaki Hatori, Mitsuru Ishida, Shigekazu Okumura, Tomoyuki Akiyama, Yoshiaki Nakata, Hiroji Ebe, Mitsuru Sugawara and Yasuhiko Arakawa, Jpn. J. Appl. Phys **43,** (8B) L1124 (2004)
9. S. Fathpour, Z. Mi, P. Bhattacharya, A. R. Kovsh, S. S. Mikhrin, I. L. Krestnikov, A. V. Kozhukhov, and N. N. Ledentsov, Appl. Phys. Lett. **85,** 5164 (2004)
10. C. Y. Liu, S. F. Yoon, Q. Cao, C. Z. Tong and H. F. Li, Appl. Phys. Lett. **90,** 041103 (2007)
11. P. M. Smowton, I. C. Sandall, H. Y. Liu and M. Hopkinson, J. Appl. Phys. **101,** 13107 (2005)
12. N. F. Massé, S. J. Sweeney, I. P. Marko, A. R. Adams, N. Hatori and M. Sugawara, Appl. Phys. Lett. **89,** 191118 (2006)
13. I. C. Sandall, P. M. Smowton, C. L. Walker, T. Badcock, D. J. Mowbray, H. Y. Liu and M. Hopkinson, Appl. Phys. Lett. **88,** 111113 (2006)
14. I. P. Marko, N. F. Massé, S. J. Sweeney, A. D. Andreev, A. R. Adams, N. Hatori and M. Sugawara, Appl. Phys. Lett. **87,** 211114 (2005)
15. K. Gündoğdu, K. C. Hall, Thomas F. Boggess, D. G. Deppe and O. B. Shchekin, Appl. Phys. Lett. **85,** 4570 (2004)

16. O. B. Shchekin, D. G. Deppe, and D. Lu, Appl. Phys. Lett. **78**, 3115 (2001)

17. Jong-Lam Lee, Long Wei, Shoichiro Tanigawa, and Mitsuo Kawabe, J. Appl. Phys. **69**, 6364 (1991)

18. Jong-Lam Lee, Long Wei, Shoichiro Tanigawa, and Mitsuo Kawabe, J. Appl. Phys. **70**, 674 (1991)

19. P. M. Smowton, I. C. Sandall, D. J Mowbray, Hui Yun Liu, M. Hopkinson, IEEE J. Select. Topics Quantum Electron. **13**, (5) 1261 (2007)

20. S. Sanguinetti, M. Henini, M. Grassi Alessi, M. Capizzi, P. Frigeri, and S. Franchi, Phys. Rev. B **60**, 8276 (1999)

21. I. P. Marko, A. R. Adams, S. J. Sweeney, D. J. Mowbray, M. S. Skolnick, H. Y. Liu, K. M. Groom, IEEE J. Select. Topics Quantum Electron. **11**, (5) 1041 (2005)

22. I.C. Sandall; P.M. Smowton; C.L. Walker; H.Y. Liu; M. Hopkinson; D.J. Mowbray; IEEE Photon. Technol. Lett. **18**, (8) 965 (2006)

23. Kohki Mukai, Nobuyuki Ohtsuka, Hajime Shoji, and Mitsuru Sugawara, Appl. Phys. Lett. **68**, 3013 (1996)

24. M. Grundmann and D. Bimberg, Phys. Rev. B **55**, 9740 (1997)

25. D. V. Regelman, E. Dekel, D. Gershoni, E. Ehrenfreund, A. J. Williamson, J. Shumway, A. Zunger, W. V. Schoenfeld, and P. M. Petroff, Phys. Rev. B **64**, 165301 (2001)

26. F. Guffarth, R. Heitz, A. Schliwa, O. Stier, M. Geller, C. M. Kapteyn, R. Sellin, and D. Bimberg, Phys. Rev. B **67**, 235304 (2003)

27. E. C. Le Ru, J. Fack, and R. Murray, Phys. Rev. B **67**, 245318 (2003)

28. Z. Y. Xu, Z. D. Lu, X. P. Yang, Z. L. Yuan, B. Z. Zheng, J. Z. Xu, W. K. Ge, Y. Wang, J. Wang, and L. L. Chang, Phys. Rev. B **54**, 11528 (1996)

29. I. C. Sandall, P. M. Smowton, J. D. Thomson, T. Badcock, D. J. Mowbray, H.-Y. Liu and M. Hopkinson, Appl. Phys. Lett. **89**, 151118 (2006)

30. Jin, C.-Y.; Badcock, T. J.; Liu, H.-Y.; Groom, K. M.; Royce, R. J.; Mowbray, D. J.; Hopkinson, M.; IEEE J. Quantum Electron. **42**, (12) 1259 (2006)

31. Mitsuru Sugawara, Kohki Mukai, and Yoshiaki Nakata, Appl. Phys. Lett. **74**, 1561 (1999)

32. H. H. Nilsson, J.-Z. Zhang, and I. Galbraith, Phys. Rev. B **72**, 205331 (2005)

33. C. Y. Jin, H. Y. Liu, K. M. Groom, Q. Jiang, M. Hopkinson, T. J. Badcock, R. J. Royce, and D. J. Mowbray, Phys. Rev. B **76**, 085315 (2007)

34. R. Heitz, A. Kalburge, Q. Xie, M. Grundmann, P. Chen, A. Hoffmann, A. Madhukar, and D. Bimberg, Phys. Rev. B **57**, 9050 (1998)

35. G. Rainò, G. Visimberga, A. Salhi, M. De Vittorio, A. Passaseo, R. Cingolani, and M. De Giorgi, Appl. Phys. Lett. **90**, 111907 (2007)

36. R. Oulton, J. J. Finley, A. I. Tartakovskii, D. J. Mowbray, M. S. Skolnick, M. Hopkinson, A. Vasanelli, R. Ferreira, and G. Bastard, Phys. Rev. B **68**, 235301 (2003)

37. F. Guffarth, R. Heitz, A. Schliwa, O. Stier, M. Geller, C. M. Kapteyn, R. Sellin, and D. Bimberg, Phys. Rev. B **67**, 235304 (2003)

38. K. W. Sun, A. Kechiantz, B. C. Lee and C. P. Lee, Appl. Phys. Lett. **88**, 163117 (2006)

39. Basu, P. K. Basu 'Theory of optical processes in semiconductors : bulk and microstructures' Oxford : Clarendon Press, 1997.

40. S. Ghosh, P. Bhattacharya, E. Stoner, J. Singh, H. Jiang, S. Nuttinck and J. Laskar, Appl. Phys. Lett. **79**, 722 (2001)

41. M. Grundmann, R. Heitz, D. Bimberg, J.H.H. Sandmann, J. Feldmann, phys. stat. sol. (b) **203**, (1) 121 (1997)

42. S. Sanguinetti, D. Colombo, M. Guzzi, E. Grilli, M. Gurioli, L. Seravalli, P. Frigeri, and S. Franchi, Phys. Rev. B **74**, 205302 (2006)

43. J. Siegert, S. Marcinkevičius, and Q. X. Zhao, Phys. Rev. B **72**, 085316 (2005)

44. Xiaodong Mu, Yujie J. Ding, Boon S. Ooi and Mark Hopkinson, Appl. Phys. Lett. **89**, 181924 (2006)

45. A. Fiore and P. Borri, W. Langbein, J. M. Hvam, U. Oesterle, R. Houdré, R. P. Stanley, and M. Ilegems, Appl. Phys. Lett. **76**, 3430 (2000)

46. P. D. Buckle, P. Dawson, S. A. Hall, X. Chen, M. J. Steer, D. J. Mowbray, M. S. Skolnick, and M. Hopkinson, J. Appl. Phys. **86**, 2555 (1999)

47. D. S. Citrin, Superlattices Microstruct. **13**, 303 (1993)

48. M. Gurioli, A. Vinattieri, M. Zamfirescu, M. Colocci, S. Sanguinetti, and Richard Nötzel, Phys. Rev. B **73**, 085302 (2006)

49. Yu. I. Mazur, J. W. Tomm, V. Petrov, G. G. Tarasov, H. Kissel, C. Walther, Z. Ya. Zhuchenko, and W. T. Masselink, Appl. Phys. Lett. **78**, 3214 (2001)

50. Y. D. Jang, H. Lee, D. Lee, J. S. Kim, J. Y. Leem, and S. K. Noh, J. Appl. Phys. **99**, 096101 (2006)

51. P. W. Fry PhD. Thesis (University of Sheffield, 2001)

52. P. W. Fry, I. E. Itskevich, S. R. Parnell, J. J. Finley, L. R. Wilson, K. L. Schumacher, D. J. Mowbray, M. S. Skolnick, M. Al-Khafaji, A. G. Cullis, M. Hopkinson, J. C. Clark, and G. Hill, Phys. Rev. B **62**, 16784 (2000)

53. P. W. Fry, L. Harris, S. R. Parnell, J. J. Finley, A. D. Ashmore, D. J. Mowbray, M. S. Skolnick, M. Hopkinson, G. Hill, and J. C. Clark, J. Appl. Phys. **87**, 615 (2000)

54. P. N. Brunkov, A. Patanè, A. Levin, L. Eaves, P. C. Main, Yu. G. Musikhin, B. V. Volovik, A. E. Zhukov, V. M. Ustinov, and S. G. Konnikov, Phys. Rev. B **65**, 085326 (2002)

55. D. A. Miller, D. S. Chemla, T. C. Damen, A. C. Gossard, W. Wiegmann, T. H. Wood, and C. A. Burrus, Phys. Rev. B **32**, 1043 (1985)

56. P. W. Fry, I. E. Itskevich, D. J. Mowbray, M. S. Skolnick, J. J. Finley, J. A. Barker, E. P. O'Reilly, L. R. Wilson, I. A. Larkin, P. A. Maksym, M. Hopkinson, M. Al-Khafaji, J. P. David, A. G. Cullis, G. Hill, and J. C. Clark, Phys. Rev. Lett. **84**, 733 (2000)

57. M. A. Cusack, P. R. Briddon, and M. Jaros, Phys. Rev. B **54**, R2300 (1996)

58. M. A. Migliorato, A. G. Cullis, M. Fearn, and J. H. Jefferson, Phys. Rev. B **65**, 115316 (2002)

59. Peng Jin, C. M. Li, Z. Y. Zhang, F. Q. Liu, Y. H. Chen, X. L. Ye, B. Xu, and Z. G. Wang, Appl. Phys. Lett. **85**, 2791 (2004)

60. J. J. Finley, M. Sabathil, P. Vogl, G. Abstreiter, R. Oulton, A. I. Tartakovskii, D. J. Mowbray, M. S. Skolnick, S. L. Liew, A. G. Cullis, and M. Hopkinson, Phys. Rev. B **70**, 201308 (2004)

Chapter 6

InAs QD structures with a thin Antimony containing cap layer

6.1 Introduction

Whilst the use of an InAs-InGaAs DWELL structure can result in emission beyond 1.3μm, it is found that the optical quality degrades significantly once 1.3μm is exceeded. It is believed that this degradation results from the high degree of strain present in the structure, a result of the need to use a large In composition in the InGaAs QW, which causes the formation of defects. Hence there appears to be no prospect of using DWELL structures to obtain emission at the 1.55μm telecommunications band from a GaAs-based system. 1.55μm emitting QDs on GaAs will hence require a new approach. One possibility is to grow on metamorphic buffer layers[1], which reduces the strain level in the InAs QDs and hence their effective band gap. Alternatively, low levels of either Sb or N may be incorporated into InAs QDs, both of which should result in a significant reduction of the emission energy, due to the strong compositional dependence of the alloy bandgap in these material systems. This chapter discusses attempts to obtain room temperature emission at 1.55μm from Sb containing InAs QD structures. It is found that direct incorporation of Sb into InAs QDs is difficult but by capping the QDs with a thin GaAsSb layer, emission up to and beyond 1.55μm is possible. A detailed optical spectroscopic study of InAs QDs capped with GaAsSb layers of different Sb compositions is presented.

6.2 InAs(Sb)-GaAs QD Structures

Initial work concentrated on attempts to incorporate various quantities of Sb directly into InAs QDs grown on GaAs. Five structures, each with a single layer of InAs(Sb) QDs, were grown. The QDs were formed by depositing 2.9 ML of InAs at 0.1 ML/sec with a substrate temperature of 500 °C, whilst an overpressure of Sb was maintained. Typically, the flux of a given group V element is determined by the "beam equivalent pressure" measured in mbar, which is then converted to

atoms/s.cm^2 Unfortunately since the ion gauge, which measures the beam pressure, was out of operation the only means of measuring the Sb flux was in terms of the degree of opening of the valve in the Sb cracker cell. Fig. 6.1 shows the low temperature PL of each sample, excited using a HeNe laser under low injection conditions (< 1 W/cm^2). In contrast to the expected red shift with increasing Sb flux, and hence expected Sb composition in the QDs, the PL blueshifts significantly and also broadens and reduces in intensity (the latter is not shown in the figure because of the normalisation of the intensities). Near band-edge emission from the GaAs matrix is also present for each sample.

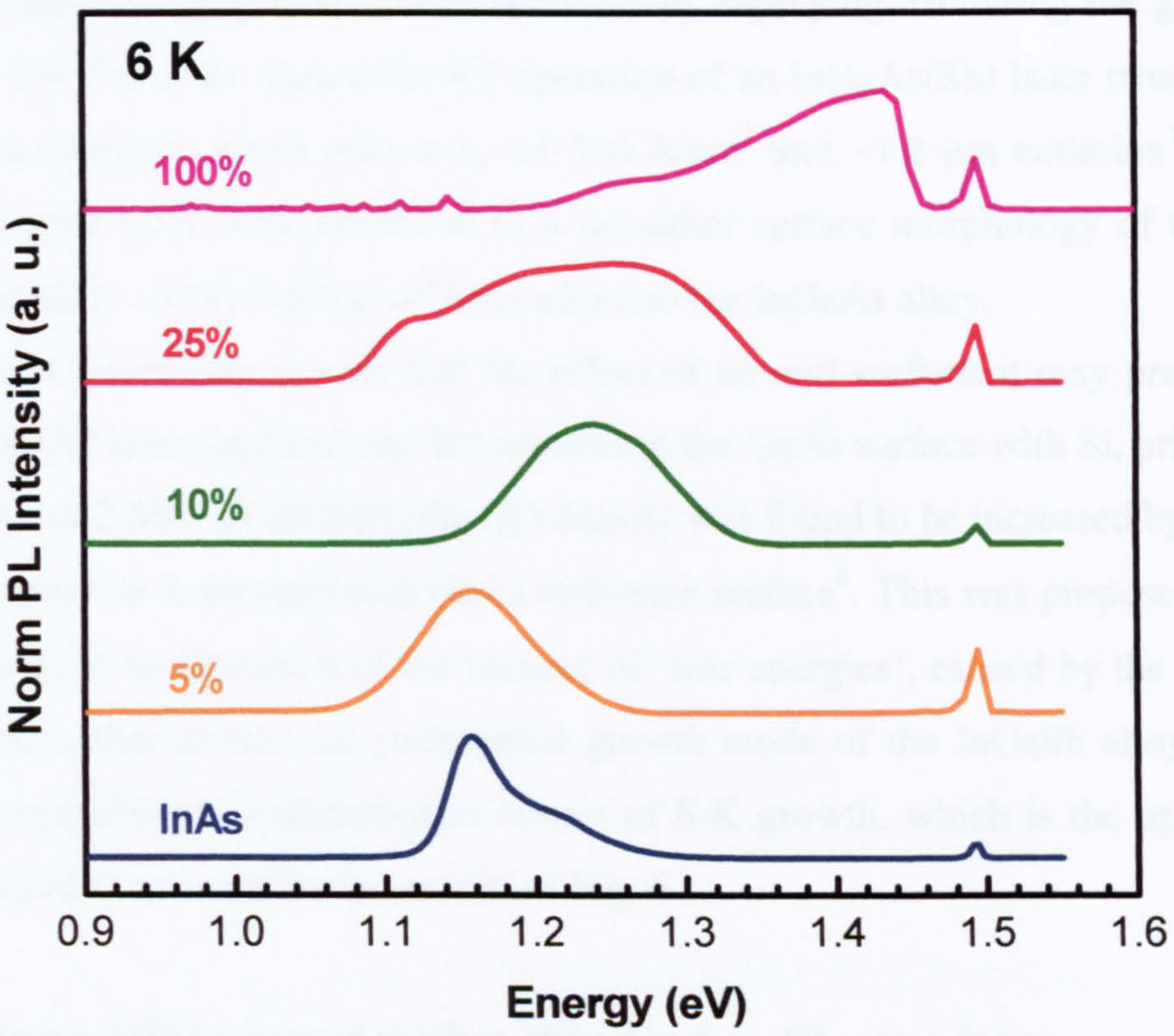

Fig. 6.1 Normalised low power PL at 6K for the In(Sb)As QD samples. The nominal Sb fraction is given in terms of a percentage, reflecting the relative opening of the shutters of the Sb cracker valve.

Since the dependence of the PL emission wavelength on the Sb flux is in contrast to what is expected for an In(Sb)As alloy of increasing Sb content[2], ie. the peak blueshifts rather than redshifts, it is unlikely that the Sb is being incorporated into the QDs in the desired manner. A similar blueshift in the PL emission of MBE grown In(Ga)As QDs in the presence of an Sb flux has been reported previously[3,4].

The Sb atoms are proposed to act as a surfactant at the QD growth front, decreasing the surface free energy and therefore increasing the critical thickness for QD nucleation. Consequently, the QDs that form are smaller and possibly have a lower density than for growth without the presence of Sb. The reduction in QD density is ascribed to a surfactant-induced increase in the surface diffusion length of the In adatoms, which may only be reduced by decreasing the growth temperature in this diffusion limited regime[5].

Analogous to the InAs/GaAs QD system, various growth techniques are currently being investigated that may allow In(Ga)As QWs to reach 1.3 μm and beyond. Recently, simultaneous enhancements of the PL intensity and uniformity of the emission wavelength have been achieved by supplying Sb during the growth of InGaAs QWs[6] and the successful RT operation of an InGaAs(Sb) laser structure has been demonstrated, albeit with a J_{th} of 350 A/cm^2 and ~1.2 μm emission[7]. These improvements have been attributed to a smoother surface morphology of the QWs when a small (< 10%) fraction of Sb is added to the InGaAs alloy.

It is interesting to note that the effect of an *anti*-surfactant may prove to be useful for QD laser applications. By irradiating the GaAs surface with Si, prior to the deposition of 2 MLs of InGaSb, the QD density was found to be increased by a factor of ~100, relative to an untreated GaAs reference surface[8]. This was proposed to be a direct result of an alteration of the balance of 'free energies', caused by the presence of Si atoms, that dictate the preferential growth mode of the InGaSb alloy. In this case the equilibrium is disturbed in favour of S-K growth, which is the opposite to that required to account for the results of Fig. 6.1.

6.3 InAs QDs capped with a thin $GaAs_{1-x}Sb_x$ cap layer

Detailed growth studies have revealed that Sb has a beneficial effect when introduced *after*, or during the latter stages of, the QD deposition. A technique utilising an Sb-irradiation step following a 40s growth interruption (GI) after the QD growth has been shown to redshift the PL by ~200 nm[9]. In a sample where this sequence is reversed, i.e. the Sb was deposited prior to the GI, the PL intensity was reduced by an order of magnitude and the QD height decreased by more than a factor of 2. This result is consistent with the Sb-irradiation initiating a change in the surface energy of the newly grown QDs, causing them to dissolve and collapse (as is the case

with high temperature GaAs capping). By using a GI, the QDs are allowed to achieve an energetically favourable shape before the capping process begins. The effect of the Sb may therefore be to prevent interface mixing between the cap and QDs, and therefore better preserving the structural properties of the QDs.

To investigate such a possibility, a single layer test structure was grown with QDs deposited under nominally identical conditions to those described in the previous section, but without the Sb flux during their growth. Instead, a 6 nm GaAsSb strain reducing layer (SRL) was grown above the QD layer with an Sb composition of 14%, as determined by X-Ray diffraction measurements. The PL properties, as shown in Fig. 6.2, of this sample demonstrated an improvement on those of the GaAs-capped InAs QD structure (see Fig. 6.1).

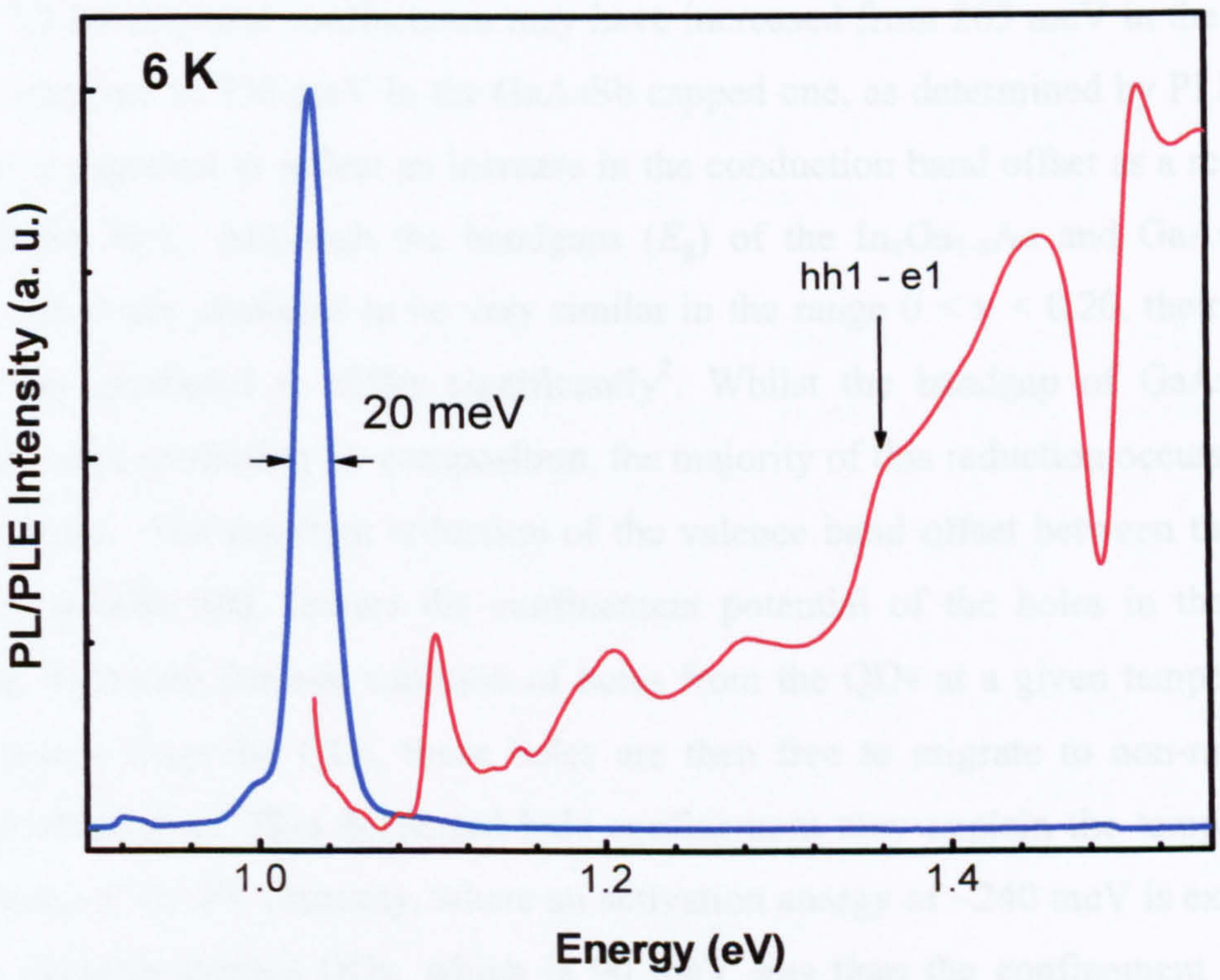

Fig. 6.2 6 K PL (blue line) and PLE (red line, detected at the PL peak) spectra for a single QD layer structure, capped with a 6nm $GaAs_{0.86}Sb_{0.14}$ layer. The PL was excited using semi-monochromatic light from the tungsten lamp source at a wavelength of ~770 nm.

For example, with respect to the GaAs capped structure (see Fig 6.1), the 6 K PL peak wavelength is redshifted from 1072 nm to 1202 nm (124 meV) in the sample containing the GaAsSb capped QDs. Furthermore, the 6 K linewidth of 20 meV in the GaAsSb structure is considerably narrower than the 50 meV value

obtained in a comparable single QD layer InGaAs capped structure (Vn 137, see Chapter 4 section 4.4.2). It even compares favourably with the lowest reported values for ensembles of self-assembled InAs QDs[10]. This high degree of QD homogeneity is reflected in the well-resolved phonon related features, related to discrete intra-QD carrier relaxation steps that can be resolved in the PLE spectrum shown in Fig. 6.2. Two broader peaks, above 1.35 eV, are attributed to transitions between states within the WL/SRL. Their separation is increased to ~80 meV and the hh-e1 transition is redshifted by 50 meV relative to the same features in GaAs capped InAs QD structures, reflecting the thicker nature of the composite SRL and In(Ga)As WL. However since the redshift of the lowest energy SRL/WL state is less than the corresponding QD PL peak shift between the two samples (~ 130 meV), carrier confinement should be larger in the GaAsSb capped QDs.

Whilst the *total* confinement may have increased from 263 meV in the GaAs capped structure to 330 meV in the GaAsSb capped one, as determined by PLE, this increase is expected to reflect an increase in the conduction band offset as a result of the GaAsSb SRL. Although the bandgaps (E_g) of the $In_xGa_{1-x}As$ and $GaAs_{1-x}Sb_x$ ternary alloys are predicted to be very similar in the range $0 < x < 0.20$, their band-lineups are predicted to differ significantly[2]. Whilst the bandgap of $GaAs_{1-x}Sb_x$ decreases with increasing Sb composition, the majority of this reduction occurs in the valence band. The resultant reduction of the valence band offset between the QDs and the GaAsSb SRL lowers the confinement potential of the holes in the QDs, allowing increased thermal emission of holes from the QDs at a given temperature. Once ejected from the QDs, these holes are then free to migrate to non-radiative recombination sites. This decreased hole confinement may explain the temperature dependence of the PL intensity, where an activation energy of ~240 meV is extracted for the GaAsSb capped QDs, which is 90 meV less than the confinement energy determined from PLE. It is generally assumed that the thermal escape process from the QD GS to the matrix is excitonic, i.e. that the carriers escape simultaneously as a correlated electron-hole pair. As mentioned in previous chapters however, there is a growing body of evidence that such a simple representation of the carrier escape dynamics is incorrect[11]. Certainly, when the band offsets are as asymmetric as they are expected to be in this system, the thermal escape of holes is likely to dominate

the PL quenching. This may account for the discrepancy between the activation and confinement energies found for the present sample.

Despite the predicted reduction of the hole confinement in the QDs, it was decided that the approach of covering the QDs with a GaAsSb alloy would be investigated further and higher Sb compositions would be incorporated into the SRL, with the aim of extending the emission towards 1.55 μm.

6.4 Low Power PL of InAs/GaAs QD structures capped with $GaAs_{1-x}Sb_x$

Two sample sets were grown, in different reactors and at different times. In all samples a 6 nm $GaAs_{1-x}Sb_x$ Strain Reducing Layer (SRL) was grown immediately above each layer of QDs. The growth temperature of the SRL was reduced from 500 °C, used for the QD growth, to 470 – 480 °C in order to prevent Sb segregation. The QDs themselves were formed under nominally identical conditions in each sample (2.9 ML InAs deposited at ~0.1 ML/s on GaAs).

One series of samples consisted of five structures, each comprising 5 QD layers separated by 50 nm GaAs spacer layers grown using the 'conventional' HGTSL technique[12]. A second series of single QD layer samples was also grown, in a different reactor and approximately one year later, but otherwise with the same growth parameters. The range of Sb compositions used in each set of structures was similar. Sb compositions were estimated by the growers from X-ray diffraction measurements. Because the Sb containing layer is very thin these values are subject to significant errors. Low power, low temperature PL spectra are shown in Fig. 6.3 a) and b) for the 5-layer and single layer sets respectively.

The PL spectra reveal that as the Sb content in the SRL increases the emission redshifts and broadens, with the strongest effect appearing to occur for compositions above ~17%. However, it is clear from a comparison of the peak positions of structures in the first and second series that have nominally identical Sb contents, that good repeatability in the growth cannot be achieved for x>0.14. It is known that the Sb:As ratio incorporated into the Group V sub-lattice is a very sensitive function of the growth temperature (T_G). During the growth of the 5-layer series it was suggested that there was some uncertainty in T_G, due to a problem with

the thermocouple in the substrate holder[13], which may explain the differences between the two sets of samples. However, the differences between the two sample sets do not obscure the overall dependence of the PL peak energy with nominal Sb composition; a strong redshift with increasing composition.

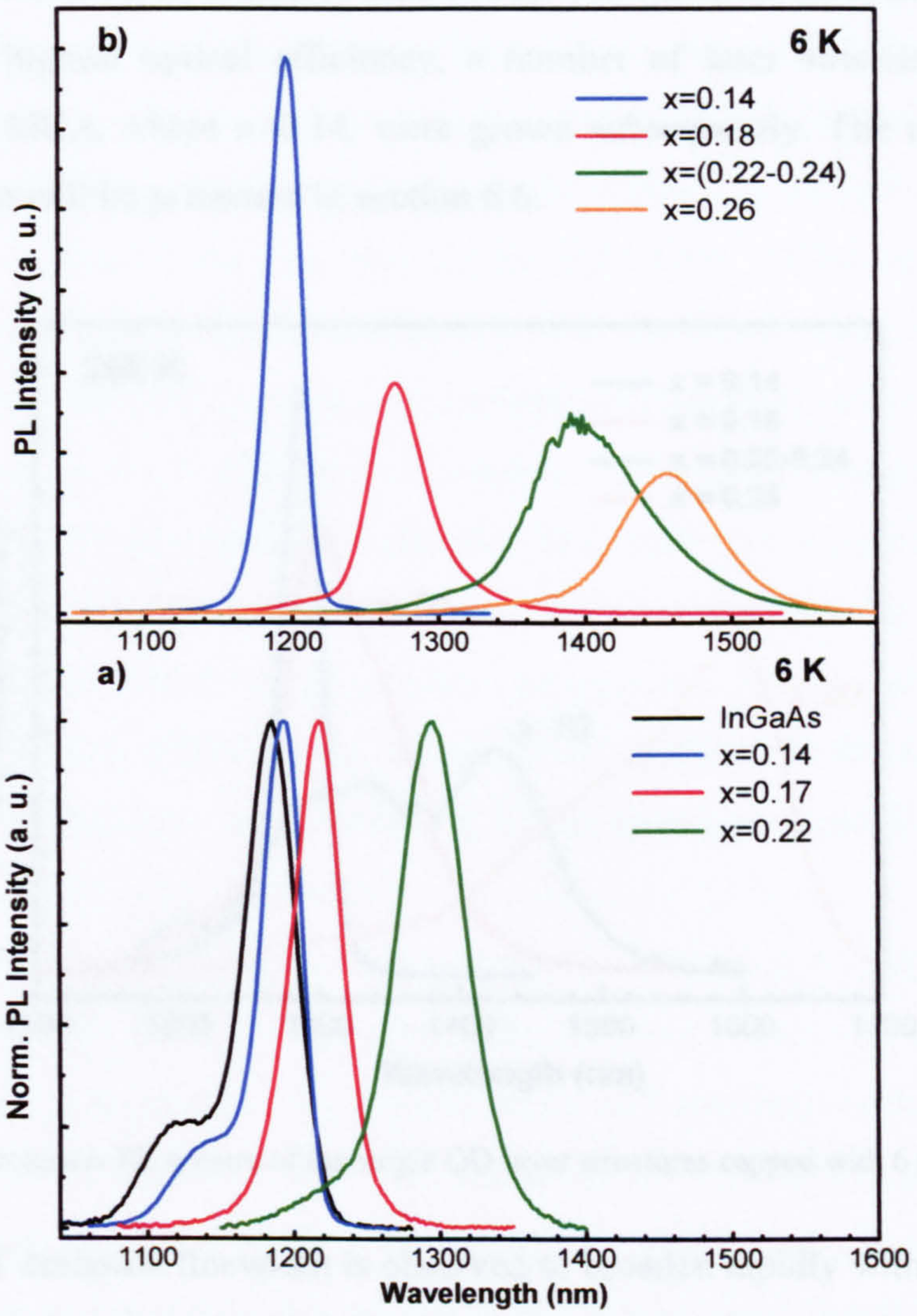

Fig. 6.3 6 K Low power PL spectra of the 5-layer (a) and single QD layer structures (b), containing 6 nm $GaAs_{1-x}Sb_x$ SRLs.

There are four possible mechanisms responsible for the redshift of the PL (QD GS emission) with increasing Sb content: reduced hydrostatic QD strain; incorporation of Sb into the QDs; increase in QD size and lowering of the confinement potential surrounding the QDs. It will be shown that the latter dominates the redshift when x>0.14. However, the presence of Sb in the capping layer is also

suggested to increase the QD height, as reported in AFM[14] and STM[15] studies, resulting in reduced quantisation energies for the QD states.

At low temperature, the integrated emission intensities are similar for all samples, decreasing by less than a factor of 2 between x=0.14 and 0.26. However, when comparing their RT PL intensities, the optical efficiency is seen to reduce markedly when x>0.14, as is clearly seen in Fig. 6.4. Since the structure with x=0.14 possesses the highest optical efficiency, a number of laser structures containing $GaAs_{0.86}Sb_{0.14}$ SRLs, where x~0.14, were grown subsequently. The results of their characterisation will be presented in section 6.6.

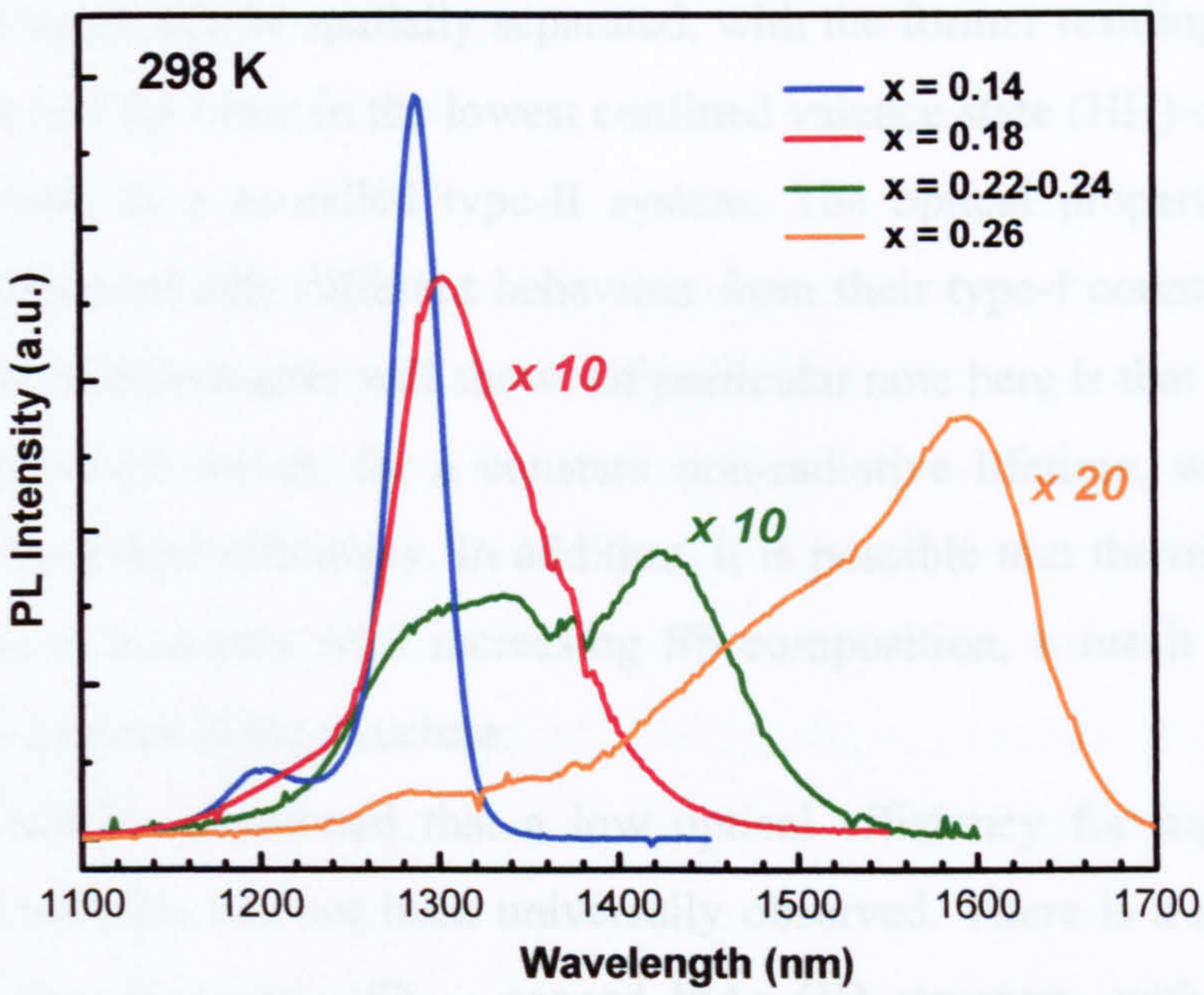

Fig. 6.4. RT Low power PL spectra of the single QD layer structures capped with 6 nm $GaAs_{1-x}Sb_x$

The RT emission linewidth is observed to broaden rapidly with increasing Sb content, in contrast to a much weaker increase observed at 6 K (x=0: 37 meV, x=0.22: 40 meV). The low temperature increase most likely reflects additional inhomogeneity due to Sb and width fluctuations in the GaAsSb layer. As will be shown below, the electronic structure changes significantly above Sb compositions of ~0.14[16].

At the time of the growth of the initial 5 layer sample set, the only other reported PL study of GaAsSb capped QDs came from the NICT group in Japan, who also showed that increasing the Sb composition increased the emission wavelength beyond 1.3 μm[17]. Despite the similar growth temperatures and rates used by this

group and the growers in Sheffield (H-Y Liu and M J Steer), there is more noise present in PL spectra of the samples grown in Japan, suggesting a poorer optical efficiency and hence that their MBE growth conditions were not well optimised.

The origin of the RT PL intensity degradation, observed for x>0.14, is not entirely clear. The optical efficiency of a QD structure is a function of a number of parameters, including the density of non-radiative centres, the confinement potential for electrons and holes and the radiative lifetime of carriers in the QDs. As discussed previously, with increasing Sb composition the valence band offset between the InAs QDs and GaAsSb SRL reduces and eventually the valence band-edge of the GaAsSb SRL falls below that of the HH state in the InAs QDs. When this occurs cold electrons and holes will be spatially separated, with the former residing in the GS of the InAs QDs and the latter in the lowest confined valence state (HH) of the GaAsSb SRL; this results in a so-called type-II system. The optical properties of type-II excitons display markedly different behaviour from their type-I counterparts, as the remaining part of this chapter will show. Of particular note here is that their radiative lifetime is increased which, for a constant non-radiative lifetime, will result in a decrease in the optical efficiency. In addition, it is possible that the number of non-radiative centres increases with increasing Sb composition, a result of the higher level of strain present in the structure.

It should be mentioned that a low optical efficiency for high Sb content (x>0.14) QD samples has not been universally observed. There is a report of a 1.4 μm emitting $In_{0.18}Ga_{0.82}As_{0.75}Sb_{0.25}$ capped InAs QD structure, with an activation energy of ~530 meV (obtained from an Arhennius fit to the temperature dependent PL intensity) and strong RT PL[18]. It may be that by adding In to the GaAsSb alloy, the morphology of the growth can be improved, as suggested for InGaAsSb QWs[7]. Perhaps of more relevance to the present work is a growth study in which different configurations of thin GaSb and GaAs layers were used to cover the InAs QDs[19]. In this study it was argued that the critical thickness for dislocation formation is easily exceeded when GaSb is deposited directly on the QDs, due to the high quantity of strained material, which then causes a strong quenching of the PL.

6.5 Type – II excitons in Ga(As)Sb/(In)GaAs hetero-structures

6.5.1 GaAsSb/GaAs QWs

Various experimental and theoretical works have focussed on the effect of the Sb composition on the emission and absorption properties of $GaAs_{1-x}Sb_x$/GaAs QWs. In this material system, there is considerable uncertainty in the values of the conduction and valence band offsets (ΔE_C and ΔE_V respectively) for a given 'x', and consequently, the band-offset ratios (Q_C and Q_V) are not clearly known. There are several reasons why this is so. First, it is not entirely straightforward to obtain the Sb composition. Atomic clustering, ordering and phase separation effects have previously been observed in scanning tunnelling microscopy (STM) images of GaAsSb compounds[20]. These all serve to restrict the precision of a measurement of x using high resolution X-ray diffraction. Second, experimental knowledge of the unstrained $GaAs_{1-x}Sb_x$ band-gap is scarce, with reported values showing considerable scatter. In addition, the deformation potentials required for a precise calculation of the strain-induced modification of the band structure are not known with certainty[21]. All of these factors contribute to the fairly disparate conclusions found in the literature regarding the exact form of the band line-ups in this system.

The magnitude and polarity of ΔE_V and Q_V are of particular importance when trying to optimise a laser structure, since the optical gain is highly sensitive to the extent of the electron and hole wavefunction overlap[22]. In the case of a single GaAsSb QW embedded in GaAs, a type-II structure is formed when $Q_V > 1$, ie. the lowest energy heavy-hole state is confined in the GaAsSb QW and the electrons are delocalised in the GaAs barrier material. Such a scenario is depicted schematically in Fig. 6.5.

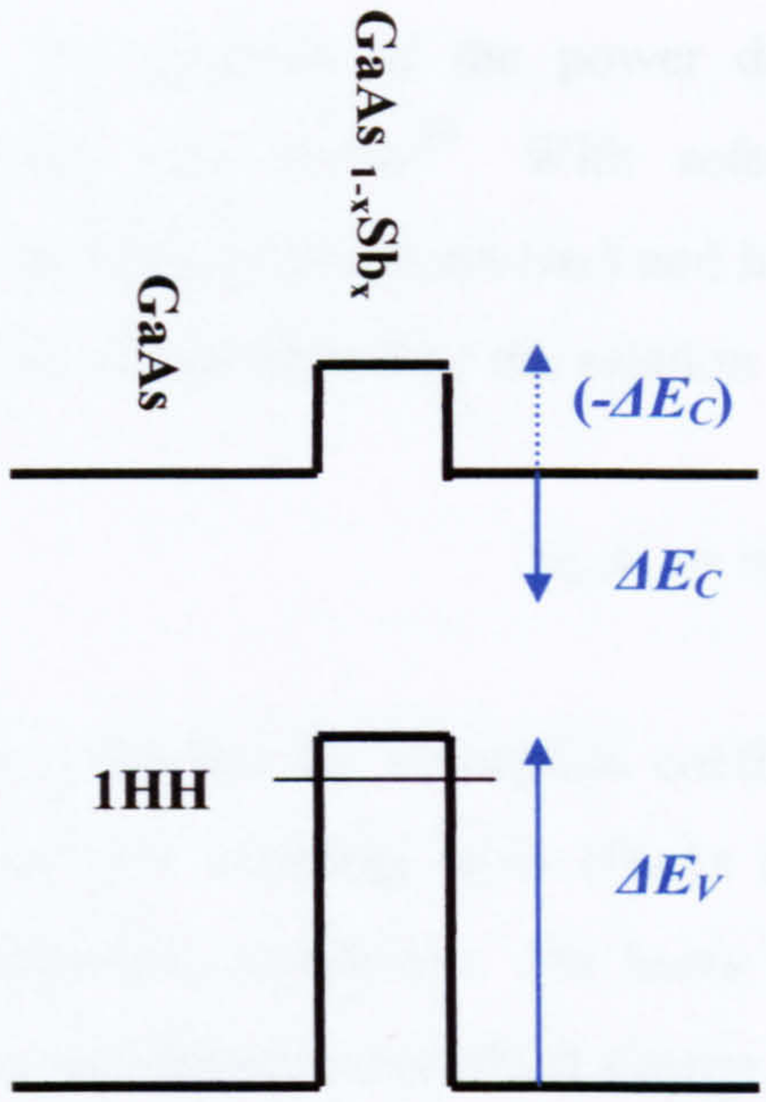

Fig. 6.5 Schematic diagram of the band line-up for a $GaAs_{1-x}Sb_x/GaAs$ hetero-junction showing the conduction and valence band offsets, ΔE_C and ΔE_V respectively.

To give a brief overview of some of the most extreme variations in the reported values of these parameters: a temperature and composition independent Q_V value of 1.05 has been inferred from PL studies of a range of samples of known Sb content in the GaAsSb QW[21], contrary to both the predictions of model-solid theory where Q_V increases to 2.75 for the GaSb/GaAs interface[23] and the experimental finding of a type-I alignment for x=0.1 – 0.3[24].

One of the consequences of a type-II band line-up is the spatial separation of injected electrons and holes, since the lowest energy electron and hole states no longer exist in the same material: for the GaAs-GaAsSb system the lowest energy hole state lies in the GaAsSb QW and the electrons are delocalised in the GaAs barriers. The build-up of two 'planes' of oppositely charged carriers results in the formation of a system analogous to that of a parallel plate capacitor which produces an electric field (E) directed parallel to the growth direction. The establishment of space charge regions also results in a modification of the electron and holes energies, with typically a triangular potential being formed at the interface between the two materials. The quantisation energies in these potentials are a strong function of the degree of charge build-up, which in turn is dependent on the excitation power used for the PL measurements. With increasing power the charge build-up increases, increasing the confinement energies and resulting in a strong power dependent blue-shift of the emission. This power dependent blue shift of the PL is a classic signature of a type-II hetero-junction system.

An analysis of the power dependent blue shift has been developed by Weisbuch and Vinter[25]. With reference to Fig. 6.5, the steady state sheet concentrations of electrons (n_W) and holes (p_W) generated in a thin layer by a photon flux I are characterised by the relation

(Eq. 1.1)

$$n_W p_W = n_W^2 = \frac{\alpha I (L+l)^2}{\gamma} \qquad \text{(Eq. 6.1)}$$

Where α denotes the absorption coefficient, L the width of the GaAsSb layer, l the multiple QW cladding layer (GaAs in this case) thickness, and γ is the radiative recombination coefficient. The holes in the GaAsSb QW are strongly localised and form a two-dimensional sheet charge, which, produces an approximately triangular potential in the GaAsSb layer and an electric field given by

$$\varepsilon = \frac{2\pi e n_W}{\varepsilon_0} \propto \sqrt{I} \qquad \text{(Eq. 6.2)}$$

The hole ground state in this potential is given by

$$E_e^{GS} = \text{Const. } \varepsilon^{2/3} \equiv bI^{1/3} \qquad \text{(Eq. 6.3)}$$

with

$$b = \left(\frac{9\pi}{8}\right)^{2/3} \left(\frac{\hbar}{2m_e}\right)^{1/3} \left(\frac{2\pi e^2}{\varepsilon_0}\right)^{2/3} \left(\frac{\alpha (L+l)^2}{\gamma}\right)^{1/3} \qquad \text{(Eq. 6.4)}$$

The hole quantisation energy is thus predicted to increase as the cube root of the excitation density. This electrostatic 'band-bending' results in a PL peak blueshift with increasing excitation density.

Numerous reports[26, 27] have validated the above model for the Ga(As)Sb/GaAs QW system, at least in the low excitation power regime. It will be shown in the next section that it can also be applied to the GaAsSb/InAs/GaAs QD system.

6.5.2 Power dependent PL of type-II InAs/GaAsSb QDs

Normalised excitation power dependent PL spectra of the 5 – layer QD structure capped by $GaAs_{0.78}Sb_{0.22}$ SRLs are shown for excitation power varying by over three orders of magnitude (0.1 – 100 mW) in Fig. 6.6. At the lowest powers, where the spectra contain only one PL peak at ~0.96 eV (peak A in Fig. 6.6) the peak position is seen to blueshift by ~20 meV. With reference to Fig. 6.7 this emission originates from the recombination of electrons in the GS of the QDs (e1) with holes in the lowest QW sub-band of the GaAsSb SRL ($HH_{T\text{-}II}$). For higher powers (> ~3 mW), a peak ~ 70 meV to higher energy emerges (Peak B) which blueshifts at the same rate as the GS peak. It is likely that Peak B originates from the recombination of electrons located in the 1st ES of the QD (e2) with $HH_{T\text{-}II}$. Both the e1 and e2 transitions are represented by orange lines in Fig. 6.7.

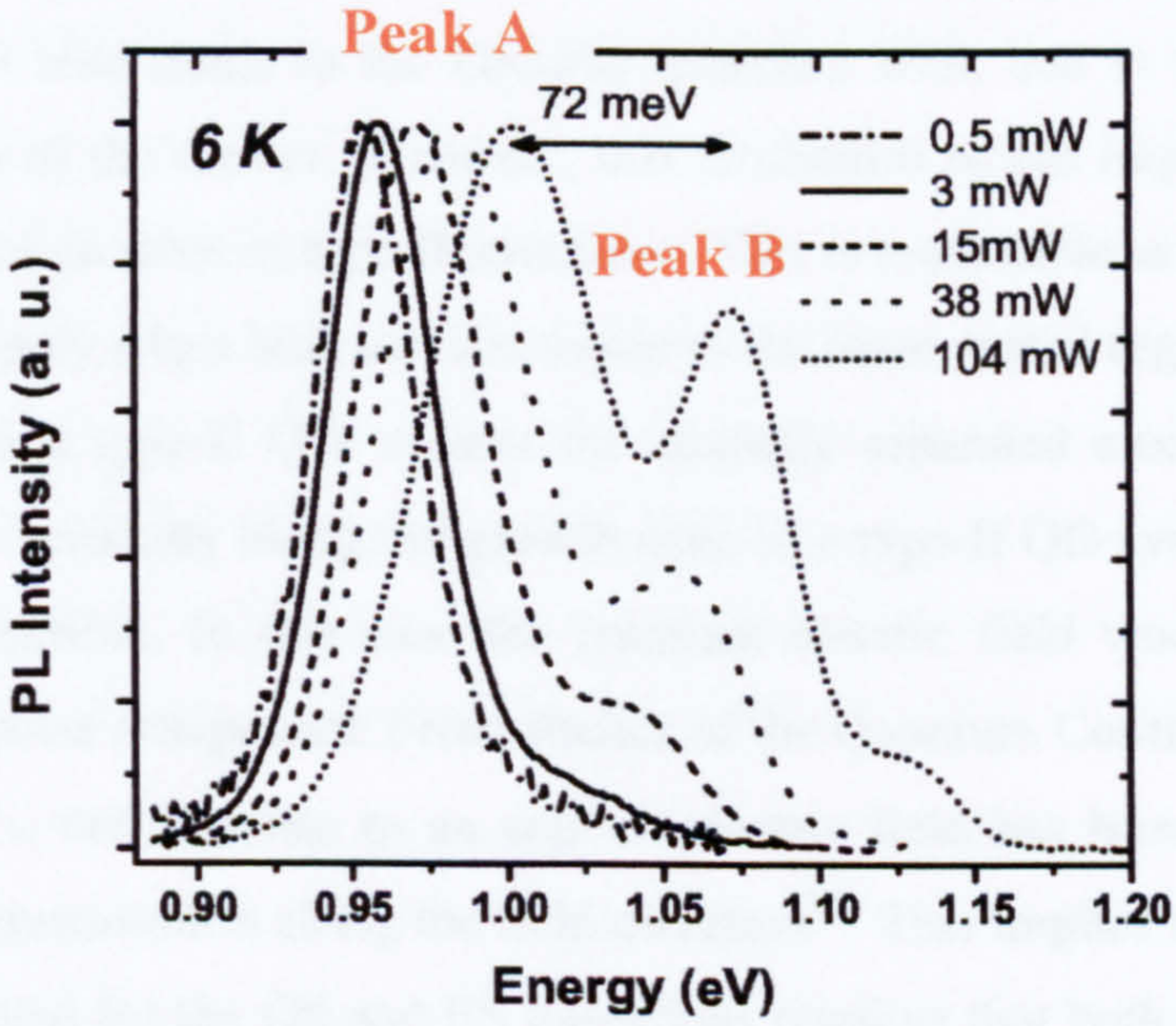

Fig. 6.6 6K power dependent PL spectra of a 5-QD layer structure capped with 6 nm $GaAs_{0.78}Sb_{0.22}$

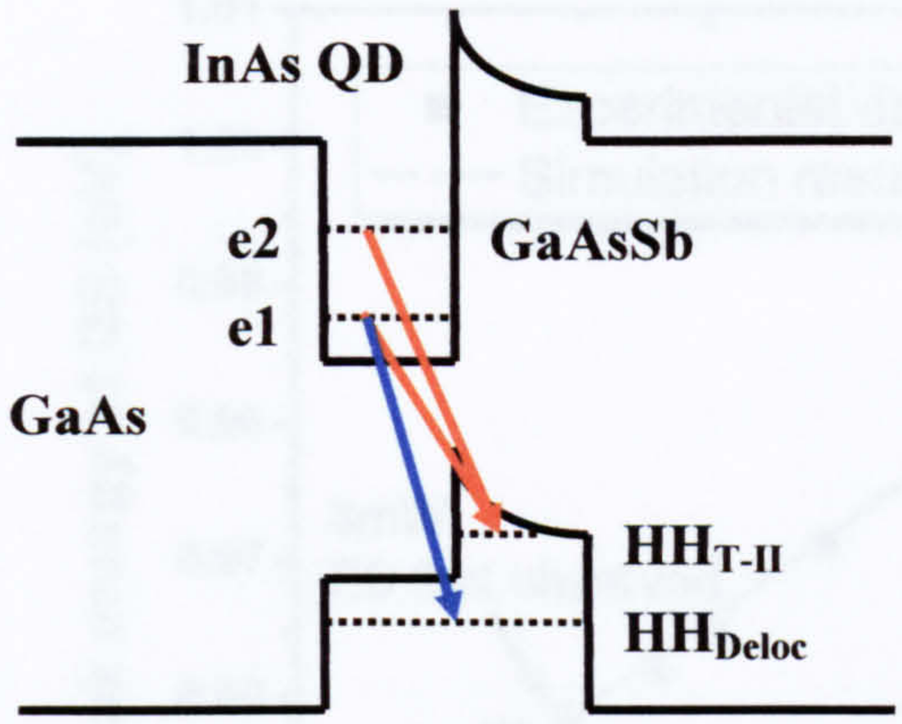

Fig. 6.7 Band diagram of InAs QDs capped with a $GaAs_{1-x}Sb_x$ SRL. The high Sb fraction in the SRL produces a type-II band alignment.

This attribution is supported by the observation of an identical shift rate for both transitions, suggesting a similar origin. In addition, it is consistent with the expected band line-up in this system (ie. the electrons being confined in the QDs) and the relative difference in the density of states between the InAs QDs and the GaAsSb SRL ie. the excited electron levels are more easily populated in the QDs than the excited hole states in the GaAsSb quantum well, due to the much lower density of states of the former. If correct, this attribution would imply the existence of 'broken' selection rules in type-II structures. This is reasonable as strong selection rules will only apply when both carriers reside in the same spatial region.

Whilst in a type-II QW system the spatially separated electrons and holes must be aligned vertically along the growth axis, in a type-II QD system an in-plane offset is also possible. In this case the resultant electric field would have both a vertical and in-plane component. From studies of the Quantum Confined Stark Effect (QCSE) in QWs, the response to an applied electric field has been shown to be a function of the quantisation along the field direction[28]. This implies that the identical blueshifts observed for the GS and ES transitions requires that both the electron and hole states have an identical quantization along the field direction. Since the GS and ES in the QDs differ in their quantization normal to the growth direction (because the height of the QDs is significantly smaller than their in-plane extent), it can be concluded that the electric field resulting from the charge build-up is oriented predominantly along the growth axis. This requires that the holes in the GaAsSb are localized above the QDs.

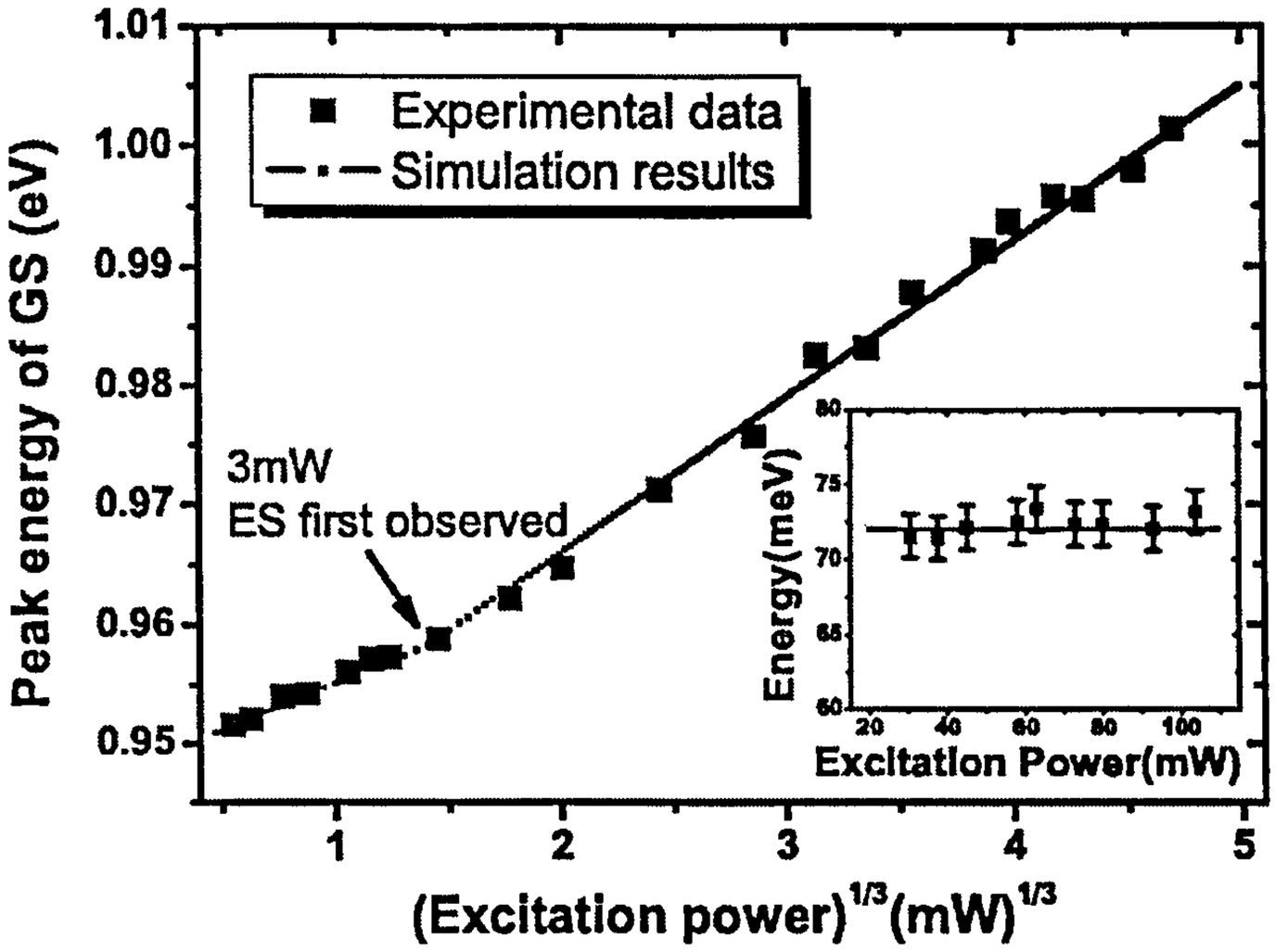

Fig. 6.8 Blueshift of the GS emission as a function of the cube root of the excitation power.

Fig. 6.8. shows the energy of the GS emission (E_{GS}) plotted against the cube root of the excitation power. As discussed previously the observed $E_{GS} \propto P^{1/3}$ behaviour has been observed previously in type-II quantum well systems[27] and also in the present QD system[29]. The data of Fig. 6.8 shows that the gradient changes at 3mW, corresponding to the excitation power where the ES transition is first observed. Above this power the emission shifts more rapidly. In order to analyze this behaviour quantitatively, a theoretical model was developed by C. Jin in the E&EE department at the University of Sheffield, using the arguments presented in section 6.5.1.

The total rate of spontaneous recombination from the GS and ES can be written as

$$\alpha P = B_{es} n_{es}^{d} p_{gs}^{w} + B_{gs} n_{gs}^{d} p_{gs}^{w} \qquad \text{(Eq. 6.5)}$$

where P is the injected photon density, α is the total absorption of the structure, B_{gs} and B_{es} are the spontaneous recombination coefficients for the GS and first ES respectively, n_{es}^{d} and n_{gs}^{d} are the electron densities in the GS and first ES dot states respectively, and p_{gs}^{w} is the hole density in the GS of the GaAsSb QW. It is assumed that the system obeys charge neutrality, from which:

$$p_{gs}^{w} = \frac{V_{dots}}{V_{w}} (n_{gs}^{d} + n_{es}^{d}) \qquad \text{(Eq. 6.6)}$$

where V_{dots} is the total volume of the QDs, and V_w is the volume of the GaAsSb well.

The electric field close to the top of the dots is given by:

$$\varepsilon = \frac{ep_{gs}^{w}d}{\varepsilon_0\varepsilon_r} \qquad \text{(Eq. 6.7)}$$

where d is the width of the GaAsSb QW. For excitation powers below the ES emission threshold (~ 3mW), and hence before the QD electron excited state is significantly populated, Eq. 6.5 can be simplified to:

$$\alpha P = \frac{V_{dots}}{V_w} B_{GS} (n_{gs}^{d})^2 \qquad \text{(Eq. 6.8)}$$

The GS energy in a QW with a triangular potential is given by

$$E_{GS}^{e} \cong \left(\frac{\hbar^2}{2m}\right)^{1/3}\left(\frac{9\pi e\varepsilon}{8}\right)^{2/3} = \left(\alpha\frac{V_w}{V_{dots}}\frac{\hbar^2}{2mB_{gs}}\right)^{1/3}\left(\frac{9\pi e^2 d}{8\varepsilon_0\varepsilon_r}\right)^{2/3} P^{1/3} \qquad \text{(Eq 6.9)}$$

which is a modified form of Eq 6.4 in section 6.5.1.

With the first ES transition present, Eq. 6.8 can be rewritten as:

$$\alpha P = \frac{V_{dots}}{V_w} B'(n_{es}^{d} + n_m)^2 \qquad \text{(Eq 6.10)}$$

where $n_m = 2/V_0$ is the saturated carrier density of the GS, V_0 the volume of a single QD and B' the equivalent spontaneous recombination coefficient given by

$$B' = B_{GS}\left(\frac{cn_{es}^{d} + n_m}{n_{es}^{d} + n_m}\right) \qquad \text{(Eq. 6.11)}$$

where $c = B_{es}/N_{gs}$ is the ratio of the spontaneous recombination coefficients. The electron GS energy is now given by

$$E_{GS}^{e} \cong \left(\alpha\frac{V_w}{V_{dots}}\frac{\hbar^2}{2mB'}\right)^{1/3}\left(\frac{9\pi e^2 d}{8\varepsilon_0\varepsilon_r}\right)^{2/3} P^{1/3} \qquad \text{(Eq. 6.12)}$$

On comparing Eq.s 6.9 and 6.12, it can be seen that the only difference in the calculated blueshift (E_{GS}^{e}) under mild and strong carrier injection respectively, is in the value for the effective spontaneous recombination coefficient (B). The accelerated blue shift observed once the ES is populated requires that $B_{ES} < B_{GS}$. The

physical significance of $B_{ES} < B_{GS}$ is that carrier accumulation is easier in the ES, resulting in enhanced electrostatic band bending and the resultant accelerated blue shift. The underlying reason for this disparity in the recombination coefficients for the GS and ES is unknown and requires further investigation. However, it is likely to be related to differences in the extent of the electron-hole wavefunction overlap for the two transitions.

As is shown in Fig. 6.10 Eq. 6.12 describes the experimental results fairly accurately. The following parameters were used in the simulation: $\alpha = 0.4$, an effective mass $m = 0.075m_0$ which includes the effects of both the electrons and holes, an unperturbed emission energy $E_C^0 = 1.3$, $V_0 = 6.75\times10^{-25}\text{m}^3$, $B_{GS} = 1.5\times10^{-16}\ \text{m}^6\text{s}^{-1}$, and $c = 0.25$, where $c = B_{ES}/B_{GS}$.

To further investigate the nature of the optical emission from the type-II QD structure, the GS integrated intensity is plotted against excitation power in Fig. 6.9.

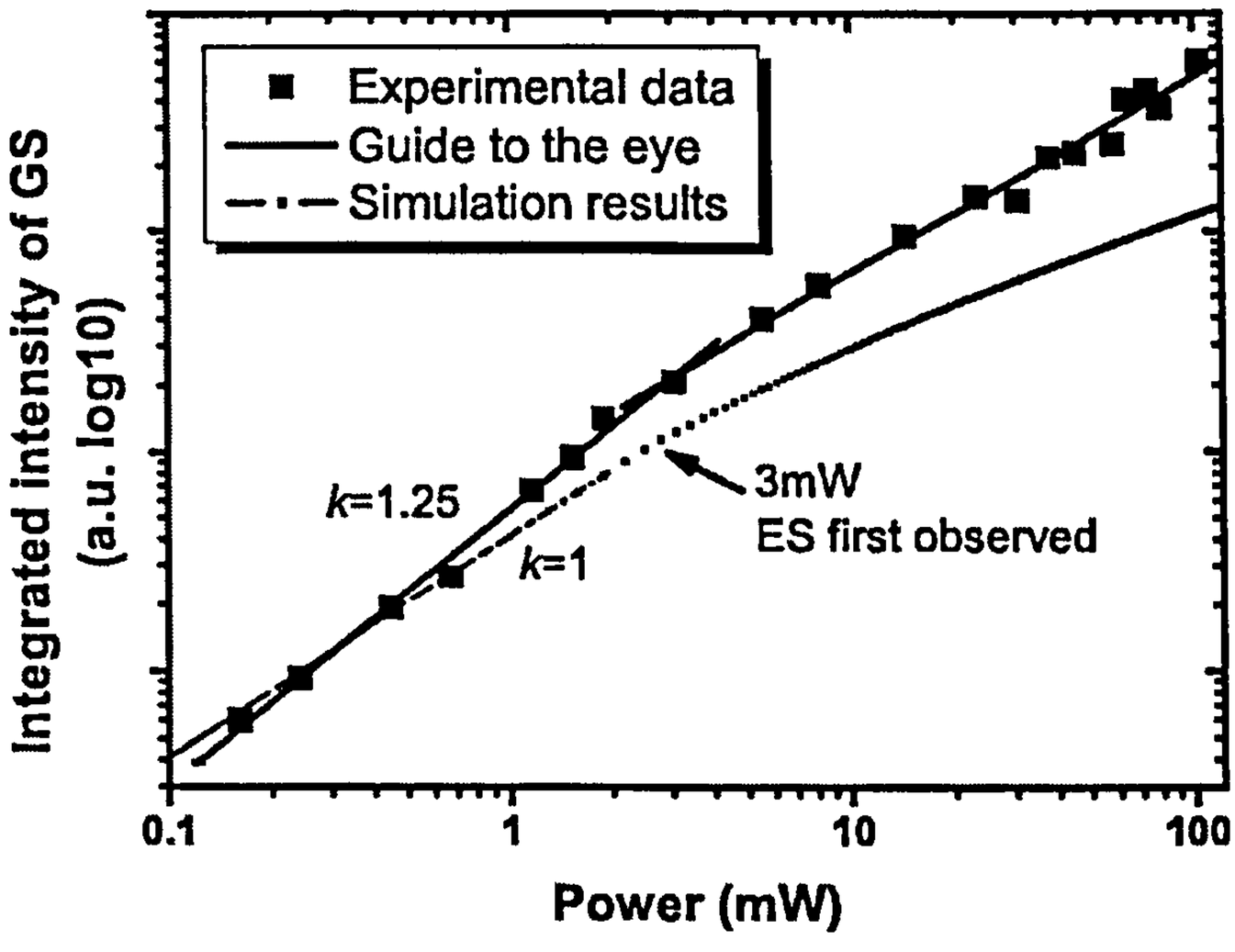

Fig. 6.9 Log-Log plot showing the variation of the integrated intensity of the GS emission as a function of the incident laser power.

The emission intensity increases at a slower rate once the ES emission is observed but no saturation of the intensity or the blue shift occurs, in contrast to the behaviour reported for a type-II QW structure[27]. This difference suggests that state filling effects are intrinsically different in type-II QW and QD systems, this requires further study. The power dependence of the integrated GS intensity was simulated using the same model and parameters discussed previously and the results are

included in Fig. 6.9. It is interesting to note that whilst a super-linear behaviour is found experimentally, theoretically a linear behaviour ($k = 1$) is predicted. A super-linear power dependence has been previously reported for type-I QDs at high temperatures and low excitation powers and attributed to either the uncorrelated capture of electrons and holes[30] or the presence of a non-radiative process[31]. It is possible that the, at least, partial *in - plane* delocalisation of holes in the GaAsSb layer may allow their migration to non-radiative centres. However this process cannot be overly significant since the optical efficiency of this sample is only weaker by a factor of two compared with a type-I (14 % Sb) structure (see Fig 6.4). In addition, magneto-PL measurements presented in section 6.5.6 indicate that the holes in the GaAsSb SRL are localised close to the QD interface.

6.5.3 PLE of InAs/GaAsSb QDs

Fig. 6.10 shows low temperature, low power PL and PLE spectra recorded from the four single layer InAs/$GaAs_{1-x}Sb_x$ structures grown in the second series. The PL and PLE were excited using monochromated light from a tungsten-halogen lamp, with a power density on the samples of ~1 W/cm^2. For the x=0.14 sample a number of features are observed in the PLE spectrum in the energy window close to the QD GS transition (950 – 1150 nm). The absolute energies of these resonances shift rigidly with detection energy. They can therefore be related to carrier relaxation processes within the QDs involving the emission of LO phonons, as has been reported many times before in the InAs/GaAs QD system[32]. These features are not present in the PLE spectra of the samples with higher Sb composition, consistent with a different dominant carrier relaxation mechanism in these structures.

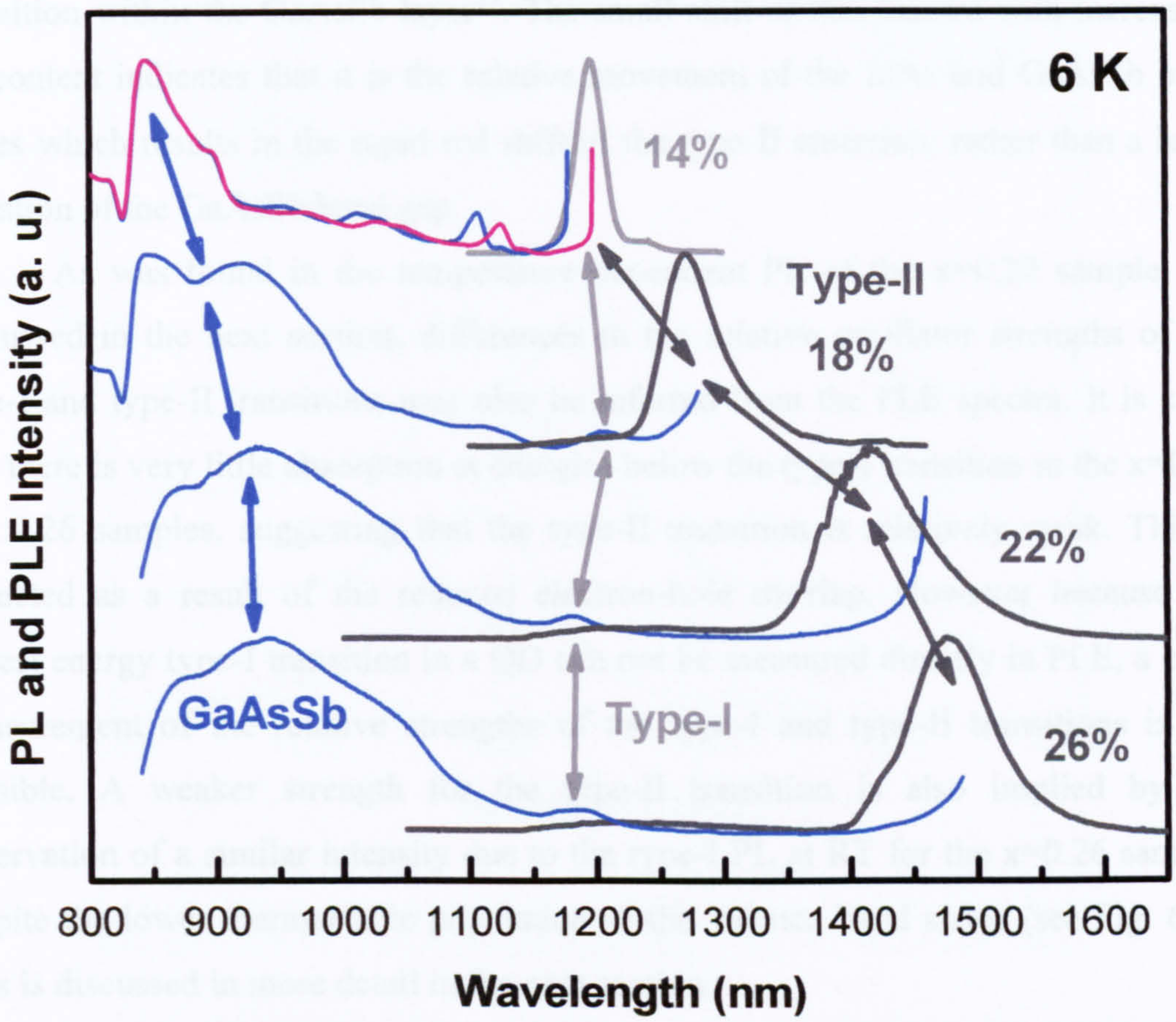

Fig. 6.10 Normalised PL and PLE at 6K, detected at the respective PL peak of the single QD layer samples capped with GaAsSb SRLs.

In addition to the LO phonon features specific to the x=0.14 sample, there are three main features observable in the PL and PLE spectra of all the higher Sb content samples. First, there is the emission between 1200 and 1500 nm which redshifts strongly with increasing Sb content and is attributed to a type-II transition occurring between the electron GS in the QDs and the lowest energy hole states in the QW. Second, the absorption feature at approximately 1200 nm in the three highest Sb content samples and the corresponding emission in the x=0.14 sample is attributed to the type-I internal QD transition. It is important to note that the far smaller variation of this feature (~12 meV) compared to the PL redshift (196 meV) over the range of Sb compositions investigated (x=0.14-0.26) indicates that it is the formation of a type-II system that is primarily responsible for the large emission redshift with increasing Sb content, and not a significant variation in the electronic structure of the QDs. Finally, there is an absorption feature in the region 900-1050 nm which redshifts weakly with increasing Sb composition. This is ascribed to the type-I

transition within the GaAsSb layer[33]. The small shift of this feature with increasing Sb content indicates that it is the relative movement of the InAs and GaAsSb band edges which results in the rapid red shift of the type-II emission, rather than a large variation of the GaAsSb band gap.

As was found in the temperature dependent PL of the x=0.22 sample and discussed in the next section, differences in the relative oscillator strengths of the type-I and type-II transitions may also be inferred from the PLE spectra. It is clear that there is very little absorption at energies below the type-I transition in the x=0.22 and 0.26 samples, suggesting that the type-II transition is relatively weak. This is expected as a result of the reduced electron-hole overlap. However because the lowest energy type-I transition in a QD can not be measured directly in PLE, a clear measurement of the relative strengths of the type-I and type-II transitions is not possible. A weaker strength for the type-II transition is also implied by the observation of a similar intensity due to the type-I PL at RT for the x=0.26 sample, despite the lower thermal hole population of the valence band states (see Fig. 6.4). This is discussed in more detail in the next section.

6.5.4 Temperature dependent PL of type-II InAs/GaAsSb QDs

As discussed in the previous section, the peculiar form of the temperature dependent PL spectra in the x=0.22 sample illustrates very clearly the difference in oscillator strength between the type-I and type-II transitions. Fig. 6.11 shows spectra obtained under low excitation, for temperatures between 77 and 290 K.

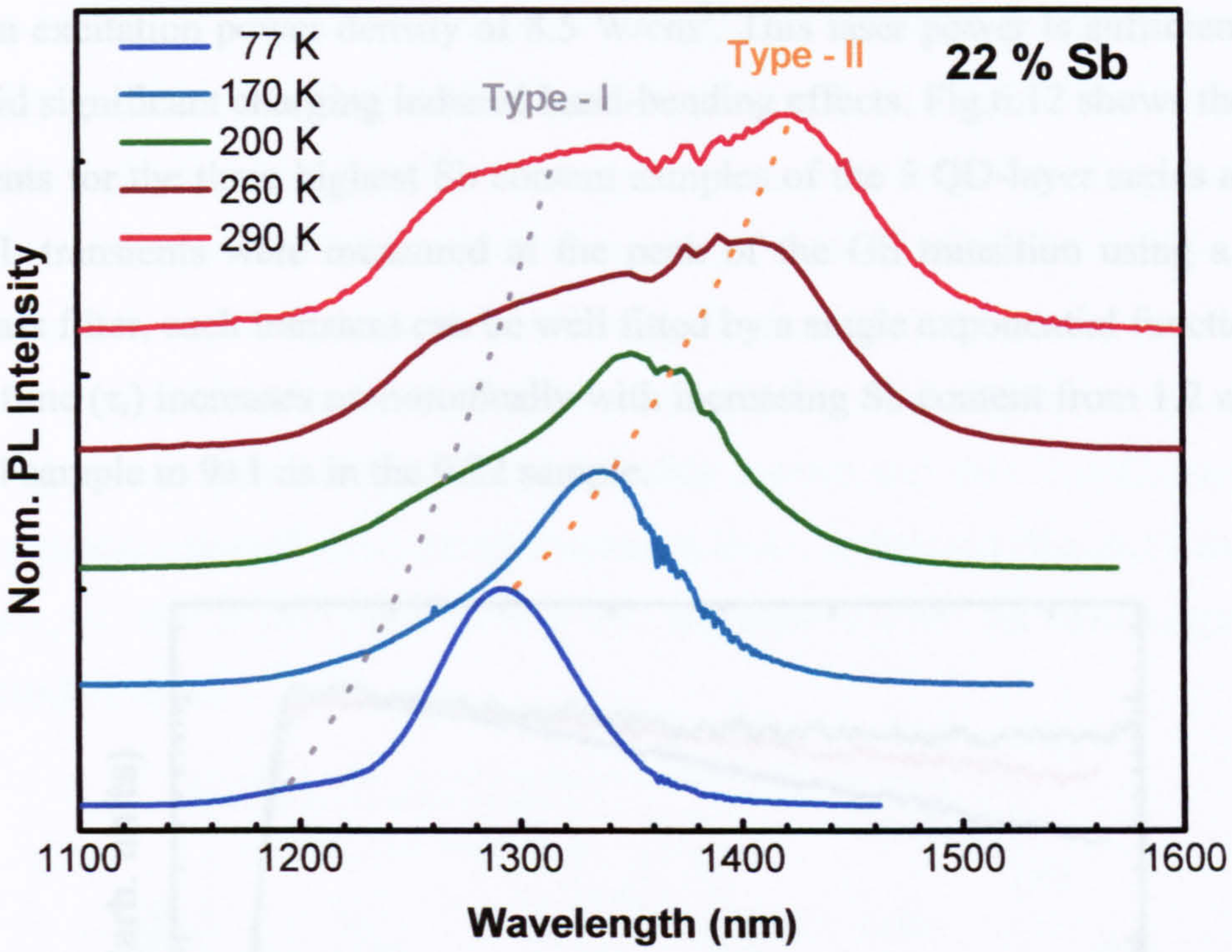

Fig. 6.11 Normalised temperature dependent PL spectra, excited using a 5 mW HeNe laser, of a 5-QD layer structure containing $GaAs_{1-x}Sb_x$ SRLs with x=0.22.

At 77 K, the emission from the type-II transition dominates the spectrum. As the temperature increases, holes begin to be thermally promoted from the HH GS in the GaAsSb SRL to the lowest energy hole state in the QDs and excited hole states in the GaAsSb SRL, as depicted in the schematic diagram of Fig. 6.7. Although the population of the holes in the HH GS of the QDs cannot exceed that of the HH GS in the GaAsSb SRL, it is feasible that the greater oscillator strength of the type-I transition may result in approximately equal emission intensities for the type-I and type-II transitions.

6.5.5 Time resolved PL of GaAsSb capped InAs QDs

The spatial separation of the electron-hole pairs involved in a type-II transition should result in a longer radiative recombination lifetime (τ_r), since this is proportional to the square of the overlap integral of the electron and hole (e-h) wavefunctions. τ_r can be extracted from the decay transients obtained in TR-PL measurement at low temperature, where non-radiative recombination is assumed to be negligible. Such measurements were performed by Yudong Jang (Chungnam University, South Korea) using a mode locked Ti:Sapphire laser, tuned to 740 nm,

with an excitation power density of 8.5 W/cm^2. This laser power is sufficiently low to avoid significant charging induced band-bending effects. Fig.6.12 shows the decay transients for the three highest Sb content samples of the 5 QD-layer series at 10 K. The PL transients were measured at the peak of the GS transition using a 10 nm bandpass filter, each transient can be well fitted by a single exponential function. The decay time (τ_r) increases monotonically with increasing Sb content from 1.2 ns in the x=0.14 sample to 9±1 ns in the 0.22 sample.

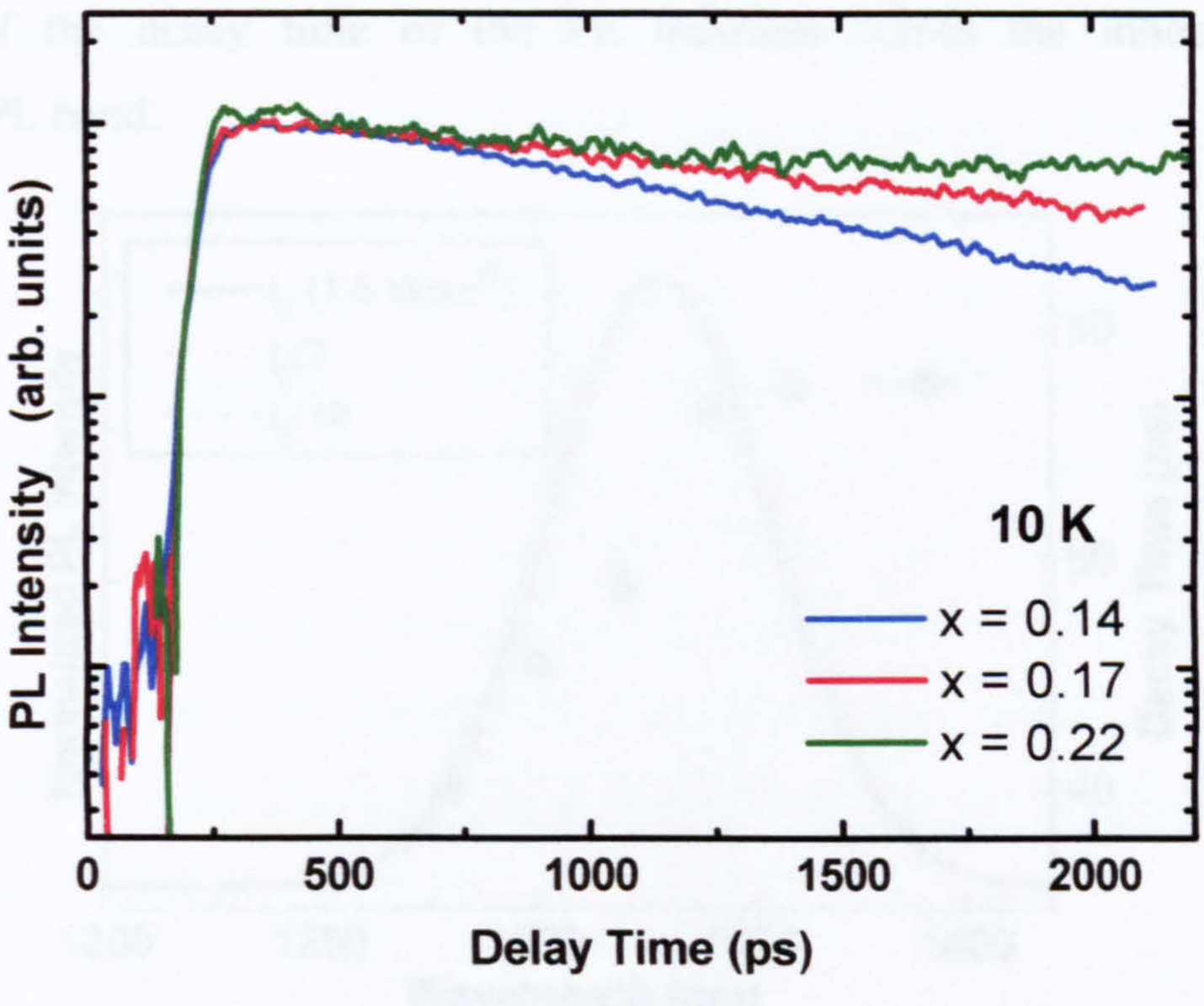

Fig. 6.12 10 K decay transients, detected at the PL peak, for three 5-QD layer samples containing $GaAs_{1-x}Sb_x$ SRLs.

This dependency is consistent with a decrease in the e-h wavefunction overlap due to the formation of a type-II system with increasing Sb content. In the x=0.17 sample, the QD/GaAsSb SRL hetero-junction is expected to be weakly type-II (~3 meV blueshift with increasing excitation density when the incident laser power is varied between 1 and 100 mW). Hence, although the hole wavefunction may be mostly localised in the GaAsSb SRL, the expected small valence band offset will allow significant hole wavefunction penetration into the QDs and therefore a significant overlap with the QD GS electron wavefunction, perhaps aided by the attractive e-h Coulomb interaction. However, even the relatively long τ_r of 9 ns is shorter than those reported for similar low-dimensional GaAsSb systems. For example, in a GaAsSb/GaAs single QW structure τ_r was determined to be ~15 ns [34]

and in GaSb/GaAs QDs a long-lived component of ~23 ns was found[35]. This relatively low enhancement for the present type-II system suggests that the electron and hole remain close together, a conclusion supported by magneto-optical measurements of the spatial extent to the exciton size presented in the next section.

In fact, due to the type-II band line-up in the x=0.22 % structure, τ_r has been shown to be sensitive to the excitation power density used. Further measurements, using a time correlated single photon counting system and low (5 MHz) repetition rate excitation, allowed much lower excitation levels to be used. Fig. 6.13 shows the variation of the decay time of the PL transient across the inhomogeneously broadened PL band.

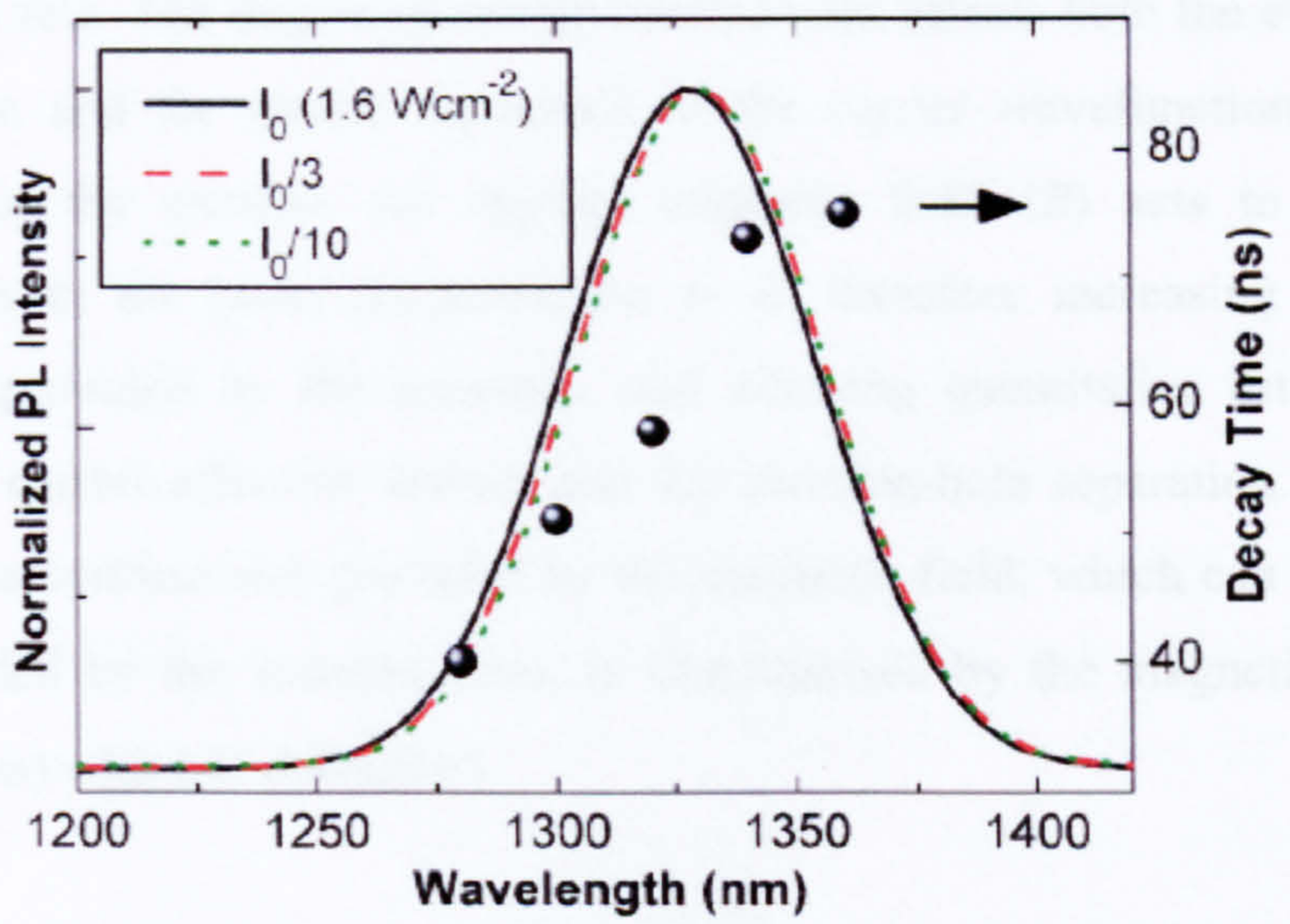

Fig. 6.13 Detection energy dependence of the decay time (solid symbols) for the x=0.22 $GaAs_{1-x}Sb_x$ SRL structure, measured at 17 K. PL spectra, recorded at different excitation densities are shown by the solid and dashed lines.

The longer decay times, measured using this system, represent the true radiative lifetime of the GS exciton in the type-II sample. τ_r increases from 40 to 75 ns as the detection energy is moved across the emission band[36]. The increase in τ_r with decreasing emission energy is most likely to be the result of compositional fluctuations in the GaAsSb capping layer, which is consistent with the broader FWHM of the PL of this sample compared to the type-I structure. In addition, variations in the QD size may also affect the extent of the electron and hole wavefunction overlap. Smaller, higher GS energy QDs are expected to have electron

wavefunctions which penetrate further out of the QD into the GaAsSb SRL and therefore have a greater overlap with the hole wavefunction in the SRL.

6.5.6 Low dimensional semiconductor structures in magnetic fields

Magneto-PL experiments are a useful technique for obtaining valuable information about the confinement environment of the carriers in low-dimensional semiconductor structures. Such measurements have been used to examine a wide range of physical effects in QDs, for example the Zeeman effect[37], the relationship between lateral confinement and exciton binding energy[38, 39], the electronic coupling of confined states[40] and the influence of substrate orientation on QD formation[41, 42], to name but a few. The degree of carrier confinement affects both the effective mass of the exciton and the spatial separation of the carrier wavefunctions, hence the spatial size of the exciton. An applied magnetic field (B) acts to localise the wavefunctions in the plane perpendicular to B, therefore increasing the intrinsic confinement provided by the structure, and allowing quantitative estimates to be made for the carrier effective masses and the electron-hole separation. The relative strength of the confinement provided by the magnetic field, which can be compared to that provided by the nanostructure, is characterised by the magnetic length (ℓ_0) (Larmor radius) which is defined by

$$\ell_0 = \sqrt{\hbar / eB} \qquad \text{(Eq. 5.13)}$$

The magnetic length decreases with increasing field, with a value of 8.2 nm reached at a field of 10T. At low fields ℓ_0 is larger than the relevant dimension of the structure and hence both electrons and holes are strongly spatially confined by the physical boundaries of the structure. In this *diamagnetic* regime, the applied field causes only a small perturbation to the energy levels of the electron and hole states in the QDs, which are blueshifted by

$$\Delta E_{e,h} = \frac{e^2 \left\langle \rho_{e,h}^2 \right\rangle B^2}{8 m_{e,h}} \qquad \text{(Eq. 5.14)}$$

where $\sqrt{\langle \rho_{e,h}{}^2 \rangle}$ and $m_{e,h}$ are the electron (hole) effective radius and mass respectively in the plane perpendicular to B[43]. When ℓ_0 becomes less than the smallest in-plane

dimension of the QD, the cyclotron energy associated with the field overcomes the Coulomb energy of the exciton and the energy varies linearly with B, equivalent to the lowest Landau level with a correction for the exciton binding energy:

$$\Delta E_{e,h} = \frac{\hbar eB}{2\mu^*} \qquad \text{(Eq. 5.15)}$$

where μ^* describes the reduced exciton effective mass. By combining Eqs 5.14 and 5.15 in the relevant limits, the PL peak position (E_{PL}) can be fitted as function of B

$$E_{PL} = E_{PL}^0 + \frac{e^2\langle\rho^2\rangle}{8\mu}B^2 \quad \text{for } B < \frac{2\hbar}{e\langle\rho^2\rangle} \qquad \text{(Eq. 5.16)}$$

$$E_{PL} = E_{PL}^0 - \frac{\hbar^2}{2\mu\langle\rho^2\rangle} + \frac{\hbar eB}{2\mu} \quad \text{for } B > \frac{2\hbar}{e\langle\rho^2\rangle} \qquad \text{(Eq. 5.17)}$$

where E_{PL}^0 is the PL peak energy at B=0 and $\sqrt{<\rho^2>}$ is the effective electron and hole radii. The combining of the separate diamagnetic shifts (Eq. 5.14) for the electron and holes into a single term in equations 5.16 and 5.17 requires the assumption that the effective electron and hole radii are identical. This is probably a reasonable assumption for type-I dots where both electron and hole wavefunctions are confined within the dot but may not hold for type-II dots[43]. When the effective radii are different the particle with the larger radius will reach the high field limit first and the effective mass initially measured in the high field limit will be that of this particle[43]. In addition, where the electron and hole wavefunction extents are appreciably different it would seem that the values of $\sqrt{<\rho^2>}$ in equations. 5.16 and 5.17 are not necessarily the same, with the value in the latter representing the exciton length scale. In the present system, as discussed below, there is little evidence that the high field limit is reached, even for the highest fields used of 50T. Hence the complication of different electron and hole radii can largely be ignored.

The transition from a quadratic to linear behaviour occurs at $B_{tr,}=\frac{2\hbar}{e\langle\rho^2\rangle}$

where $\ell_0 = \sqrt{\langle\rho^2\rangle/2}$. Given that dc superconducting magnets have a maximum field strength of ~25 T, the high field regime may only be reached for structures in which

$\sqrt{<\rho^2>}$ is greater than ~7.5 nm. This is typically larger than $\sqrt{<\rho^2>}$ for InAs QDs[44, 45] and so the linear shift should not be observed using such systems. Only pulsed magnets, with peak fields of ~50 T, are able to produce confinement lengths comparable with the excitonic extent in QDs and narrow QWs. Such systems are hence required to fully probe the properties of these nanostructures.

6.5.6.1 Experimental Details

PL measurements in pulsed magnetic field were conducted in the Pulsed Field Group at the Katholieke Universiteit of Leuven, under the direction of Dr Manus Hayne and with the assistance of Thomas Nuytten. PL was performed at 4.2 K in pulsed magnetic fields of up to 50 T. The sample surface was oriented relative to the field such that B was directed either parallel ($\|$) or perpendicular ($\perp$) to the growth direction (z). These configurations are referred to as the Faraday and Voigt geometries respectively. The PL was excited using a frequency doubled neodymium:yttrium-aluminium-garnet laser (532 nm) via an optical fibre with a core diameter of 200 μm. Six surrounding optical fibres collected the PL and fed it into a 30 cm monochromator, where it was dispersed and detected by a LN_2 cooled InGaAs array. Pulsed field coils coupled to a 5 kV, 600 kJ capacitor bank delivered 22 ms pulses, during which time 10-20 spectra could be acquired, depending on the integration time of the InGaAs array (itself determined by the optical efficiency of the sample).

6.5.6.2 Objectives of magneto-PL measurements on type-II QDs

Low temperature (4.2 K) magneto-PL measurements were performed, in both Faraday and Voigt geometries and with various excitation levels (20 – 700 mW), on both series of samples to examine the effect of increasing Sb content on the spatial extent of the GS wavefunctions. In the Faraday configuration, where the lateral size of the wavefunctions is probed, the spatial extent of the hole wavefunction is expected to increase as the system becomes type-II (i.e. when $x \geq 0.14$) due to the motion of the holes now being unconfined in the plane of the GaAsSb QW.

As a further consequence (and verification) of the type-II nature of the higher Sb content samples, a change in the in-plane value extracted for $\sqrt{<\rho^2>}$ with incident

laser power may also be expected. The charge imbalance across the hetero-interface that produces the band-bending may act to screen the Coulomb interaction between the QD-bound electron and the holes in the GaAsSb QW, resulting in a reduction of the exciton binding energy (E_B) and an extension of $\sqrt{<\rho^2>}$, presumably for the holes as they are able to move further from the QD. Alternatively, the optical pumping of the QDs with electrons may increase the attractive Coulomb force between the bound electron and delocalised hole, therefore increasing E_B and reducing $\sqrt{<\rho^2>}$. The interplay between the carrier-carrier interaction energies and the screening length will determine how E_B and $\sqrt{<\rho^2>}$ vary with carrier density. In type-II GaSb/GaAs QDs for example, the optical charging of the QDs with *holes* is posited to increase the binding energy of the type-II exciton[46]. If this effect exists for the InAs/GaAsSb QDs studied in this chapter it is unlikely to be so pronounced, since there are fewer electron states – the confined carrier in this system – than hole states in the GaSb QDs[47]. Nonetheless, the presence, or otherwise, of these effects can be confirmed by comparing the changes in diamagnetic shift (ΔE_{PL}) of a type-I and type-II sample for different excitation levels. It is expected that ΔE_{PL} in the type-I structure will display little dependence on the excitation intensity, whereas in contrast, the type-II structure(s) should be sensitive to changes in carrier density. The x=0.22, 5-layer sample was deemed a suitable choice for studies of a type-II structure.

6.5.6.3 Magneto PL at 6K in the Faraday Geometry (500 mW)

Fig. 6.14 shows several PL spectra of the control InGaAs SRL sample (Rm 2027) using a laser power of 500 mW in the Faraday geometry. Each spectrum was obtained over a 0.5ms interval during one 22ms field pulse, or 'shot'. The field variation for any particular spectrum is less than ±3%. Short acquisition times, which allow more spectra to be taken per shot, could only be used on the brighter, low Sb content ($x \leq 0.14$) samples.

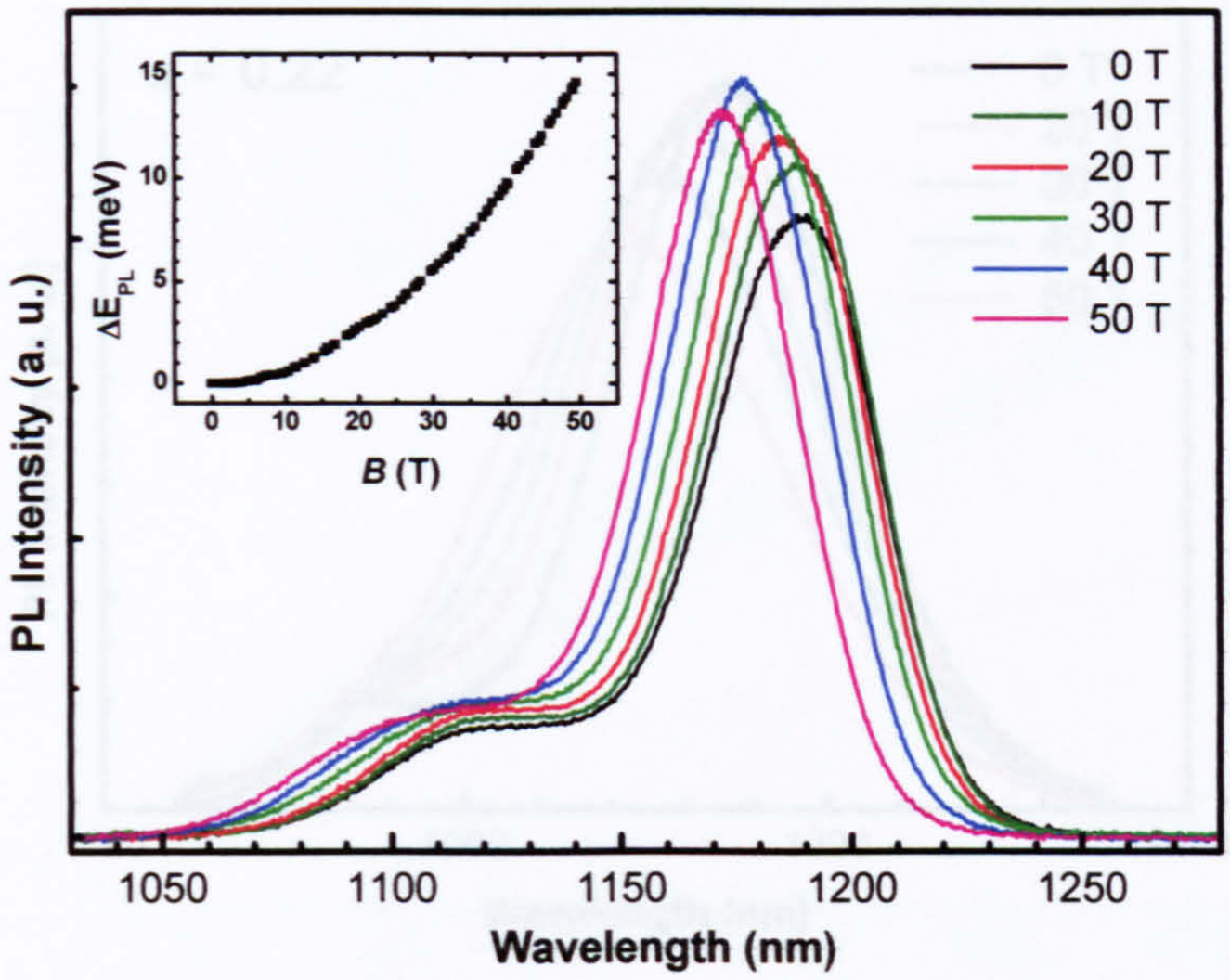

Fig. 6.14 6 K Magneto-PL spectra of the InGaAs SRL reference sample using an incident laser power of 500 mW. The spectra were acquired at various times during the 22 ms *B*-field pulse. The PL peak shifts (ΔE_{PL}) from B=0 T are plotted as a function of B in the inset.

The PL spectra exhibit a blueshift with increasing B and there is a slight increase in the peak PL intensity. Although the variation in the PL intensity with B will not be described quantitatively some of the physical processes responsible will be discussed briefly in section 6.5.6.5 In the inset to Fig. 6.14, the change in the PL peak energies (ΔE_{PL}) are plotted as a function of B between B=0 and 50 T.

The PL spectra of the x=0.22 Sb sample are shown in Fig. 6.15, also recorded over the full range of accessible B values during a single shot at a laser power of 300 mW. Only a single spectrum was able to be acquired during each magnet shot, due to the weaker emission in this sample.

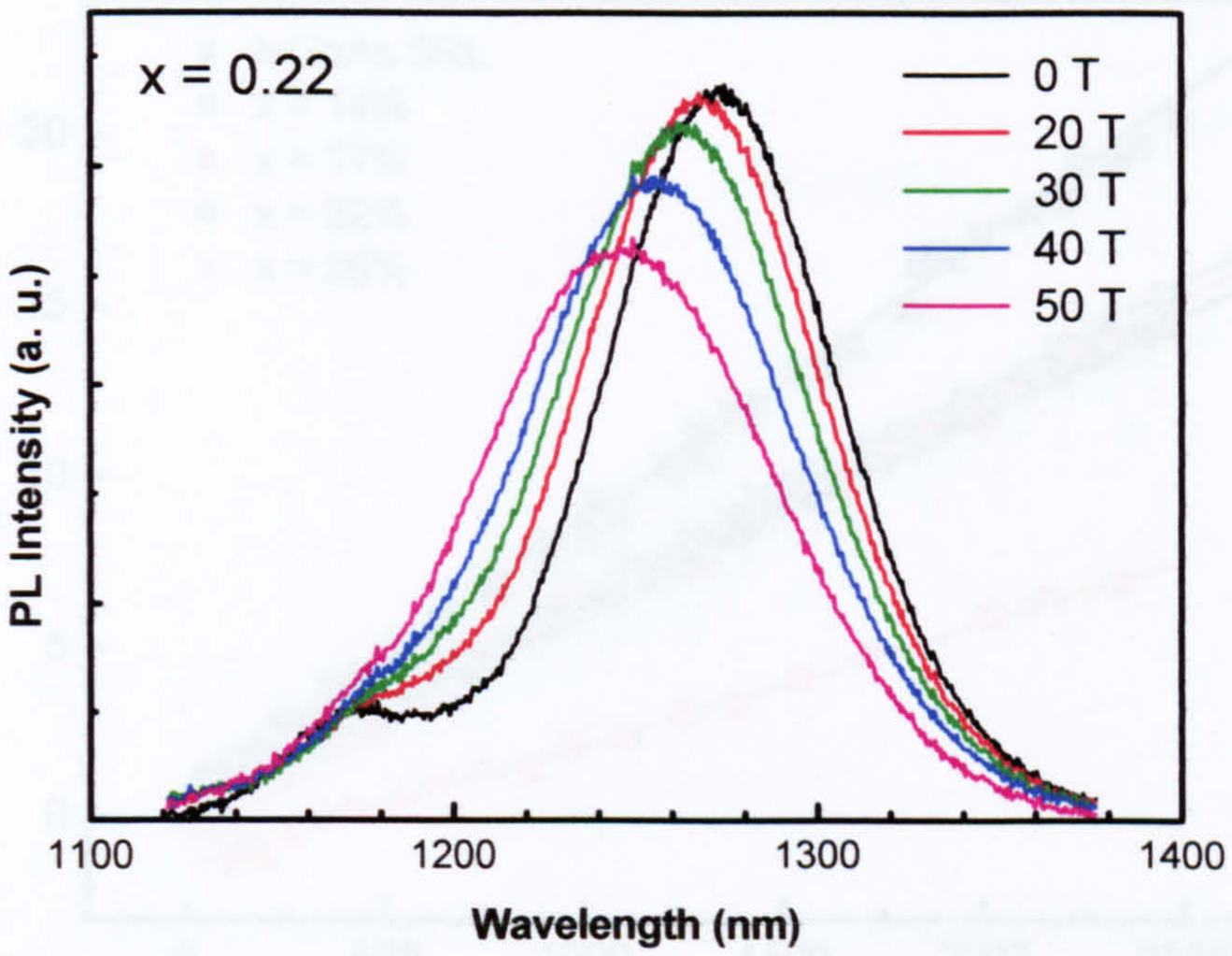

Fig. 6.15 6 K Magneto-PL spectra of the 5 – QD layer $GaAs_{1-x}Sb_x$ SRL sample with x=0.22.

In Fig. 6.16, ΔE_{PL} is plotted as a function of B^2. A linear dependence of ΔE_{PL} on B^2 is observed for all samples over the entire 0 – 50 T field range, indicating that the behaviour remains diamagnetic up to the highest fields available (the straight lines in Fig 6.16 are guides to the eye). Only by observing the transition to a sub-linear dependence on a B^2 plot is it possible to determine $\sqrt{\langle\rho^2\rangle}$ independently of μ. Since this cannot be obtained for the present samples, the current results allow only an upper limit to be placed on the in-plane value of $\sqrt{\langle\rho^2\rangle}$. Substituting $B = 50$ T into Eqns 5.16 and 5.17 yields $\sqrt{\langle\rho^2\rangle}|_{max} \approx 5.1$ nm, for all the samples. Hence even in the type-II QDs the hole, which is expected to be in the GaAsSb layer, is strongly localised.

It can also be seen that the overall trend in the behaviour is very similar for all the samples containing <18% Sb in the SRL, implying that $\sqrt{\langle\rho^2\rangle}$ and μ remain fairly constant with increasing Sb content until x=0.18.

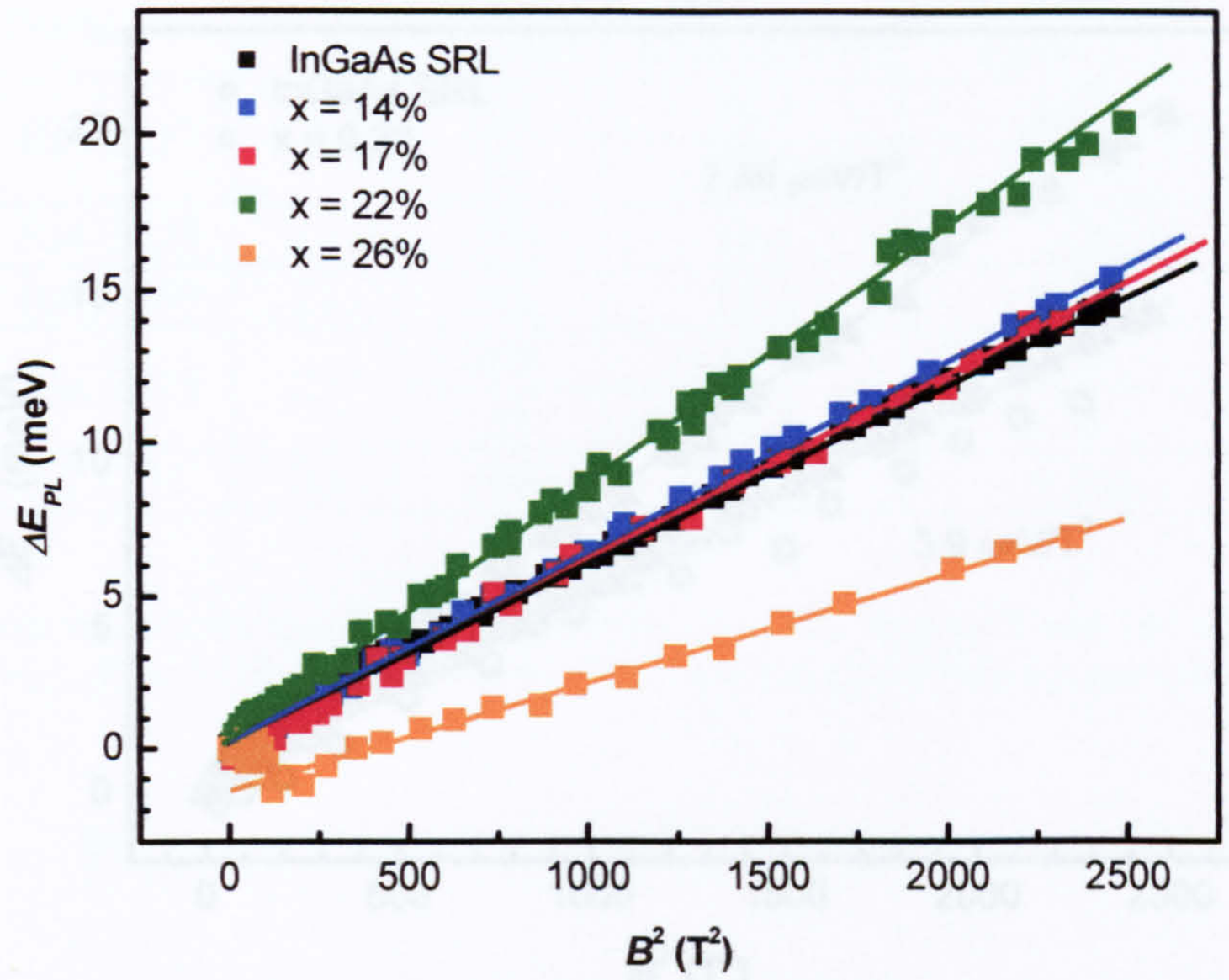

Fig. 6.16 6 K diamagnetic shift (ΔE_{PL}) of the 5 – QD layer $GaAs_{1-x}Sb_x$ SRL samples plotted as a function of B^2. The solid lines are guides to the eye.

However, when x ≥ 0.18, the trend in the dependence of ΔE_{PL} on B^2 varies non-systematically with increasing x. ΔE_{PL} is greater in the x=0.22 structure than for the lower Sb content samples, for all B. Yet when x=0.26, ΔE_{PL} reduces to approximately half of the value in the x ≤ 0.18 sample at any corresponding value of B. Again the fact that for no sample is a sub-linear $\Delta E_{PL} - B^2$ dependence observed, implies that the samples remain in the low field regime up to at least 50 T, indicates the presence of strong spatial hole localisation in the type-II structures. As will be discussed in 6.5.6.5, it may be necessary to invoke inhomogeneity of the GaAsSb in order to explain the anomalous trend in the $\Delta E_{PL} - B$ dependence with increasing x.

6.5.6.4 Excitation dependence of diamagnetic shift (Faraday)

Fig. 6.17 compares ΔE_{PL} for the InGaAs SRL and 22% Sb structures as a function of B^2 in the Faraday geometry and for two different laser excitation levels: 20 and 300 mW. The dependencies are diamagnetic over the full field range for both structures at both excitation levels. Since ΔE_{PL} can be considered to be purely diamagnetic, the diamagnetic coefficient ($\gamma_{Dia} = e^2\langle\rho^2\rangle/8\mu$) can be extracted from the gradient of the plot.

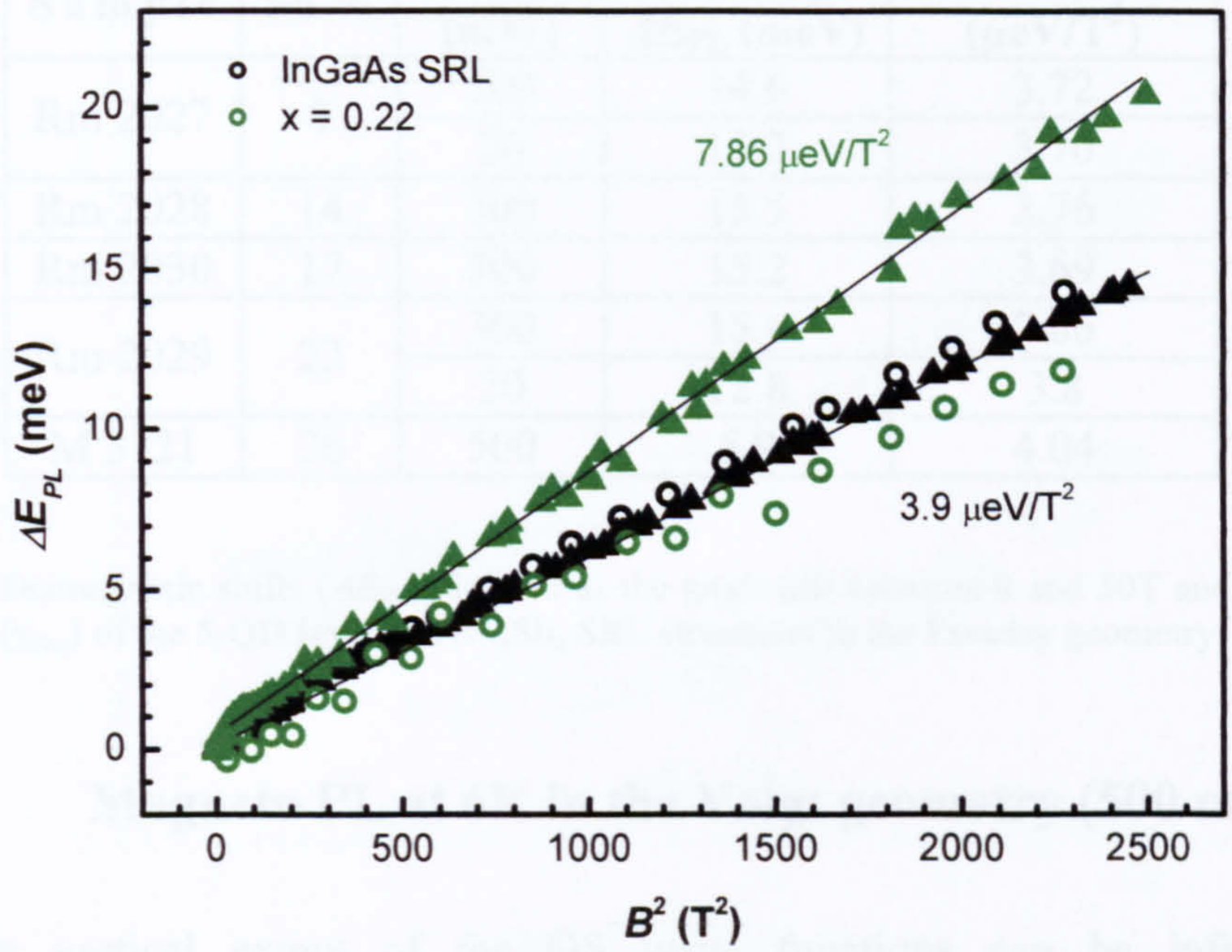

Fig. 6.17 6 K laser power dependent diamagnetic shift (ΔE_{PL}) of the 5- QD layer $GaAs_{0.78}Sb_{0.22}$ SRL sample and the InGaAs SRL reference sample plotted as a function of B^2. Circles and triangles correspond to laser powers of 20 and 300 mW respectively.

For the InGaAs SRL sample, γ_{Dia} displays a negligible dependence on photoexcited carrier density, remaining constant at ~3.7 μeV/T^2. This is not the case for the x=0.22 Sb sample, in which γ_{Dia} undergoes a two-fold increase from 3.8 to 7.9 μeV/T^2 as the power is increased from 20 to 300 mW. Within an exciton model confinement influences both $\sqrt{<\rho^2>}$ and μ, with stronger confinement decreasing $\sqrt{<\rho^2>}$ and increasing μ^*, both of which lead to a decrease in γ_{Dia}[48]. This suggests that increasing the photoexcited carrier density weakens the effective electron-hole attraction, possibly by screening the Coulomb interaction between the electron and hole. A reduction in the Coulomb interaction was cited to account for a similar trend, observed in type-I InAs/GaAs QDs under high excitation[45], which is not seen for the present InGaAs capped QDs. The diamagnetic shift between 0 and 50T and diamagnetic coefficients are listed for all the investigated samples in the Faraday geometry in Table 6.18

Sample	Sb %	Power (mW)	Faraday ΔE_{PL} (meV)	Faraday γ_{Dia} ($\mu eV/T^2$)
Rm 2027	0	500	14.6	3.72
		20	15.2	3.70
Rm 2028	14	500	15.5	3.76
Rm 2030	17	500	15.2	3.69
Rm 2029	22	300	15.4	7.86
		20	12.8	3.8
M 3121	26	500	6.9	4.04

Table. 6.18 Diamagnetic shifts (ΔE_{PL}), defined as the total shift between 0 and 50T and diamagnetic coefficients (γ_{Dia}) of the 5-QD layer $GaAs_{1-x}Sb_x$ SRL structures in the Faraday geometry.

6.5.6.5 Magneto PL at 6K in the Voigt geometry (500 mW)

The vertical extent of the GS wave functions can be inferred from measurements of ΔE_{PL} as a function of B, where B is applied in the QD plane (Voigt geometry). Since the QD (and GaAsSb QW) height is less than the lateral size of the QDs, the carriers are more strongly confined in this direction. As stated in section 6.5.6.4, increased confinement is associated with a lower γ_{Dia}. On inspection of Fig. 6.19 it is therefore not unexpected that between 0 and 50 T, ΔE_{PL} is >50% smaller for this field orientation (for the type-I samples). The corresponding diamagnetic shifts and coefficients are listed in Table 6.20 for the reference InGaAs and GaAsSb capped samples. As in the Faraday geometry, a diamagnetic shift is observed up to the highest applied field of 50T.

What is most surprising about the Voigt geometry data, however, is the ΔE_{PL} – B dependence of the higher Sb content type-II samples (17, 22 and 26% Sb), which all show an unexpected *red*shift of the PL energy between 0 and ~25 T, before exhibiting the expected blueshift at higher fields. At 25 T, E_{PL} is ~2 meV less than E_{PL}^0 for all three samples. This unusual behaviour has been noted previously in studies of type-I InAs/GaAs QDs[49], but no explanation was offered. In contrast, the present type-I structures (samples with the InGaAs SRL and an Sb composition of 14%) exhibit the expected blue shifting diamagnetic behaviour over the full field range. The 26% Sb sample also shows the same behaviour in the Faraday geometry (see Fig. 6.18), exhibiting a pronounced minimum at ~ 12 T followed by a diamagnetic blue shift at higher fields.

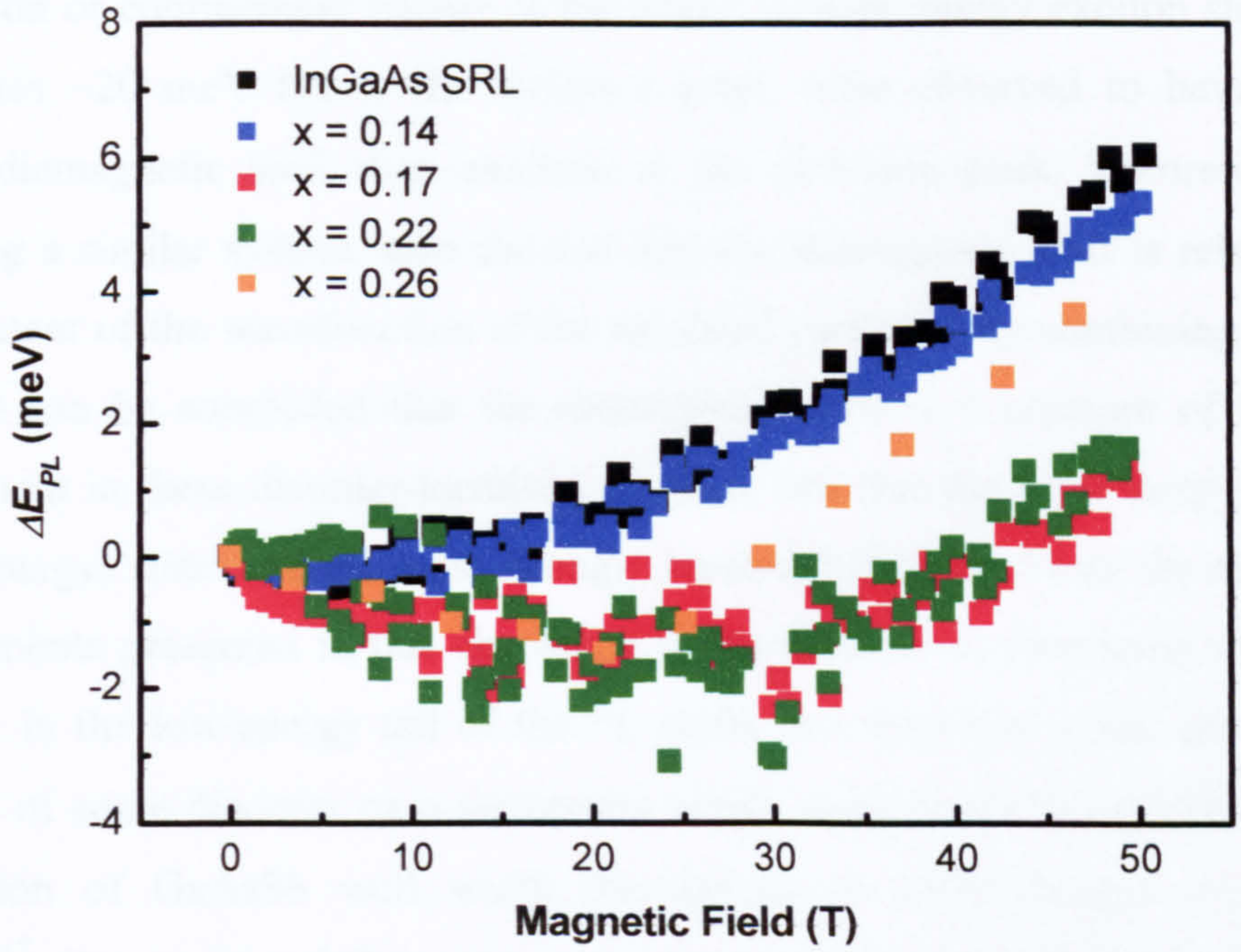

Fig. 6.19 6 K Voigt geometry magnetic field shift (ΔE_{PL}) of the PL energy for 5 – QD layer samples, capped with $GaAs_{1-x}Sb_x$ SRLs ($0.14 \leq x \leq 0.26$). A negative ΔE_{PL} is observed between 0 and 25 T when $x \geq 0.17$. Data for the reference sample with the InGaAs SRL is also shown.

Whilst this behaviour is not well understood, it may be related to the non-systematic change in γ_{Dia} with increasing Sb fraction in the Faraday geometry (see Fig 6.16). Since the observed change in γ_{Dia} between the 22% Sb and 26% Sb samples is the opposite of what is expected, ie. γ_{Dia}[26% Sb] < γ_{Dia}[22% Sb], the onset of strong carrier localisation effects may be important in the high Sb composition structures.

Sample	Sb %	Power (mW)	Voigt ΔE_{PL} (meV)	Voigt γ_{Dia} ($\mu eV/T^2$)
RM 2027	0	500	6.0	4.15
RM 2028	14	500	5.3	4.37
RM 2030	17	500	1.3	-
RM 2029	22	500	1.6	-

Table. 6.20 Diamagnetic shifts (ΔE_{PL}) and coefficients (γ_{Dia}) of the 5-QD layer $GaAs_{1-x}Sb_x$ SRL structures, measured between 0 and 50T, in the Voigt geometry.

Magneto – μPL studies of disorder localised excitons in GaAs/AlGaAs QWs reveal that there is a positive correlation between the in-plane γ_{Dia} and the

localisation or confinement energy of the state[50]. Lower energy exciton states, lying at energies ~20 meV below the emission peak, were observed to have a ~50% smaller diamagnetic shift than excitons at the emission peak. Theoretical work, modelling a similar system, also showed that the diamagnetic shift is related to the lateral extent of the wavefunction of the localised carrier[51]. By combining these two results it can be concluded that the diamagnetic shift is a measure of the lateral confinement in these disorder-localised systems, and that the more deeply confined (lower energy) states are the most strongly localised laterally. From the macro – PL measurements presented in this chapter, it is not possible to determine whether the emission in the low-energy tail of the PL shifts less than that at the peak, but the presence of some disorder on a nanometre length scale is not inconsistent with the observation of GaAsSb well width fluctuations in TEM images of a similar structure[17]. Compositional fluctuations are also possible, although these have not yet been studied. TEM investigations, performed in the E&EE department in Sheffield, indicate that the GaAsSb capping layer does not cover the larger QDs entirely (see Fig. 6.21) in the single layer sample with x=0.26.

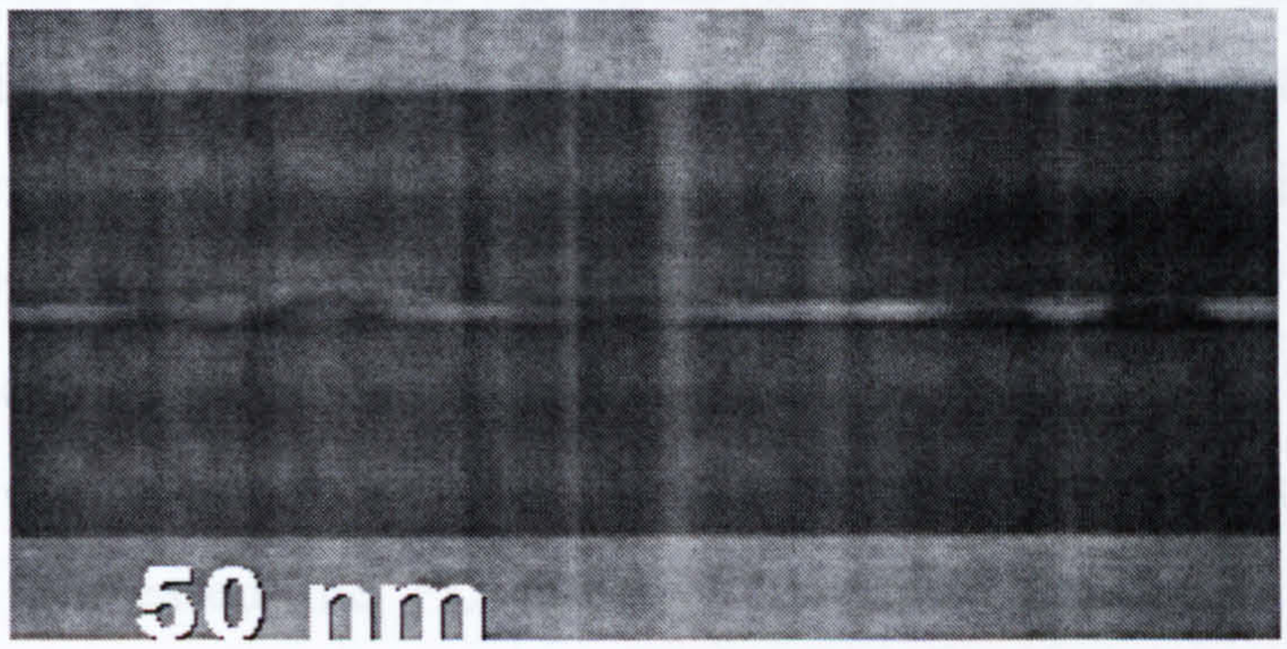

Fig. 6.21 Dark field cross-sectional TEM image of a single-QD layer sample with a $GaAs_{0.74}Sb_{0.26}$ SRL. The in-plane coverage of the SRL is seen to be non-uniform.

It is likely that this incomplete coverage of the QDs is a result of the enhanced lattice mismatch between these larger QDs and the GaAsSb capping material, initiating the migration of the capping material away from the apex of the QD. As has been mentioned previously, the Sb composition depends critically on the growth temperature. In fact, this sensitivity to the growth temperature extends to the final QD/capping layer configuration, as shown in a recent cross-sectional STM study of samples grown in the same reactor as the present structures[16]. For a sample

in which the QDs (grown at 500°C) were capped with GaAsSb at 475 °C, the GaAsSb layer was found to be continuous, fully covering the QDs. When the capping took place at 500 °C however, the deposited GaAsSb is able to migrate away from the top of the QDs, thereby minimising the strain, and the QDs are not fully capped. Hence there is some evidence for GaAsSb well width fluctuations in the high Sb composition structures and it appears likely that the diffusion of material away from the top of the QDs may result in significant compositional fluctuations. Both may act to increase the hole localisation, explaining the reduced diamagnetic shift observed for the highest Sb composition (Fig. 6.16). Again, however, the hole must be localised close to the QD given the relatively high PL efficiency of the structures.

The magnetic field behaviour of the PL intensity also displays a dependence on the Sb composition. For the reference InGaAs SRL sample the PL intensity increases slightly as the field increases from 0 to 50 T (Fig. 6.14). However for the GaAsSb capped QDs, not only does the size of the increase in the PL intensity between 0 and 50 T decrease with increasing Sb% in the Faraday geometry, but for x = 0.22 and 0.26 the PL intensity actually decreases with applied field (see Fig. 6.15). In low temperature (2K) magneto-PL studies of InAs/GaAs QD ensembles it was found that application of a magnetic field in the Faraday geometry caused a reduction in the PL intensity and that this reduction became stronger as the QD density decreased[52]. This behaviour was explained by the magnetic field increasing the localisation of carriers in potential fluctuations in the wetting layer, hence reducing the probability of transport to the QDs. In contrast, above 100K the application of a magnetic field increased the PL intensity, this was attributed to a magnetic confinement of the exciton wavefunction which increases the probability of carrier capture by the dot and also reduced the radiative lifetime due to the smaller exciton volume. The results for the present high Sb composition structures are hence consistent with the low temperature behaviour of the InAs/GaAs QDs, again suggesting that carrier localisation by potential minima in the GaAsSb layer may be significant. It is not clear, however, why the low Sb structures and the reference InGaAs SRL structure behave so differently. If potential minima in the InAs wetting layer and GaAsSb (low Sb composition) or InGaAs SRL were very weak then it is possible that the effects observed by Larsson et al[52] at high temperatures may be

observed at low temperatures, although it seems unlikely that the fluctuations would be that weak.

6.5.6 Carrier wavefunction locations in type-II InAs/GaAsSb QDs

In previous sections evidence has been presented for the formation of a type-II system for Sb compositions above ~17%. In such systems there is potential for a very large electron – hole separation, with the electron tightly confined in the QDs but with the hole able to reside in the GaAsSb layer above the wetting layer and between the QDs. However, despite the relatively long radiative lifetime (~ 60 ns) of the type-II structure, the magneto-optical studies imply that the hole is strongly localised close to the QDs.

One possible mechanism for this hole localisation is the Coulombic attraction by the electron which has been suggested to occur in GaSb/GaAs self-assembled QDs However a possible stronger mechanism in the present system is a spatial modulation of the strain state of the GaAsSb layer. The very thin nature of the wetting layer deposited between the QDs will result in the GaAsSb being grown on a matrix with essentially the GaAs lattice constant. This will give a compressive strain in the GaAsSb. In contrast the relaxation back towards the lattice constant of InAs towards the top of the QDs will result in the GaAsSb deposited above the dots having a tensile strain. This spatial modulation of the strain will result in a potential minimum above the dots, acting to localise the holes in this region. This mechanism would hence explain the strong localisation of the holes close to the QDs. This is a rather simplistic model and the situation in the real structures is likely to be much more complicated. For example structural studies (including the TEM studies discussed above) have shown that the GaAsSb SRL does not always completely cover the QDs[15] and it is possible that the Sb content of the layer is also spatially modulated. A full understanding of this behaviour hence requires detailed structural studies of the form of the GaAsSb layer, followed by calculations of the electronic band structure using these structural results as input parameters.

6.6 QD Laser structures containing GaAsSb SRLs

6.6.1 Laser characterisation of low antimony content SRL structures (x=0.14)

As was determined in 6.4.5, a Sb fraction of 0.14 in the $GaAs_{1-x}Sb_x$ is optimum for intense 1.3 μm emission from the underlying InAs QDs. Therefore, a number of 5 layer laser structures were grown that contained active regions with approximately x=0.14 Sb in the SRL. Due to the previously mentioned complications with the reactor, the control of the growth was not optimal, hence the growth recipes were repeated, with minor adjustments being made between the growth of each sample. As before, 3 ML of InAs was deposited directly on GaAs to form the QDs. These were covered with 6nm of $GaAs_{0.86}Sb_{0.14}$ (SRL) at the same growth temperature (~510 °C). 50nm GaAs High Growth Temperature Spacer Layers were used to separate the QD/SRL layers. A reference structure was also grown in which the SRLs were composed of $In_{0.15}Ga_{0.85}As$. In all other respects the design of the devices was identical. The design of the AlGaAs waveguiding/cladding layers for all structures followed that described in chapter 3, section 3.3.1. From these wafers, optical access mesas and 5 and 3 mm laser cavities were processed as described previously.

The main part of Fig. 6.22 shows the below and above threshold EL from a 5 mm cavity of a $GaAs_{1-x}Sb_x$ capped device at RT and 130 °C. The lasing wavelength at RT (25 °C) is 1294 nm and the cw J_{th} is 78 A/cm^2. The high material quality of this particular device is evident from the persistence of GS lasing up to 130 °C in pulsed mode.

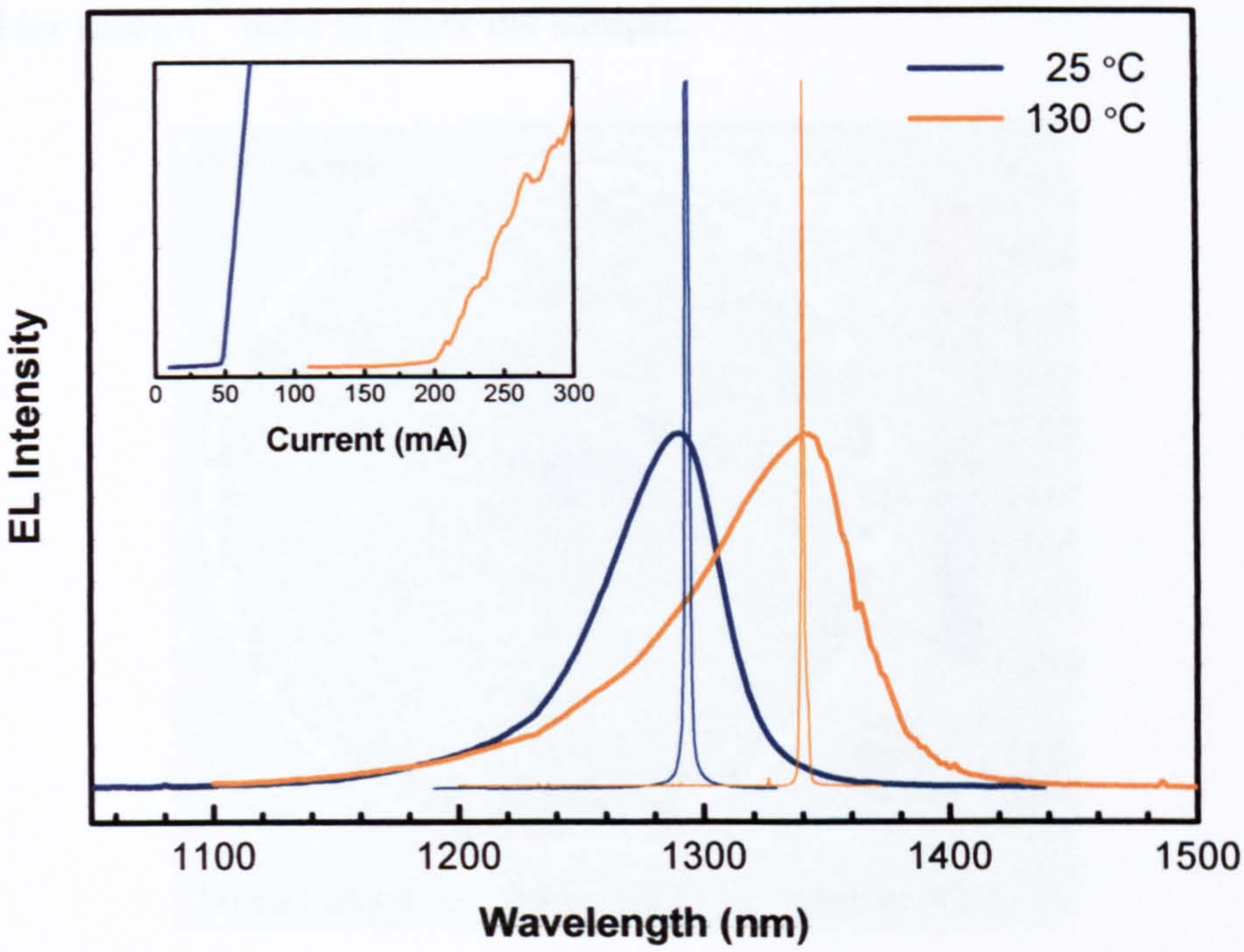

Fig. 6.22 Sub – threshold and lasing EL spectra taken from a 5 mm, 5 – QD layer $GaAs_{1-x}Sb_x$ capped QD laser structure. Inset shows the LIs at the corresponding temperatures

However, this good performance does not extend to all devices fabricated from this wafer, as deduced from the markedly inferior characteristics of the 3 mm device (see Table 6.25). Although the J_{th}'s may be expected to be slightly increased in this shorter cavity structure, the absence of cw lasing at RT and twofold increase in the pulsed RT J_{th} cannot result purely from the increased mirror losses. It will now be shown that the inconsistency in these laser results is not unique to this sample but is likely to be due to spatial inhomogeneities within the growth of individual Sb containing wafers.

A PL mapping study of all the samples grown in this series reveals that there are large fluctuations in PL peak wavelength and intensity across the wafer, which may be spatially correlated with in-plane non-uniformities in the growth. The results of a RT PL map of M 3116 are displayed in Fig. 6.23, where the PL peak wavelength is plotted as a function of the spatial position across the wafer. The wavelength varies between ~1250 and 1300 nm, with the longer wavelength region occurring along the perimeter of half of the wafer. The pattern of the spatial variation in the PL peak wavelength suggests that a spatial variation in the temperature profile across the wafer is responsible for the non-uniform growth. Such a process is entirely consistent with the grower's reports of a poor thermal coupling of the wafer to substrate holder

in this older reactor[13] used to grow the sample.

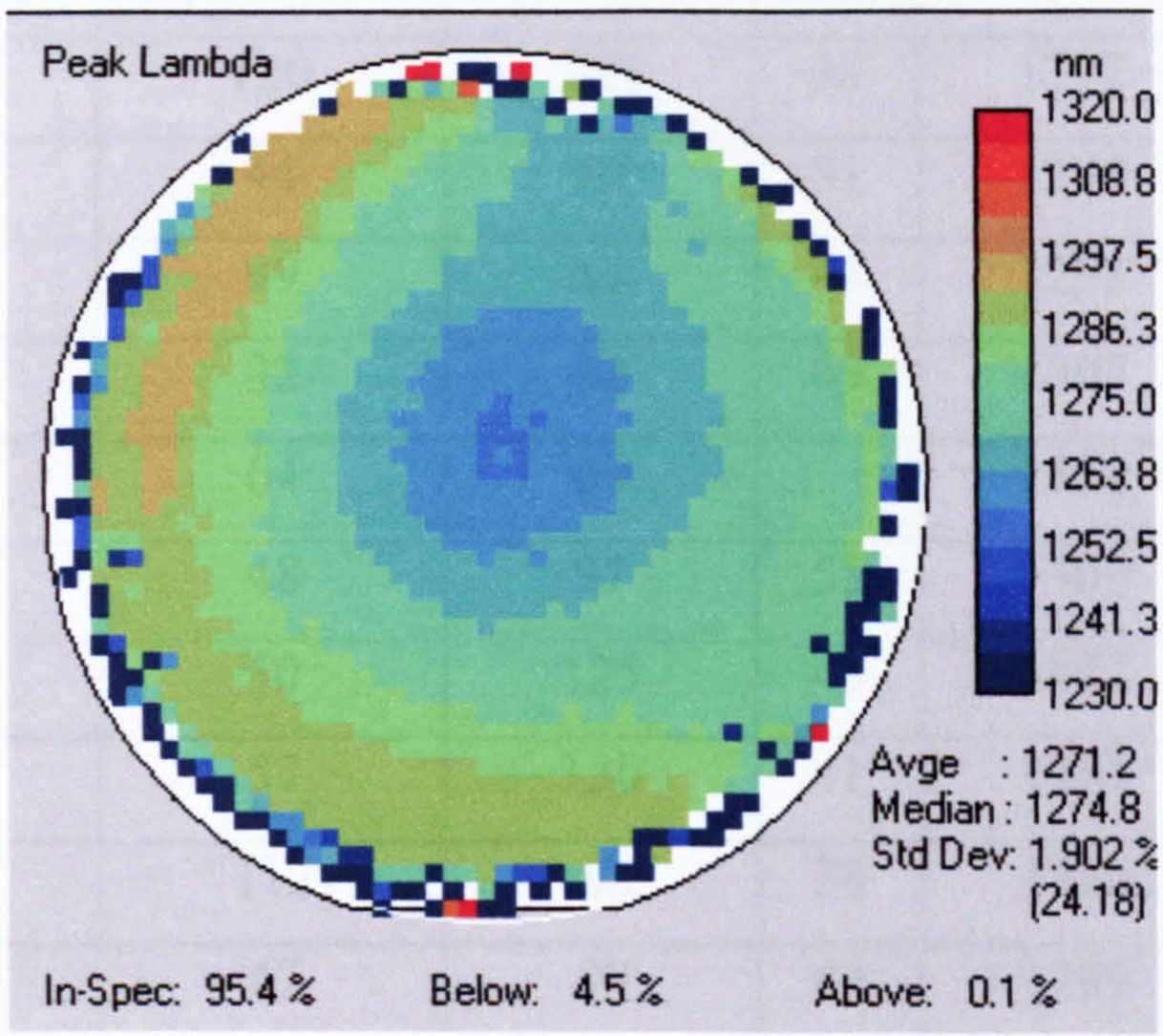

Fig. 6.23 RT PL map of a 5 – QD layer structure capped with $GaAs_{0.86}Sb_{0.14}$ (M 3116). The PL peak wavelength varies from 1250 at the centre of the wafer to 1300 nm near the edge.

Clearly, such non-uniformity in the QD growth within a wafer poses a problem when it comes to establishing 'unique' parameters to characterise the material. This point is illustrated in Table 6.24, where a comparison can be made between the lasing characteristics of devices processed from different parts of the M3116 wafer: 'a' material was cleaved from a portion within the horseshoe-shaped region near the left-hand edge region shown in Fig. 6.23 and 'b' material was taken from an area roughly halfway between the edge and the centre of the wafer.

On inspection of the tabulated parameters in Table 6.24, it is clear that devices fabricated from the 'a' material possess better characteristics i.e. longer lasing wavelengths and lower J_{th}'s. Furthermore, these devices have J_{th}'s which are less sensitive to cavity length (L_c). This latter point suggests that the material quality may be better near the edge of the wafer. As will be discussed in the following section, it is known that the competition between Sb/As for incorporation into the group V sub-lattice is strongly temperature dependent, which may explain the pronounced variation in the PL peak across the wafer if there are non-uniformities in the temperature of the underlying substrate.

Sample	L_C (mm)	RT Pulsed J_{th} (A/cm^2)	RT cw J_{th} (A/cm^2)	T_0 (K)	RT lasing λ (nm)	Max GS cw lasing T (°C)
Rm 2040	5	120	180	36	1292	-
M 3114	5	44	80	51	1294	60
	3	99	n/a	43	1291	2
M 3115 (InGaAs)	5	32	52	69	1307	90
	3	64	60		1298	110
M 3116 a	5	48	97	55	1309	60
	3	50	125	45	1315	50
M 3116 b	5	57	130	41	1294	60
	3	112	n/a	38	1286	17
M 3124	5	47	89	44	1289	50

Table. 6.24 Parameters extracted from laser characterisation of structures capped with $GaAs_{1-x}Sb_x$ SRLs

The full $J_{th} - T$ dependence is shown in Fig. 6.25 for 5 mm cavities of M 3115 (InGaAs SRL reference structure), M 3116 (a) and M 3116 (b). The RT cw J_{th}'s are 52, 97 and 130 A/cm^2 respectively. The T_0's are consistent with this trend, being 69, 55 and 41 K respectively. In the inset to Fig. 6.26 the respective RT lasing spectra are shown. In each structure lasing occurs at the peak of the low-bias spontaneous emission. There is a 15 nm blueshift in the lasing wavelength of M 3116 (b) with respect to M 3116 (a).

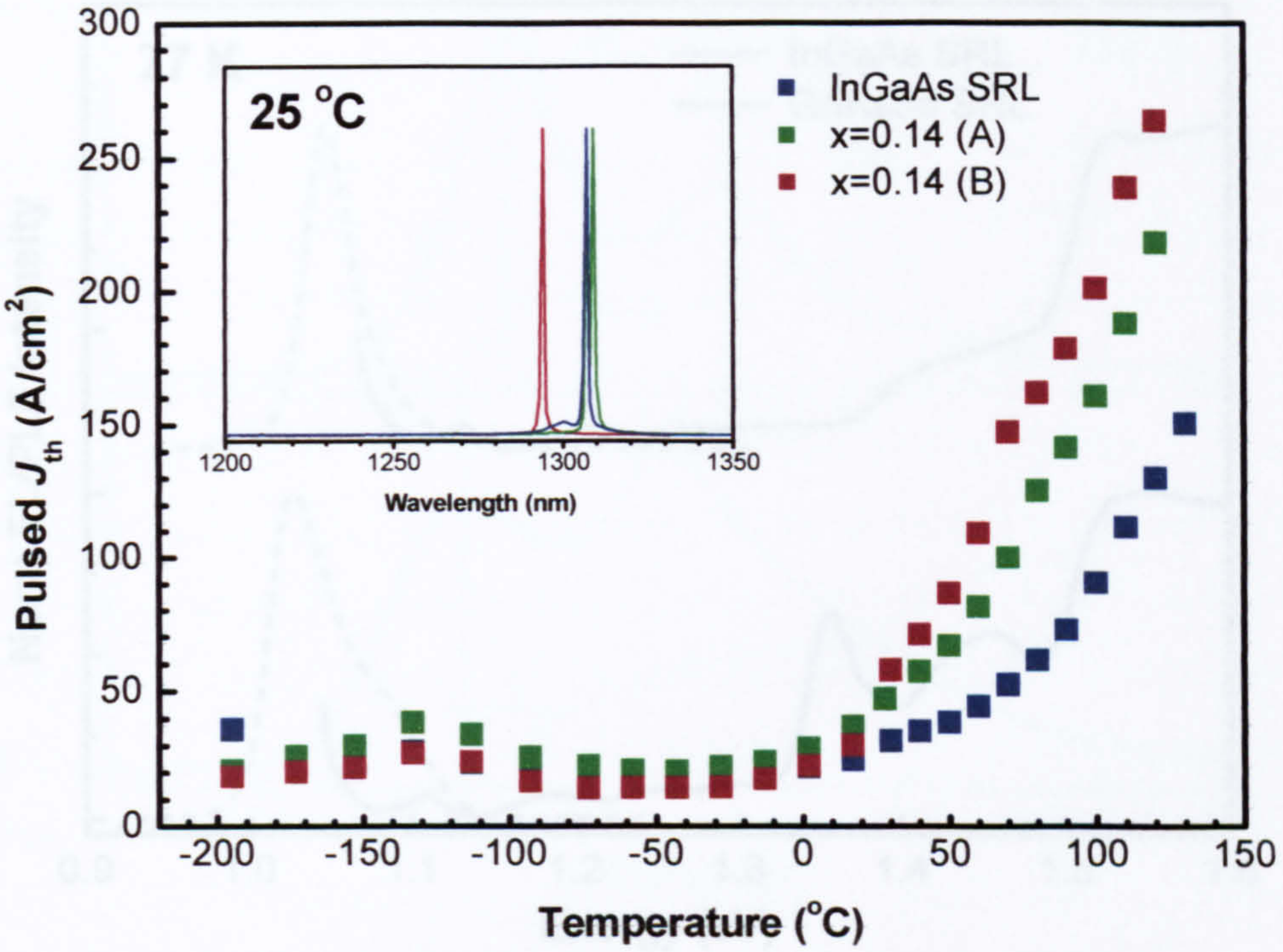

Fig. 6.25 Pulsed J_{th}'s as a function of temperature for 5 mm cavities of a $GaAs_{0.86}Sb_{0.14}$ capped 5 – QD layer structure (M 3116) processed from spatially distinct regions of the wafer. Data is also shown for the InGaAs capped reference structure.

Prior to the fabrication of these devices, the only other report of lasing from QDs capped with GaAsSb was from NICT in Japan[53]. Their results were poor, with RT pulsed lasing occurring at ~1200 nm with a J_{th} of ~ 11 kA/cm^2, this was attributed to primitive processing techniques. It is therefore encouraging that our results represent an improvement on this, even if the effect of the Sb in the SRL does not improve on the lasing performance of the $In_{0.15}Ga_{0.85}As$ capped reference device.

6.6.2 Absorption properties of InAs/GaAsSb QD devices

6.6.2.1 Low antimony content SRLs (x=0.14)

77K low injection current spontaneous emission spectra, collected from 400 μm diameter mesa devices processed from the 'b' material of the M 3116 wafer and M 3115 are shown in Fig. 6.26 along with the PLE detected at the respective PL peaks.

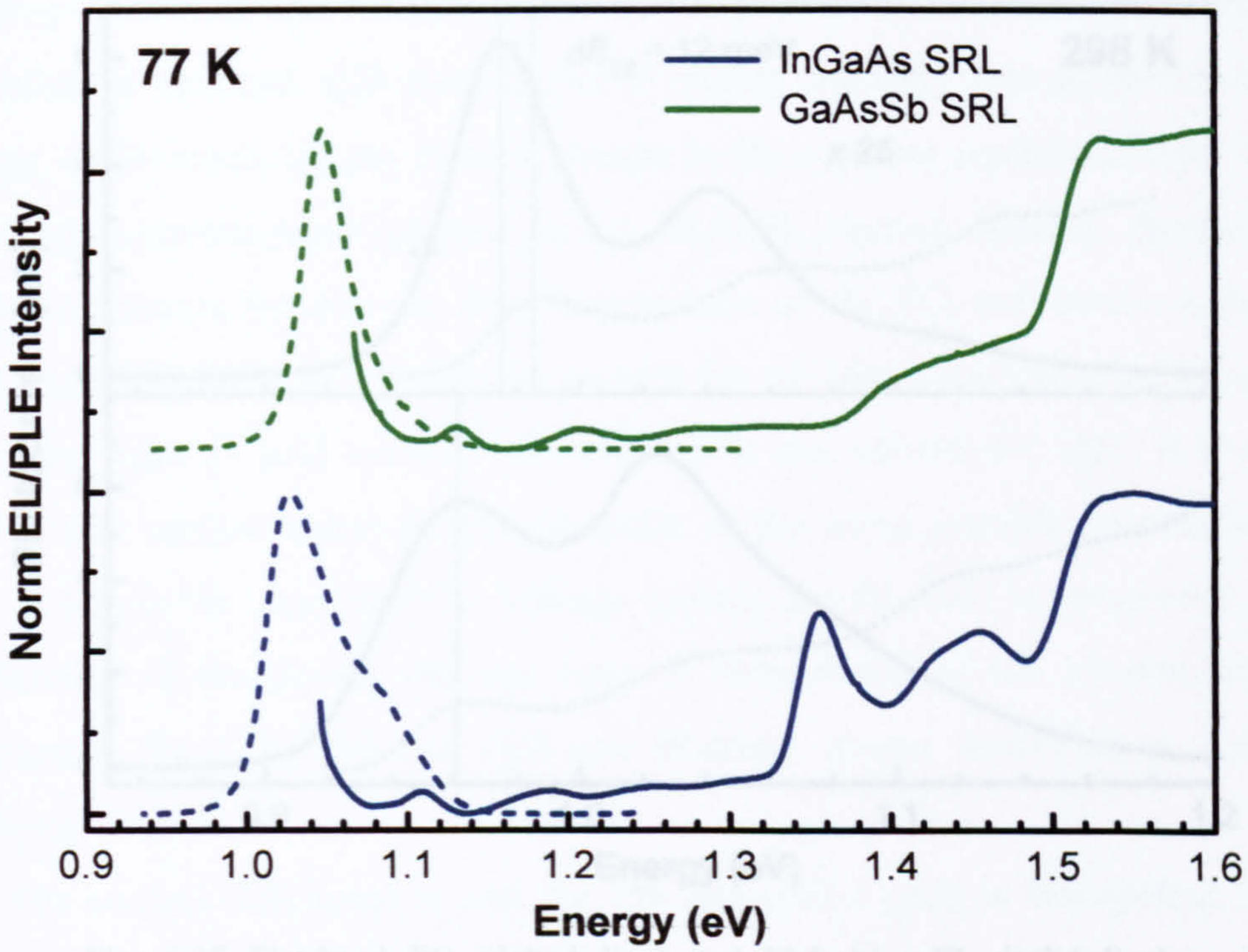

Fig. 6.26 PLE (solid line) and low bias EL (dotted line) measured at 77 K for a $GaAs_{0.86}Sb_{0.14}$ capped 5 – QD layer structure (M 3116) (green line) and the InGaAs capped reference structure (navy line).

Somewhat surprisingly, the linewidth of the GS emission is greater in the Sb containing structure than in InGaAs capped reference one, However, the greater homogeneity of the Sb containing structure is restricted to the emitting QD states, with features attributed to the GaAsSb SRL being weaker and less homogeneous than the corresponding feature in the InGaAs capped structure; possibly reflecting a greater degree of disorder in the GaAsSb SRL. Despite this, the intra-QD relaxation processes, appear to be unaffected by the capping material, occurring at coincident energies and having a similar spectral form for both GaAsSb and InGaAs capped structures

From Fig. 6.26 the lowest energy transition in the GaAsSb SRL is seen to occur at ~1.4 eV, an energy approximately 50 meV higher than the corresponding state in the InGaAs SRL. This would be consistent with a greater potential barrier height for electron escape in the Sb containing structure. However, it is clear that the higher energy confinement layer does not prevent the degradation of J_{th} above RT in the GaAsSb capped structures.

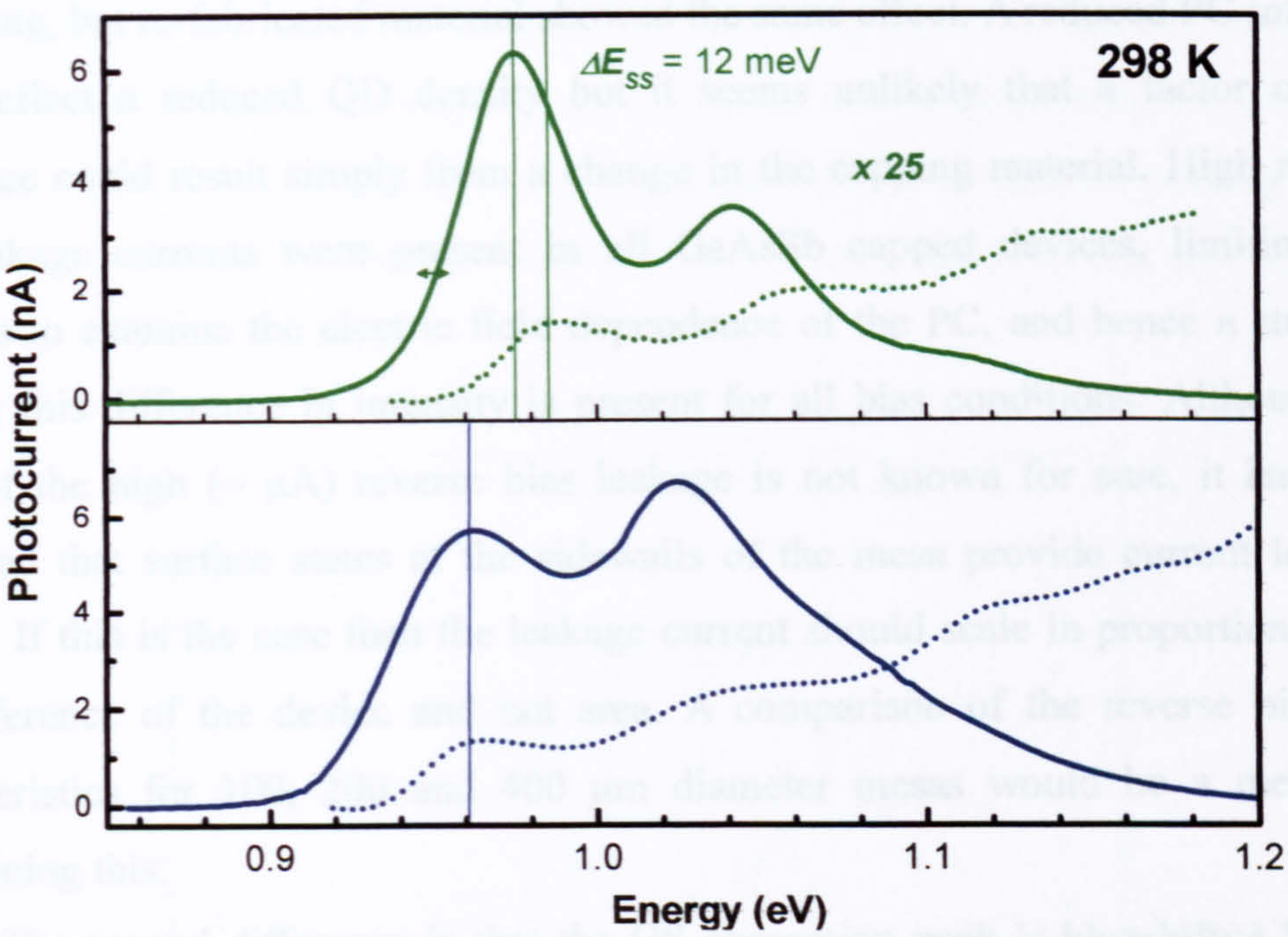

Fig. 6.27 Flat-band PC (dotted line) and high bias EL (solid line) measured at RT for a $GaAs_{0.86}Sb_{0.14}$ capped 5 – QD layer structure (M 3116) (green line) and the InGaAs capped reference structure (navy line).

RT EL and PC measurements are shown in Fig. 6.27. The EL was taken under a pulsed injection level of 60 mA and the PC was recorded with zero bias across the structure. From the EL, the GS to first ES separation energy is determined to be ~65 meV in each structure, although the first ES transition is more clearly resolved in GaAsSb capped device. This almost identical energy level separation suggests a very similar QD structure when capped with either $In_{0.15}Ga_{0.85}As$ or $GaAs_{0.86}Sb_{0.14}$. As discussed previously there is some evidence from structural studies that QDs capped with GaAsSb have a larger height than dots capped with GaAs, although no data is available for InGaAs capped dots. This suggests that the dot height is sensitive to the capping material. However the separation between confined states is mainly a function of the in-plane size and is relatively insensitive to changes in the dot height.

The PC spectra are similar in form, yet there are two pronounced differences. First, relative to the $In_{0.15}Ga_{0.85}As$ capped reference structure (M 3115), the magnitude of the PC is a factor of ~25 weaker in the $GaAs_{0.86}Sb_{0.14}$ capped structure processed from material between the edge and the centre of the wafer (M 3116b), although the emission intensities are comparable. Initially it was thought that the reduction in the PC signal was due to defects being introduced in the structure during

processing, but re-fabricated material showed the same effect. A reduced PC intensity could reflect a reduced QD density but it seems unlikely that a factor of ~25 difference could result simply from a change in the capping material. High reverse bias leakage currents were present in all GaAsSb capped devices, limiting any attempts to examine the electric field dependence of the PC, and hence a study of whether this difference in intensity is present for all bias conditions. Although the cause of the high (~ μA) reverse bias leakage is not known for sure, it has been suggested that surface states at the sidewalls of the mesa provide current leakage paths[54]. If this is the case then the leakage current should scale in proportion to the circumference of the device and not area. A comparison of the reverse bias I-V characteristics for 100, 200 and 400 μm diameter mesas would be a means of determining this.

The second difference is that the GS absorption peak is blueshifted by ~12 meV with respect to the emission peak in the GaAsSb structure, whereas the PC and EL are coincident for the InGaAs capped QDs. By measuring the GS EL energy for low injection levels, it was confirmed that the GS energy observed in the 60 mA pulsed EL is not subject to a redshift as a result of Joule heating in the device. Therefore, the Stokes shift between emission and absorption is a real effect. As there should be no Stokes shift for a single QD this effect must be a consequence of studying an inhomogeneously broadened ensemble of QDs, with different QDs within this ensemble contributing different strengths to emission and absorption. For example the quantum efficiency in emission or carrier extraction efficiency in absorption could vary across the distribution. Alternatively, photogenerated carriers could be emitted and preferentially recaptured in larger QDs, giving a higher spectral weighting to these dots in emission. It is not clear, however, why the two samples behave so differently. A Stokes shift could be expected for a type-II structure due to the hole residing in an alloy material. However the present GaAsSb capped sample is believed to be type-I given the Sb composition of 14%.

6.6.2.2 High antimony content (x=0.22 – 0.26) SRLs

The performance of devices with higher Sb content, operating at longer wavelengths, was universally poor. Fig. 6.28 shows pulsed EL from a 5-layer device

with a 5 mm cavity length and GaAsSb SRLs covering the QDs. The Sb composition was approximately 26%. Lasing is only obtainable at low temperatures (100 K) and at a high J_{th} (423 A/cm^2). By RT, only weak spontaneous emission, peaking around 1350 nm, is observable. These wavelengths are considerably shorter than expected for this high Sb composition.

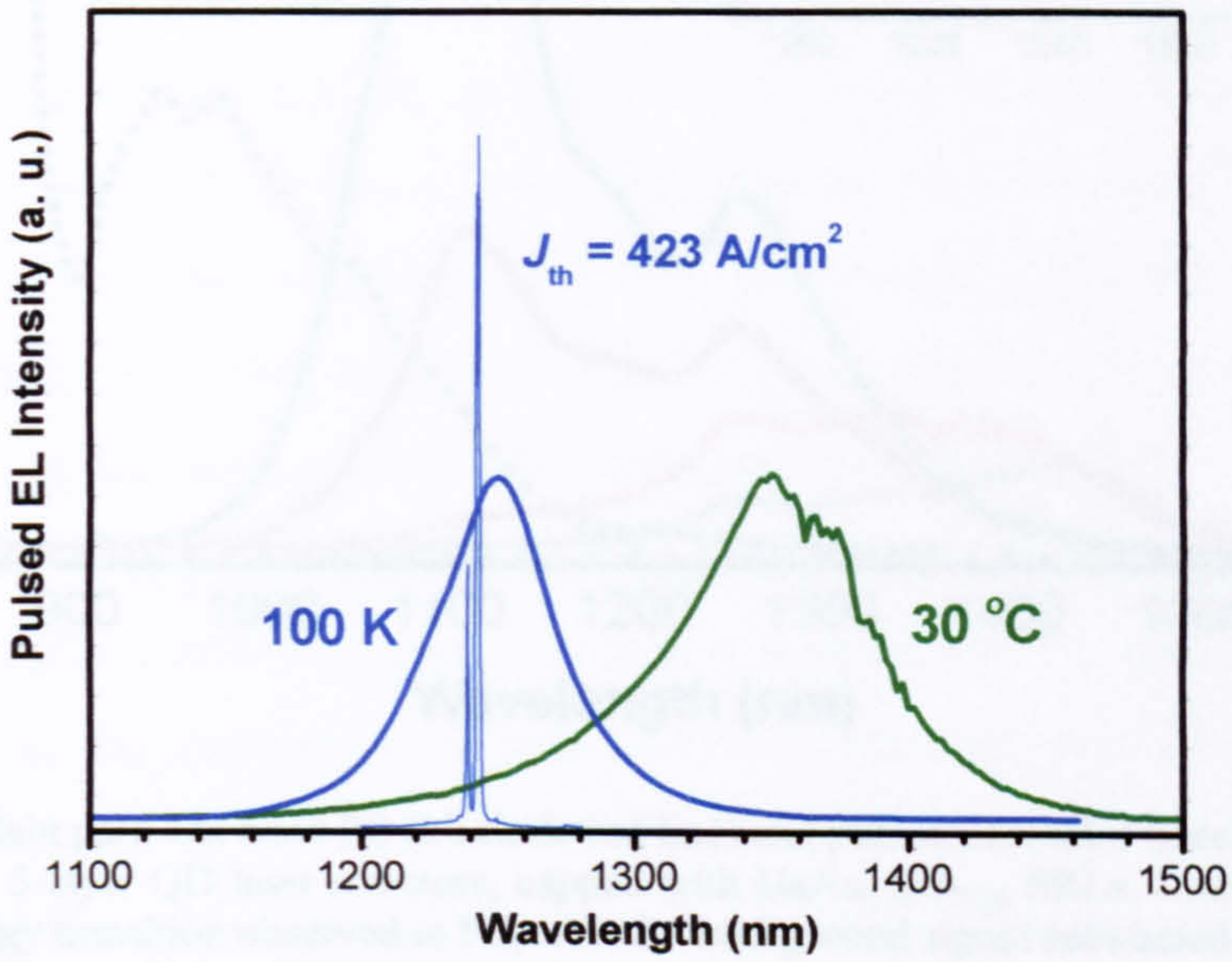

Fig. 6.28 Pulsed spontaneous and lasing EL spectra at 100 K (blue lines) for a 5 mm cavity of a 5-QD layer laser structure capped with $GaAs_{0.74}Sb_{0.26}$ SRLs. At RT (green line) only spontaneous emission occurs.

Fig. 6.29 shows RT PC and EL spectra of a 5-layer structure with nominally 26% Sb in the SRL. The type-II nature of the lowest energy transition at ~1440 nm is revealed by the blueshift of the EL with increasing injection current. Eventually this emission is quenched and the type-I emission centred at 1255 and 1110 nm emerges. The emission at 1255 nm may be the result of a transition involving excited (n=2) electron and hole states within the QDs. The 1110 nm peak is attributed to a purely type-I transition occurring in the GaAsSb SRL.

These assignments are supported by the large differences in their absorption strengths, as inferred from the PC: the GaAsSb QW having a much greater density of states than the ensemble of QD states. Again, there is evidence for a Stokes shift (~17 meV) for the transition corresponding to emission at 1255 nm; in PC the same transition occurs at 1234 nm (see inset to Fig. 6.29). However in this sample a Stokes shift is understandable if the hole is localised in the GaAsSb alloy material.

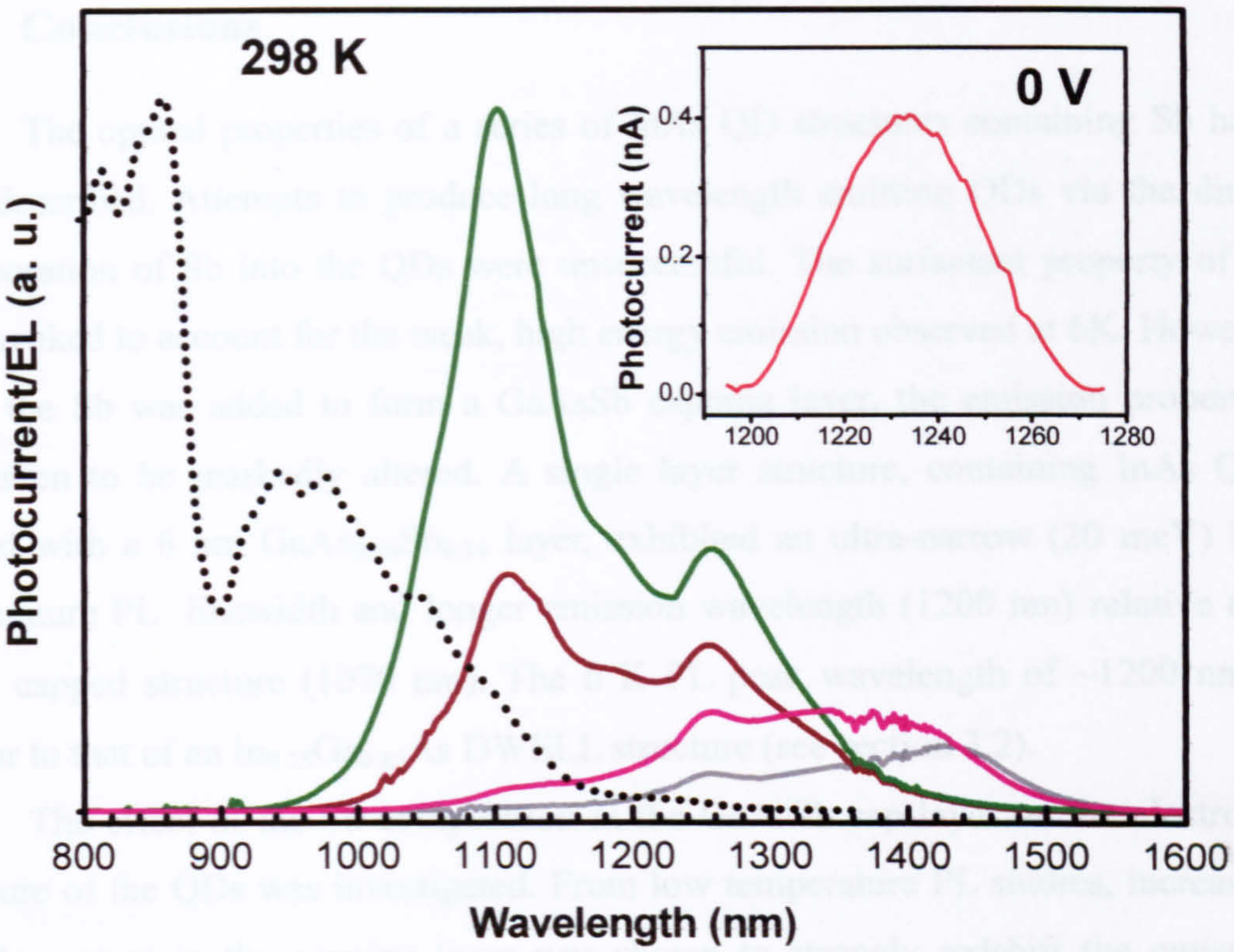

Fig. 6.29 Main part: flat band PC (black dotted line) and pulsed EL (solid lines), measured at RT, of a 5-layer QD laser structure, capped with $GaAs_{0.74}Sb_{0.26}$ SRLs. Inset shows the lowest energy transition observed in PC, with the background signal subtracted.

A laser device was fabricated from this material with an Sb composition of 26%, but no lasing was observed at any temperature. This could reflect either a low material quality, with a large non-radiative centre density (extrinsic effect), or a low oscillator strength for the type-II transition, and hence insufficient gain for lasing (intrinsic effect). Very recently, lasing has been reported for a type-II structure consisting of GaSb/GaAs QDs capped with InGaAs[55]. As in Fig. 6.29, a blueshifting EL peak was observed with increasing injection current, with RT lasing occurring at 1033 nm and J_{th} = 678 A/cm^2 from a 5 mm as-cleaved cavity. In addition, lasing at ~4 μm has been reported from a type-II InAs/InGaSb/InAs/AlSb QW system[56]. These results indicate that a type-II system can support lasing action and suggests that, given the possible compact nature of the excitons in the present system, lasing may also be possible if the basic material quality could be improved sufficiently.

6.7 Conclusions

The optical properties of a series of InAs QD structures containing Sb have been described. Attempts to produce long wavelength emitting QDs via the direct incorporation of Sb into the QDs were unsuccessful. The surfactant property of Sb was invoked to account for the weak, high energy emission observed at 6K. However, when the Sb was added to form a GaAsSb capping layer, the emission properties were seen to be markedly altered. A single layer structure, containing InAs QDs capped with a 6 nm $GaAs_{0.86}Sb_{0.14}$ layer, exhibited an ultra-narrow (20 meV) low temperature PL linewidth and longer emission wavelength (1200 nm) relative to a GaAs capped structure (1070 nm). The 6 K PL peak wavelength of ~1200 nm is similar to that of an $In_{0.15}Ga_{0.85}As$ DWELL structure (see section 3.2).

The effect of the Sb composition in the GaAsSb cap layer on the electronic structure of the QDs was investigated. From low temperature PL studies, increasing the Sb content in the capping layer was shown to strongly redshift the emission wavelength. In addition, it is found that for a composition above ~14% the PL strongly blue shifts with increasing excitation power. This latter behaviour is characteristic of the formation of a type-II system and this is postulated as the dominant mechanism for the redshift with increasing Sb content. PLE indicated an alteration to the carrier relaxation mechanisms in the type-II structures ($x \geq 0.14$) and the contrast in oscillator strengths of the type-I and type-II transitions.

The type-II band alignment for structures with $x \geq 0.14$, results in longer radiative lifetimes for the GS excitons in these structures. TR PL studies confirm that that the radiative lifetime in the $x=0.22$ structure increases to ~60 ns. Analysis of the power dependent blue-shift of the emission indicates that the hole is localised above the QD. Magneto-PL measurements in pulsed fields, used to probe the 3D extent of the wavefunctions, suggest that the electron and hole wavefunctions are relatively closely spaced in the type-II structures. A lateral modification of the strain state of the GaAsSb layer was postulated to account for the localisation of the hole close to the QD. In addition, in high Sb content samples there is evidence for carrier localisation by fluctuations of the GaAsSb width or composition.

A series of laser structures containing $GaAs_{1-x}Sb_x$ SRLs were grown. For $x \sim 0.14$ their performance was comparable to that of a reference structure containing

an $In_{0.15}Ga_{0.85}As$ SRL, although in no respect was an improvement observed. Despite this, the results presented represent the state of the art for this particular design of QD laser. Structures with $0.22 < x < 0.26$ in the $GaAs_{1-x}Sb_x$ SRLs, engineered to emit at ~1.55 μm, failed to lase at RT, but exhibited novel emission and absorption properties. It remains unclear if this lack of lasing is a result of a weak type-II oscillator strength (intrinsic) or defects associated with the high Sb content (extrinsic).

References

1. L Ya Karachinsky, T Kettler, I I Novikov, Yu M Shernyakov, N Yu Gordeev, M V Maximov, N V Kryzhanovskaya, A E Zhukov, E S Semenova, A P Vasil'ev, V M Ustinov, G Fiol, M Kuntz, A Lochmann, O Schulz, L Reissmann, K Posilovic, A R Kovsh, S S Mikhrin, V A Shchukin, N N Ledentsov and D Bimberg, Semicond. Sci. and Tech. **21**, 691 (2006)

2. C. E. Pryor and M.-E. Pistol, Phys. Rev. B **72**, 205311 (2005)

3. Tetsuya Matsuura, Tomoyuki Miyamoto, Takeo Kageyama, Masataka Ohta, Yasutaka Matsui, Tatsuya Furuhata and Fumio Koyama, Jpn. J. Appl. Phys. **43**, (5A) L605 (2004)

4. Makoto Kudo, Toshihiro Nakaoka, Satoshi Iwamoto and Yasuhiko Arakawa, Jpn. J. Appl. Phys. **44**, (1) L45 (2005)

5. Denis Guimard, Masao Nishioka, Shiro Tsukamoto, and Yasuhiko Arakawa, Appl. Phys. Lett. **89**, 183124 (2006)

6. Yi-An Chang, Hao-Chung Kuo, Ya-Hsien Chang, and Shing-Chung Wang, Appl. Phys. Lett. **87**, 61908 (2005)

7. Takeo Kageyama, Tomoyuki Miyamoto, Masataka Ohta, Tetsuya Matsuura, Yasutaka Matsui, Tatsuya Furuhata, and Fumio Koyama, J. Appl. Phys. **96**, 44 (2004)

8. Naokatsu Yamamoto, Kouichi Akahane, Shinichirou Gozu, and Naoki Ohtani, Appl. Phys. Lett. **86**, 203118 (2005)

9. T. Matsuura, T. Miyamoto, M. Ohta, Y. Matsui, T. Furuhata and F. Koyama, J. Cryst. Growth **278**, (1-4) 51 (2005)

10. Zetian Mi and Pallab Bhattacharya, J. Appl. Phys. **98**, 023510 (2005)

11. P. Dawson, O. Rubel, S. D. Baranovskii, K. Pierz, P. Thomas, and E. O. Göbel, Phys. Rev. B **72**, 235301 (2005)

12. H. Y. Liu, I. R. Sellers, T. J. Badcock, D. J. Mowbray, M. S. Skolnick, K. M. Groom, M. Gutiérrez, M. Hopkinson, J. S. Ng, J. P. R. David, R. Beanland, Appl. Phys. Lett. **85**, 704 (2004)

13. Hui-Yun Liu and M J Steer (Private communication)

14. Tetsuya Matsuura, Tomoyuki Miyamoto, and Fumio Koyama, Appl. Phys. Lett. **88**, 183109 (2006)

15. J. M. Ulloa, I. W. D. Drouzas, P. M. Koenraad, D. J. Mowbray, M. J. Steer, H. Y. Liu, and M. Hopkinson, Appl. Phys. Lett. **90**, 213105 (2007)

16. J. M. Ripalda, D. Granados, Y. González, A. M. Sánchez, S. I. Molina, and J. M. García, Appl. Phys. Lett. **87**, 202108 (2005)

17. Kouichi Akahane, Naokatsu Yamamoto and Naoki Ohtani, Physica E **21**, (2-4) 295 (2004)

18. Wei-Sheng Liu, David M. T. Kuo, and Jen-Inn Chyi, Wen-Yen Chen, Hsing-Szu Chang and Tzu-Min Hsu, Appl. Phys. Lett. **89**, 243103 (2006)

19. J. M. Ripalda, D. Alonso-Álvarez, B. Alén, A. G. Taboada, J. M. García, Y. González, and L. González, Appl. Phys. Lett. **91**, 012111 (2007)

20. S. L. Zuo, Y. G. Hong, E. T. Yu and J. F. Klem, J. Appl. Phys. **92**, 3761 (2002)

21. R. Teissier and D. Sicault, J. C. Harmand, G. Ungaro and G. Le Roux, J. Appl. Phys. **89**, 5473 (2001)

22. Guobin Liu, Shun-Lien Chuang and Seoung-Hwan Park, J. Appl. Phys. **88**, 5554 (2000)

23. S. M. North, P. R. Briddon, M. A. Cusack, and M. Jaros,Phys. Rev. B. **58**, 12601 (1998)

24. A. D. Prins, D. J. Dunstan, J. D. Lambkin, E. P. O'Reilly, A. R. Adams, R. Pritchard, W. S. Truscott, and K. E. Singer, Phys. Rev. B. **47**, 2191 (1993)

25. Quantum semiconductor structures : fundamentals and applications / Claude Weisbuch, Borge Vinter. London : Academic Press Inc, 1991

26. N. N. Ledentsov, J. Bőhrer, M. Beer, F. Heinrichsdorff, M. Grundmann, D. Bimberg, S. V. Ivanov, B. Ya. Meltser, S. V. Shaposhnikov, I. N. Yassievich, N. N. Faleev, P. S. Kop'ev, and Zh. I. Alferov, Phys. Rev. B **52**, 14058 (1995)

27. Y. S. Chiu, M. H. Ya, W. S. Su, and Y. F. Chen, J. Appl. Phys. **92**, 5810 (2002)

28. D. A. Miller, D. S. Chemla, T. C. Damen, A. C. Gossard, W. Wiegmann, T. H. Wood, and C. A. Burrus, Phys. Rev. B **32**, 1043 (1985)

29. T. T. Chen, C. L. Cheng, Y. F. Chen, F. Y. Chang, H. H. Lin, C.-T. Wu, and C.-H. Chen, Phys. Rev. B **75**, 033310 (2007)

30. E. C. Le Ru, J. Fack, and R. Murray, Phys. Rev. B **67**, 245318 (2003)

31. S. Sanguinetti, M. Henini, M. Grassi Alessi, M. Capizzi, P. Frigeri, and S. Franchi, Phys. Rev. B **60**, 8276 (1999)

32. R. Heitz, M. Veit, N. N. Ledentsov, A. Hoffmann, D. Bimberg, V. M. Ustinov, P. S. Kop'ev, and Zh. I. Alferov, Phys. Rev. B **56**, 10435 (1997)

33. H. Y. Liu, M. J. Steer, T. J. Badcock, D. J. Mowbray, M. S. Skolnick, F. Suarez, J. S. Ng, M. Hopkinson, and J. P. R. David, J. Appl. Phys. **99**, 046104 (2006)

34. X. D. Luo, C. Y. Hu, Z. Y. Xu, H. L. Luo, Y. Q. Wang, J. N. Wang, and W. K. Ge, Appl. Phys. Lett. **81**, 3795 (2002)

35. C.-K. Sun, G. Wang, J. E. Bowers, B. Brar, H.-R. Blank, H. Kroemer, and M. H. Pilkuhn, Appl. Phys. Lett. 68, 1543 (1996)

36. Y. D. Jang, T. J. Badcock, D. J. Mowbray, M. S. Skolnick, J. Park, D. Lee, H. Y. Liu, M. J. Steer, and M. Hopkinson, Appl. Phys. Lett. 92, 251905 (2008)

37. R. Rinaldi, P. V. Giugno, R. Cingolani, H. Lipsanen, M. Sopanen, J. Tulkki, and J. Ahopelto, Phys. Rev. Lett. 77, 342 (1996)

38. M. Bayer, S. N. Walck, T. L. Reinecke, and A. Forchel, Phys. Rev. B 57, 6584 (1998)

39. P. D. Wang, J. L. Merz, S. Fafard, R. Leon, D. Leonard, G. Medeiros-Ribeiro, M. Oestreich, P. M. Petroff, K. Uchida, N. Miura, H. Akiyama, and H. Sakaki, Phys. Rev. B 53, 16458 (1996)

40. R. Provoost, M. Hayne, V. V. Moshchalkov, M. K. Zundel and K. Eberl, Appl. Phys. Lett. 75, 799 (1999)

41. J. Maes, M. Hayne, V. V. Moshchalkov, A. Patanè, M. Henini, L. Eaves, and P. C. Main, Appl. Phys. Lett. 81, 1480 (2002)

42. S. Godefroo, J. Maes, M. Hayne, V. V. Moshchalkov, M. Henini, F. Pulizzi, A. Patanè, and L. Eaves, J. Appl. Phys. 96, 2535 (2004)

43. M. Hayne, R. Provoost, M. K. Zundel, Y. M. Manz, K. Eberl, and V. V. Moshchalkov, Phys. Rev. B 62, 10324 (2000)

44. L. R. Wilson, D. J. Mowbray, M. S. Skolnick, M. Morifuji, M. J. Steer, I. A. Larkin, and M. Hopkinson, Phys. Rev. B 57, R2073 (1998)

45. P. P. Paskov, P. O. Holtz, B. Monemar, J. M. Garcia, W. V. Schoenfeld, and P. M. Petroff, Phys. Rev. B 62, 7344 (2000)

46. M. Hayne, J. Maes, S. Bersier, V. V. Moshchalkov, A. Schliwa, L. Müller-Kirsch, C. Kapteyn, R. Heitz, and D. Bimberg, Appl. Phys. Lett. 82, 4355 (2003)

47. M. Hayne, O. Razinkova, S. Bersier, R. Heitz, L. Müller-Kirsch, M. Geller, D. Bimberg, and V. V. Moshchalkov, Phys. Rev. B 70, 081302 (2004)

48. N. Schildermans, M. Hayne, V. V. Moshchalkov, A. Rastelli, and O. G. Schmidt, Phys. Rev. B 72, 115312 (2005)

49. I. E. Itskevich, M. Henini, H. A. Carmona, L. Eaves, P. C. Main, D. K. Maude and J. C. Portal, Appl. Phys. Lett. 70, 505 (1997)

50. M. Erdmann, C. Ropers, M. Wenderoth, R. G. Ulbrich, S. Malzer, and G. H. Döhler, Phys. Rev. B 74, 125412 (2006)

51. M. Grochol, F. Grosse, and R. Zimmermann, Phys. Rev. B 71, 125339 (2005)

52. M. Larsson, E. S. Moskalenko, L. A. Larsson, P. O. Holtz, C. Verdozzi, C.-O. Almbladh, W. V. Schoenfeld, and P. M. Petroff, Phys. Rev. B 74, 245312 (2006)

53. Kouichi Akahane, Naokatsu Yamamoto, Shin-ichiro Gozu and Naoki Ohtani, Physica E 26, (1-4) 395 (2005)

54. P D Buckle (Private Communication)

55. J. Tatebayashi, A. Khoshakhlagh, S. H. Huang, G. Balakrishnan, L. R. Dawson, D. L. Huffaker, D. A. Bussian, H. Htoon, and V. Klimov, Appl. Phys. Lett. 90, 261115 (2007)

56. Chih-Hsiang Lin, S. S. Pein H., Q. Le, J. R. Meyer and C. L. Felix, Appl. Phys. Lett. 71, 3281 (1997)

Chapter 7

Conclusion and future work

This thesis has presented a detailed optical characterisation of InAs quantum-dot-in-a-well (DWELL) laser structures aimed primarily at the development of commercially viable 1.3μm emitting devices. Basic structures consist of InAs QDs grown within an InGaAs-GaAs quantum well, this structure being required to extend the emission wavelength out to 1.3μm. From PL studies of DWELL test structures, an In composition of 15% was found to be optimum for optically efficient 1.3 μm emission at room temperature. The use of a DWELL structure was also found to increase the QD density. A ground state exciton confinement energy of 310 meV, independent of x, was determined from PLE studies. This finding confirmed that the stimulated decomposition of the $In_xGa_{1-x}As$ DWELL and/or reduction in hydrostatic QD strain dominates the redshift of the QD emission with increasing x.

Initial multi-QD layer full laser structures incorporating $In_{0.15}Ga_{0.85}As$ DWELLs and 50nm thick GaAs spacer layers exhibited poor performance. Transmission Electron Microscopy (TEM) investigations revealed the presence of dislocated QDs, originating in the second QD layer and propagated upwards to the higher layers via threading dislocations in the GaAs spacer layers. From an Atomic Force Microscopy study of the QD nucleation surface, the GaAs was shown to be insufficiently planarised following the QD growth, with remaining roughness promoting the formation of dislocated QDs. The low growth temperature (510 °C) used for the GaAs spacer layers in these initial structures was attributed as the cause of this surface roughness. This finding motivated the development of a new technique for the GaAs spacer layer growth.

To increase the Ga ad-atom mobility and therefore the planarisation rate during the GaAs spacer layer growth, the growth temperature for the upper 35 nm portion of the spacer layer was increased to 580 °C. Spacer layers grown using this two-temperature method were referred to as High Growth Temperature Spacer Layers (HGTSLs). TEM images confirmed that the HGTSL technique was able to reduce the dislocation density by over three orders of magnitude, translating into greatly improved RT optical efficiencies and laser performance. A 5-layer laser

structure was now able to maintain cw ground state lasing at room temperature down to a cavity length of 1.5 mm. A 5mm cavity of the same structure operated cw from the ground state up to 85 °C. The eradication of defective QDs produced some of the lowest reported J_{th}s in the literature for 1.3 μm QD laser devices e.g. a double HR coated 1 mm cavity of a 3 layer structure with 70 nm HGTSLs lased cw at RT with a $J_{th} = 19$ A/cm^2.

In spite of the excellent cw performance, the highest T_0 achieved for any of the initial devices was only ~90 K, at best only comparable to values for quantum well lasers. Possibly related to this poor high temperature performance was the observation of dual-state lasing at and above RT. This behaviour indicated that the devices suffered from a significant temperature induced reduction in the saturated ground state gain. Temperature dependent studies of the spontaneous emission highlighted the impact of the bimodal QD size distribution on the optical properties. The presence of two QD 'sub-sets' resulted in the enhancement of thermal carrier redistribution effects which are specific to inhomogeneously broadened systems. Above ~220 K, non-radiative processes, possibly involving defect or excited states are shown to contribute significantly to the increase in J_{th}. From studies of annealed DWELL test structures, the origin of the bimodal QD size distribution, observed in all the laser structures studied in this thesis, was attributed to an *in situ* annealing process of the QDs during the high temperature growth of the upper AlGaAs cladding layer.

In an attempt to increase the material gain of the devices, a new series of structures was grown including 7 and 10-layer structures. Despite the increase in the ground state absorption strength with layer number, confirmed by PC spectroscopy, there was no marked improvement in the high temperature performance of the 10-layer device. However, there was no evidence that the radiative efficiency *per QD layer* changed significantly with the number of layers in the structure, although there may be proportionally more large QDs in higher layer number structures. In addition, the GaAs/AlGaAs waveguide thickness was shown to have little effect on the temperature dependence of J_{th}, confirming that the modal gain was not being unduly limited by a lower optical confinement factor.

By modifying the HGTSL technique, a structure containing 35 nm GaAs spacer layers, in which the upper 20 nm was deposited at 620°C, allowed a 1mm

cavity length device to operate cw from the ground state at temperatures up to 60°C. This enhanced performance was attributed to a reduction in both the inhomogeneous broadening of the QD emission and the amount of non-radiative recombination. Again, a smoother nucleation surface for the QDs is believed to be the reason for this improvement.

p-type modulation doping of the QDs has been shown to improve the temperature stability of J_{th} although with an increase in its absolute value. For a device doped with 15 acceptors/QD both a low J_{th} (less than 50 A cm^{-2} at room temperature) and a negative characteristic temperature between -50 and 45°C is obtained. The spectral form of the emission at low temperature and low current injection indicates that the dopants do not affect the physical structure of the QDs. Likewise, no charging induced shifts of the emission energy are observed for doping levels up to 50 acceptors/QD. At low temperatures, both the optical efficiency and the carrier lifetime decrease as the level of doping increases. An Auger process, involving the extrinsic holes, was invoked to account for this behaviour. However, the dependence of the Auger recombination rate on the extrinsic hole density is observed to be weaker than that observed in higher dimensionality systems, a result of the discrete QD states and strong optical selection rules. Pump-probe and PLE studies provided evidence for faster carrier capture and relaxation in doped QDs.

Studies of the emission linewidth and relative populations of the two QD sub-sets suggested that the attainment of a thermal carrier distribution within the QD ensemble occurs at a higher temperature in the doped structures. This is believed to be the result of a deeper confinement potential for the electrons in the doped QDs, due to the attractive potential arising from the extrinsic holes. As a consequence, the negative T_0 region (observed in undoped devices around ~ -100°C) was observed at around room temperature in the 15 acc/QD structure. The predictions of a photon coupling model, based on the interaction between ground and excited states in the inhomogeneously broadened ensemble, was shown to be able to reproduce the observed temperature dependence of J_{th} in undoped and 15 acceptor/QD doped devices. Photocurrent spectroscopy confirmed the expected hole state blocking of the QD transitions in the doped structures. In addition, measurements of the Quantum Confined Stark Effect suggest that the permanent dipole is reduced in highly doped (>12 acceptors/QD structures).

By capping the QDs with a thin layer of GaAsSb, it was shown that emission beyond 1.3 μm may be obtained from InAs QDs. The emission was observed to redshift strongly with increasing Sb content. For Sb compositions above ~14%, the PL blueshifted with increasing laser excitation and the radiative lifetime of the GS exciton increased (up to ~ 65 ns), consistent with the formation of a type-II system in which the electron is located in the QD and the hole is in the GaAsSb. Analysis of the PL blueshift indicates the hole is localised above the QD, perhaps by a lateral modification of the strain within the GaAsSb layer. Magneto-PL in fields up to 50T was used to probe the spatial extent of the excitons in both type-I and type-II structures. Although room temperature lasing at 1.3 μm was obtained from QD structures with dots capped with low Sb composition (x~14%) layers, the performance of these devices did not exceed that of reference InGaAs capped devices. Structures containing $0.22<x<0.26$ Sb failed to lase at RT but exhibited emission that blueshifted with increasing injection. It is unclear whether the absence of lasing is due to the poor material quality of the type-II structures or due to the low oscillator strength of the type-II transition.

Some examples of future experimental work will now be listed.

1) A more detailed series of EL measurements on the multilayer structures discussed in chapter 4. By performing spectrally resolved measurements using various absolute current densities and constant current densities per layer, a more complete understanding of the effects of increasing layer number on the optical efficiency may be achieved. State-filling effects could also be examined.

2) Single QD layer *p*-type doped samples, with monomodal size distributions, could be re-grown and incorporated into *p-i-n* devices without the thick AlGaAs cladding layers. The study of single layer samples would simplify the treatment of the internal electric field induced by the dopants and extrinsic holes, allowing a better understanding of the PC properties. Further temperature dependent interband pump - intraband probe studies would also be useful.

3) For the Sb containing structures, a temperature dependent study of the radiative lifetime of the GS exciton in the type-II structure ($x=0.22$) would be interesting. Also more PC studies of the type-II devices structures, with passivated mesa sidewalls, enabling electric field dependence of the absorption to be studied.

4) Perhaps some QD bi-layer structures could be grown, in an attempt to increase the emission wavelength to ~1.5 μm, whilst preserving a narrow linewidth.